JOHANNES GUTENBERG UNIVERSITÄT MAINZ

JG|U

Effective Field Theory Phenomenology and Scattering Amplitudes

Dissertation

zur Erlangung des Grades „Doktor der Naturwissenschaften“
am Fachbereich Physik, Mathematik und Informatik
der Johannes Gutenberg-Universität in Mainz

Rafael Aoude

geb. in Brazil
Mainz, June 9, 2020

date of submission: 15.06.2020
date of defense: 02.09.2020

Abstract

The Standard Model (SM) is an effective description of Nature and experimental evidences indicates that beyond SM physics ought to exist. The series of the LHC null results for many searches for specific models have shifted the interest towards a model-independent effective description. Effective Field Theories (EFTs) provide a framework not only to parametrize the unknown but also to make efficient calculations with the right degrees of freedom. The most simple candidate for an effective extension of the SM is called Standard Model Effective Field Theory (SMEFT), which assumes that the scalar boson discovered by the LHC belongs to a doublet under the SM Electroweak symmetry. This thesis focus on the study of the SMEFT via phenomenological imprints at the LHC and using new modern methods for scattering amplitudes.

In the first part, we study the diboson production at the LHC and the impact of flavour data in SMEFT global fits. The former probes the nature of the electroweak symmetry breaking mechanism via anomalous triple-gauge-couplings and can be studied with an observable sensitive to only one higher-dimensional operator, which is rare in LHC SMEFT signals. Using jet substructure techniques, we analyse the azimuthal angles of the hadronic and semileptonic diboson production final states. In the latter, we study how flavour data can constrain the unknown parameters of SMEFT, the Wilson coefficients. Flavour low-energy measurements are known to put strong bounds on deviations of the SM flavour structure. Usually, these bounds are avoided in model building by assuming some kind of flavour symmetry in the ultraviolet. We study two flavour assumptions: leading-order Minimal Flavour Violation and $U(3)^5$. We show that the flavour data still put strong constraints on models of new physics, even in the most flavourless scenario. Global fits are of extreme importance for model building, since a lot of new physics models can be matched to SMEFT. The bounds on the Wilson Coefficients set the allowed space of the EFT and, consequently, on the allowed parameter space of the respective model.

In the second part, we use modern methods for scattering amplitudes to study the SMEFT. These new methods rely on spinor-helicity variables, recursion relations and generalized unitarity. They provide efficient tools to calculate higher-multiplicity and multi-loops amplitudes. We study the three-point SMEFT amplitudes in a new covariant massive spinor-helicity formalism and discuss the construction of higher point amplitudes via recursion relations and consistent factorization. The results on massive on-shell SMEFT amplitudes will allow precise computations in this EFT for the LHC.

Keywords: Effective Field Theories, Scattering Amplitudes.

Contents

Overview of Publications

This thesis contains the work of the author during his PhD. In this section we provide an overview of all the publications and the respective contribution of the author.

- [1] **Jet Substructure Measurements of Interference in Non-Interfering SMEFT Effects**, Rafael Aoude and William Shepherd.

  We perform a complete analysis of this azimuthal interference pattern in hadronic decays of W bosons using jet substructure techniques to tag the bosons and measure their azimuthal decay angles. This technique provides a valuable cross-check to purely-leptonic measurements of interference resurrection in diboson production.

  All the simulations, calculations and figures were made by the author under the supervision of William Shepherd. Both authors contributed to the manuscript. The majority of the publication has been literally copied into Section 4 of this thesis. One subsection was omitted and explained in detail in Chapter 3.

- [2] **The Rise of SMEFT On-shell Amplitudes**, Rafael Aoude and Camila S. Machado

  We present a map between the tree-level Standard Model Effective Theory (SMEFT) in the Warsaw basis and massive on-shell amplitudes. As a first step, we focus on the electroweak sector without fermions. We describe the Feynman rules for a particular choice of input scheme and compare them with the 3-point massive amplitudes in the broken phase. Thereby we fix an on-shell basis which allows us to study scattering amplitudes with recursion relations.

  All the calculations were performed independently by both authors and cross-checked. Both authors contributed to the manuscript.

- [3] **The impact of flavour data on global fits of the MFV SMEFT**, Rafael Aoude, Tobias Hurth, Sophie Renner and William Shepherd.

  We investigate the information that can be gained by including flavour data in fits of the Standard Model Effective Field Theory (SMEFT) with the assumption of Minimal Flavour Violation (MFV). Starting from a theory with no tree level flavour changing neutral currents, we calculate effects in flavour changing processes at one loop, and the resulting constraints on linear combinations of SMEFT coefficients. By doing a global fit including electroweak, Higgs and low energy precision measurements among others, we show that flavour observables put strong constraints on previously

unconstrained operator directions. Our findings demonstrate that flavour remains a stringent test for models of new physics, even in the most flavourless scenario.

Parts of the text was modified to fit in the thesis. The discussion of reparametrization invariance was added to explain the flat directions encountered in LEPI data. The author contributed to the coding of matching results, discussions and cross-checking calculations. Figures 12 and 13 were done by the author, while the other figures were done by Sophie Renner.

The preprint is currently under review for publication in JHEP.

- [4] **Soft Theorems and the KLT-Relation**, Rafael Aoude and Andreas Helset.

  We find new relations for the non-universal part of the Yang-Mills amplitudes by combining the Kawai-Lewellen-Tye-relation and the soft behavior of gauge and gravity amplitudes. We also extend the relations to include contributions from effective operators.

  This publication was done during the PhD of the author but is not discussed in this thesis.

- [5] **On-shell heavy particle effective theories**, Rafael Aoude, Kays Haddad and Andreas Helset.

  We introduce on-shell variables for Heavy Particle Effective Theories (HPETs) with the goal of extending Heavy Black Hole Effective Theory to higher spins and of facilitating its application to higher post-Minkowskian orders. These variables inherit the separation of spinless and spin-inclusive effects from the HPET fields, resulting in an explicit spin-multipole expansion of the three-point amplitude for any spin. By matching amplitudes expressed using the on-shell HPET variables to those derived from the one-particle effective action, we find that the spin-multipole expansion of a heavy spin-s particle corresponds exactly to the multipole expansion (up to order 2s) of a Kerr black hole, that is, without needing to take the infinite spin limit. Finally, we show that tree-level radiative processes with same-helicity bosons emitted from a heavy spin-s particle exhibit a spin-multipole universality.

  This publication was done during the PhD of the author but is not discussed in this thesis.

1 Introduction

The discovery of the Higgs boson in 2012 by the Large Hadron Collider (LHC) [6, 7] at CERN is the most important recent event in particle physics. It completes an epoch of experimental searches of the Standard Model (SM) particles as we know today. Before its discovery, perturbative unitarity in boson scattering was violated, more specifically, in the longitudinal components of the two gauge bosons, as shown in Fig. 1.1. As the energy of the process is taken to infinity, the amplitude is unbounded without the Higgs boson. An absence of a well behaved high-energy limit leads to unitarity violation. The Higgs model is the most economical solution that has an exact cancellation of this high-energy behaviour and where unitarity is preserved. The discovery completed the SM and gave the first evidence of the mechanism of electroweak symmetry breaking.

Figure 1.1: $W_L Z_L$ tree-level scattering without the Higgs boson. This amplitude in the high-energy limit grows as $\lim_{s\to\infty} i\mathcal{M}(W_L Z_L \to W_L Z_L) \to -t/v^2$, where v is the vacuum expectation value (vev) and $t = (p_1 - p_3)^2$.

However, after the discovery, the value of its mass was still unexplained. If one assumes that physics beyond Standard Model (BSM) lies at the ultraviolet (UV) scale Λ, quantum corrections would make the Higgs mass dependent on the UV. This unnatural dependence would require an undesired amount of fine-tuning to fix the mass as it is given by the LHC Higgs data. Many models were constructed to explain this hierarchy problem and explain a possible Higgs substructure, ranging from Composite Higgs models to extra-dimensions. Between them, one of the most promising was supersymmetry, that would explain the Higgs mass and also predict the appearance of a plethora of new particles, that would keep particle physicists busy for years. However, up to the current date, the only state seen at LHC was the Higgs boson.

We are nowadays in the Higgs and nothing else scenario[1], where the lack of striking new physics results at the LHC leads to the resurgence of model-independent parametrizations, shifting the attention towards the use of effective field theories. In this framework, we minimize the number of UV assumptions and parametrize the unknown systematically. In particular, we adopt the Standard Model as the baseline, with the insertion of higher-dimensional, non-renormalizable operators to parametrize the potential effects of new

[1]At the moment that this thesis is being written, the five sigma of flavour anomalies are still not confirmed.

physics too heavy to have been seen yet at the LHC. The goal of an "effective field theorist" is to not only to sharpen the tools required for physics predictions but also to look for distinct signals at LHC and other experiments.

Within the EFT framework for the SM, two effective theories can be used to parametrize new physics, where their difference lies on whether the standard model electroweak symmetry $\mathrm{SU(2)_L} \otimes \mathrm{U(1)_Y}$ is assumed or not. With this assumption, the Standard Model Effective Field Theory (SMEFT) is built systematically by enlarging the possible operators to higher mass dimensions. The main focus is on dimension-six operators that provide possible signals at the LHC. This effective theory comes with three elements: An expansion scale Λ, the effective operators, and their coefficients, called Wilson coefficients. The operators $\mathcal{O}_{\mathrm{IR}}$ parametrize the infrared effects while the Wilson coefficients c_{UV} entail the ultra-violet new physics effects. The goal is either to predict a LHC signal for a value of c_{UV} and Λ or to use the data to put bounds on these coefficients.

This thesis is divided in two parts, effective field theories and scattering amplitudes. In the first part, we search for clear signals at the LHC from EFT higher dimension operators in diboson production at the LHC. Moreover, we analyse the impact of experimental data at different scales, in particular, how flavour data compete with other sectors, such as Higgs and Electroweak data. In the second part, we look into the SMEFT scattering amplitudes from a different point of view. The usual approach to calculate these amplitudes is to derive them from Lagrangians and apply Feynman Rules. The new modern methods for scattering amplitudes provide a new machinery to calculate them more efficiently. These methods also shed light on new hidden structures and lead to incredible simplifications. They are based on on-shell recursion relations and spinor-helicity variables.

The search for signals at the LHC is a challenge within SMEFT due to the proliferation of possible operators contributing. Finding observables which are sensitive to few operators is crucial to have clean new physics signals. In the first result of this thesis, we study the diboson production $\bar{\psi}\psi \to VV$ at the LHC within SMEFT. This process is important to test the triple-gauge coupling (TGC) vertex, which probes the nature of the electroweak sector. Due to helicity selection rules, it is well known that there is no interference between the SM and the EFT amplitudes for this four-point amplitude. However, when the bosons decay, forming a six-point amplitude $\bar{\psi}\psi \to VV \to \bar{\psi}\psi\bar{\psi}\psi$, the interference is recovered. Considering this final state, it is possible to construct an asymmetry observable sensitive to only one CP conserving operator $\mathcal{O}_W = \epsilon^{IJK} W_\mu^{I\nu} W_\nu^{J\rho} W_\rho^{K\mu}$, which makes use of the azimuthal angles in the final state. We analyse the tails of the hadronic and semileptonic final state distributions using jet substructure techniques and put bounds on this single operator.

While new physics at the tails of the distributions probe the high-energy behaviour of the theory, precision experiments at low energy probe the infrared behaviour of the theory and can put competitive constraints on the same coefficients. In the second result of this

thesis, we look into flavour measurements and how they impact the SMEFT Wilson Coefficients. Low-energy measurements such as meson oscillations, $b \to s$ transitions, put strong constraints on any deviation of the SM flavour structure. Usually, in model building, these constrains are avoided by imposing flavour symmetries at the UV, for example, Minimal Flavour Violation (MFV) or a fully-symmetric flavour theory $U(3)^5$. After imposing these flavour symmetries one would expect to escape from flavour low-energy bounds. However, we will show that, after a one-loop matching, the flavour data can still have competitive constraints to Higgs and electroweak physics data.

In the second part of the thesis, we look into modern methods for scattering amplitudes. Mostly used for massless amplitudes, these methods are rooted in three pillars: spinor-helicity variables, recursion relations and generalized unitarity. The value of the first one is that these variables not only represent momenta but also the polarization vectors, being the fundamental building blocks for all the amplitude's kinematic. The second one allows the recursive construction of higher-point amplitudes from lower-point ones, while the third pillar enables efficient loop-order calculations. However, massive amplitudes were not fully explored until recently [8], where a covariant formalism for massive spinor-helicity variables was built.

Understanding the same physics from a different perspective always leads to new insights. For example, the null entries of the SMEFT anomalous dimension matrix were beautifully understood from on-shell unitarity cuts [9]. Therefore, is it important to understand the SMEFT from other points of view. In this work, we use these massive modern methods to understand this effective theory. In particular, we draw a map between the three-point amplitudes for SMEFT and the Lagrangian formalism. This is done in the broken phase of SMEFT, i.e. when the particles acquire masses. We find compact expression and study the construction of higher-multiplicity amplitudes, via recursion relations, from the three-points amplitudes.

This thesis has the following structure: In Chapter 2, we describe EFTs and its fundamental concepts, including the decoupling theorem, Renormalization Group Equations (RGE) and matching. These concepts are then applied in Chapter 3 for the SMEFT, where its construction is given. Once SMEFT is constructed with all its operators, we make use of this theory to look into the LHC signal for the diboson production, and we study the impact of low-energy measurements in the SMEFT Wilson Coefficients in Chapter 4 and 5. In the second part of the thesis, we explain the Modern Methods for Scattering Amplitudes in Chapter 6 and find the map of the amplitudes of SMEFT in Chapter 7. Finally, we conclude the thesis in Chapter 8.

2 Effective Field Theories

Describing phenomena in physics requires the use of appropriate tools. One does not need to understand the properties of the Higgs boson to use Newtonian Mechanics. These are problems with two different energy scales and each one requires its particular set of tools. The idea behind effective field theories is that phenomena can be studied without the knowledge of the full theory. As using Cartesian coordinates to describe a spherical problem or using Quantum Mechanics to study Classical Gravity, the use of the wrong variables for a problem just add extra complications [2]. Therefore, before tackling any problem, we need to identify the scale we are interested in, the correct variables (or degrees of freedom) to work with, and the symmetries of the problem.

Quantum Field Theory is the unification of Special Relativity and Quantum Mechanics, and the variables to use are the quantum fields. As Weinberg derived in his book [11], *"The Cluster decomposition principle together with Lorentz invariance thus makes it natural that the interaction density should be constructed out of annihilation and creation fields."* Although quantum fields are the particle physics degrees of freedom (d.o.f), all the three ingredients mentioned still need to be decided. Choosing the transfer momenta p small compared to the mass of a particle M, defines a separation of scale which is given by an expansion parameter $\delta = p/M$. Thus, choosing whether or not to include a term will depend on the power counting formula in this parameter. The relevant d.o.f. of the problem are chosen considering just a set of particles and choosing the correct representations of them under a symmetry group. The last ingredient is this chosen symmetries. For instance, at very low-energy one does not expect QCD to manifest explicitly since there are no free quarks and gluons but one should expect chiral symmetry for the mesons. All the allowed terms in the Lagrangian will be given by power counting and the symmetries. Based on these observations, two approaches are known:

- **Top-Down**: the full theory of the problem is known and one 'integrates out' the unneeded ultraviolet degrees of freedom in order to have a low-energy description. In this description, the Wilson Coefficients can be obtained from the full theory. Examples of Top-Down are Heavy Quark Effective Theory, Soft-Collinear Effective Theory and Weak Effective Theory.

- **Bottom-Up**: based on the low-energy symmetries, the relevant d.o.f are chosen to describe the problem, and the known theory is enlarged with higher-dimension operators that entail the deviations to the theory. These operators parametrize our ignorance of the full theory and the Wilson Coefficients are undetermined variables. SMEFT and Chiral Perturbation Theory are examples of a bottom-up approach.

[2] However, this is not completely true. It has been proved the advantages of using the on-shell unitarity methods techniques for classical gravity calculations. See [10] and the references therein.

One nice example of the machinery of EFT at work is the very famous case of Fermi theory, which describes the nuclear beta decay. Before the discovery of the W-boson, the interaction was described by a four-fermion operator, as an example of bottom-up construction. However, nowadays we know the particle content of the SM and that the Fermi interaction can be obtained from $\mathrm{SU(2)_L \times U(1)_Y}$ by 'integrating out' the electroweak gauge bosons, as an example of a top-down approach. Another bottom-up example is the Chiral Perturbation Theory (χPT), which is constructed based on the Chiral symmetry of QCD. The d.o.f are the low-energy mesons, which are the pseudo Goldstone bosons of the spontaneous symmetry breaking of the chiral symmetry $SU(3)_L \otimes SU(3)_R \to SU(3)_V$. In this case, the UV theory, QCD, is known but the non-perturbative regime makes it impractical to use it at low energies.

Several concepts of EFT are important for its success. In Fig. 2.1, we show pictorially how both approaches, *top-down* and *bottom-up* work and some important concepts behind them. Throughout this chapter, we will explain them and connect to the work of this thesis, in particular with the SMEFT.

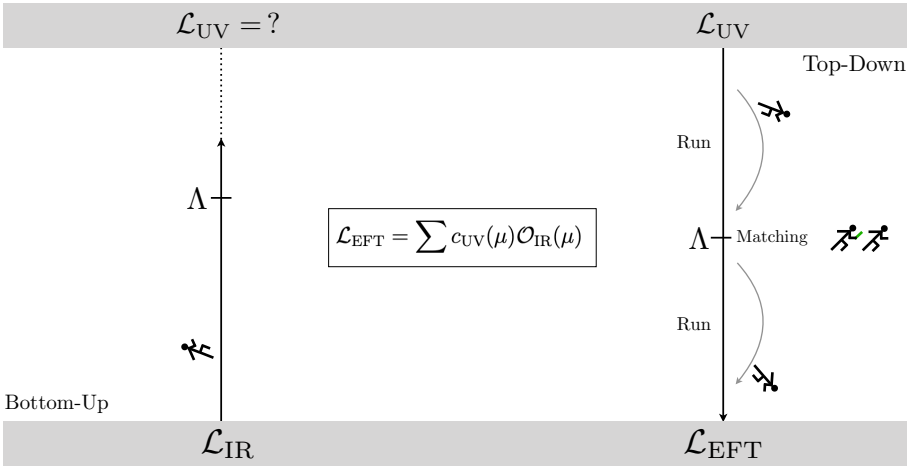

Figure 2.1: Important EFT concepts for the *bottom-up* and *top-down* approaches

Central to this picture, we have the separation of the ultraviolet and the infrared effects in the Lagrangian. As we will see, the coefficients c_{UV} are called Wilson Coefficients and entail the ultraviolet physics that was integrated out or is a unknown parameter to be measured, depending on top-down or bottom-up. The composite operators $\mathcal{O}_{\mathrm{IR}}$ describe the infrared physics. Both terms are subjected to renormalization and therefore are defined at a specific scale μ. The operators to include are determined by a power-counting formula, in terms of a small expansion parameter δ, also known as *power counting*

parameter [12]. Any computation is then done in a given expansion order n in δ and consequently, the error associated to this result comes at the next order, δ^{n+1}. These computations can be performed as precise as required but at higher orders the proliferation of complicated diagrams and additional operators can become troublesome.

For a long time, non-renormalizable theories were considered unable to make predictions, since they would require an infinite number of counterterms to cancel all the UV divergences. For example, an EFT has an infinite tower of higher-dimensional operators but we still have predictive power since if we want to calculate an observable with error $\mathrm{O}(\delta^{n+1})$, we need to add all the consistent diagrams and counterterms at order δ^n and therefore, theory is predictive at this given order. Many of the developments are rooted in the Wilsonian picture of the renormalization group equations [13].

Given the renormalization order-by-order, how to construct the low-energy description? On this, Weinberg formulated the so-called Folks' Theorem [14]:

> *"If one writes down the most general possible Lagrangian, including all terms consistent with assumed symmetry principles, and then calculates matrix elements with this Lagrangian to any given order of perturbation theory, the result will simply be the most general possible S-matrix consistent with perturbative unitarity, analyticity, cluster decomposition, and the assumed symmetry properties."*

This theorem gives us a recipe on how to built a consistent EFT. Thus, it is worthwhile to describe in detail each one of the S-matrix's properties.

- **Perturbative Unitarity**: Formally, the unitarity of the S-matrix implies that $S^\dagger S = \mathbb{1}$. In practice, the unitarity condition is approximate, in perturbative calculations and sizeable violations indicate the breakdown of the power expansion $\delta = p/\Lambda$. Thus, perturbative unitarity constrains the validity of the theory.

- **Analyticity**: The singularity structure of the amplitude is, at most, poles and branch cuts. Together with locality, the poles can only come from single-propagators, branch cuts and points where more than one propagator are simultaneously singular.

- **Cluster Decomposition**: The connected S-matrix does not have delta-function singularities.

Since any theory's S-matrix should obey these properties, they serve as one of the guidelines when constructing an EFT and connecting it to the UV. They are especially important in the context of on-shell EFTs later in Section 7.

The general EFT Lagrangian $\mathcal{L} = \sum c_{\mathrm{IR}}\, \mathcal{O}_{\mathrm{UV}}$ has Wilson coefficients which in the bottom-up approach have to be fixed by data before giving any predictions. In the top-down, one can simply obtain the EFT coupling constants from it by matching it to the UV theory. This is a crucial step for making predictions with an EFT. It is tempting to ask

at this point: *If the UV theory is known, why not use it?* Effective theories pick out the right degrees of freedom and make the calculation way simpler; therefore, in some cases, is more convenient to use it. Furthermore, it performs the resummation of large-logs arising due to infrared effects using the same RGE technology familiar for the UV divergences. These are advantages in a top-down approach; in a bottom-up case, in which the UV is not known, the EFT parametrizes our ignorance and is obligatory. All these advantages will be discussed throughout this chapter.

2.1 Matching

The Wilsonian ideas are a very successful way to understand the importance of each type of operators — irrelevant, marginal and relevant — but the common practice to go from a full theory to its infrared effective description is given by the **matching** procedure (🏃🏃). To this end, one calculates the matrix elements in the full and effective theories and equates both at the matching scale. This equality gives the Wilson coefficients as a function of the UV theory parameters. For instance,

$$\langle p_1 ... p_a | \mathcal{O}^{\rm UV}(p^2) | k_1 ... k_b \rangle_{p^2 \ll \Lambda^2} \equiv \langle p_1 ... p_a | \mathcal{O}^{\rm EFT}(p^2) | k_1 ... k_b \rangle \tag{2.1}$$

To illustrate this procedure we give two examples of such **matching**. The first one is the textbook tree-level matching of the muon-decay, and the second one is a one-loop matching relevant to one of the papers [3] this thesis is based on.

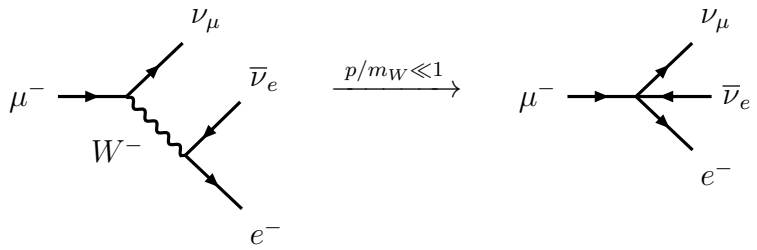

Figure 2.2: Integrating out the W boson in a muon decay

In the process $\mu \to e\,\bar{\nu}_e\,\bar{\nu}_\mu$, the muon decays via a intermediate gauge W boson (See Fig. 2.2), in the full theory, and has a momentum transfer below the mass of the W, i.e. $p^2 \ll m_W^2$. Thus, the EFT power counting parameter is $\delta = p/m_W$ and the process is described by the following four-fermion interaction [15]:

$$\mathcal{L}_{\rm EFT} \supset -\frac{4G_F}{\sqrt{2}} \left(\bar{\nu}_\mu \gamma^\alpha P_L \mu\right) \left(\bar{e} \gamma_\alpha P_L \nu_e\right), \tag{2.2}$$

where $P_L = (1-\gamma_5)/2$ and G_F is the Fermi's constant. In the full theory, this four-point amplitude is given by

$$\begin{aligned} i\mathcal{A}_4^{\rm UV} &= \bar{u}(p_\nu)\left(\frac{ig}{\sqrt{2}}\gamma^\alpha P_L\right)u(p_\mu)\cdot i\frac{g_{\alpha\beta}}{q^2-m_W^2}\cdot\bar{u}(k_e)\left(\frac{ig}{\sqrt{2}}\gamma^\beta P_L\right)v(k_\nu) \\ &= \frac{ig^2}{2(q^2-m_W^2)}[\bar{u}(p_\nu)\gamma^\alpha P_L u(p_\mu)][\bar{u}(k_e)\gamma_\alpha P_L v(k_\nu)] \\ &= -\frac{ig^2}{2m_W^2}[\bar{u}(p_\nu)\gamma^\alpha P_L u(p_\mu)][\bar{u}(k_e)\gamma_\alpha P_L v(k_\nu)] + \mathcal{O}(q^2/m_W^2) \end{aligned} \tag{2.3}$$

where in the last line, we have expanded the momentum around $q \ll m_W^2$. The same process, in the EFT is given by the following

$$i\mathcal{A}_4^{\rm EFT} = -\frac{4iG_F}{\sqrt{2}}[\bar{u}(p_\nu)\gamma^\alpha P_L u(p_\mu)][\bar{u}(k_e)\gamma_\alpha P_L v(k_\nu)] \tag{2.4}$$

Equating both terms, we have:

$$i\mathcal{A}_4^{\rm UV} = i\mathcal{A}_4^{\rm EFT} \qquad \rightarrow \qquad G_F = \frac{g^2}{4\sqrt{2}m_W^2} \tag{2.5}$$

which gives the Fermi constant (an example of a Wilson coefficient in the general case) in terms of the UV parameters. This matching was done at tree level since no loops were involved. The m_W-dependence of the result should be expected by power counting because a four-point amplitude has zero mass-dimension and each Dirac spinor has mass dimension $+1/2$, therefore $[G_F] = -2$.

Figure 2.3: Penguin and Box diagrams contributing to the $b \to s$ transitions. In the penguin diagram, the photon could also couple the a lepton in the final state.

We give now a one-loop matching example, where the structure naturally gets more difficult but also more interesting [16]. Consider the $b \to s$ transition, where we have a photon or a lepton pair in the final state. In the SM, this process is generated only at one-loop by the penguin and box diagrams, illustrated in Fig. 2.3, generating several kinematical structures. In the EFT, we can write down the higher-dimensional operators contributing to it

$$\mathcal{L}_{b\to s}^{\rm EFT} \supset 4\frac{G_F}{\sqrt{2}}\lambda_t^s\left(C_7Q_7 + C_8Q_8 + C_9Q_9 + C_{10}Q_{10}\right) \tag{2.6}$$

where

$$Q_7 = \frac{e\, m_b}{16\pi^2}(\bar{b}_R \sigma^{\mu\nu} s_L) F_{\mu\nu} \qquad Q_8 = \frac{g_s m_b}{16\pi^2}(\bar{b}_R \sigma^{\mu\nu} T^A s_L) G^A_{\mu\nu}$$
$$Q_9 = \frac{1}{2}(\bar{b}_L \gamma^\mu s_L)(\bar{\ell}\gamma_\mu \ell) \qquad Q_{10} = \frac{1}{2}(\bar{b}_L \gamma^\mu s_L)(\bar{\ell}\gamma_\mu \gamma_5 \ell) \tag{2.7}$$

Performing the one-loop matching requires equating the matrix element of $b \to s\gamma$ and $b \to s\ell\ell$ processes in both UV and the effective theory. From the matching onto all low energy operators, we can pick out the theoretically clean matching to C_{10A}, which gives at the scale m_W

$$C_{10}(m_W) = \frac{g^2}{8\pi^2}\frac{x_t}{8}\left[\frac{4 - x_t}{1 - x_t} + \frac{3\, x_t}{(1 - x_t)^2}\ln x_t\right], \quad x_t = \frac{m_t^2}{m_W^2} \tag{2.8}$$

Note that in this matching, we have a non-decoupling effect of the top mass. One would naively expect that, once the particle is integrated out, the IR description is insensitive to its effects when the same mass is taken to infinity. However, in $C_{10A}(m_W)$ if one takes $m_t \to \infty$ the Wilson coefficient blows up. The origin of the non-decoupling effect is the Glashow, Iliopoulos, and Maiani (GIM) mechanism [17]. The one-loop penguin diagrams contributing to the $b \to s\gamma$ process have a sum over the internal quarks, with a CKM and mass dependence $\mathcal{M} = \sum_i V_{ib}^* V_{is} f(m_i)$, where $f(m_i)$ are the Inami-Lim [18] functions which have the property that for small $x_i\, m_i/m_W$, the function is proportional to x_i but is constant whenever $x_i > 1$. The GIM mechanism says that the one loop amplitudes carry the x_i factors, where i is summed, and therefore for m_t this contribution does not decouple. We can also understand the non-decoupling to be due to $\mathrm{SU(2)_L}$ violation involved in integrating out only part of the multiplet.

2.2 The decoupling theorem

The IR-description behaviour whenever Λ is taken to infinity divides the effective landscape in two categories. The non-decoupling EFT contains UV effects of Λ, while the decoupling, as expected, decouples. This concept can be summarized by the decoupling theorem [19, 20]

> *For any one-particle-irreducible Feynman graph with external vector mesons only but containing internal fermions, when all external momenta are small relative to Λ^2, then apart from the coupling constant and field strength renormalization the graph will be suppressed by some power of m relative to a graph with the same number of external vector mesons but no internal fermions.*

While the statement is given in terms of a specific theory, was later proved the generalization for arbitrary field theories in terms of all n-point Green's function as [20]

$$\prod_i^N Z_i G^n_{\rm UV}(1,2,...,n;\mu) = \prod_j^M Z_j G^n_{\rm EFT}(1,2,...,n;\mu) + \frac{1}{\Lambda^2}\prod_i^k Z_i G'^n_{\rm EFT}(1,2,...,n;\mu) \quad (2.9)$$

where Z_i are wave function renormalization of the fields in each Green function. The ones on the left correspond to the full theory renormalization and the ones on the right side, from the EFT. The immediate consequence of the decoupling theorem is one of the guidelines of effective theories: one does not need to know the UV to calculate EFT amplitudes. In other words, the IR description of the full theory is the same as the effective theory, where the UV information is encoded in the Wilson Coefficients. Thus, we can write down the effective Lagrangian in the following way:

$$\mathcal{L}_{\rm EFT} = \sum_i c_{\rm UV}(\mu)\mathcal{O}_{\rm IR}(\mu) \quad (2.10)$$

where the Wilson Coefficients vanish whenever $\Lambda \to \infty$. The difference between the UV of the full theory and the effective theory is fixed by the matching procedure, where the $c_{\rm UV}(\mu)$ will absorb the UV dependence. In this thesis we will use the decoupling theorem for SMEFT, which considers that the possible UV completion of the SM decouples at low-energy.

However, as we have seen previously, this theorem has important exceptions where traces of the UV are still present in the IR. For example, when a heavy state, which is in the same representation as the light state, is integrated out from the theory. This was exactly the $b \to s\gamma$ transition, where the the top-quark is integrated out. This non-decoupling will be extremely relevant for our phenomenological analysis of the one-loop matching between SMEFT and the Weak Effective Theory(WET), where the gauge bosons $W^{\pm}/Z$ and the top quark are integrated out, in Section 5. In this case, the limit of the WET Wilson coefficients do not vanish, $\lim_{m_W\to\infty} c_{IR} \neq 0$.

In this thesis we are going to focus mostly on the SMEFT, where EFT techniques will provide us a systematic way to parametrize new physics. One of the ingredients to construct an EFT is the number of terms we need to use at a particular accuracy order δ^n. The answer to that comes with the aid of power counting.

2.3 Power Counting

An efficient way to organize the perturbative orders of an EFT is with power counting formulas. In particular, we want to count the mass dimensions of each term in the Lagrangian. In natural units, any action is dimensionless[3] and can be written as the

[3]In non-natural units, the action has units of angular momentum [$\hbar$].

integral of the Lagrangian density

$$S = \int d^{\mathsf{d}}x\, \mathcal{L}(x) \quad \rightarrow \quad [\mathcal{L}(x)] = \mathsf{d} \tag{2.11}$$

Writing down all the possible operators in a Lagrangian as a sum

$$\mathcal{L}(x) = \sum_i c_i\, \mathcal{O}_i(x) \tag{2.12}$$

and labelling the dimension of each operator with mass dimension D, the coefficient with these operators will have mass dimension $\mathsf{d} - D$. The fields in QFT have mass dimension given by their kinetic term. For instance, the scalar field obeys the Klein-Gordon Lagrangian, which contains two derivatives while the fermionic field respects the Dirac Lagrangian with one derivative, with $[\partial] = 1$. For a gauge field, the kinetic term comes from two field strengths contracted and each one contains one derivate. Another observation is that the covariant derivative $D_\mu = \partial_\mu + igA_\mu$ has mass dimension one, giving us the coupling mass dimension $[g]$. Thus,

$$\begin{aligned} [\psi] &= \frac{1}{2}(\mathsf{d}-1), \qquad [\phi] = \frac{1}{2}(\mathsf{d}-2), \qquad [A_\mu] = \frac{1}{2}(\mathsf{d}-2), \\ [g] &= \frac{1}{2}(4-\mathsf{d}), \qquad [y] = \frac{1}{2}(4-\mathsf{d}), \qquad [\lambda] = (4-\mathsf{d}) \end{aligned} \tag{2.13}$$

The last two terms are the couplings from a Yukawa interaction, $y\,\phi(\bar{\psi}\psi)$, and a $\lambda\phi^4$ term. Important building blocks for the construction of SMEFT are bispinors and field strengths $X^{\mu\nu} = (\partial^\mu A^\nu - \partial^\nu A^\mu)$, that in $\mathsf{d} = 4$ have the following dimensionality

$$[\bar{\psi}\psi] = 3, \qquad [X] = 2, \qquad [D_\mu] = 1, \qquad [\phi] = 1 \tag{2.14}$$

In section 3, the construction of the Standard Model Effective Field Theory will be given in more details. For the moment, consider the dimension-six Lagrangian

$$\mathcal{L}_6 = \sum_i \frac{c_i}{\Lambda^2}\mathcal{O}_i, \qquad [c_i] = 0, \quad [\Lambda] = 1 \quad \text{and} \quad [\mathcal{O}_i] = 6 \tag{2.15}$$

Each operator is given as a product of the building blocks

$$\mathcal{O}_i \sim (\bar{\psi}\psi)^{N_F}(X)^{N_X}(D)^{N_D}(\phi)^{N_\phi} \rightarrow [\mathcal{O}_i] = 3N_F + 2N_X + N_D + N_H = 6. \tag{2.16}$$

With this counting of fields contribution, all operators for a dimension-six Lagrangian can be found. However, they are not independent since some of them can be connected through Equations of Motion (EOM) and/or Integration-by-parts (IBP). Finding the minimal set of operators that form a basis is essential to describe the amplitudes. In SMEFT, the most used basis is the Warsaw basis, in which the number of derivatives is minimized.

The reason for that is that a low-derivative basis makes loop-calculations easier but also stems from unitarity. Given a simple scalar theory with higher derivative operators [21]

$$\mathcal{L} = -\frac{1}{2}\phi\left(\Box + c\frac{\Box^2}{\Lambda^2} + m^2\right)\phi + \mathcal{L}_{\text{int}}(\phi) \tag{2.17}$$

the effective operator would lead to the Källen-Lehmann representation of the two-point function to converge faster than without the dimension-six term, *i.e* $\lim_{p^2\to\infty}\Pi(p^2) = -\frac{1}{c}\frac{\Lambda^2}{p^4}$. Such behaviour would violate the bound given by **positivity** of the spectral density function, which is a consequence of S-matrix unitarity. Therefore, in order to construct a basis for the dimension-six SMEFT operators, one should avoid bilinear higher derivatives terms. However, given that we naïvely have these higher derivatives terms, a way to remove it is to use EOM or, more generally, field redefinitions.

2.4 Equations of Motion

In QFT, we normally compute the correlation functions from the Lagrangians and use the Lehmann-Symanzik-Zimmermann (LSZ) reduction formula in order to obtain the S-matrix elements. They are then squared to obtain the cross-section, which is the real observables in a scattering experiment. The S-matrix elements are obtained by picking out the external particle poles from the Greens' function. This formula depends solely on the fact that the external particle described by the field $\phi(x)$ produces a single state $|p\rangle$ out of the vacuum, i.e. $\langle p|\phi(x)|0\rangle \neq 0$.

The insensitivity to the interpolating field of the LSZ formula can be understood as change of integration variable in the path-integral formalism. For a scalar theory, we have the path-integral for ϕ, which under the change of the integration variable $\phi(x) = F[\phi'(x)]$ becomes [22]

$$Z[J] = \int [D\phi]\, e^{i\int_x \mathcal{L}[\phi]+J\phi} \to Z[J] = \int [D\phi']\left|\frac{\delta F}{\delta\phi'}\right| e^{i\int_x \mathcal{L}'[F[\phi']]+JF[\phi']} \tag{2.18}$$

The Jacobian of this transformation is unity in dimensional regularization[4], and dropping the primes labels on the variables we have

$$Z[J] = \int [D\phi]\, e^{i\int_x \mathcal{L}'[F[\phi]]+JF[\phi]} \tag{2.19}$$

This calculation tells us that the same generating function $Z[J]$, which gives the Green's function calculated with ϕ and the Lagrangian $\mathcal{L}[\phi]$, will also provide another Green function, but this time by using the interpolating field $F[\phi]$ and a new Lagrangian $\mathcal{L}'[F[\phi]]$.

[4]We are doing for scalar theory here but a generalization is possible. In the fermionic case, we can have chiral anomalies.

Upon a local field redefinition, $\phi(x) = F[\phi'(x)]$ the S-matrix does not change as long as the new interpolating field produces the same single state, i.e. $\langle p|F[\phi(x)]|0\rangle \neq 0$. These field redefinitions are familiar to us in the context of renormalizable theories whenever we perform a linear transformation $\phi'_j = C_{ij}\phi_i$ to put the kinetic term in the canonical form. With the incorporation of higher dimension operators in the theory, we have more freedom in the field redefinitions as long as it respects power counting [22].

The EOM plays a crucial role in the quest for the minimal basis. Whenever defining a basis of higher dimension operators, one needs to find the minimal set of independent operators. To find them, a usual approach is to use EOM to relate different operators. To illustrate the procedure, we consider the following simple Lagrangian [22]

$$\mathcal{L} = \frac{1}{2}\partial_\mu\phi\partial^\mu\phi - \frac{1}{2}m^2\phi^2 - \frac{1}{4!}\lambda\phi^4 + \frac{c_1}{\Lambda^2}\phi^3\partial^2\phi + \frac{c_6}{\Lambda^2}\phi^6 + ... \tag{2.20}$$

which has the following equation of motion

$$E[\phi] = -\partial^2\phi - m^2\phi - \frac{1}{3!}\lambda\phi^3 + .. \tag{2.21}$$

where the higher dimension operators will contribute to a higher order and do not need to be considered. Using the field redefinition $\phi \to \phi + \frac{c_1}{\Lambda^2}\phi^3$, we can rewrite the Lagrangian as

$$\mathcal{L} \to \mathcal{L}' = \mathcal{L} + \frac{c_1}{\Lambda^2}\phi^3\left[-\partial^2\phi - m^2\phi - \frac{1}{3!}\lambda\phi^3 + ...\right] \tag{2.22}$$

$$= \frac{1}{2}\partial_\mu\phi\,\partial^\mu\phi - \frac{1}{2}m^2\phi^2 - \frac{1}{4!}\tilde{\lambda}\phi^4 + \frac{\tilde{c}_6}{\Lambda^2}\phi^6 + ... \tag{2.23}$$

where

$$\frac{1}{4!}\tilde{\lambda} = \frac{1}{4!}\lambda + \frac{c_1}{\Lambda^2}m^2 \quad \text{and} \quad \frac{\tilde{c}_6}{\Lambda^2} = \frac{c_6}{\Lambda^2} - \frac{c_1}{\Lambda^2}\frac{\lambda}{3!} \tag{2.24}$$

Both Lagrangians give the same S-matrix, as physics should be basis-independent. In the former, the propagators are modified and new poles appear in the calculations, while in the low derivative basis, the poles are only due to the particles' masses. At tree-level, the addition of a new pole might not seem harmful, but at loop-level, this could become cumbersome. Thus, removing the higher-derivative operators which change the two-point function makes the EFT computations easier.

2.5 Running of Composite operators

The tree level picture of the muon decay where the W boson is integrated out, leaving a four-fermion interaction is very simple and intuitive. However, we could only use the

four-fermion interaction near the matching scale, where large-logs are not relevant. In practice, we would like to provide predictions at lower physical scales, for instance, at the B meson mass scale. In order to do so, we need to consider the running (🏃) of the Wilson coefficients when we change the scales. One of the real advantages of using EFT comes from resumming these loop corrections.

Loop integrals need to have their divergences regulated and removed and, therefore, always come with a renormalization scheme. The common practice in EFT calculations is to use the $\overline{\text{MS}}$ renormalization scheme and dimensional regularization (dim-reg) [20]. In this scheme, the dimension of the problem d is arbitrary, allowing one to evaluate the integrals without facing the infinities. Later, one specifies the d to be a fractal dimension $d = 4 - 2\epsilon$ and finally, takes the small ϵ-limit.

In the one-loop matching, logarithms of the form $\left(\frac{g^2}{4\pi}\ln\frac{\mu^2}{m_W^2}\right)$ appear in both theories. Choosing the appropriate physical scale μ can lead to big contributions in the next orders, given by large-logs. EFTs show their real power when come to the task of resumming the logarithms, which is done by means of renormalization group equations (RGEs). For instance, if one operator satisfies the one-loop RGE [22]

$$\mu\frac{d}{d\mu}c(\mu) = \gamma_0\frac{g^2(\mu)}{16\pi^2}c(\mu), \quad \text{where} \quad \mu\frac{dg(\mu)}{d\mu} = -b_0\frac{g^3(\mu)}{16\pi^2} \tag{2.25}$$

we can integrate it to get

$$\frac{c(\mu_1)}{c(\mu_2)} = \left[\frac{\alpha_s(\mu_1)}{\alpha_s(\mu_2)}\right]^{-\gamma_0/(2b_0)} \approx 1 + \gamma_0\frac{\alpha_s}{4\pi}\log\frac{\mu_1}{\mu_2} - \frac{1}{2}\gamma_0(2b_0-\gamma_0)\left[\gamma_0\frac{\alpha_s}{4\pi}\log\frac{\mu_1}{\mu_2}\right]^2 + ... \tag{2.26}$$

where $\alpha_s(\mu) = g^2(\mu)/4\pi$. From this equation it is clear that the RGE resum all the leading log (LL) series of $\alpha_s^n\log^n$. The next terms to this series would come at two-loops, where the next-to-leading-log (NLL) series of $\alpha_s^n\log^{n-1}$ appears.

For more than one operator, there is a mixing between the operators and one has to deal with an anomalous-dimension matrix. The effective Lagrangian when the running is accounted can be written as [22]

$$\mathcal{L}_{\text{EFT}} = \sum_{n=0}^{\infty}\sum_i \frac{C_i^{(n)}(\mu)}{M^n}\mathcal{O}_i^{(n)}(\mu) \tag{2.27}$$

The set of composite operators can be renormalized as

$$\mathcal{O}_{i,0}^{(n)} = \sum_j Z_{ij}^{(n)}\mathcal{O}_j^{(n)}(\mu) \tag{2.28}$$

where in the left-hand side we have the bare composite operators. Acting with a derivative $d/d\ln\mu$ in this equation leads to the running of the operators

$$\frac{d\mathcal{O}_i(\mu)}{d\ln\mu} \equiv -\gamma_{ij}(\mu)\mathcal{O}_j(\mu), \quad \text{where} \quad \gamma_{ij} = (Z^{-1})_{ik}(\mu)\frac{dZ_{kj}}{d\ln\mu} \tag{2.29}$$

Therefore, expanding γ_{ij} in powers of the coefficients, integrating the RGE equation gives operator dependence at different energy scales, again resumming the large-logs.

Effective Field Theories are quantum field theories with a regularization and renormalization scheme like any other QFT and are predictive order-by-order in δ. Besides being a theory in its own, they provide a toolbox to efficiently calculate matrix elements and observables which are either impossible or extremely complicated in the full theory. Moreover, they can be used as an efficient way to parametrize new physics, and provide a well-defined cross-talk with experimental data. In the following chapters, we are going to apply the concepts illustrated here to the Standard Model Effective Field Theory.

3 Standard Model Effective Field Theory

3.1 Standard Model

The Standard Model [23–25] of particle physics describes the strong and electroweak interactions. It is build upon gauge symmetries respected by matter and gauge fields. The massive particles acquired their masses through a spontaneous symmetry breaking mechanism. The SM group is broken by vacuum expectation value (vev) of the Higgs doublet.

$$\mathrm{G_{SM}} = \mathrm{SU(3)_c} \times \mathrm{SU(2)_L} \times \mathrm{U(1)_Y} \to \mathrm{SU(3)_c} \times \mathrm{U(1)_{EM}} \tag{3.1}$$

where the $\mathrm{SU(2)_L} \times \mathrm{U(1)_Y}$ symmetry is broken down to electromagnetism at the electroweak scale. The SM is constructed using the action principle and formulated with the Lagrangian formalism, where the system's dynamics are determined by the principle of least action and the symmetries by Noether's currents.[5]

Quantum field theory unifies quantum mechanics and special relativity. As a consequence, particles are *irreducible representations* of the Lorentz group in the Hilbert space and single-particle states are created by the interpolating fields, which are the solutions of the cluster decomposition principle requirement. The SM matter content has the following representations under the $\mathrm{G_{SM}}$ and the Lorentz group.[6]

Field	$\mathrm{SU(3)_c}$	$\mathrm{SU(2)_L}$	$\mathrm{U(1)_Y}$	$\mathrm{SO^+(3,1)}$
$q_i = (u_L^i, d_L^i)^T$	**3**	**2**	1/6	(1/2,0)
$u_i = \{u_R, c_R, t_R\}$	**3**	**1**	2/3	(0,1/2)
$d_i = \{d_R, s_R, b_R\}$	**3**	**1**	-1/3	(0,1/2)
$\ell_i = (\nu_L^i, e_L^i)^T$	**1**	**2**	-1/2	(1/2,0)
$e_i = \{e_R, \mu_R, \tau_R\}$	**1**	**1**	-1	(0,1/2)
H	**1**	**2**	1/2	(0,0)

In the Table, we have our fermion fields ($'qud\ell e'$), where i runs over the three different flavours, and the Higgs H, which is a $\mathrm{SU(2)_L}$ scalar doublet. The SM Lagrangian can be

[5] Alternative constructions of the Standard Model, where the concept of Lagrangians are bypassed, have being recently explored via on-shell formalism and will be discussed in more details in Section 7.

[6] The $\mathrm{SO^+(3,1)}$ is the proper-orthocronus subgroup of the Lorentz Group. The (a, b) labels the Weyl 2 components spinors of the group $SU(2) \otimes SU(2)$, which is locally isomorphic to $\mathrm{SO^+(3,1)}$ [20].

written in a very compact form, where the conventions of [20] are used

$$\mathcal{L}_{\rm SM} = -\frac{1}{4}G^A_{\mu\nu}G^{A\mu\nu} - -\frac{1}{4}W^I_{\mu\nu}W^{I\mu\nu} - \frac{1}{4}B_{\mu\nu}B^{\mu\nu} + \sum_{\psi=q,u,d,\ell,e}\bar{\psi}i\not{D}\psi$$
$$+ (D_\mu H)^\dagger(D^\mu H) - \lambda(H^\dagger H - \frac{1}{2}v^2)^2 - [H^{\dagger j}\bar{d}Y_d q_j + \tilde{H}^{\dagger j}\bar{u}Y_u q_j + H^{\dagger j}\bar{e}Y_e\ell_j + \text{h.c.}].$$

In the first line, the first three terms are kinetic terms of the gauge fields of each simple subgroup of $\rm G_{SM}$[7]. Since the two first symmetries are non-abelian, these terms also contain three- and four-point interactions.[8] The next two derivatives terms are the kinetic and the gauge interactions for the fermion and the Higgs fields. The gauge covariant derivative is given by

$$D_\mu = \partial_\mu + ig_3T^AG^A_\mu + ig_2t^IW^I_\mu + ig_1y_iB_\mu, \tag{3.2}$$

where the last three terms give the gauge-matter interactions for each symmetry. In this notation is implicit that the connection of the covariant derivative does not act on singlets under that symmetry. The quark and lepton fields are written in the weak eigenbasis

$$q_1 = \begin{bmatrix}u_L\\ d'_L\end{bmatrix}, \quad q_2 = \begin{bmatrix}c_L\\ s'_L\end{bmatrix}, \quad q_3 = \begin{bmatrix}t_L\\ b'_L\end{bmatrix}, \quad \ell_1 = \begin{bmatrix}\nu^{e'}_L\\ e_L\end{bmatrix}, \quad \ell_2 = \begin{bmatrix}\nu^{\mu'}_L\\ \mu_L\end{bmatrix}, \quad \ell_3 = \begin{bmatrix}\nu^{\tau'}_L\\ \tau_L\end{bmatrix}. \tag{3.3}$$

The matrix which relates the mass basis with the weak basis $(d'_L, s'_L, b'_L)^{\rm T} = V_{\rm CKM}\,(d_L, s_L, b_L)^{\rm T}$ is the Cabibbo-Kobayashi-Maskawa matrix [30, 31]. Last but not least, there is the the Higgs potential and the Yukawa interactions. The Higgs field H can be written as

$$H = \begin{bmatrix}\phi^+\\ \phi^0\end{bmatrix} = \frac{1}{\sqrt{2}}\begin{bmatrix}i\phi_1 + \phi_2\\ \phi_4 - i\phi_3\end{bmatrix} \to \begin{bmatrix}i\phi_1 + \phi_2\\ v + h - i\phi_3\end{bmatrix} \tag{3.4}$$

where in the last step, we expanded it around the minimum of its potential. The $\phi_{1,2,3}$ are 'eaten' Goldstone bosons, providing masses to the $W^\pm$ and Z.

The SM successfully describes the experimental data probed by LHC up to $\sqrt{s} \leq 3\,\text{TeV}$ [9], failing to explain:

- **Neutrino masses**: Oscillations of neutrinos were first observed in solar neutrinos [33–36] and later on in atmospheric [37]. The oscillations are not compatible with massless neutrinos and are explained by a small mass where the flavour and the mass eigenstates are not the same. In the SM, neutrinos are massless.

[7] We omit the presence of interaction between the field strength and its dual $\text{Tr}[X_{\mu\nu}\tilde{X}^{\mu\nu}]$ terms. The term for EW can be neglect due to the accidental B+L symmetry in the SM while for QCD is strongly constrained from the neutron electric dipole moment measurements [26–29].

[8] In Sec 6, we will see that the four-point is only required to satisfy gauge symmetry for off-shell particles. In on-shell formalism, the massless three-point vertices contain all the required information to constructed higher-point amplitudes.

[9] Flavour anomalies [32] are unexplained by the SM. However, the experiment still has not found the five sigma to claim a discovery.

- **Dark matter**: Rotation curves of galaxies [38, 39], CMB power spectrum [40] and the Bullet cluster offer strong evidences that the amount of matter in the Standard Model is not enough to explain the Universe, requiring a component of Dark Matter.

- **Baryogenesis**: One of the Sakharov conditions for a matter-antimatter asymmetry in the Universe is the presence of C and CP violation. In the SM, the latter comes from the quark sector and it is well known that the SM CP violation is not enough to meet the observed matter-antimatter asymmetry [41, 42].

- **Lepton CP violation**: T2K experiment [43] observed CP violation $\delta_{\rm CP}$ in the Leptonic sector. Differently form the quark sector, the flavour and mass eigenstates are the same in the SM. From neutrinos masses, we know that this is not true and, in reality, the flavours are mixtures of the mass states given by the Pontecorvo-Maki-Nakagawa-Sakata (PMNS) matrix [44, 45].

- **Strong CP problem**: Neutron EDM [26–29] poses a constraint on the strong CP phase, $\bar{\theta}$. The smallness of the $\bar{\theta}$ compared to the large value of CP violation in the weak sector is known as the strong CP problem.

- **Unification with gravity**: Gravitational effects are not accounted for in the SM. Gravity can be treated as an EFT derived from the Einstein-Hilbert Lagrangian, which is a non-renormalizable theory, where the relevant scale is $M_{\rm Plank} \sim 10^{19}$ GeV. In this scale, quantum corrections and all the terms in the EFT Lagrangian are expected to be important, and prediction at higher energies are not possible using this theory.

On top of that, theoretical arguments provide more hints that the SM Higgs mechanism is an effective description at low energies. The idea of the Higgs mechanism, as we know, is similar to description of Cooper pairs, which at low energies are described by the Landau-Ginzburg theory [20]. As the latter is not a fundamental theory, there is an expectation that the Higgs mechanism could also be an effective description of a more fundamental theory. Furthermore, quantum arguments pose more questions on the Higgs boson substructure. Since the Higgs mass operator $(H^\dagger H)$ has mass dimension two, it is a *relevant* operator and therefore receives contributions from possible heavy states. For instance, assuming the existence of a beyond standard model scenario that couples to the Higgs, loop corrections to its mass come in the form of

$$\bar{m}_h^2 = m_h^2 + \delta m_h^2, \qquad \delta m_h^2 \sim \pm \frac{1}{16\pi^2} |g_{\rm UV}|^2 m_{\rm UV}^2 \tag{3.5}$$

where $\pm$ depends on the new physics particle to be a fermion or a boson. We see that the IR physics of our problem, $\bar{m}_h^2$, is sensitive to the UV physics $m_{\rm UV}^2$. One of the relevant scales in the UV is the Plank Mass, $\Lambda \sim M_{\rm Pl} \sim 10^{19}$GeV, which this scale one would

need the bare mass of the Lagrangian to be $m_h^2 = (1 + 10^{-34})\Lambda^2$, since the Higgs pole mass is $\bar{m}_h^2 \approx 125$ GeV [21]. This sensitivity is called fine-tuning and the fact that these two scales are widely separated but the IR is sensitive to the UV goes by the name of the gauge hierarchy problem. This problem is related with the concept of naturalness, which requires all the fundamental parameters of a Lagrangian to be order one. Another view on the naturalness problems is called technical naturalness [46], which state that a parameter in the theory is allowed to be small if an enhanced symmetry appears when the parameter is taken to zero. In the case of the Higgs boson, no such enhanced symmetry exits and, therefore, its mass would not be technical natural. However, the statements on the fine-tuning is given for the bare mass of the Lagrangian, which is not an observable itself and one could argue that this is not a problem since we do not have access to such parameter [22].

These theoretical hints together with the experimental evidence that the SM is incomplete supplicate for an extension.[10] During the past decades, numerous models were built upon the assumption of a *naturalness problem* and the fine-tuning for the Higgs mass. The series of LHC null results for these theories and the discovery of no new particles has pushed forward a model independent way to look at high-energy particle physics. Trying to minimize the model assumptions when reporting bounds has become a common and essential practice for LHC data analysis. EFTs not only provide a framework with the minimal set of assumptions but also a systematic way to report bounds from data.

However, even describing the low energy limit of physics beyond the SM requires its own assumptions. The more crucial one is regarding the presence of the SM Higgs doublet. When this doublet is present, the effective description is called Standard Model Effective Field Theory and is the theory assumed in this thesis. In the absence of this doublet, we have the Higgs Effective Field Theory (HEFT). At the present time, there are no striking experimental evidence towards any of these possibilities. Thus, it is important to set clear the assumptions there are made when comparing theoretical predictions with data.

3.2 Enlarging the Standard Model

Convinced that an effective extension of the SM is needed, we still need to choose between SMEFT and HEFT. In the SM, we require the existence of [20]

- (a) Three goldstone bosons, eaten by the EW gauge bosons,
- (b) A scalar particle that ensures unitarity in the longitudinal scattering of these EW bosons.

However, the latter condition can be relaxed since unitarity only needs to be true within the validity of the EFT, i.e. only at order $O(1/\Lambda^0)$ the longitudinal scattering is broken

[10] Furthermore, the SM is not well-defined for all energies due to presence of a Laundau pole. However, this pole occurs way further than the Planck Scale.

by the higher dimensional operators. Assuming or not (b) tells HEFT/SMEFT apart. The latter requires both assumptions and the Higgs field H is part of the $\mathrm{SU(2)_L}$ doublet together with the three goldstone bosons.

The construction without the second assumption is the guideline of Higgs Effective Field Theory, where after the 125 GeV scalar discovery, a scalar degree of freedom h, which is not part of the doublet, was included in its Lagrangian [47, 48]. This model is the parametrization of the scalar sector with the minimal IR assumptions. We can then state

$$\mathrm{SM}(\mathrm{H} \in \mathrm{SU(2)_L},\ \Lambda \to \infty) \subset \mathrm{SMEFT}(\mathrm{H} \in \mathrm{SU(2)_L},\ \Lambda \neq \infty) \subset \mathrm{HEFT}(h,\ \Lambda \neq \infty)$$

An important step towards the construction of a low-energy description is to minimize the UV assumptions. A more general setup leads to more coefficients while a more restrictive one, less. The SMEFT seems a good compromise between complexity and generality given the current data by LHC. As less assumptions are made in HEFT, more operators are expected order-by-order in Λ. For instance, for $n_f = 1$ flavours, HEFT contains 148 operators (plus the hermitian conjugates) whereas SMEFT contains 'only' 76. Due to the proliferation of operators even for SMEFT, starting with a simple model (with more assumptions) seems more appealing.

This effective theory is build upon enlarging the SM with higher dimension operators

$$\mathcal{L}_{\mathrm{SMEFT}} = \mathcal{L}_{\mathrm{SM}} + \sum_{d>4} \mathcal{L}^{(d)}, \qquad \mathcal{L}^{(d)} = \sum_{i=1}^{n_d} \frac{c_i^{(d)}}{\Lambda^{d-4}} \mathcal{O}_i^{(d)}. \tag{3.6}$$

Each term in the Lagrangian has a mass order dictated by power of Λ, a set of operators and Wilson coefficients c_i, which are dimensionless[11]. Explicitly, these terms are

$$\mathcal{L}_{\mathrm{SMEFT}} = \mathcal{L}_{\mathrm{SM}} + \mathcal{L}^{(5)} + \mathcal{L}^{(6)} + \mathcal{L}^{(7)} + \mathcal{L}^{(8)} + ... \tag{3.7}$$

The first term that appears in the expansion is $\mathcal{L}^{(5)}$, which contains only one operator

$$\mathcal{L}^{(5)} = C_{5,rs} \epsilon^{ij} \epsilon^{kl} (\ell_{ir}^T\, C\, \ell_{ks}) H_j H_\ell + \mathrm{h.c}, \tag{3.8}$$

where r, s are flavour indices[12]. This $\Delta L = 2$ term gives the Majorana mass to neutrinos whenever the Higgs field acquires its vacuum expectation value. This term would not enter in our analysis since the mass of the neutrinos are very small and therefore this operator should be highly suppressed. Moreover, it was shown that [49]

$$\frac{1}{2}(\Delta B - \Delta L) = d, \qquad \mathrm{mod} \quad 2, \tag{3.9}$$

[11] A notation where the Λ scale is absorbed could also be used: $C_i^{(d)} = c_i^{(d)}/\Lambda^{d-4}$.

[12] We always use the letters p, r, s, t for the flavour indices and i, j, k, l for the SU(2) indices

and therefore $\Delta B - \Delta L = 0$ only happens for operators with even dimensions. We focus on the second part of the Lagrangian, the dimension-six $\mathcal{L}^{(6)}$. In its full glory, it contains 2499 of $\Delta B = \Delta L = 0$ hermitian operators, which accounts for the three flavours. The non-hermitian operators $\mathcal{O}$ have a CP-even $\mathcal{O} + \mathcal{O}^\dagger$ and a CP-odd part $\mathcal{O} - \mathcal{O}^\dagger$ and comes with two real Wilson Coefficients. These operators count as two hermitian operators, *i.e* the number of real coefficients are the same as the hermitian operators [22]. One could also add to it 6 of $\Delta L = 2$ and 273 of $\Delta B = \Delta L = 1$ operators and their hermitian conjugate, but we are going to focus on the trivial case. In the table below, we classify them accordingly with their field content.

purely-bosonic	mixed	fermionic
X^3, H^6	$\psi^2 H^3, \psi^2 X H,$	ψ^4
$H^4 D^2, X^2 H^2$	$\psi^2 H^2 D$	

Since this is an expansion in Λ, higher order terms are neglected. The $\mathcal{L}^{(7)}$ Lagrangian does contribute to $\Delta B = \Delta L = 0$ while $\mathcal{L}^{(8)}$ can have a interplay with the dimension-six operators but are suppressed by an additional factor of $1/\Lambda^2$. A basis for the dimension-eight operators was recently found by two independent groups [50, 51] and the number of operators of each term $\mathcal{L}^{(k)}$ is known and determined by the Hilbert series [52–54]. The General Relativity (GR) mixed SMEFT operators were also constructed using this method [55]. Regarding the dimension-eight operators, many derivatives are inserted to construct them which leads to unitarity-violating behaviour at large energies. Such high derivative terms have their signs constrained by positive bounds, reducing the allowed coefficient space [56, 57]. Although very powerful, positivity bounds only applies to dimension eight operators, and we are interested in the dimension-six ones. In the following, we describe in detail how to obtain the minimal set of dimension-six operators, which is regarded as a *basis*.

3.3 Warsaw Basis construction

We focus on the dimension-six Lagrangian using the Warsaw Basis. The search for the basis started with the study of [58], and the minimal set of operators was only found 20 years later in [59]. This construction made use of three essential identities

- **Equations of Motion:** We can use the classical EOM to remove derivatives from operators. For e.g., whenever there is a gauge field derivative

$$(D^\rho G_{\rho\mu})^A = g_s(\bar{q}\gamma_\mu T^A q + \bar{u}\gamma_\mu T^A u + \bar{d}\gamma_\mu T^A d) \tag{3.10}$$

we observe that right-hand-side does not contain any derivative. Therefore, if two operators are related by the EOM, we can swap the derivative term for other non-derivative ones, which will lead to the same physical effect [60, 61]

$$\text{If} \quad \mathcal{O}_a = \mathcal{O}_b + \mathcal{O}_c \frac{\delta S_{\text{kin}}}{\delta \phi_j}, \quad \text{then} \quad \mathcal{O}_a \sim \mathcal{O}_b \tag{3.11}$$

The EOM can also be understood as just a change of the integration variable in the path-integral formalism, as explained in Sec 2.4.

- **Fierz Identities:** These identities relates fermion fields such as

$$(\bar{\psi}_L \gamma_\mu \psi_L)(\bar{\chi}_L \gamma^\mu \chi_L) = (\bar{\psi}_L \gamma_\mu \chi_L)(\bar{\chi}_L \gamma^\mu \psi_L) \tag{3.12}$$

which we can make use when building the minimal set of four-fermion operators.

- **Integration by Parts:** If two operators are related by a total derivative, then they are equivalent

$$\text{If} \quad \mathcal{O}_a = \mathcal{O}_b + d\mathcal{O}_c, \quad \text{then} \quad \mathcal{O}_a \sim \mathcal{O}_b \tag{3.13}$$

since $\int_{\mathcal{M}} d\mathcal{O} = 0$ and $\mathcal{M}$ is the spacetime manifold.

With these three ingredients, we can then define the basis for the dimension-six Lagrangian. A very elegant way is to use invariants and Hilbert series [53, 54]. But here we follow the approach of [59]. First, from Section 2, we know that the the building blocks in SMEFT are given by[13]

$$\mathcal{O}_i \sim (\bar{\psi}\psi)^{N_F} (X)^{N_X} (D)^{N_D} (H)^{N_H} \to 3N_F + 2N_X + N_D + N_H = 6 \tag{3.14}$$

For $N_F = 2$, we have the four-fermion operators and characterizing all the possible contractions will depend on the Fierz identities, this class of operators is known as the **Class 8** and we discuss it below.

In SMEFT, the Higgs field is a doublet under $\text{SU}(2)_L \times \text{U}(1)_Y$ which forces us to pick an **even** number of Higgs fields for purely bosonic operator. The same happens for covariant derivatives due to Lorentz invariance. We understand each possible combination as a 'mass class', which want to be lowered in the number of derivatives, these are:

$$N_F = 1, 2: \qquad \{\psi^4, \psi^2 X D, \psi^2 X H, \psi^2 D^3, \psi^2 D^2 H^1, \psi^2 D H^2, \psi^2 H^3\} \tag{3.15}$$

$$N_F = 0: \qquad \{X^3, X^2 D^2, X^2 H^2, X H^4, X D^4, X D^2 H^2, H^6, D^4 H^2, D^2 H^4\} \tag{3.16}$$

[13] Since we are dealing with SMEFT, the Higgs is assumed to be linearly realized. See Ref. [12] for a more general power counting when the Higgs can also be non-linear realized.

From this set of operators, XH^4 and XD^4 can be ignored due to the anti-symmetrization of the field-strength and lack of Lorentz indices. In the case of XD^4, one finds out that if the Lorentz indices are contracted (including contraction with $\epsilon_{\mu\nu\rho\sigma}$) one always ends up with $[D_\mu, D_\nu] \sim X_{\mu\nu}$, putting it in the X^2D^2 class.

For the purely bosonic case, the mass classes H^2D^4, H^2XD^2 and X^2D^2 reduce to X^3, X^2H^2, H^6 and H^4D^2 via EOM. Writing them down for the Higgs[14]

$$D^2H_k + 2\lambda(H^\dagger H - \frac{1}{2}v^2)H_k - \bar{d}Y_d q_k - \bar{q}_j Y_u^\dagger u\epsilon_{jk} + \bar{e}Y_e\ell_k = 0, \tag{3.17}$$

which reduces the derivatives to H^3, H and $\bar{\psi}\psi$. Using those, we want to remove the number of derivatives. For instance, the operator H^2D^4

$$(D^\mu D_\mu H^k)(D^\rho D_\rho H_k) = (D^\mu D_\mu H^k)(2\lambda(H^\dagger H - \frac{1}{2}v^2)H_k - \bar{d}Y_d q_k - \bar{q}_j Y_u^\dagger u\epsilon_{jk} + \bar{e}Y_e\ell_k) \tag{3.18}$$

downgrading it to the classes H^4D^2, ψ^2HD^2 and dimension-four operator multiplied by v^2. We finally find the following substitutions

$$\begin{aligned} H^2XD^2 \quad &\rightarrow \quad H^4D^2, \quad H^2X^2 \quad \text{and} \quad \psi^2H^2D \\ X^2D^2 \quad &\rightarrow \quad X^3, \quad H^2XD^2 \quad \text{and} \quad \psi^2XD \end{aligned} \tag{3.19}$$

Allowing us to write down all possible gauge-invariant realizations of the minimal set of the four purely bosonic mass classes X^3, X^2H^2, H^6 and H^4D^2 [59]. The most simple one is H^6 (**Class 2**), since we have to contract the $\mathrm{SU}(2)_L$ indices, the only possibility is $\mathcal{O}_H = (H^\dagger H)^3$. In the case of X^2H^2 **Class 4**, two H can form a singlet or a triplet under $\mathrm{SU}(2)_L$, *i.e* $(H^\dagger H)$ or $(H^\dagger\tau^I H)$, where the latter has to be contracted with $W^I_{\mu\nu}$ and that one of $X^{\mu\nu} \in G^A_{\mu\nu}, W^I_{\mu\nu}, B^{\mu\nu}$ can be the dual. Therefore, for the gluons we have:

$$\mathcal{O}_{HG} = (H^\dagger H)G^A_{\mu\nu}G^{\mu\nu}_A \quad \text{and} \quad \mathcal{O}_{H\widetilde{G}} = (H^\dagger H)\widetilde{G}^A_{\mu\nu}G^{\mu\nu}_A \tag{3.20}$$

The same appears for only B's or only W's:

$$\mathcal{O}_{HB} = (H^\dagger H)B_{\mu\nu}B^{\mu\nu} \quad \text{and} \quad \mathcal{O}_{H\widetilde{B}} = (H^\dagger H)\widetilde{B}_{\mu\nu}B^{\mu\nu} \tag{3.21}$$

$$\mathcal{O}_{HW} = (H^\dagger H)W^I_{\mu\nu}W^{I\mu\nu} \quad \text{and} \quad \mathcal{O}_{H\widetilde{W}} = (H^\dagger H)\widetilde{W}^I_{\mu\nu}W^{I\mu\nu} \tag{3.22}$$

Now, considering the possibility of the two Higgs to form a triplet we have to contract the index with only one W and the other has to be a B, since gluons would require colour indices, then:

$$\mathcal{O}_{HWB} = (H^\dagger\tau^I H)W^I_{\mu\nu}B^{\mu\nu} \quad \text{and} \quad \mathcal{O}_{H\widetilde{W}B} = (H^\dagger\tau^I H)\widetilde{W}^I_{\mu\nu}B^{\mu\nu} \tag{3.23}$$

[14]Note since we are interested in operators at order $\mathcal{O}(\frac{1}{\Lambda^2})$, we can ignore the higher dimension operators in the EOM, so we just have to use the SM-EOM, not the SMEFT-EOM. If one wants to understand dimension eight effects, then SMEFT-EOM at $\mathcal{O}(\frac{1}{\Lambda^2})$ should be used.

The next class to analyse is H^4D^2 (**Class 3**). The two derivatives must act on different fields or the SM-EOM moves it to a lower class. Again, the Higgs can form a triplet or a singlet

$$(H^\dagger\tau^I H)[(D_\mu H)^\dagger\tau^I(D^\mu H)^\dagger)] \quad \text{and} \quad (H^\dagger H)[(D_\mu H)^\dagger(D^\mu H)^\dagger)] \tag{3.24}$$

In the first one, we can use Fierz for the Pauli matrices $\tau^I_{jk}\tau^I_{mn} = 2\delta_{jn}\delta_{mk} - \delta_{jk}\delta_{mn}$ where we obtain an independent term and the second one, where we can use EOM to reduce it as below:

$$(H^\dagger\tau^I H)[(D_\mu H)^\dagger\tau^I(D^\mu H)^\dagger)] = 2(H^\dagger D_\mu H)^*(H^\dagger D^\mu H) - (H^\dagger H)[(D_\mu H)^\dagger(D^\mu H)^\dagger)] \tag{3.25}$$

$$(H^\dagger H)[(D_\mu H)^\dagger(D^\mu H)^\dagger)] = \frac{1}{2}(H^\dagger H)\Box(H^\dagger H) + \psi^2H^3 + H^6 + m^2H^4 + ...$$

where we call then

$$\mathcal{O}_{H\Box} = (H^\dagger H)\Box(H^\dagger H) \quad \text{and} \quad \mathcal{O}_{HD} = (H^\dagger D^\mu H)^*(H^\dagger D^\mu H) \tag{3.26}$$

Last but not least, the X^3 operator or the **Class 1**, which is the most important operator for the diboson production result. For this, assume that they can be different X, Y and Z (where we allow one to be dual and do not need to consider the $\epsilon^{\mu\nu\rho\sigma}$) and all the indices must be contracted, which has the Lorentz structure $X^\mu_\nu Y^\nu_\rho Z^\rho_\mu$. This implies that the three tensor must be different, otherwise $X_{\alpha\mu}X_{\beta\nu}Z^{\mu\nu}g^{\alpha\beta} = 0$ by antisymmetry of the Z. Also, two tensor cannot be dual because $X^\nu_\mu\widetilde{X}^\rho_\nu = -\frac{1}{4}\delta^\rho_\mu X_{\alpha\beta}\widetilde{X}^{\alpha\beta}$ is symmetric in $\mu\rho$ and Z is antisymmetric, this vanish the possibility of $B^\nu_\mu W^{I\rho}_\nu\widetilde{W}^{I\mu}_\rho = 0$, symmetric singlets in products of two adjoint representations are absent. The only option is then to contract the three different tensor with f^{ABC} or ϵ^{IJK}, leading to:

$$\begin{aligned} \mathcal{O}_G &= f^{ABC}G^{A\nu}_\mu G^{B\rho}_\nu G^{C\mu}_\rho \qquad & \mathcal{O}_{\widetilde{G}} &= f^{ABC}\widetilde{G}^{A\nu}_\mu G^{B\rho}_\nu G^{C\mu}_\rho \\ \mathcal{O}_W &= \epsilon^{IJK}W^{I\nu}_\mu W^{J\rho}_\nu W^{K\mu}_\rho \qquad & \mathcal{O}_{\widetilde{W}} &= \epsilon^{IJK}\widetilde{W}^{I\nu}_\mu W^{J\rho}_\nu W^{K\mu}_\rho \end{aligned} \tag{3.27}$$

With this, the purely bosonic part of the SMEFT dimension-six Lagrangian is fully obtained. For the fermionic part, a similar analysis can be made but with the essential aid of Fierz identities. There are three possibilities of fermion content here, only leptons, quarks and leptons, and only quarks. Regarding the first option, a four-fermion operator with left-handed lepton fields can have the following contractions

$$\mathcal{O}^{(1)}_{\ell\ell} = (\bar{l}_{ip}\gamma^\mu l^i_r)(\bar{l}_{js}\gamma_\mu l^j_t) \qquad \text{and} \qquad \mathcal{O}^{(3)}_{\ell\ell} = (\bar{l}_{ip}\gamma^\mu[\tau^a]^i_j l^j_r)(\bar{l}_{ks}\gamma_\mu[\tau^a]^k_m l^m_t) \tag{3.28}$$

Applying SU(2) Fierz identity, we relate with delta functions

$$[\tau^a]^i_j[\tau^a]^k_m = 2\delta^i_m\delta^k_j - \delta^i_j\delta^k_m \tag{3.29}$$

and can rewrite the $\mathcal{O}_{\ell\ell}^{(3)}$ operators as a combination of two singlet with flavour indices swapped. However, this would not be true in the mixed case, where one of the bilinear is made out of quarks. In this case, the two structures are independent and we need both of them, $\mathcal{O}_{lq}^{(1)} = (\bar{l}_{ip}\gamma^\mu l_r^i)(\bar{q}_{\alpha js}\gamma_\mu q_t^{\alpha j})$ and $\mathcal{O}_{lq}^{(3)} = (\bar{l}_{ip}\gamma^\mu [\tau^a]_j^i l_r^j)(\bar{q}_{\alpha ks}\gamma_\mu [\tau^a]_m^k q_t^{\alpha m})$. For the four-quark operators, we can write the product of the bilinears as

$$(\bar{q}_p\gamma^\mu\Gamma q_r)(\bar{q}_s\gamma_\mu\Gamma q_t), \quad \text{where} \quad \Gamma\otimes\Gamma \quad \propto \quad 1\otimes 1,\, T^A\otimes T^A,\, \tau^I\otimes\tau^I,\, T^A\tau^I\otimes T^A\tau^I.$$

Now, quarks have SU(2) and SU(3) indices that can be contracted within the same bilinear (direct) of across them (swapped). The Fierz identity relates the quarks over different bilinears, therefore the case where both SU(2) and SU(3) indices are swapped is the same as a direct product. Similarly, SU(2) swapped is the same as SU(3) swapped. Thus there are only two independent structures since $T^A\otimes T^A$ and $T^A\tau^I\otimes T^A\tau^I$ can be rewritten using the Fierz identities, which are $1\otimes 1$ and $\tau^I\otimes\tau^I$

$$\mathcal{O}_{qq}^{(1)} = (\bar{q}_p\gamma^\mu q_r)(\bar{q}_s\gamma_\mu q_t) \qquad \text{and} \qquad \mathcal{O}_{qq}^{(3)} = (\bar{q}_p\gamma^\mu\tau^I q_r)(\bar{q}_s\gamma_\mu\tau^I q_t) \tag{3.30}$$

The derivation of the mixed terms, which includes fermions and bosons, can be found in [59] and we explicitly show in App. J the complete Warsaw basis with all operators.

This construction is based on listing all possibilities, analysing the consistency of each operator and removing redundancies. Clearly, this becomes unrealistic for dimensions greater than six. Using the Hilbert series methods, the authors of [53, 54] obtained the operators for general dimensions. They have shown that the operators in EFTs are controlled by a conformal algebra which deals with EOM and IBP organizing the operators into irreducible representations of a conformal group.

3.4 Electroweak Redefinitions

The effective operators change the usual definitions of the Electroweak coefficients. These new definitions play an important role for the SMEFT phenomenological analysis. For instance, the introduction of the operator $\mathcal{O}_H \equiv (H^\dagger H)^3$ changes the minimum of the Higgs potential [62]

$$V(H^\dagger H) = \lambda(H^\dagger H - \frac{1}{2}v^2)^2 - C_H(H^\dagger H)^3 \tag{3.31}$$

which yields to a new minimum, up to order $\mathcal{O}(\Lambda^{-2})$

$$\langle H^\dagger H\rangle = \frac{v^2}{2}\left(1 + \frac{3C_H v^2}{4\lambda}\right) \equiv \frac{1}{2}v_T^2 \tag{3.32}$$

where we are assuming an expansion on the mass gap. This is one of the expansion parameter we are going to deal in SMEFT calculations $\bar{v}_T^2/\Lambda^2 < 1$. After finding the

new minimum, we can expand the Higgs doublet around it. In the unitary gauge [63], we obtain

$$H = \frac{1}{\sqrt{2}} \begin{bmatrix} 0 \\ [1 + C_{H,\text{kin}}]h + \bar{v}_T \end{bmatrix}, \qquad C_{H,\text{kin}} \equiv \left(C_{H\Box} - \frac{1}{4} C_{HD} \right) \tag{3.33}$$

Another important issue, is to put the modified kinetic term in the canonical form.

$$G_\mu^A = \mathcal{G}_\mu^A (1 + C_{HG}), \quad W_\mu^I = \mathcal{W}_\mu^I (1 + C_{HW}), \quad B_\mu = \mathcal{B}_\mu (1 + C_{HB}) \tag{3.34}$$

which also redefine the coupling constants

$$\bar{g}_3 = g_3 (1 + C_{HG}), \quad \bar{g}_2 = g_2 (1 + C_{HW}), \quad \bar{g}_1 = g_1 (1 + C_{HB}) \tag{3.35}$$

which keeps $g_3 G_\mu^A = \bar{g}_3 \mathcal{G}_\mu^A$ and the others unchanged. In order to rotate from $\{\mathcal{W}_\mu^3, \mathcal{B}_\mu\}$ to the $\{\mathcal{Z}_\mu, \mathcal{A}_\mu\}$, we also need to keep track of the $\mathcal{L}^{(6)}$ terms

$$\begin{bmatrix} \mathcal{W}_\mu^3 \\ \mathcal{B}_\mu \end{bmatrix} = \begin{bmatrix} 1 & -\frac{1}{2} C_{HWB} \\ -\frac{1}{2} C_{HWB} & 1 \end{bmatrix} \begin{bmatrix} \cos\bar{\theta} & \sin\bar{\theta} \\ -\sin\bar{\theta} & \cos\bar{\theta} \end{bmatrix} \begin{bmatrix} \mathcal{Z}_\mu \\ \mathcal{A}_\mu \end{bmatrix} \tag{3.36}$$

where the rotation angle is given by

$$\tan\bar{\theta} = \frac{\bar{g}_1}{\bar{g}_2} + \frac{C_{HWB}}{2} \left(1 - \frac{\bar{g}_1^2}{\bar{g}_2^2} \right) \tag{3.37}$$

The new definitions will be important in the relevant processes of this thesis since they involve the electroweak sector. A new approach to define these parameters in terms of geometrical quantities, such as curvature in the scalar field space, is called Geometric SMEFT [64].

Usually, in order to make a prediction in any theory, the first step is to perform a finite set of measurements and then one can calculate observables in order to make new predictions. The set of measurements are called input parameters. However, with dimension-six operators, masses and couplings now contain Wilson coefficients and change the relation with the input parameters. It is important to have control of the proliferation of the coefficients such that we can always trace back the input scheme dependence in the final answer.

3.5 Input Schemes

We have mainly two schemes: α-scheme and m_W-scheme [65]. Historically, the former has been used more in the literature due to the Large-Electron Positron Collider (LEP) influence. It is characterized by the electromagnetic structure constant $\hat{\alpha}$ extracted from the Thomson scattering. The latter goes by the name of m_W-scheme, which did not become a common practice due to the lack of precision on the W mass during LEP data analysis. However, this input scheme has more advantages.

3.5.1 $\hat{\alpha}$-Scheme

In this input parameter scheme, the measured quantities are $\{\hat{\alpha}, \hat{m}_Z, \hat{G}_F, \hat{m}_h\}$. Then, in the unitary gauge, we can define the parameters

$$\hat{e} = \sqrt{4\pi\hat{\alpha}}, \quad \hat{v}_T = \frac{1}{2^{1/4}\sqrt{\hat{G}_F}}, \quad s^2_{\hat{\theta}} = \frac{1}{2}\left[1 - \sqrt{1 - \frac{4\pi\hat{\alpha}}{\sqrt{2}\hat{G}_F\hat{m}_Z^2}}\right], \tag{3.38}$$

$$\hat{g}_1 = \frac{\hat{e}}{c_{\hat{\theta}}}, \qquad \hat{g}_2 = \frac{\hat{e}}{s_{\hat{\theta}}}, \qquad \hat{m}_W^2 = \hat{m}_Z^2 c^2_{\hat{\theta}}, \tag{3.39}$$

3.5.2 $\hat{m}_W$-Scheme

In this scheme, we have then the following definitions

$$\hat{e} = 2 \cdot 2^{1/4}\hat{m}_W s_{\hat{\theta}}\sqrt{\hat{G}_F}, \qquad \hat{v}_T^2 = \frac{1}{\sqrt{2}\hat{G}_F}, \qquad s^2_{\hat{\theta}} = 1 - \frac{\hat{m}_W^2}{\hat{m}_Z^2}, \tag{3.40}$$

$$\hat{g}_1 = 2 \cdot 2^{1/4}\hat{m}_W\sqrt{\hat{G}_F} \qquad \hat{g}_2 = 2 \cdot 2^{1/4}\hat{m}_W\sqrt{\hat{G}_F\left(1 - \frac{\hat{m}_W^2}{\hat{m}_Z^2}\right)} \tag{3.41}$$

This input scheme has two main benefits: The first one is due to the flat directions present in global fits of the LEPI data. This experiment is based on a $\bar{\psi}\psi \to V \to \bar{\psi}\psi$ scattering and when performing a global fit with SMEFT presents two flat directions that cannot be constrained [65]. This issue is explained by a *reparametrization invariance*. Consider the simple Lagrangian

$$\mathcal{L} = \frac{1}{2}m_V^2 V^\mu V_\mu - \frac{1}{4}V^{\mu\nu}V_{\mu\nu} - g\bar{\psi}_i\gamma^\mu\psi_j V_\mu - g\kappa\bar{\psi}_k\gamma^\mu\psi_l V_\mu + ... \tag{3.42}$$

then the change of the vector field and coupling $(V, g) \leftrightarrow (V'(1+\epsilon), g'(1-\epsilon))$ does not change the $\bar{\psi}\psi \to V \to \bar{\psi}\psi$ scattering since they keep $gV \to g'V'$ invariant. We will come across these flat directions in Sec. 5.

In order to lift these flat directions, LEP II data with $\bar{\psi}\psi \to \bar{\psi}\psi\bar{\psi}\psi$ was introduced. When calculating the amplitudes, one need to expand around the pole of the $W^\pm$ boson. In this expansion, the $\hat{\alpha}$-scheme introduces a shift in the mass pole which is the same order as the SMEFT corrections. This however does not occur in the $\hat{m}_W$-scheme [65]. The second important benefit is that the $\hat{m}_W$-scheme is easier to implement in one loop corrections [66, 67]. In App. D, we show the expressions for the one-loop matching in both schemes and it is clear that the expressions for $\hat{m}_W$-scheme are simpler. During this thesis we are going to use both schemes and compare when it is appropriate.

We can introduce the 'bar-hat' notation to understand the shift to the Lagrangian parameters. Due to SMEFT, leading order shift in a parameter P from the SM Lagrangian, is defined as $\delta P = \bar{P} - \hat{P}$. The bar parameters are accompanied by the canonically

normalized SMEFT Lagrangian, where the hat is the input parameter. An example of a leading order shift in both schemes is

$$\hat{\alpha}\text{-scheme}: \qquad \delta s_\theta^2 = \frac{s_{2\hat{\theta}}}{8c_{2\hat{\theta}}}\left[s_{2\hat{\theta}}\left(C_{HD} + 2\sqrt{2}\delta G_F\right) + 4C_{HWB}\right] \tag{3.43}$$

$$\hat{m}_W\text{-scheme}: \qquad \delta s_\theta^2 = -\frac{\hat{m}_W^2}{2\hat{m}_Z^2}C_{HD} - \frac{\hat{m}_W}{\hat{m}_Z}\sqrt{1-\frac{\hat{m}_W^2}{\hat{m}_Z^2}}C_{HWB} \tag{3.44}$$

3.6 Triple-Gauge-Coupling in the SMEFT

The first result of this thesis is based on the study of anomalous triple-gauge couplings (TGC) in SMEFT via diboson production at LHC. These particular couplings give imprints on the nature of the electroweak symmetry breaking. We are going to explore this in more details in the next chapter. Here, we introduce this sector and connect directly with the previous discussions. The anomalous TGC Lagrangian, in the SMEFT, has been historically written as

$$\frac{-\mathcal{L}_{\text{TGC}}^{\text{SMEFT}}}{g_{VWW}} = i\bar{g}_1^V(\mathcal{W}^+_{\mu\nu}\mathcal{W}^{-\mu} - \mathcal{W}^-_{\mu\nu}\mathcal{W}^{+\mu})\mathcal{V}^\nu + i\bar{\kappa}_V\mathcal{W}^+_\mu\mathcal{W}^-_\nu\mathcal{V}^{\mu\nu} + i\frac{\bar{\lambda}_V}{\bar{M}_W^2}\mathcal{V}^{\mu\nu}\mathcal{W}^{+\rho}_\nu\mathcal{W}^-_{\rho\mu}, \tag{3.45}$$

where $\mathcal{W}_\mu$ and $\mathcal{V}_\mu = \mathcal{Z}_\mu$ or $\mathcal{A}_\mu$ are the canonically normalized gauge fields. The couplings above can be written as [68]

$$\begin{gathered} g_{AWW} = \hat{e}, \quad g_{ZWW} = \hat{e}\cot\hat{\theta}, \quad \bar{g}_1^V = g_1^V + \delta g_1^V \\ \bar{\kappa}_V = \kappa_V + \delta\kappa_V, \quad \bar{\lambda}_V = \lambda_V + \delta\lambda_V\,, \end{gathered} \tag{3.46}$$

where the hat notation indicates a measured coupling constant value, *i.e* the input parameter. The coupling shifts of the Lagrangian form in Eq. 3.45 can be directly calculated in terms of the SMEFT Warsaw basis operators, given here using the $\{\hat{\alpha}, \hat{G}_F, \hat{m}_Z\}$ input scheme[15]:

$$\delta g_1^A = 0, \qquad \delta g_1^Z = \frac{1}{2\sqrt{2}\hat{G}_F}\left(\frac{s_{\hat{\theta}}}{c_{\hat{\theta}}} + \frac{c_{\hat{\theta}}}{s_{\hat{\theta}}}\right)C_{HWB} + \frac{1}{2}\left(\frac{1}{s_{\hat{\theta}}^2} + \frac{1}{c_{\hat{\theta}}^2}\right), \tag{3.47}$$

$$\delta\kappa_A = \frac{1}{\sqrt{2}\hat{G}_F}\frac{c_{\hat{\theta}}}{s_{\hat{\theta}}}C_{HWB}, \quad \delta\kappa_Z = \frac{1}{2\sqrt{2}\hat{G}_F}\left(-\frac{s_{\hat{\theta}}}{c_{\hat{\theta}}} + \frac{c_{\hat{\theta}}}{s_{\hat{\theta}}}\right)C_{HWB} + \frac{1}{2}\left(\frac{1}{s_{\hat{\theta}}^2} + \frac{1}{c_{\hat{\theta}}^2}\right), \tag{3.48}$$

$$\delta\lambda_A = 6s_{\hat{\theta}}\frac{\hat{m}_W^2}{g_{AWW}}C_W, \qquad \delta\lambda_Z = 6c_{\hat{\theta}}\frac{\hat{m}_W^2}{g_{ZWW}}C_W, \tag{3.49}$$

where the Wilson coefficients correspond to the operators:

$$\mathcal{Q}_{HWB} = H^\dagger\tau^I H W^I_{\mu\nu}B^{\mu\nu} \quad \text{and} \quad \mathcal{Q}_W = \epsilon^{IJK}W^{I\nu}_\mu W^{J\rho}_\nu W^{K\mu}_\rho, \tag{3.50}$$

[15]Even thought the clear advantages of $\hat{m}_W$, we have used the alpha scheme for this particular work [1].

It is clear that in the SM, the couplings are $g_1^V = \kappa_V = 1$ and $\lambda_V = 0$. In the chosen input parameter scheme, gauge-invariance at order Λ^{-2} requires that $\delta\kappa_Z = \delta g_1^Z - t_{\hat{\theta}}^2 \delta\kappa_A$, $\delta g_1^A = 0$ and $\delta\lambda_A = \delta\lambda_Z$ [69].

Generic values of the coupling shifts δg_1^V and $\delta\kappa_V$ spoil the SM cancellation of amplitude terms that grow with energy in the charged current diagrams, also known as CC03 diagrams, resulting in a growing effect of these coupling corrections in the high-energy tails of the distribution. This is a somewhat unique feature in the SMEFT, as usually the source of growing-with-energy terms are operators which contain extra dynamical fields or derivatives, but in this case operators which are functionally dimension-4 after Higgs vev insertions still lead to growing effects. This also maps to propagator corrections.

On the other hand, the operator $\mathcal{Q}_W$, related to $\bar{\lambda}_V$, couples only to three-boson combinations which all have identical helicities. Since the SM couplings always lead to the production of two opposite-helicity vector bosons at leading order, this leads to a non-interference between SM and the $\mathcal{Q}_W$-induced BSM four-point amplitudes for diboson production. In Sec 4, we are going to construct an observable which is only sensitive to this operator.

3.7 Weak Effective Theory

Precision calculations in flavour physics are challenging due to the contribution of several scales. In order to control the scales and expansions, effective theories make themselves very useful. For instance, if one wants to study precisely the CKM matrix and its unitarity condition, a flavour decay could give insights. The decay of a B into a D meson probes the elements of the CKM matrix. However, this process occurs at low-energy scale, below the W-mass, and the QCD corrections are important. The problem is that, large logarithms appear of the form of $\alpha_s \ln\left(\frac{m_W}{m_b}\right)$. Using EFT tools, one can accomplish the resummation of large-logs by means of RGE [21], which is one of the greatest advantages of using effective theories. Thus, a theory where all the particles with masses above the electroweak scale are integrated out is a suitable model for this problem.

The Weak Effective Theory[16] is obtained from the Standard Model after the Electroweak bosons and the top quark are integrated out. Naturally, below the EW scale, QCD and QED are still preserved symmetries and the previous EW currents are now given by four-fermion operators. The construction of the interaction Hamiltonian is given by writing down all the possible operators for four-fermion interactions and matching with the SM at the electroweak scale m_W.

In this thesis we will be interested in the subset of WET that describes the flavour-changing neutral currents in the down-sector, *i.e* $d_i \to d_j\gamma$ and $d_i \to d_j\ell^+\ell^-$. This is

[16] Also known as Low Energy Effective Theory (LEFT).

described by the following Hamiltonian [70]

$$\mathcal{H}_{\text{eff}}^{\ell\ell} \supset 4\frac{G_F}{\sqrt{2}}\left[-\frac{1}{(4\pi)^2}V_{td_j}^* V_{td_i}\sum_{k=3}^{10} C_k^{d_i d_j}\mathcal{O}_k^{d_i d_j} + \sum_{q=u,c} V_{qd_j}^* V_{qd_i}(C_1^{d_i d_j}\mathcal{O}_1^{q,d_i d_j} + C_2^{d_i d_j}\mathcal{O}_2^{q,d_i d_j})\right] \tag{3.51}$$

with the following operators

$$\mathcal{O}_1^{q,d_i d_j} = (\bar{d}_i^\alpha \gamma_\mu P_L q^\beta)(\bar{q}^\beta \gamma^\mu P_L d_j^\alpha), \qquad \mathcal{O}_2^{q,d_i d_j} = (\bar{d}_i^\alpha \gamma_\mu P_L q^\alpha)(\bar{q}^\beta \gamma^\mu P_L d_j^\beta), \tag{3.52}$$

for the second part of the Hamiltonian. For the first part, the operators $\mathcal{O}_{3..6}$

$$\mathcal{O}_3^{d_i d_j} = (\bar{d}_i \gamma_\mu P_L d_j)(\bar{q}\gamma^\mu q), \qquad \mathcal{O}_4^{d_i d_j} = (\bar{d}_i T^A \gamma_\mu P_L d_j)(\bar{q} T^A \gamma^\mu q), \tag{3.53}$$

$$\mathcal{O}_5^{d_i d_j} = (\bar{d}_i \gamma_\mu \gamma_\nu \gamma_\rho P_L d_j)(\bar{q}\gamma^\mu \gamma^\nu \gamma^\rho q), \quad \mathcal{O}_6^{d_i d_j} = (\bar{d}_i T^A \gamma_\mu \gamma_\nu \gamma_\rho P_L d_j)(\bar{q} T^A \gamma^\mu \gamma^\nu \gamma^\rho q), \tag{3.54}$$

and our main interest will be on

$$\mathcal{O}_7^{d_i d_j} = e\hat{m}_{d_i}(\bar{d}_j \sigma^{\mu\nu} P_R d_i) F_{\mu\nu}, \qquad \mathcal{O}_8^{d_i d_j} = g_s \hat{m}_{d_i}(\bar{d}_j \sigma^{\mu\nu} T^A P_R d_i), G_{\mu\nu}^A \tag{3.55}$$

$$\mathcal{O}_9^{d_i d_j} = e^2(\bar{d}_j \gamma^\mu P_L d_i)(\bar{\ell}\gamma_\mu \ell,) \qquad \mathcal{O}_{10}^{d_i d_j} = e^2(\bar{d}_j \gamma^\mu P_L d_i)(\bar{\ell}\gamma_\mu.\gamma_5 \ell) \tag{3.56}$$

With this organization of the Hamiltonian, it becomes clear that the long-distance physics is represented by the operators $\mathcal{O}_{1,..,9}$ while the short distance (ultra-violet) is given by the Wilson coefficients.

In Sec. 2 we saw the one-loop matching between the SM operators and the WET Hamiltonian, where the Wilson coefficients were obtained as a function of the SM couplings. The implicit assumption is that the UV-theory is the Standard Model, therefore the paramaters are known. As we have argued, a extension of this theory is required and the main effective candidate is SMEFT. Thus, it seems reasonable to take SMEFT as the UV-theory and perform the one-loop matching with it. In this case, the SMEFT WCs are free parameters to be determined.

The second result of this thesis focus on the phenomenological implications of this one-loop matching and how the low-energy data can constrain the SMEFT WCs. The result focus on the flavour changing neutral currents in the down sector [3, 71]. The schematic procedure of running via RGE and matching at one-loop is shown in Fig 5.2.

As we pointed out previously, one of the biggest bottlenecks for SMEFT computations and viable phenomenological constrains are the four-fermion operators and their flavour indices. In this work, we have studied two flavour assumption, the $U(3)^5$ and the leading-order Minimal Flavour Violation.

3.8 Minimal Flavour Violation

The cumbersome part of the SMEFT is naturally the four-fermion operators where the proliferation of flavour indices make an impossible task to extract any feasible bound from

the SMEFT in its full glory. An easy indication of the flavour power comes when we count the number of operators as a function of flavour number N_f, which for $N_f = 1, 2, 3$ give us $76, 582, 2499$ hermitian operators, respectively. Therefore, flavour ultraviolet assumptions help to simplify the phenomenological analysis. In the SM, there is a $U(3)^5$ flavour-symmetry in the vanishing Yukawa limit

$$U(3)^5 = U(3)_{Q_L} \times U(3)_{u_R} \times U(3)_{d_R} \times U(3)_{L_L} \times U(3)_{e_R} \tag{3.57}$$

where each field has the following representation under this group

$$q_L \sim (3,1,1,1,1) \quad u_R \sim (1,3,1,1,1) \quad d_R \sim (1,1,3,1,1) \tag{3.58}$$

$$\ell_L \sim (1,1,1,3,1) \quad e_R \sim (1,1,1,1,3) \tag{3.59}$$

A first natural assumption is that all the higher-dimension operators respect this symmetry and therefore are identity-like in the flavour-space, *i.e* the indices p, r, s, t are diagonal. The flavour breaking of this $U(3)^5$- symmetry in the SM comes from the Yukawa coupling matrices, therefore the second natural assumption is that all the flavour-breaking pattern comes only via the Yukawa matrices. This goes by the name of Minimal Flavour Violation (MFV) [72]. To understand it, we can perform a spurion analysis, upgrading the Yukawa matrices to spurion fields which should have the following representation in order to respect the flavour-symmetry

$$Y_u \sim (3, \bar{3}, 1, 1, 1) \qquad Y_d \sim (3, 1, \bar{3}, 1, 1) \tag{3.60}$$

Therefore, if we have the operator $(\bar{Q}_i \sigma^{\mu\nu} u_j) B_{\mu\nu}$, which have the representation $(\bar{3}, 3, 1)$ under the quark flavour part, then we need to include $(Y_u)_{ij}$ to compensate and preserve the symmetry. A systematic analysis of the structure and operators will be done in Sec 5.

3.9 Holomorphic SMEFT

In Fig. 2.1, we can see that to run SMEFT from the UV down to the electroweak scale, the anomalous dimension matrices are required. The complete RGEs of SMEFT were calculated in [73–75]. The authors realized that the anomalous matrices have several null entries, which respect holomorphy [75]. These zeros in the anomalous matrices were later explained by [9] using on-shell unitarity cuts in one-loop amplitudes. These results were recently generalized by [76] where new 'zeros' at higher loops order were found.

The on-shell results for SMEFT and the null entries were understood on a different presentation of the SMEFT Lagrangian that seems more natural when dealing with on-shell amplitudes. This construction categorizes the SMEFT operators as (anti-)holomorphic and non-holomorphic. If we consider only one flavour, there are 59 operators which can be classified accordingly with their field content. A fermion ψ can be left-handed (L) or right-handed (R), D is the covariant derivative and let X be any field strength. Then,

we have $X^3, H^6, H^4D^2, X^2H^2, \psi^2H^3, \psi^2HX, \psi^2H^2D$ and the four-fermion ψ^4, which can be separated in three sub-categories: $(\bar{L}R)(\bar{L}R)$, $(\bar{L}R)(\bar{R}L)$ and the current-current JJ, which consist of $(\bar{L}L)(\bar{L}L)$, $(\bar{R}R)(\bar{R}R)$ and $(\bar{L}L)(\bar{R}R)$. We can introduce then the 'complex' field strengths

$$X^{\pm}_{\mu\nu} = \frac{1}{2}\left(X_{\mu\nu} \mp i\tilde{X}_{\mu\nu}\right), \qquad \tilde{X}^{\pm}_{\mu\nu} = \pm iX^{\pm}_{\mu\nu} \tag{3.61}$$

The authors from [75] define: *"The holomorphic part of the Lagrangian, $\mathcal{L}_h$, is the Lagrangian constructed from the fields $X^+, R, \bar{L}$ but none of their hermitian conjugates"*. For example, take the triple-gauge coupling operator

$$\mathcal{Q}_X = f^{ABC}X^{A\nu}_{\mu}X^{B\rho}_{\nu}X^{C\mu}_{\rho} \quad \mathcal{Q}_{\tilde{X}} = f^{ABC}\tilde{X}^{A\nu}_{\mu}X^{B\rho}_{\nu}X^{C\mu}_{\rho} \tag{3.62}$$

$$\mathcal{Q}_{X,\pm} \equiv \frac{1}{2}(\mathcal{Q}_X \mp i\mathcal{Q}_{\tilde{X}}) = f^{ABC}X^{\pm A\nu}_{\mu}X^{\pm B\rho}_{\nu}X^{\pm C\mu}_{\rho} \tag{3.63}$$

where $\mathcal{Q}_{X,+}$ is holomorphic and $\mathcal{Q}_{X,-}$ is anti-holomorphic. Therefore the triple-gauge coupling Lagrangian can be rewritten as

$$\mathcal{L}_{\text{SMEFT}} \supset C_X\mathcal{Q}_X + C_{\tilde{X}}\mathcal{Q}_{\tilde{X}} = C_{X,+}\mathcal{Q}_{X,+} + C_{X,-}\mathcal{Q}_{X,-} \tag{3.64}$$

where $C_{\pm} \equiv (C_X \pm iC_{\tilde{X}})$. The similar approach can be made for the operators X^2H^2 and ψ^2HX, while the four-fermion operator $(\bar{L}R)(\bar{L}R)$ is holomorphic. The rest of the operators are classified as non-holomorphic[17]. Thus,

$$\begin{aligned} \mathcal{L}_{\text{SMEFT}} &= \mathcal{L}_h + \mathcal{L}_{\bar{h}} + \mathcal{L}_n = C_h\mathcal{Q}_h + \mathcal{Q}_{\bar{h}}Q_{\bar{h}} + C_n\mathcal{Q}_n \\ \mathcal{Q}_h &\subset \{X^3, X^2H^2, \psi^2XH, (\bar{L}R)(\bar{L}R)\} \\ \mathcal{Q}_n &\subset \{H^6, H^4D^2, \psi^2H^3, \psi^2H^2D, (\bar{L}R)(\bar{R}L), JJ\} \end{aligned} \tag{3.65}$$

The authors found that the holomorphic part of the Lagrangian does not mix under the renormalization group evolution, *i.e* the holomorphic coefficient dependence is $C_h(\mu) = C_h(\{C_h(\mu_0)\}, \mu_0/\mu)$, which is called the weak holomorphy condition. This translates into the anomalous dimension matrix as

$$\dot{C}_i \equiv 16\pi^2\mu\frac{d}{d\mu}C_i = \sum_{j=h,\bar{h},n}\gamma_{ij}C_j, \quad \text{for} \quad i = h, \bar{h}, n. \tag{3.66}$$

The anomalous dimension matrix γ_{ij} is a non-holomorphic function of the SM parameters. Under weak holomorphy, the entry $\gamma_{h\bar{h}} = \gamma_{hn} = 0$ but no constraints are set to γ_{nh}.

All this analysis is based in the electroweak symmetric phase, where the particles are massless. In Sec 7 we will be interested in applying new massive on-shell methods [8] for the bosonic part of the SMEFT, which are the first two operators of the $\mathcal{Q}_h$ and $\mathcal{Q}_n$ sets.

[17]The operators ψ^2H^3 is holomorphic but behave as non-holomorphic

4 Diboson interference resurrection via jet substructure

This section is based on the paper ***'Jet substructure measurements of interference in non-interfering SMEFT effects'*** *[1].*

The LHC physics program has already had a great success in the discovery of the Higgs boson [6, 77], completing the Standard Model (SM) and providing the first direct probe of the mechanism of electroweak symmetry breaking. Unfortunately, the plethora of new particles expected to explain the otherwise unnatural parameter values needed to fix the Higgs mass and vacuum expectation value (VEV) to those required by data have not made themselves known to us. Nonetheless, naturalness remains a compelling argument that new physics ought to exist near the electroweak scale. This circumstance has led to a resurgence of techniques treating the SM as an effective field theory (EFT), explicitly allowing the existence of higher-dimensional, non-renormalizable operators to parametrize the potential effects of new physics too heavy to have been seen yet at the LHC. There are two physically distinct and perfectly reasonable ways of treating the SM as an EFT; the difference between them hinges on what assumptions are made about the nature of the experimentally measured scalar.

If one treats the 125 GeV scalar h as potentially already having a new physics origin, at least in part, then the logical expansion to perform is a simultaneous expansion in $\frac{h}{v}$ and $\frac{D}{\Lambda}$, where h is the scalar discovered at the LHC, v the SM Higgs vacuum expectation value (vev), D is a covariant derivative, and Λ is the characteristic scale of new physics (other than that already assumed to be incorporated in h). As v is generally comparable to or below the scale at which measurements are being made to constrain this EFT, it is necessary to expand in relation to Λ only, with all the vev-suppressed terms resummed and treated as a form factor instead. This treatment is known as the Higgs EFT or HEFT, and has been investigated in depth; for recent status of constraints in this framework, see [78].

If instead one is satisfied by the thus-far agreement of the LHC measurements with the SM predictions for the Higgs boson, it is possible to insist that the h is in fact the Higgs, embedded in an electroweak doublet with the would-be Goldstone bosons which become the longitudinal modes of the $W^{\pm}$ and Z bosons. This assumption forbids the separate series in $\frac{h}{v}$, leaving a simpler EFT with just one characteristic scale. This approach has come to be called the SMEFT, and is the one we will adopt for this study. For a recent review of this approach, see [20].

The primary virtue of any EFT treatment is its independence from the underlying UV physics; it is precisely our agnosticism regarding the precise nature of the solution to the hierarchy problem of the SM which motivates us to adopt these methods, rather than directly studying the specific model which we find most pleasing, aesthetically or

otherwise. If used properly, these EFT techniques will allow for bounds to be placed on any model of heavy new physics, importantly including models which have not yet been invented. In order to retain this virtue, it is important that the analyses performed in SMEFT not make unwarranted UV assumptions, even implicitly. In particular, we need to allow for multiple different operators to be active at once, and study all those operators which have an impact on the observable being measured simultaneously.

Much foundational effort has already been invested in the SMEFT, with the full basis of operators at leading order (dimension 6) having been sought by many [58, 79–86], and ultimately found [59]. Once a complete and non-redundant basis was known, it became possible to study the bounds which can be placed on EFT operators in a UV independent way by performing global fits which allow all the Wilson coefficients which are relevant to the data being considered to vary simultaneously. These analyses at tree level have now been performed on the full set of precision electroweak data [68], on diboson production data from LEP [87], on measurements of Higgs properties [66,67,88,89], and combinations of these [90–92]. These tree-level analyses were able to meaningfully constrain the subset of operators which contribute directly to two to two scattering on the Z and Higgs poles at tree level in the narrow width approximation.

Given this non-redundant basis, it also became possible to study the behavior of the leading EFT effects under SM renormalization [62, 93, 94], and that work enabled many analyses of EFT effects at one-loop order, such as corrections to Higgs, tops and Z decays [66, 95–101], QCD and EW radiative corrections [67, 100, 102] and some processes such as single top production [103], Higgs production in association with a $t\bar{t}$ pair [104], and next-to-leading order (NLO) QCD effects in anomalous triple gauge couplings and Drell-Yan processes at the LHC [105–107]. These loop-level calculations introduce dependence (at the order of 10% corrections to the tree-level EFT effect) on new operators which did not contribute at tree level to these observables. They thus make manifest the need for additional data, beyond that of single on-shell particle production and decay, in order to successfully constrain or measure the Wilson coefficients of the SMEFT at accuracy comparable to that available in the data on the poles.

The series expansion in Λ^{-1} in the SMEFT behaves differently away from poles than on them. The dominant beyond SM (BSM) effects on data at a pole arise from insertions of the Higgs vev in dimension d operators leading to corrections to couplings already present in the SM. All other effects are suppressed relative to these contributions by the width of the particle being singly produced. Off the pole, however, other operators are important, and generically scale in relation to the SM contribution as $\frac{E^2}{\Lambda^2}$, where E is the characteristic energy of the process. The scaling can arise in two different ways: a shift in the SM couplings can violate the energy growth cancellation in would-be SM amplitudes, or an operator can explicitly contain a greater number of dynamical fields or derivatives. This has motivated many studies of EFT effects in the high-energy tails of distributions, most notably those for quark compositeness [108, 109]. This growth greatly increases the signal

effect due to the presence of the EFT correction, but it also hints at the breakdown of our perturbative expansion, necessitating an appropriate treatment of theoretical errors due to unknown yet-higher-dimensional operators. A consistent approach to these searches gives notably weaker, but much more theoretically robust, constraints [110, 111].

In studying the potential effects of the SMEFT, it has been found that certain operators are not able to interfere with the SM in two-to-two scatterings [112]. In particular, the operators X^3, composed of three insertions of a gauge field strength tensor, do not interfere at leading order. These non-interference phenomena are due to amplitude total helicity selection rules forcing the final state gauge bosons to have distinct helicities when generated by SM interactions, while their helicities are required to be the same in order for the X^3 operator to couple to them. However, interference effects return once higher-point amplitudes are considered, either due to the decay of unstable particles or the radiation of an additional gluon or photon [113–115]. In both of these cases nontrivial angular correlations occur, and in fact the case of particle decays has angular structure which causes the contribution to again vanish if the azimuthal decay angles are integrated over, as they normally are for the purposes of counting "2 to 2" events treating such an unstable particle as a final state. Thus, accessing the interference effects in diboson production, for instance, requires measuring these decay angles. This of course benefits greatly from knowing the full kinematics of the events, which is generally not possible in leptonic vector boson decays due to the presence of neutrinos in the final state.

Expanding the differential cross-section in powers of Λ, the first new physics term appearing, at Λ^{-2} order, is due to the interference between SM and BSM amplitude from a dimension-6 operator insertion, followed by the BSM amplitude squared and the interference between a dimension-8 operator (or pair of dimension-6 operators) in one matrix element and the SM amplitude, at Λ^{-4} .

$$d\sigma = d\sigma_{\mathrm{SM}} + \frac{1}{\Lambda^2} d\sigma_{\mathrm{SM}\times\mathrm{BSM}_6} + \frac{1}{\Lambda^4}\left(d\sigma_{\mathrm{BSM}_6^2} + d\sigma_{\mathrm{SM}\times\mathrm{BSM}_8}\right) + ... \tag{4.1}$$

However, since a complete dimension-8 basis for SMEFT is not known, it is best not to treat the $d\sigma_{\mathrm{BSM}_6^2}$ piece as signal for this analysis. We follow the treatment of [110, 111], truncating the expansion at order Λ^{-2} for the signal and considering the dimension-6 squared term as an estimation of the theory error associated with the neglect of higher orders in the perturbation series in powers of Λ^{-2}.

Tagging techniques for jets which are due to decaying heavy particles are well advanced and accepted in both the experimental and theoretical communities [116–118], and will give access to fully-reconstructable kinematics in diboson processes. In this article we explore the application of these techniques to measure the decay angles and improve the resulting reach of LHC data for these operators, while performing for the first time an analysis of diboson observables which estimates consistently the theory error due to neglecting effects higher order in Λ^{-1}.

We find that these angular-only interference effects have multiple unusual properties compared to the more typical SMEFT analysis; nontrivial azimuthal decay angle effects can only arise from interference effects between bosons of differing helicity, and even then only interferences between amplitudes for which it is impossible to choose all helicities to match are able to give rise to the asymmetry which we shall use to perform this analysis. Therefore, these analyses are sensitive to very few operators, giving a much cleaner signal model and more straightforward interpretation than usual in terms of constraints on Wilson coefficients. Additionally, this feature leads to the extremely unusual fact that the errors due to higher-dimensional operators on these observables also generically do not contribute to these asymmetries beyond correcting the overall diboson rate and thus altering the statistical fluctuations of the asymmetry variable. This stands in stark contrast to the usual state of consistent SMEFT measurements, where the number of possible causes of a deviation from the SM in any given observable is generally vast, and the theoretical uncertainties arising from higher-order EFT contributions is often significant and occasionally the dominant source of errors.

In the next section, we review the arguments for non-interference between certain SMEFT operators and SM amplitudes, and then investigate the source and nature of the azimuthal correlations that arise when the decay of the intermediate weak bosons is consistently applied. We then discuss the jet substructure techniques which we shall use to differentiate between weak bosons and ordinary QCD jets, and discuss as well how the azimuthal angles are recoverable from the standard tools already regularly used in substructure-based searches in 4.2. In 4.3, we describe in detail the search design for the LHC which can exploit these azimuthal correlations, and discuss our signal and background modelling. We then present the resulting sensitivities in 4.4 and conclude in 4.5. We include explicit calculations of the two-to-four amplitudes and an exploration of the impact of naïvely interfering operators in A.

4.1 Non-interference in the SMEFT

We work in the Warsaw basis [59], which has been constructed by systematically using the SM equations of motion to reduce the number of derivatives in the retained operators in favor of instead including more fields. This has multiple advantages, but the most important for the purposes of this article are that it ensures that corrections to propagators are due only to corrections to input parameters and retain their SM form, and it avoids couplings at higher-point vertices which have momentum dependence able to cancel the propagator of one of the particles incident on the vertex.

4.1.1 Interference obstruction for $2 \to 2$ processes

Within a derivative-reduced basis like the Warsaw basis [59], it is possible to identify the helicities of particles which can be coupled to by SM and SMEFT operators in a two-

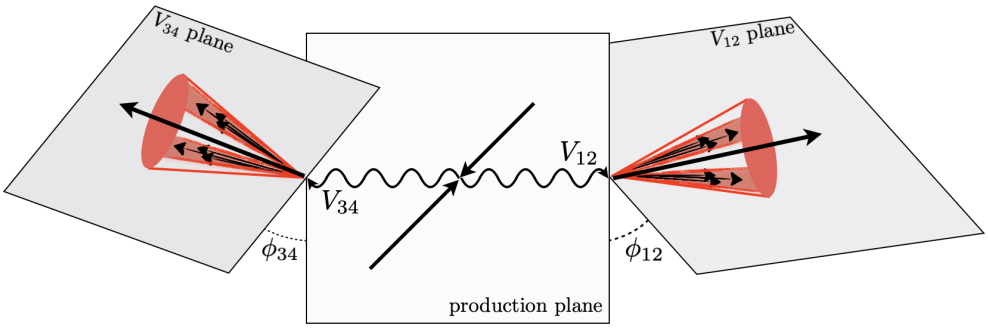

Figure 4.1: Diboson production planes and boson hadronic decay planes. For the semileptonic channel, one of the fat jets is a dilepton system but the kinematics is similar. The relevant azimuthal angles for this analysis is the angle between the production plane and the boson decay planes.

to-two scattering process by constructing the amplitude out of on-shell three-point subamplitudes. If there were a contribution that corrected the propagator in a non-standard way or a vertex with momentum dependence which could cancel the propagator on an incoming particle this would not be possible in general. Investigating the implications of these techniques, Ref. [112] finds that there are some classes of operators which do not interfere with the SM amplitudes at leading order in two-to-two scattering of definite-helicity particles, and thus have leading-order in cutoff scale interactions which do not grow with energy in the way generically expected of higher-dimensional operators, instead scaling as $\frac{m^2}{\Lambda^2}$, where m is the mass of the heaviest particle whose helicity can be flipped to allow interference with the SM amplitude.

The authors recommend to study the effect of the square of the dimension-6 operator amplitude, but the effects at this order in the inverse cutoff scale expansion are not predicted solely by the dimension-6 basis, and are thus best treated as theoretical errors rather than signal contributions [110, 111]. This non-interference has long been known in the context of higher-dimensional couplings of gluons [115], with proposals for how to probe this operator in spite of the non-interference similar to those in the electroweak case.

Multiple investigations of how best to recover from this non-interference effect have been undertaken since then, focusing on the fact that the weak bosons ultimately are not final-state particles but also decay [113,114,119]. Their decays revive the interference effect in two-to-four scattering in such a way that if the decay kinematics are not explicitly measured the interference effects again largely cancel.

4.1.2 Azimuthal structures in decay angles

All dependence on azimuthal angles in decays arises from the angular momentum portion of the gauge boson wavefunction, proportional to $e^{i\lambda\phi}$ for helicity λ and decay azimuthal angle ϕ relative to the production plane. The azimuthal angles and the relevant planes are illustrated in Figure 4.1, where the final state fermions are taken to be quarks. When an amplitude of fixed helicity is squared, these phases trivially cancel, but interfering amplitudes with different helicities will yield trigonometric functions of the decay angles. At tree level, the only imaginary contribution to the amplitude comes from the gauge boson decay and any CP violating coupling. Therefore, any CP-conserving operator gives a structure composed of cosines of the azimuthal angle of the decaying bosons. On the other hand, a CP-odd operator leads to a combination of sines due to the factor of i that appears on the operator [120]. In this article, we focus on new physics which is not CP-violating, as CP violation is generally strongly constrained by precisely-measured low-energy observables. The inclusion of $\mathcal{Q}_{\widetilde{W}}$ generates non-negligible contribution at 1-loop to the neutron electric dipole moment, therefore its Wilson coefficient should be highly suppressed [121].

Whether or not this structure is observable depends on the nature of the event being measured, though. If we are unable to distinguish experimentally between the two decaying bosons, as is the case for a fully-hadronic event, then the decay angle is not experimentally defined from 0 to 2π but rather from 0 to π, as it is experimentally not possible to orient the production plane in this case, despite the fact that quantum mechanically it is in principle observable in the full range. If, additionally, we also cannot tell apart the particle from the antiparticle in the boson decay, then the angle is actually defined only on the interval from 0 to $\frac{\pi}{2}$. In order to map the azimuthal behavior into this observable variable, it is necessary to perform two "foldings" of the distribution in each decay angle, defining the observable angular function $f(\phi)$ as [18]

$$2f(\phi) = g(\phi) + g(\pi - \phi), \qquad 2g(\phi) = h(\phi) + h(2\pi - \phi), \tag{4.2}$$

where $h(\phi)$ is the appropriate trigonometric function resulting from the helicity interference in question. In this way, $f(\phi)$ is now defined only in the observable range. Some angular distributions $h(\phi)$ vanish after being folded in this way, notably cosines of $(2n+1)\phi$, which are odd under 2π-folding.

We divide the remaining functions into two sets based on their parity under the operation $(\phi_{12}, \phi_{34}) \to \left(\frac{\pi}{2} - \phi_{12}, \frac{\pi}{2} - \phi_{34}\right)$. The set of functions which is even under this transformations are cosines of angle sums and arises in interferences of amplitudes which also are able to interfere with identical helicities. The set of functions odd under this parity are sum of cosines and can arise at tree level only from the interference of amplitudes which cannot be combined to interfere identical helicities for both gauge bosons.

[18] Here the dependence on the second decay angle is implicit for simplicity.

We calculate all the relevant amplitudes for the interference effect we are searching for, the SM background processes, and the theory uncertainty effects due to the squared BSM amplitude in **??**, and those due to the effects of other operators in **??**. After the proper foldings, the single-insertion SMEFT amplitude is:

$$\frac{d\sigma_{\rm int}(s)}{d\phi_{12}d\phi_{34}} \sim \left(-\frac{\delta\lambda_Z\, s}{m_W^2}\right)(\cos 2\phi_{12} + \cos 2\phi_{34}). \tag{4.3}$$

Strikingly, only the effects of naïvely non-interfering operators interfering with the SM give rise to angular structures which are odd under this parity transformation. The purely SM amplitude has azimuthal dependence, but that dependence is even underthis parity, as is the azimuthal dependence of the non-interfering SMEFT amplitude squared or the naïvely-interfering SMEFT operators interfering with the SM. As a result, the ability to measure an asymmetry corresponding to these odd distributions probes only the non-interfering operators, which is just $\mathcal{Q}_{\rm W}$ at leading order in $\sqrt{s}$. No other operator can produce this distribution with comparable growth in the energy tails; they either require a vev-insertion or occur only with slower energy growth.

4.2 Jet substructure with azimuthal decay angles

In the last decade, particle identification based on substructure techinques has developed explosively, with the appearance of many new techniques [116–118]. They were mainly developed to distinguish boosted tops and $W/Z/h$ bosons from QCD jets. In particular, boosted Higgs analyses led to the development of the BDRS subjet/filter algorithm [122], which made feasible the study of $pp \to HV, H \to b\bar{b}$ at the LHC. In early studies, the ATLAS and the CMS experiments used the so-called "YSplitter" [123] and the "Hopkins" top-tagger [124] to study hadronically top decay and efficiently distinguish them from QCD jets. Latter, the HEPTopTagger [125] proposed to reconstruct a not so highly boosted top, particularly useful in SUSY searches.

The jet substructure techniques can be broadly divided into two categories: jet grooming and object discrimination. The former one is built in order to remove, as much as possible, initial state radiation, underlying event, and pileup effects from the hard event of interest. The Soft Drop algorithm [126] is another example of object discrimination, built for use in tagging W/Z hadronic decays at CMS. Since it is known that QCD mostly produces 1-prong structures while W/Z and tops produces 2- and 3-prong jets, it is useful to use a tagging algorithm to discriminate 1-prong from N-prong structures, characterizing the discrimination algorithms. In this study, in order to successfully identify the boosted W boson decaying hadronically, we employ the *N-subjettiness* [127] algorithm, which introduces the jet shape variables τ_N:

$$\tau_N = \frac{1}{d_0}\sum_k p_{T,k}\min\{\Delta R_{1,k}, \Delta R_{2,k}, ..., \Delta R_{N,k}\}, \tag{4.4}$$

where $p_{T,k}$ is the transverse momentum of the particle k and $\Delta R_{J,k} = \sqrt{(\Delta\eta)^2 + (\Delta\phi)^2}$ is the rapidity-azimuth pseudo-angular distance between the subjet axis candidate J and the jet constituent particle k. The normalization is defined as $d_0 = \sum_k p_{T,k} R_0$, where R_0 is the jet radius.

This variable was designed to be minimal whenever the N-subjet hypothesis describes the jet well, i.e. there is not a need for more than N subjets, and the normalisation ensures that τ_N is near one when the jet is poorly described. However, the ratio τ_N/τ_{N-1} actually has a better discrimination power than τ_N itself. Two prong structures are well identified by smaller values of $\tau_{21} \equiv \tau_2/\tau_1$, meanwhile the other τ ratios (e.g $\tau_{32} \equiv \tau_3/\tau_2$) approach one, as both values are comparably small. We make use of τ_{32} to reject top jets and τ_{21} to separate decaying electroweak bosons from QCD background events.

In this study, we consider two decay channels: The **semileptonic** channel, where a diboson $W^{\pm}Z$ is produced with the Z decaying leptonically and $W^{\pm}$ into a fat jet and the **hadronic** channel, where a $W^{+}W^{-}$ or $W^{\pm}Z$ pair is produced and both intermediate vector bosons decay hadronically. In both channels, the final state includes boson-jets arising from the hadronically-decaying $W^{\pm}$ which are reconstructed initially as 'fat jets'. In order to look inside them and fully reconstruct the decay kinematics of the vector boson, we utilize N-subjettiness.

In Figure 4.2, we show the ratios τ_{21} and τ_{23} of the single $R = 1.0$ fat jet produced in the semileptonic channel, for the BSM single insertion of $\delta\lambda_Z$, for the diboson SM production and for the SM background Z+jets. As we can clearly see, τ_{21} is small for BSM and SM and peak around 0.6 for Z+jets, which suggests that the two former channels have a 2-prong structure most of the time, while for the Z+jets the τ's behaviour does not favour this hypothesis. In Figure 4.3, we see a similar behaviour for the hadronic channel, where we obtain the 2-prong structure for BSM and SM diboson production but not for multijet production. The substructure tagging efficiencies for both channels considered in this study are shown in Table 4.1 and 4.2. In both channels we have confirmed that the search design cuts consider in Section 4.3 does not affect this behaviour. Note that the propensity for the BSM signal events to be two-prong-like with low τ_{21} is even greater than that for the SM diboson events; this arises from the fact that this interference process effectively causes the polar decay angle to behave in a way reminiscent of longitudinal gauge bosons, even though it is the result of interfering transverse bosons of opposite helicity; see A for details.

After identifying the tagged events, we need to reconstruct the azimuthal angles of the decay plane. As a proxy for the decay product partons' directions of travel, we utilize the subjet axes which appear in the definition of the N-subjettiness. These axes depend on a recombination scheme, for which we utilize One-pass Winner-Take-All (WTA) k_T algorithm; this matches quite well the partonic momenta [128], and we have confirmed explicitly that One-pass E-Scheme k_T Axes do not yield noticeably different results.

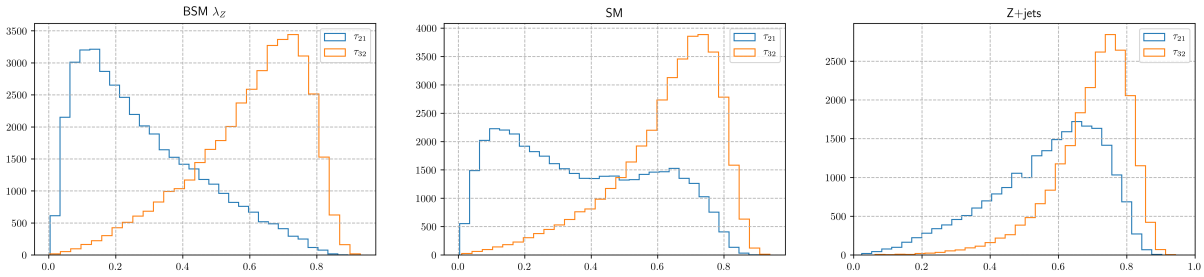

Figure 4.2: *N-subjettiness* ratios τ_{21} and τ_{32} for the single fat jet in the Semileptonic channel, plotted separately for the signal case as well as the SM irreducible background diboson processes and the SM QCD background due to Z boson and jet associated production.

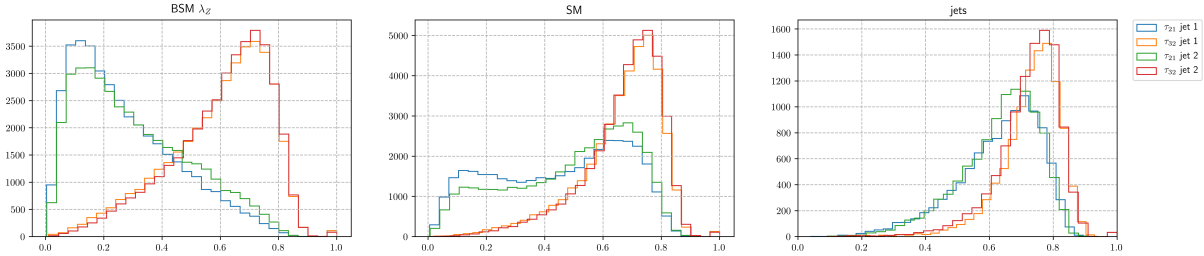

Figure 4.3: *N-subjettiness* ratios τ_{21} and τ_{32} for both fat jets in the fully hadronic channel, plotted separately for the signal case as well as the SM irreducible background diboson processes and the SM QCD background due to multijet production.

4.3 Search design at the LHC

We implemented the relevant operators for this analysis in `FeynRules` [129] and the simulation for the hadronic and semileptonic channel was performed using `MadGraph5` [130], followed by showering/hadronization via `PYTHIA 8` [131]. The fat jets were reconstructed with $R = 1.0$ using anti-k_T and E-scheme recombination. Each fat jet is then required to have 2 subjets and its axes are reconstructed using WTA k_T. The subjet reconstruction was done using `FastJet` [132, 133].

The calorimeter cannot resolve tracks that lie within the same cell (0.1×0.1) in $(\phi \times \eta)$ and also does not identify soft particles $p_T < 0.5$. We performed the analysis with and without the calorimeter granularization and no non-trivial structure is introduced due to the calorimeter; we retain this constraint on our simulated calorimeter to remain conservative in our estimates of what sensitivity can be reached.

We also investigated the effects of two techniques of jet grooming for pileup suppression applicable to anti-k_T jets: Jet Trimming ($R_{\text{trim}} = 0.3$ and $p_{\text{T,frac}} = 0.05$) and Pruning ($R_{\text{cut}} = 0.1$ and $z_{\text{cut}} = 0.05$). The signal events exhibited no relevant modifications in the

azimuthal pattern nor in cut efficiencies, indicating reasonable robustness of this analysis technique against pileup effects.

Several backgrounds contribute to diboson production; for the fully-hadronic case, the expected background for this search consists of multijet events ($pp \to jj, jjj, jjjj$), SM W^+W^- production, $t\bar{t}$, $W+$ jets and tW production. In the semileptonic analysis, we have Z+jets, $t\bar{t}$ production and SM WZ production. While none of these backgrounds intrinsically contribute to the asymmetry we search for here, care must be taken to ensure that the analysis cuts do not induce such an asymmetry accidentally; we've explored the effect of each cut and confirmed that they do not cause such azimuthal distortions in the background distributions.

Although the signal diboson cross-section for the hadronic channel is larger than that for the semileptonic due to the greater hadronic branching ratios and inclusion of the W^+W^- intermediate state, it suffers from more background contamination due to the presence of pure-QCD backgrounds. With a good choice of topology and tagging cuts we can largely eliminate peaking backgrounds without spoiling the BSM interference pattern, which are shown in Tables 4.1 and 4.2. Background suppression cuts importantly include an acoplanarity cut to ensure a back-to-back diboson production and a cut requiring a small p_T asymmetry, defined as $(p_{T_1} - p_{T_2})/(p_{T_1} + p_{T_2})$, between the two fat jets (or the fat jet and the dilepton system) in order to remove events with one poorly reconstructed jet. Tagging cuts include a fat jet mass requirement (or dilepton mass in the semileptonic case), small τ_2/τ_1 for the fat jet, and an 3-prong structure rejection, which means a large τ_3/τ_2. The cut values we employ are:

- fat jet mass: $40 \leq m_j \leq 100$ GeV (hadronic) and $65 \leq m_j \leq 105$ GeV (semileptonic)
- dilepton mass: $80 \leq m_{\ell\ell} \leq 100$ GeV
- acoplanarity: $\Delta\phi < 0.5$
- $\mathrm{p_T}$ asymmetry: $\Delta p_{\mathrm{T}} < 0.15$
- tagging: $(\tau_2/\tau_1 < 0.45)$ and $(\tau_3/\tau_2 > 0.45)$ for all fat-jets

We note that the SM diboson distributions do not exhibit strong dependence on the azimuthal decay angles (see A for parton-level details), and neither do any backgrounds after passing these cuts. Meanwhile, these cuts do not change the azimuthal behaviour for the BSM interference term. We show both channels for the particular center-of-mass energy 0.9 TeV $\leq \sqrt{\hat{s}} \leq$ 1.1 TeV in Figure 4.4.

In order to construct an asymmetry variable to maximize the sensitivity to new physics effects, we define two regions of the azimuthal plane:

$$\text{Region A}: \ \phi_{V_i} \in [\pi/4, \pi/2] \quad \text{and} \quad \text{Region B}: \ \phi_{V_i} \in [0, \pi/4]\,, \tag{4.5}$$

cut	BSM($\delta\lambda_Z$) [%]		SM [%]		W+jets [%]		tW [%]		$t\bar{t}$ [%]		jets [%]
fat jet mass	68.4	68.4	28.2	28.2	1.66	1.66	15.4	15.4	14.0	14.0	-
acoplanarity	15.3	32.9	34.9	13.1	18.76	0.77	20.3	6.1	20.6	5.3	-
p_T asymmetry	89.0	31.3	76.2	11.9	35.98	0.59	38.3	4.3	39.8	3.8	-
tagging	39.1	15.3	18.8	6.1	2.62	0.20	12.5	2.0	11.7	1.7	-
total	15.3		6.1		0.20		2.0		1.7		10^{-3}

Table 4.1: Efficiency table for topology and tagging cuts for the hadronic case for the center-of-mass-energy 0.5 TeV $\leq \sqrt{\hat{s}} \leq$ 2.1 TeV. The first (second) column of each background represent the individual (sequential) cut efficiency. For the jets background, we assumed the ATLAS [134] efficiency; note that our tagging efficiency for bosons is actually slightly below the ATLAS number, so this efficiency is a conservative estimate.

cut	BSM($\delta\lambda_Z$) [%]		SM [%]		Z+jets [%]		$t\bar{t}$ [%]	
fat jet and dilepton mass	60.7	60.7	31.8	31.8	7.10	7.10	7.73	7.73
acoplanarity	47.8	29.9	30.8	12.1	7.10	0.57	7.99	0.62
p_T asymmetry	93.5	29.2	57.1	10.8	20.46	0.08	14.13	0.04
tagging	63.3	21.7	44.9	8.5	22.95	0.05	24.69	0.02
total	21.7		8.5		0.05		0.02	

Table 4.2: Efficiency table for topology and tagging cuts for the semileptonic case for the center-of-mass-energy 0.5 TeV $\leq \sqrt{\hat{s}} \leq$ 2.1 TeV. As in the hadronic case, the first (second) column is the individual (sequential) cut efficiency.

where $i = 1, 2$ and VV is W^+W^- in the hadronic case and $W^\pm Z$ in the semileptonic. These regions are replicated to the other quadrants after the foldings described in 4.2. Then, the asymmetry is defined as

$$\mathcal{A}(s) \equiv \frac{N_A - N_B}{N_A + N_B}, \tag{4.6}$$

where $N_{A(B)}$ is the number of events in respective region.

The number of events in each region is proportional to the total reconstructed cross-section including SM backgrounds and the single-insertion interference cross-section. While the BSM term has opposite sign between regions A and B, which add up in the numerator and cancels in denominator, the dominant backgrounds, *i.e.* jets (Z+jets) for the hadronic (semileptonic), are effectively flat in this angular space, resulting in the opposite effect. Therefore one naïvely expects that the asymmetry should exhibit quadratic growth with $\sqrt{s}$; this is indeed the case when SM diboson production is treated as the sole as background. However, this is not the largest background for this process. The QCD jets (Z+jets) are the dominant background; including them, the asymmetry does grow but

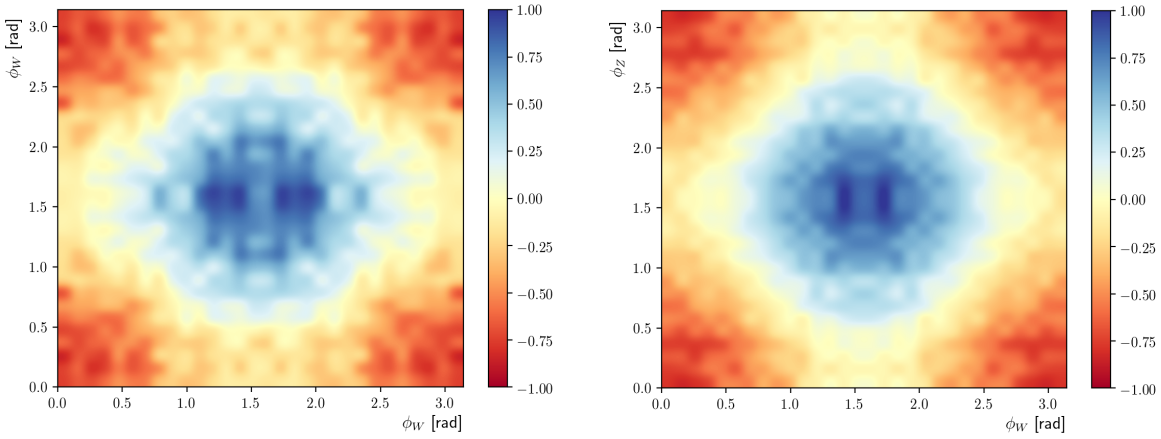

Figure 4.4: Hadronic (left) and Semileptonic (right) SMEFT-SM interference cross-sections after the reconstruction, calorimeter granularization and analysis cuts. (z axis in arbitrary units). After the foldings, Region A (B) is largely overlapping with the blue (red) region.

it is no longer quadratic. This arises due to the access of the background processes to PDF components with different momentum-fraction dependence compared to those of the diboson processes.

In general, the effects of generic SMEFT contributions grow with energy compared to the SM backgrounds, thus it is best to consider the measured asymmetry as a function of the center-of-mass energy. In Figure 4.5, we plot the absolute asymmetry, including all backgrounds, for the LEP 2σ maximal bound[19] of $\max(|\delta\lambda_Z|) = 0.059$ [135], with the illustrative assumed systematic error of 0.1% on the asymmetry and statistical errors assuming an LHC integrated luminosity of 3 ab^{-1}. Note that the theory errors, illustrated as the blue region around the prediction, remain subdominant in all regions of parameter space due to their not contributing directly to the asymmetry, and instead only altering the symmetric background rate.

[19] The LEPII analysis, much like many others, was driven by the EFT contribution at order Λ^{-4}, which is incompletely calculated as the square of the EFT contribution and subject to the effects of many other (neglected) operators; Here, with our analysis cuts, vector bosons are effectively on-shell and the signal prediction is appropriately truncated, yielding an observable which is sensitive to just this operator.

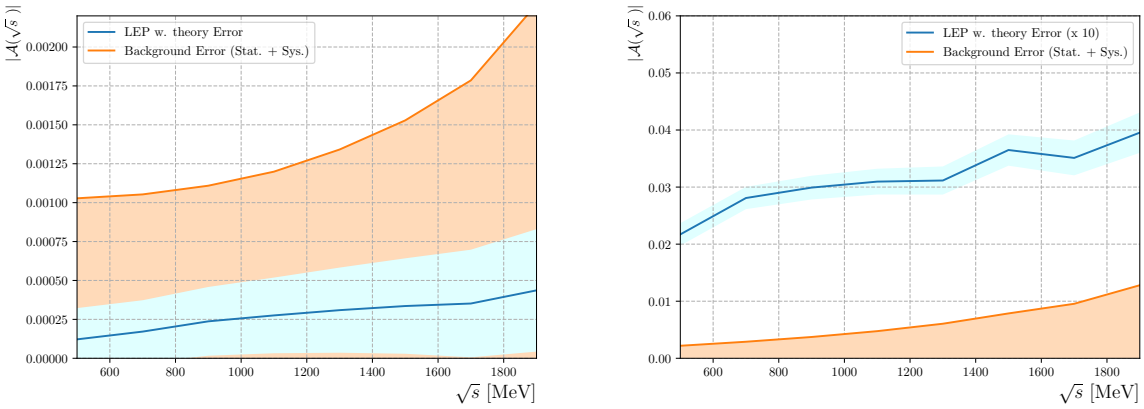

Figure 4.5: Hadronic (left) and Semileptonic (right) absolute asymmetry plots. The blue curves are the asymmetries predicted by the LEP bound value of C_W. The statistical and systematic (illustratively chosen to be 0.1% on the asymmetry) uncertainties are shown by the orange shaded region, and the theoretical error due to higher order EFT effects is the blue shaded region around the predicted asymmetry; note that the theoretical error for the semileptonic case has been increased by a factor of 10 for readability.

4.4 Detection reach at the LHC

Our sensitivity to these asymmetries is driven by the statistical uncertainty of the SM backgrounds; experimental systematic uncertainties are largely independent of these decay angles, and therefore cancel in the asymmetry. We thus present results assuming the statistical error is dominant and results assuming a systematic uncertainty on the asymmetry measurement of 0.1%, independent of the integrated luminosity.

It is of course necessary to include theoretical errors on the signal model as well. However, we note that the squared amplitude contribution of various operators do not themselves contribute to the asymmetry, only to the number of symmetric events in the background; this holds true for a number of other operator contributions which we have checked explicitly as well. Detailed parton-level calculations are presented in A. Treating the squared SMEFT contributions (with an inflated value of C_W such that $\frac{C_W}{\Lambda^2} = \frac{g}{6m_w^2}$ to remain as conservative as possible) as a theoretical uncertainty on the signal model, we find that this term produces a structure on the azimuthal plane with peaks around $\phi_V = 0$ and $\phi_V = \frac{\pi}{2}$; these two peaks cancel each other in the asymmetry. This contribution has the same pattern ($d\sigma = a + b\cos 2\phi_{12}\cos 2\phi_{34}$) as the purely-SM cross section, but with different coefficients of the two terms. These errors are shown as blue shaded areas around the predicted asymmetries in 4.5.

Our ultimate reach for detecting these asymmetries at the LHC as a function of integrated luminosity is shown in Figure 4.6. The green and orange regions represent the LHC sensitivity to the corresponding value of $|c_W/\Lambda^2|$ in the semi-leptonic and fully hadronic channels, respectively. We also indicate the LEP bound, the current LHC 2σ bound from Ref. [91] (both of which are driven by the theoretically ill-defined $\frac{1}{\Lambda^4}$ EFT contribution), and two prospective reaches, at 300fb^{-1} and 3ab^{-1}, from Ref. [113] arising from a fully-leptonic final state analysis which neglects the EFT errors due to terms of order $\frac{1}{\Lambda^4}$, but at least does not treat them as signal contributions. As expected, the more data LHC accumulates, smaller values of c_W/Λ^2 can be probed. Even though the total rejection factor for the hadronic channel background is 3 orders of magnitude better than the semileptonic and the signal cross section is larger as well, the QCD multijet background remains problematic. Ultimately, our analysis favours the semileptonic channel in detection reach. We note that, in addition to these two channels, it is also possible to study the azimuthal decay angle of a vector boson produced in association with a leptonically-decaying $W^\pm$ boson using these techniques, but have focused here on final states in which both angles can be reconstructed; single-angle events will not provide a significantly stronger constraint than the two-angle semileptonic study presented here.

4.5 Summary

We have demonstrated in this article that it is possible to obtain interference measurements in "non-interfering" four point amplitudes using jet substructure techniques. Tagging the subjets with *N-subjettiness* and reconstructing their azimuthal decay angles allows us to probe the anomalous triple gauge coupling generated by the $\mathcal{Q}_{3\text{W}}$ operator. With a single-insertion of this operator, patterns exclusive to this operator occur in the azimuthal plane, allowing the construction of an asymmetry maximally sensitive to it and that vanishes for other contributions.

This provides a cross-check of an observable which has been consistently calculated in the SMEFT, including honest theory error appraisals. Thus, it continues the work toward developing the needed machinery to perform a fully-general, model-independent analysis of the implications of precision SM measurements at the LHC and elsewhere on heavy new physics. It is interesting to note that, in the at least semi-hadronic signals considered here, the theory errors remain always subdominant to the SM statistical errors, which stands in stark contrast to the other signatures studied consistently in the SMEFT. This arises because of the unique nature of these azimuthal interference patters even within the SMEFT itself, preventing other operators from contributing to the constructed asymmetry. The errors in a purely leptonic analysis which properly truncates its signal at leading order in SMEFT effects are similarly suppressed.

It is particularly interesting that these techniques give access to observables which measure exactly one term in the Warsaw basis of the SMEFT Lagrangian, since other observables require a higgs-vev insertion and, since they do not have an extra derivative,

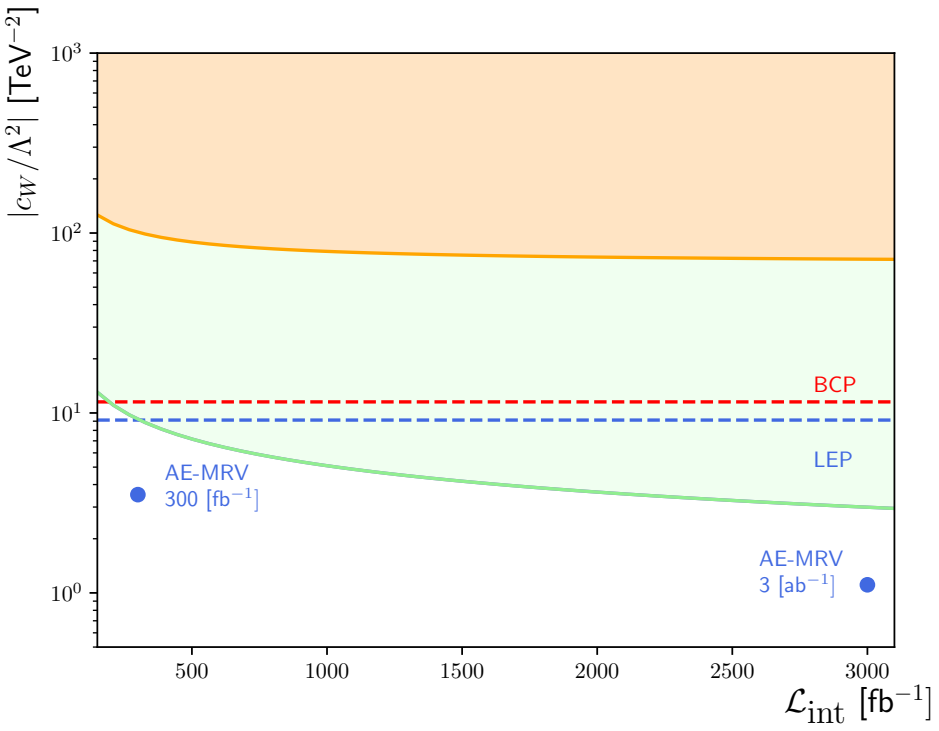

Figure 4.6: Hadronic (orange) and Semileptonic (green) detection reach as a function of the integrated luminosity. We also show the LEP 2σ bound for this operator, the recent projections (AE-MRV) from Ref. [113] for 300fb^{-1} and 3ab^{-1} and the 2σ bound (BCP) from a LHC Run II based global analysis [91], which has a similar treatment of this operator to the LEP analysis.

they do not flip one of the diboson helicities. This lack of helicity flip makes an azimuthal distribution which is not doubly-odd, therefore cancels in the asymmetry at leading order.

Another possibility of this technique is to construct a similar search for these non-interference effects in the QCD sector, as initially proposed in [115] and recently revisited in [136]. We shall explore whether these substructure techniques now make this azimuthal angular search possible in a future publication.

5 The impact of flavour data

This section is based on the paper ***'The impact of flavour data on global fits of the MFV SMEFT'****. [3]. The preprint is currently in preparation for publication in JHEP.*

5.1 Introduction

The SMEFT Lagrangian contains a large number of Wilson coefficients. As seen in Sec. 3, these are unknown parameters which need to be constrained. In order to put feasible bounds on them, one should use as much data as possible. As well as LHC measurements, we have precise data from LEP measurements, Standard Model-forbidden process experiments, high-precision measurements like parity-violating electron scattering experiments, and flavour physics experiments. Much of these have already been incorporated into EFT fits, but flavour observables have generically been applied only to explicitly flavour-symmetry violating new physics scenarios.

The flavour data puts the strongest constraints on flavour violation models[20]. Thus, new physics models usually have a flavour symmetry such that the parameter space is not ruled out by the flavour constraints. A natural way to avoid such bounds is to construct a model with similar flavour structure of the SM, which contains a $U(3)^5$-symmetry in the vanishing Yukawa matrices limit. A possible ultraviolet flavour symmetry is then to assume $U(3)^5$ or that any breaking of this symmetry is given by the Yukawa matrices, as in the SM. This goes by the name of "Minimally Flavour Violating" [72]; i.e. with new sources of flavour and CP violation only proportional to the Standard Model (SM) Yukawa matrices. This hypothesis ensures the flavour structure is similar to that in the SM, and thus significantly lowers the scale of new physics needed to be consistent with measurements in the flavour sector.

New physics effects at tree-level would be highly suppressed by the current data and, studying loop-level BSM is more than necessary. These are unavoidable even in models with no new sources of flavour breaking; loops involving W bosons will always induce flavour changing neutral currents even from flavourless interactions. In this article, we explore these loop level contributions in detail, within the framework of the leading order MFV SMEFT. Under this assumption, each dimension-six operator is multiplied by the minimum number of spurionic Yukawa matrices needed to make it formally invariant under the $U(3)^5$ flavour symmetry. This means that the theory does not contain tree level flavour changing neutral currents (FCNCs). The motivations for MFV are two-fold: one, that it allows for an approximation of the minimum, baseline effects that can be expected to be seen in flavour observables if physics beyond the Standard Model (BSM) exists; and two, that it is often used already in global SMEFT fits to electroweak and LHC data, so the value of flavour information can be analysed in this context.

[20] See Ref. [137] for bounds on flavour-changing SMEFT operators from meson mixing

Group	Operators	$d_i \to d_j\gamma$	$d_i \to d_j\, l^+l^-$	Meson mixing
1	Q_G	-	-	-
	Q_W	✔	✔	-
2	Q_H	-	-	-
3	$Q_{H\Box}$	-	-	-
	Q_{HD}	✔	✔	-
4	Q_{HG}	-	-	-
	Q_{HW}	-	-	-
	Q_{HB}	-	-	-
	Q_{HWB}	✔	✔	-
7	$Q^{(1)}_{H\ell}$	-	✔	-
	$Q^{(3)}_{H\ell}$	✔*	✔	✔*
	Q_{He}	-	✔	-
	$Q^{(1)}_{Hq}$	-	✔	-
	$Q^{(3)}_{Hq}$	✔	✔	✔
	Q_{Hu}	-	✔	-
	Q_{Hd}	-	-	-

Group	Operators	$d_i \to d_j\gamma$	$d_i \to d_j\, l^+l^-$	Meson mixing
8: $(\bar{L}L)(\bar{L}L)$	$Q_{\ell\ell}$	✔*	✔*	✔*
	$Q^{(1)}_{qq}$	-	✔	✔
	$Q^{(3)}_{qq}$	-	✔	✔
	$Q^{(1)}_{\ell q}$	-	✔	-
	$Q^{(3)}_{\ell q}$	-	✔	-
8: $(\bar{R}R)(\bar{R}R)$	Q_{ee}	-	-	-
	Q_{uu}	-	-	-
	Q_{dd}	-	-	-
	Q_{eu}	-	✔	-
	Q_{ed}	-	-	-
	$Q^{(1)}_{ud}$	-	-	-
	$Q^{(8)}_{ud}$	-	-	-
8: $(\bar{L}L)(\bar{R}R)$	$Q_{\ell e}$	-	-	-
	$Q_{\ell u}$	-	✔	-
	$Q_{\ell d}$	-	-	-
	Q_{qe}	-	✔	-
	$Q^{(1)}_{qu}$	-	-	-
	$Q^{(8)}_{qu}$	-	-	-
	$Q^{(1)}_{qd}$	-	-	-
	$Q^{(8)}_{qd}$	-	-	-

Table 5.1: Table reproduced from Ref. [71]: All operators that are invariant under CP and the $U(3)^5$ flavour symmetry. Ticks indicate that they contribute to the FCNC processes we consider. An asterisk $(*)$ signifies that the contribution is only indirect, via effects in input parameter measurements.

The matching of flavour-singlet operators to $d_i \to d_j l^+l^-$, $d_i \to d_j\gamma$ and down-type meson mixing processes was originally calculated in [71]; In Table 5.1, we reproduce the tables from [71] with the operators invariants under CP and $U(3)^5$. In this work, we provide the matching also of operators which are necessarily Yukawa-weighted in the MFV scheme. We also provide the full one-loop matching under our flavour assumptions to $d_i \to d_j\bar{\nu}\nu$ processes. The full one-loop matching for arbitrary flavour structures has been completed in [138], and we cross-check our results against theirs as appropriate. The additional steps provided by our calculations (including transforming to a physical mass basis and including the effects of SMEFT operators on input measurements) allow our results to be directly compared with measurements and straightforwardly incorporated into SMEFT fits.

The flavour structure of the MFV SMEFT was already presented in Sec. 3.8 but in the next section we explain some further assumptions made. In Section 5.3 we discuss the observables which we consider here to derive our constraints and present the linear combinations of SMEFT Wilson coefficients which contribute to those observables. We perform a simple global fit in Section 5.4 to demonstrate the impact of flavour data, and discuss our findings in Section 5.5. We present analytic results of the Yukawa-weighted operator matching and the relevant matching calculations for processes with final-state neutrino pairs, as well as numerical results for all matching calculations, in the Appendices.

5.2 Conventions and notation for the MFV SMEFT

The MFV SMEFT Lagrangian follows the description of Sec. 3.8 and Sec. 3.7. With these conventions, the Yukawa terms of the SM Lagrangian are rendered formally flavour symmetric;

$$\mathcal{L}_{\text{Yukawa}} \supset -Y_u \tilde{H} \bar{q} u - Y_d H \bar{q} d - Y_e H \bar{l} e + h.c.. \tag{5.1}$$

For the coefficient of each SMEFT operator we take only the lowest order (but non-zero) terms in the symmetry breaking parameters Y_u, Y_d and Y_e that are needed to construct a singlet under the $U(3)^5$ symmetry. To illustrate this, we can take the example of the operator $Q_{Hq}^{(1)} = (H^\dagger i \overleftrightarrow{D}_\mu H)(\bar{q}_i \gamma^\mu q_j)$. Since this operator can be made into a $U(3)^5$ singlet by contracting the two quark doublet indices, the lowest order coefficient here requires no Yukawa insertions and is simply $\delta_{ij} C_{Hq}^{(1)}$.

As shown in Sec. 3, the location of the CKM matrix is in the down sector $(d'_L, s'_L, b'_L)^{\text{T}} = V_{\text{CKM}} (d_L, s_L, b_L)^{\text{T}}$. Thus, the relation between the Yukawa matrices in the mass basis $\hat{Y}_u$ and $\hat{Y}_d$ and the interaction basis, Y_u and Y_d above, as

$$Y_u \equiv \hat{Y}_u, \qquad Y_d \equiv V \hat{Y}_d. \tag{5.2}$$

A further simplification is made, where only the top and bottom Yukawa couplings, y_t and y_b, are considered on the diagonalised Yukawa matrices. The other entries are considered to be zero. To illustrate the flavour structure, we present in Table 5.2, operators coefficient and how Yukawa insertions affect each of them. We separate the Yukawas from the dimensionful Wilson coefficients $C_a = c_a/\Lambda^2$, such that all Yukawa suppressions are explicit and all Wilson coefficients may naïvely be expected to be of similar magnitude, independent of the operator classification. This also implies that while operators can be thought of as having flavour indices (which are contracted with those of Yukawa and/or CKM matrices), SMEFT Wilson coefficients in our notation do not.[21] For example, within our assumptions there is only one C_{uB} or C_{dB}.

An extra care has to be taken with some operators, regarding the flavour indices. We can contract the flavour indices in the same Lorentz-bilinear our across them, making two possible contractions. The former one labelled unprimed while the latter comes primed. These two contractions operators includes $Q_{ll} = \left(\bar{l}_p \gamma_\mu l_r\right)\left(\bar{l}_s \gamma^\mu l_t\right)$ and $Q_{quqd}^{(1)} = (\bar{q}_i^\alpha u_j)\, \epsilon_{\alpha\beta} (\bar{q}_k^\beta d_l)$. This is illustrated by the last two examples in Table 5.2.

The one-loop matching between a $U(3)^5$-singlet SMEFT and WET for operators mediating $d_i \to d_j l^+ l^-$, $d_i \to d_j \gamma$ and $d_i \bar{d}_j \to d_j \bar{d}_i$ processes were given in Ref. [71]. Here, we take one step further and present a similar matching for all the SMEFT operators which require quark Yukawa insertions under our flavour assumptions. For example, the operator Q_{Hud} matches to $C_7^{bd_j}$ through diagrams in Figure 5.1, as well as to $C_8^{bd_j}$ through

[21] This should be kept in mind if our results are to be used in global fits, since some references instead absorb the Yukawas into the Wilson coefficients, such that they are defined as the full expressions in the last column of Table 5.2.

Transformation under $U(3)_q \times U(3)_u \times U(3)_d$	Example operator	Operator coefficient	Coefficient with only y_b, y_t nonzero
$(\bar{3} \otimes 3, 1, 1)$	$(H^\dagger i \overleftrightarrow{D}_\mu H)(\bar{q}_i \gamma^\mu q_j)$	$C_{Hq}^{(1)}\, \delta_{ij}$	$C_{Hq}^{(1)}\, \delta_{ij}$
$(\bar{3}, 3, 1)$	$(\bar{q}_i \sigma^{\mu\nu} u_j) B_{\mu\nu}$	$C_{uB}\, (Y_u)_{ij}$	$C_{uB}\, y_t \delta_{i3} \delta_{j3}$
$(\bar{3}, 1, 3)$	$(\bar{q}_i \sigma^{\mu\nu} d_j) B_{\mu\nu}$	$C_{dB}\, (Y_d)_{ij}$	$C_{dB}\, y_b V_{ib} \delta_{j3}$
$(1, \bar{3}, 3)$	$i(\tilde{H}^\dagger D_\mu H)(\bar{u}_i \gamma^\mu d_j)$	$C_{Hud}\, (Y_u^\dagger Y_d)_{ij}$	$C_{Hud}\, y_t y_b V_{tb} \delta_{i3} \delta_{j3}$
$(\bar{3} \otimes 3 \otimes \bar{3} \otimes 3, 1, 1)$	$(\bar{q}_i \gamma_\mu q_j)\, (\bar{q}_k \gamma^\mu q_l)$	$C_{qq}^{(1)}\, \delta_{ij} \delta_{kl}$ $C_{qq}^{(1)\prime}\, \delta_{il} \delta_{kj}$	$C_{qq}^{(1)}\, \delta_{ij} \delta_{kl}$ $C_{qq}^{(1)\prime}\, \delta_{il} \delta_{kj}$
$(\bar{3} \otimes \bar{3}, 3, 3)$	$(\bar{q}_i^\alpha u_j) \epsilon_{\alpha\beta} (\bar{q}_k^\beta d_l)$	$C_{quqd}^{(1)}\, (Y_u)_{ij} (Y_d)_{kl}$ $C_{quqd}^{(1)\prime}\, (Y_u)_{kj} (Y_d)_{il}$	$C_{quqd}^{(1)}\, y_t y_b V_{kb} \delta_{i3} \delta_{j3} \delta_{l3}$ $C_{quqd}^{(1)\prime}\, y_t y_b V_{ib} \delta_{k3} \delta_{j3} \delta_{l3}$

Table 5.2: Structure of Lagrangian coefficients for operators with quark flavour indices. The coefficients in the final column are given in the flavour basis defined by Eqns. (5.2). All columns apart from the last are flavour-basis-independent (if no assumptions are made about the diagonality of the Yukawa matrices).

diagrams similar to the second and sixth diagram in Figure 5.1 (with the photon replaced by a gluon):

$$C_7^{bd_j} = v^2 y_t^2 C_{Hud} \left(\frac{-5x_t^2 + 31x_t - 20}{24(x_t-1)^2} + \frac{x_t(2-3x_t)}{4(x_t-1)^3} \log x_t \right) \tag{5.3}$$

$$C_8^{bd_j} = v^2 y_t^2 C_{Hud} \left(-\frac{x_t^2 + x_t + 4}{8(x_t-1)^2} + \frac{3x_t}{4(x_t-1)^3} \log x_t \right) \tag{5.4}$$

All the matching expressions can be found in App. E and F. The contributing operators

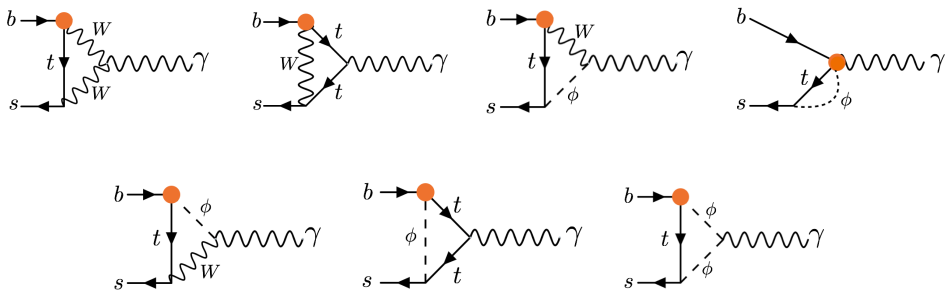

Figure 5.1: Diagrams generating contributions to $b \to s\gamma$ from the Q_{Hud} operator

and the relevant process are listed in Table 5.3; they include dipole operators, Yukawa-like operators with extra Higgs bosons, one Higgs-fermion mixed current operator which gives rise to a $W^{\pm}$ boson right-handed coupling, and scalar-current four-quark operator. Furthermore, we present the matching of all MFV SMEFT operators to $d_i \to d_j \bar{\nu}\nu$ processes, in Appendix F.

Operator	$y_t Q_{uH}^{33}$, $y_b V_{ib} Q_{dH}^{i3}$	$y_t Q_{uG}^{33}$	$y_t Q_{uW}^{33}$	$y_t Q_{uB}^{33}$	$y_b V_{ib} Q_{dG}^{i3}$, $y_b V_{ib} Q_{dB}^{i3}$	$y_b V_{ib} Q_{dW}^{i3}$	$y_b y_t V_{tb} Q_{Hud}$ $y_t y_b V_{ib} Q_{quqd}^{(1,8)}$
$d_i \to d_j \gamma$	-	✔	✔	✔	-	✔	✔
$d_i \to d_j l^+ l^-$	-	-	✔	✔	-	-	-
$d_i \to d_j \, \bar{\nu}\nu$	-	-	✔	-	-	-	-
Meson Mixing	-	-	✔	-	-	-	-

Table 5.3: All operators which are brought into flavour symmetric form with insertions of y_t and/or y_b. Tick marks indicate that the operator in that row contributes to the flavour-violating process of interest in that column. In the last column, the second operator represents $y_t y_b V_{kb} Q_{quqd}^{(1,8)} = \{y_t y_b V_{kb} Q_{quqd}^{(1)33k3}, y_t y_b V_{kb} Q_{quqd}^{(8)33k3}, y_t y_b V_{ib} Q_{quqd}^{(1)i333}, y_t y_b V_{ib} Q_{quqd}^{(8)i333}\}$

5.3 Connecting to flavour observables

Connecting SMEFT and low-energy measurements requires three steps This process is illustrated in Fig 5.2 and given the Wilson coefficients at the new physics scale Λ, one must:

- *(i)*: run (🏃) from Λ down to the electroweak scale m_W through γ_{SMEFT},
- *(ii)*: perform a one-loop matching (🏃🏃) between the SMEFT and the WET, and
- *(iii)*: run (🏃) from m_W down to the flavour observable scale. This running is given by the WET anomalous dimension matrix, γ_{WET}.

Furthermore, the effect of the two different input schemes in the electroweak input schemes has to be taken into account. This effect is explained in Sec 3. We present matching results in two common input schemes in which the electroweak input measurements are respectively $\{\alpha_{\text{em}}, m_Z, G_F\}$ and $\{m_W, m_Z, G_F\}$. Since we work consistently to $O(1/\Lambda^2)$, parameters which are already multiplying dimension 6 SMEFT coefficients in the results are unaffected by the input scheme choice.

Under the MFV assumptions, we may take the CKM parameters to be unshifted with respect to the SM. This can be justified by noting that, even when including NP effects,

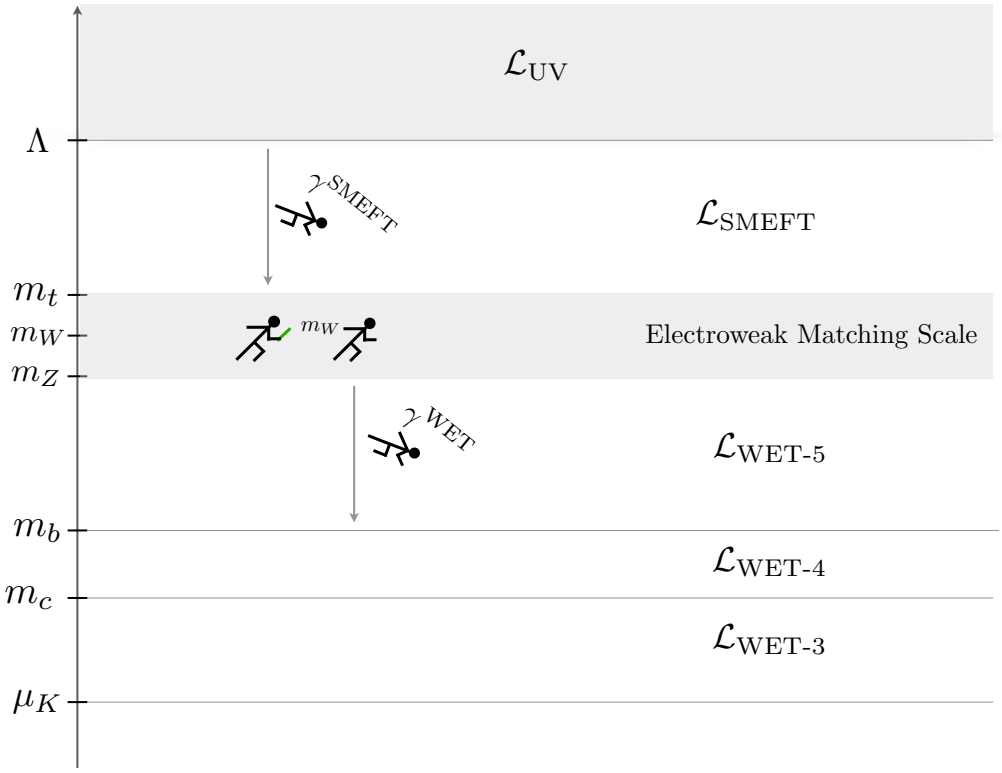

Figure 5.2: Weak Effective Theory: Running and matching procedures. The WET-5 represent the five quarks in the theory and as one run down, the number of quarks in WET decreases and the proper running and matching should be considered.

the ratio of similar processes involving different quarks will always be proportional to the same CKM ratios as in the SM. So if the values of CKM elements are fixed with an appropriate set of four or more input measurements based on ratios of observables, the extracted values will be unchanged compared to a SM fit. Recently, Ref. [139] proposed a CKM input scheme that can be applied to the general (flavour-violating) SMEFT, in which they identified four optimal inputs to fix the CKM parameters. Their particular choice of inputs was partially motivated by the fact that some processes can be complicated in the general case by the need for new unknown matrix elements and form factors, due to flavour and chirality structures in the BSM interactions which are not present in the SM. These difficulties don't arise in the MFV scenario we consider; as we shall see in more detail below, the flavour and chirality structures that result are identical to those in the SM. We therefore assume an appropriate input scheme such that the CKM matrix is unshifted in this theory (all shifts to charged-current interactions are described by corrections to the gauge coupling g_2 and/or the electroweak vev v) and FCNC processes may be used as constraints on Wilson coefficients rather than as would-be SM input parameters.

The observables considered in this analysis has take into account its sensitivity to new physics. Theoretical clean observables and well-understood are favoured. We are going to consider the down-type FCNC processes and most of the observables comes from B-physics, where we focus our attention on (semi-)leptonic and photonic meson decays, and meson mixing.

The reason for not considering up-type is twofold. First, the up-type FCNC currents $u_i \to u_j$ are suppressed by $O(m_b^2/m_t^2)$ compared to the down-type, due to the GIM mechanism. Second, theoretical uncertainties are larger in D meson system than in B meson. This is mostly due to the fact that the charm system is too heavy for χPT and too light for heavy-quark effective theory (HQET). Within the down-type sector, most of the constraints come from B-physics because the kaon equivalents observables are affected by long-distance contributions, which pollute the constrain power of these observables. Exceptions are the "golden channels" $K_L \to \pi^0\bar{\nu}\nu$ and $K^+ \to \pi^+\bar{\nu}\nu$, which we include in our analysis, and the observables ϵ and ϵ', which measure direct and indirect CP violation in kaon mixing and $K \to \pi\pi$ respectively, and which we do not include since there are no new CP violating phases in our model[22].

5.3.1 Effective theory below the electroweak scale

The matching calculations presented in Appendices E and F and Ref. [71] provide the Wilson coefficients of the WET in terms of the Wilson coefficients of the SMEFT, both at the electroweak scale. In Sec 5.2 , we presented the Hamiltonian for the $d_i \to d_j l^+ l^-$ and $d_i \to d_j \gamma$ transitions to which the flavour-symmetric SMEFT matches.

The set of operators is identical to those present in the matching of the SM alone (note the absence of any right-handed current, primed operators) as a result of the flavour symmetry imposed. Since we also match with the $d_i \to d_j \bar{\nu}\nu$ transitions, we present its WET effective Hamiltonian

$$\mathcal{H}_{\text{eff}}^{\nu\nu} \supset -\frac{4G_F}{\sqrt{2}}\frac{1}{(4\pi)^2}\frac{e^2}{\sin^2\theta_W} V_{td_j}^* V_{td_i}\, C_L^{d_i d_j} \left(\bar{d}_j \gamma^\mu P_L d_i\right)\left(\bar{\nu}_k \gamma^\mu (1-\gamma^5)\nu_k\right). \tag{5.5}$$

Last but not least, the WET effective Hamiltonian governing meson mixing is[23]

$$\mathcal{H}_{\text{eff}}^{\text{mix}} \supset \frac{G_F^2 m_W^2}{16\pi^2}\,\lambda_t^2\, C_{1,mix}^{d_i d_j}(x_t)\left(\bar{d}_j^{\,\alpha}\gamma^\mu P_L d_i^\alpha\right)\left(\bar{d}_j^{\,\beta}\gamma^\mu P_L d_i^\beta\right), \tag{5.6}$$

where α and β are colour indices, and $\lambda_t = V_{td_j}^* V_{td_i}$. The coefficients $C_{1,mix}^{d_i d_j}$ should not be confused with the coefficients $C_1^{d_i d_j}$ of the semileptonic Hamiltonian in Sec. 3.7.

[22] The inclusion of ϵ and ϵ' observables is currently under review.

[23] Here we do not include additional terms in the operator coefficient, which are functions of m_c^2/m_W^2. Due to CKM suppression these terms are negligible for B_s and B_d mixing. They should be taken account of in calculations of kaon mixing, but as mentioned, kaon mixing does not provide useful constraints on the MFV SMEFT, so we neglect it here.

5.3.2 Matching results

Our analytical matching results from the MFV SMEFT to the WET are given in Appendices E and F, and Ref. [71]. For convenience, we also provide the matching in numerical form as follows:

$$C_\alpha^{(\mathrm{WET})}(m_W) = \sum_k \left(N_{\alpha k}^{(1)} \log \frac{m_W}{\mu} + N_{\alpha k}^{(2)} \right) \frac{C_k^{(\mathrm{SMEFT})}(\Lambda)}{\mathrm{TeV}^{-2}} \tag{5.7}$$

where the coefficients $N_{\alpha k}^{(1)}$ are collected in Table G.1, and the coefficients $N_{\alpha k}^{(2)}$ are collected in Table G.2 for the $\{\alpha, m_Z, G_F\}$ input parameter scheme, or Table G.3 for the $\{m_W, m_Z, G_F\}$ input parameter scheme.[24] These tables show at a glance which SMEFT coefficients will be important in which processes. Note that the only SMEFT coefficients whose matching is changed by the choice of input scheme are C'_{ll}, C_{HD}, C_{HWB} and $C_{Hl}^{(3)}$, since these multiply the operators which enter the measured input observables in these two schemes. Throughout our calculations in the remainder of this paper, we take $\mu = 1$ TeV.

In order to make contact with experimental observables, we must run these results from the scale m_W to the appropriate scale for the FCNC observables, as illustrated in Fig. 5.2. In the case of $B_{(s,d)}$ meson observables we use $\mu_b = 4.2$ GeV, and for kaon observables we run to the scale of $\mu_K = 2$ GeV, at which the relevant matrix elements have been calculated by the lattice community [140]. The running below the weak scale is calculated using `Wilson` [141] which incorporates the anomalous dimension matrices of Ref. [142, 143].

5.3.3 Predictions for flavour observables

The main goal of this work is to incorporate the flavour data in global fits. In this section, we calculate constraints from flavour on the WET Wilson coefficients, which may then be used as pseudo-observables in fits to constrain the model.

Our flavour assumptions align the new physics effects with the SM. One the one hand, we have simpler calculations and in the other hand it limit the NP effects sensitivity. For instance, no contributions are made to operators containing right-handed flavour-changing quark currents, such as $\mathcal{O}'_9 = \hat{e}^2 \left(\bar{d}_j \gamma^\mu P_R d_i\right) \left(\bar{\ell} \gamma_\mu \ell\right)$, which are negligible also in the SM due to the chiral nature of the weak interactions. This in turn ensures that the leading NP effects are linear in the SMEFT coefficients, since there is always an interference term with the SM.

We therefore expect a rather limited number of new constraints arising from the flavour observables considered. The flavour symmetry assumptions ensure that $C_{1,\mathrm{mix}}^{bs}$ and $C_{1,\mathrm{mix}}^{bd}$

[24] Picking an input scheme effectively changes the definition of dimension 4 parameters. Since there are no dimension 4 counterterms for FCNCs, the scheme-dependent effects must be finite, and this is why we do not need two tables for the $N_{\alpha k}^{(1)}$ coefficients.

depend on the exact same linear combination of SMEFT Wilson coefficients. The same is true for C_L^{bs} and C_L^{sd}. We, therefore, expect to find a maximum of 6 new constrained directions corresponding to constraints on these two coefficients $C_{1,\text{mix}}^{bd_j}$ and $C_L^{d_i d_j}$, as well as constraints on the three coefficients C_7^{bs}, C_9^{bs} and C_{10}^{bs} from (semi)leptonic and photonic $b \to s$ transitions, and a constraint on one linear combination of C_1^{bs} and C_2^{bs} from the width difference of B_s mesons. The list of operators are given in the following.

- $B_{s,d}$ **mixing observables** $\Delta M_{s,d}$ **and** $\Delta\Gamma_{s,d}$

  One observable that can be measured in $B_{s,d}$ mixing is the mass difference of the two neutral mass eigenstates, $\Delta M_{s,d}$. In our case where $C_{1,\text{mix}}$ is the only non-zero $\Delta B = 2$ operator, the theoretical expression for the SM+NP mass difference for $B_{s,d}$ mixing, normalised to the SM, is simply [144]

$$\frac{\Delta M_{s,d}^{\text{SM+NP}}}{\Delta M_{s,d}^{\text{SM}}} = \left| 1 + \frac{C_{1,\text{mix}}^{b(s,d)}(m_W)}{S_0(x_t)} \right|, \tag{5.8}$$

  since the hadronic matrix elements and QCD corrections are identical for the SM and NP parts. The function $S_0(x_t)$ is the usual Inami-Lim function [18], given by

$$S_0(x_t) = \frac{4x_t - 11x_t^2 + x_t^3}{4(1-x_t)^2} - \frac{3x_t^3}{2(1-x_t)^3} \log x_t \approx 2.54. \tag{5.9}$$

  The measured values are [145]

$$\Delta M_d^{\text{exp}} = (0.5064 \pm 0.0019)\,\text{ps}^{-1}, \qquad \Delta M_s^{\text{exp}} = (17.757 \pm 0.021)\,\text{ps}^{-1}, \tag{5.10}$$

  while recent averaged SM predictions are [144]

$$\Delta M_d^{\text{Average 2019}} = \left(0.533^{+0.022}_{-0.036}\right)\text{ps}^{-1} = \left(1.05^{+0.04}_{-0.07}\right)\Delta M_d^{\text{exp}}, \tag{5.11}$$
$$\Delta M_s^{\text{Average 2019}} = \left(18.4^{+0.7}_{-1.2}\right)\text{ps}^{-1} = \left(1.04^{+0.04}_{-0.07}\right)\Delta M_s^{\text{exp}}. \tag{5.12}$$

  These lead to constraints on the *new physics parts* of the WET Wilson coefficients:

$$C_{1,\text{mix}}^{bs}(m_W) = 0.09 \pm 0.14, \qquad C_{1,\text{mix}}^{bd}(m_W) = 0.08 \pm 0.14, \tag{5.13}$$

  where we have symmetrised the two-sided errors conservatively by taking the largest side.

  The decay rate difference of B_s mesons, $\Delta\Gamma_s$, is sensitive to new $b \to \bar{c}cs$ effects, and is thus dependent on the coefficients C_1^{bs} and C_2^{bs} of the Hamiltonian in Eqn. 3.51.

The observable is defined $\Delta\Gamma_s = 2|\Gamma_{12}^{s,\mathrm{SM}} + \Gamma_{12}^{s,\mathrm{NP}}| \cos\phi_{12}^s$, where $\cos\phi_{12}^s \approx 1$, and [146]

$$\begin{aligned}\Gamma_{12}^{s,\mathrm{NP}} = &-G_F^2 \lambda_c^2 m_b^2 M_{Bs} f_{Bs}^2 \frac{\sqrt{1-z_c}}{36\pi} \times \\ &\Big[\Big(8(1-z_c/4)\, C_2^{\mathrm{SM}} C_2^{\mathrm{NP}} + 4(1-z_c)\left(3C_1^{\mathrm{SM}} C_1^{\mathrm{NP}} + C_1^{\mathrm{SM}} C_2^{\mathrm{NP}} + C_2^{\mathrm{SM}} C_1^{\mathrm{NP}}\right)\Big) B \\ &+ (1+z_c/2)(C_2^{\mathrm{SM}} C_2^{\mathrm{NP}} - C_1^{\mathrm{SM}} C_2^{\mathrm{NP}} - C_2^{\mathrm{SM}} C_1^{\mathrm{NP}} + 3C_1^{\mathrm{SM}} C_1^{\mathrm{NP}})\, \tilde{B}_S' \Big], \end{aligned} \tag{5.14}$$

where $z_c = 4m_c^2/m_b^2$, $\lambda_c = V_{cs}^* V_{cb}$, f_{Bs} is the B_s decay constant, B and $\tilde{B}_S'$ are bag parameters, and $C_{1,2}^{\mathrm{SM}}$ and $C_{1,2}^{\mathrm{NP}}$ are the SM and NP values respectively of $C_{1,2}^{bs}(\mu_b)$. The SM coefficients are $C_1^{\mathrm{SM}}(\mu_b) = -0.2451$, $C_2^{\mathrm{SM}}(\mu_b) = 1.008$ at NNLO in QCD [147]. For the values of hadronic parameters we refer to [148] and references therein. The SM prediction $\Delta\Gamma_s^{\mathrm{SM}}$ [149] and the measured value $\Delta\Gamma_s^{\mathrm{exp}}$ are [145]

$$\Delta\Gamma_s^{\mathrm{SM}} = (0.088 \pm 0.020)\,\mathrm{ps}^{-1}, \qquad \Delta\Gamma_s^{\mathrm{exp}} = (0.088 \pm 0.006)\,\mathrm{ps}^{-1}. \tag{5.15}$$

From this (adding experimental and theoretical errors in quadrature), we obtain a constraint at 1σ on a linear combination of the NP WET Wilson coefficients:

$$\left|C_2^{bs}(\mu_b) + 0.01 C_1^{bs}(\mu_b)\right| < 0.09, \tag{5.16}$$

where [146]

$$\begin{pmatrix} C_1^{bs}(\mu_b) \\ C_2^{bs}(\mu_b) \end{pmatrix} = \begin{pmatrix} 1.12 & -0.27 \\ -0.27 & 1.12 \end{pmatrix} \begin{pmatrix} C_1^{bs}(m_W) \\ C_2^{bs}(m_W) \end{pmatrix}. \tag{5.17}$$

The percentage error on the measurement of $\Delta\Gamma_d$, the decay rate difference of B_d mesons, is much larger than that on $\Delta\Gamma_s$ [145]. This observable is dependent on the exact same linear combination of MFV SMEFT coefficients as $\Delta\Gamma_s$, and would produce much weaker bounds, so we don't include it in our analysis.

- **Kaon decay into neutrinos:** $K \to \pi\bar{\nu}\nu$

  For NP in which the neutrinos are coupled to left-handed currents only (which is the case for the MFV SMEFT), the expressions for the branching ratios are [150, 151]

$$\mathcal{B}\left(K^+ \to \pi^+ \bar{\nu}\nu\right) = \kappa_+ (1 + \Delta_{\mathrm{EM}}) \left[\left(\frac{\mathrm{Im}\, X_{\mathrm{eff}}}{\lambda^5}\right)^2 + \left(\frac{\mathrm{Re}\,\lambda_c}{\lambda} P_c(X) + \frac{\mathrm{Re}\, X_{\mathrm{eff}}}{\lambda^5}\right)^2\right], \tag{5.18}$$

$$\mathcal{B}\left(K_L \to \pi^0 \bar{\nu}\nu\right) = \kappa_L \left(\frac{\mathrm{Im}\, X_{\mathrm{eff}}}{\lambda^5}\right)^2, \tag{5.19}$$

where $\Delta_{\rm EM} = -0.003$, and

$$\kappa_+ = (5.173 \pm 0.025) \times 10^{-11} \left[\frac{\lambda}{0.225}\right]^8, \quad \kappa_L = (2.231 \pm 0.013) \times 10^{-10} \left[\frac{\lambda}{0.225}\right]^8. \tag{5.20}$$

Here $\lambda = |V_{us}|$, $\lambda_i = V_{is}^* V_{id}$, $\Delta_{\rm EM}$ is the radiative electromagnetic correction, and κ_+ and κ_L summarise the remaining factors, including the hadronic matrix elements. The loop functions for the top and charm quark contributions, $X_{\rm eff}$ and $P_c(X)$, are given in the SM by [151]

$$P_c(X) = 0.404 \pm 0.024, \quad X_{\rm eff}^{\rm SM} = V_{ts}^* V_{td}\, X_L^{\rm SM}, \quad X_L^{\rm SM} = 1.481 \pm 0.009. \tag{5.21}$$

In the presence of the SMEFT contributions,[25] $X_{\rm eff}$ becomes

$$X_{\rm eff}^{\rm SM+NP} = V_{ts}^* V_{td} \left(X_L^{\rm SM} - C_L^{sd}(\mu_K)\right) \tag{5.22}$$

with $\mu_K = 2$ GeV. For the experimental limits, we take the recent upper bound from NA62 [152]

$$\mathcal{B}\left(K^+ \to \pi^+ \bar\nu\nu\right) < 1.85 \times 10^{-10} \ \ (90\%\ \text{CL}), \tag{5.23}$$

and from the 2015 run at KOTO [153]

$$\mathcal{B}\left(K_L \to \pi^0 \bar\nu\nu\right) < 3.0 \times 10^{-9} \ \ (90\%\ \text{CL}). \tag{5.24}$$

These lead to a bound on the *new physics part* of the WET Wilson coefficient:

$$C_L^{sd}(\mu_K) = 0.9 \pm 2.4. \tag{5.25}$$

This coefficient barely runs, so we can take $C_L^{sd}(\mu_K) \approx C_L^{sd}(m_W)$.

- **B decay into neutrinos:** $B \to K^{(*)}\bar\nu\nu$

  Following Ref. [154], the predictions for the branching ratios in the presence of the MFV SMEFT contributions can be written (in our notation)

$$\frac{\mathcal{B}\left(B \to K^{(*)}\bar\nu\nu\right)_{\rm SM+NP}}{\mathcal{B}\left(B \to K^{(*)}\bar\nu\nu\right)_{\rm SM}} = \frac{\left|C_L^{bs}(m_b) - X_t^{\rm SM}\right|}{X_t^{\rm SM}} \tag{5.26}$$

  where $X_t^{\rm SM} = 1.469 \pm 0.017$. The experimental limits on the branching ratios, measured at BaBar [155] and Belle [156] are

$$\mathcal{B}\left(B^+ \to K^+ \bar\nu\nu\right) < 1.7 \times 10^{-5} \ \ (90\%\ \text{CL}), \tag{5.27}$$

$$\mathcal{B}\left(B^0 \to K^{*0} \bar\nu\nu\right) < 5.5 \times 10^{-5} \ \ (90\%\ \text{CL}), \tag{5.28}$$

[25] neglecting the suppressed effect of NP in the charm loops

which lead to bounds on the ratios, at 90% CL, of [154]

$$\frac{\mathcal{B}\left(B^+ \to K^+ \bar{\nu}\nu\right)_{\text{SM+NP}}}{\mathcal{B}\left(B^+ \to K^+ \bar{\nu}\nu\right)_{\text{SM}}} < 4.3, \qquad \frac{\mathcal{B}\left(B^0 \to K^{*0} \bar{\nu}\nu\right)_{\text{SM+NP}}}{\mathcal{B}\left(B^+ \to K^+ \bar{\nu}\nu\right)_{\text{SM}}} < 4.4. \tag{5.29}$$

These lead to a bound on the *new physics part* of the WET Wilson coefficient:

$$C_L^{bs}(\mu_b) = 1.5 \pm 3.9. \tag{5.30}$$

As above, we can take $C_L^{bs}(\mu_b) \approx C_L^{bs}(m_W)$ since the running is very small.

- $b \to s\gamma$ **and** $b \to s l^+ l^-$ **processes**

  Processes involving the parton level transitions $b \to s\gamma$ and $b \to s l^+ l^-$, for example branching ratios and angular observables of $B \to K^{(*)} l^+ l^-$, and branching ratios of $B \to X_s \gamma$ and $B_s \to l^+ l^-$, can constrain the WET Wilson coefficients C_7^{bs}, C_9^{bs} and C_{10}^{bs}.[26] We use `flavio` [159] to find the vector $\hat{\boldsymbol{C}}$ of best fit values of the Wilson coefficients, and to numerically extract the variances and correlation matrix by expanding $\Delta\chi^2$ around the best fit point as

$$\Delta\chi^2 = \left(\boldsymbol{C} - \hat{\boldsymbol{C}}\right)^T U^{-1} \left(\boldsymbol{C} - \hat{\boldsymbol{C}}\right), \tag{5.31}$$

  where the covariance matrix U can be written in terms of the variances σ_i^2 and the correlation matrix ρ as $U_{ij} = \sigma_i \sigma_j \rho_{ij}$ (no sum). In this way we find constraints on the new physics Wilson coefficients of

$$\begin{pmatrix} C_7^{bs}(\mu_b) \\ C_9^{bs}(\mu_b) \\ C_{10}^{bs}(\mu_b) \end{pmatrix} = \begin{pmatrix} -0.001 \pm 0.011 \\ -0.96 \pm 0.23 \\ 0.31 \pm 0.15 \end{pmatrix} \tag{5.32}$$

  with the correlation matrix

$$\rho = \begin{pmatrix} 1.00 & -0.30 & 0.20 \\ -0.30 & 1.00 & -0.19 \\ 0.20 & -0.19 & 1.00 \end{pmatrix}. \tag{5.33}$$

  The observables that are included in this `flavio` fit are based on the list of rare B decay observables involving a $b \to s$ transition given in Ref. [32] (and we refer to this reference as well as Ref. [159] for the measurements and theory predictions that are included in the `flavio` code). Specifically, the observables used are: all

[26] The $b \to d$ WET coefficients C_7^{bd}, C_9^{bd} and C_{10}^{bd} depend on the same linear combinations of SMEFT Wilson coefficients under our MFV assumptions as these $b \to s$ ones. Currently, new physics in the theoretically clean $b \to d l^+ l^-$ and $b \to d\gamma$ processes is not well constrained, but this should change in the future with measurements of inclusive $b \to d$ processes at Belle II [157, 158].

relevant CP-averaged observables in semileptonic $b \to s\mu\mu$ decays that were included in the global fit of Ref. [160], high-q^2 branching ratios and angular observables of $\Lambda_b \to \Lambda\mu\mu$, the branching ratios of $B^0 \to \mu\mu$ and $B_s \to \mu\mu$, the branching ratio of the inclusive decay $B \to X_s\mu\mu$, and all observables in inclusive and exclusive radiative $b \to s\gamma$ decays included in the fit of Ref. [161], including $B \to K^*ee$ at low q^2. We do not fit to observables that test lepton flavour universality, or lepton flavour violation, since under our flavour assumptions these will not be altered from their SM predictions.

The constrained Wilson coefficients at μ_b=4.2 GeV are related to the Wilson coefficients at m_W by [141]:

$$\begin{aligned} C_7^{bs}(\mu_b) &= 0.65\, C_7^{bs}(m_W) + 9.6 \cdot 10^{-2}\, C_8^{bs}(m_W), \\ C_9^{bs}(\mu_b) &= 8.46\, C_1^{bs}(m_W) + 2.04\, C_2^{bs}(m_W) + 0.98\, C_9^{bs}(m_W), \\ C_{10}^{bs}(\mu_b) &= 1.0\, C_{10}^{bs}(m_W). \end{aligned} \tag{5.34}$$

5.4 Fit

In order to show the impact of flavour data compared to other set of data, we perform an illustrative fit using the method of least-squares, within the $\{\alpha_{em}, m_Z, G_F\}$ input scheme fit. We include all operators allowed by our flavour and CP assumptions.

5.4.1 Observables and data

Our choice of non-flavour observables is motivated by the following considerations, with the aim of getting a fair picture of the new physical information that flavour can add to a global fit: *(a)* we want to include observables which provide strong and up-to-date constraints on operators involving EW gauge bosons and Higgs fields, and *(b)* we want to include observables which depend on the same 4-fermion operators that appear at one-loop in FCNCs. With this in mind, we include the following.

- **Precision electroweak observables:** We use the LEPI observables and predictions from Table 2 of Ref. [65], as well as the W mass and the forward-backward asymmetries $A_{FB}^{0,f}$ for $f = \{c, b, \ell\}$. The measurements and their correlations come from Ref. [162]. Note that this fit contains two flat directions that what latter lifted by LEPII data.

- **LEPII W^+W^-:** We use all the data and SM predictions ([135, 163–165]) from Tables 12, 13, 14 and 15 of Ref. [68], and the definitions of the observables in terms of SMEFT parameters from Tables 2 and 3 of the same reference.

- **Higgs Run I:** We use the combined ATLAS and CMS Run I Higgs signal strength measurements from Table 8 of Ref. [166], with the correlation matrix in Figure

27 of the same reference. For the SMEFT predictions we adopt the definitions of the observables in terms of Warsaw basis Wilson coefficients provided in the `Mathematica` notebook accompanying Ref. [167].

- **Higgs Run II:** From the CMS paper [168], we use all the signal strength measurements in Table 3, and the correlation matrix from the supplementary material. From the ATLAS paper [169] we use all the cross sections times branching ratios in Table 6 and the correlation matrix in Figure 6. For the SMEFT predictions we use the definitions of the observables in terms of Warsaw basis Wilson coefficients provided in the `Mathematica` notebook accompanying Ref. [167].

- W^+W^- **production at LHC:** Following Ref. [167], we use a measurement of one bin of the differential cross section of $pp \to W^+W^- \to e^\pm\nu\mu^\pm\nu$ at ATLAS [170], using the definitions of the observable in terms of SMEFT Wilson coefficients provided in the `Mathematica` notebook accompanying Ref. [167].

- $e^+e^- \to \bar{q}q$ **off the** Z **pole:** We use the data on σ_{had} at different values of $\sqrt{s}$ from Table 6 of Ref. [87]. The original experimental results are from LEP [135] and TRIDENT [171] and the SM predictions are taken from Ref. [172].

- **Low energy precision measurements:** From the Appendix of Ref. [87], we use observables and data on Atomic Parity Violation [173, 174] and eDIS [175]. From Ref. [176], we use observables and data on neutrino-nucleon scattering (both ν_e scattering data from CHARM [177] and ν_μ scattering data from the PDG average [178]), deep inelastic scattering of polarized electrons [178, 179], and deep inelastic scattering of muons [180].

- **FCNCs:** We use the constraints on WET Wilson coefficients given in Section 5.3.3.

This is a total of 186 observables. Figure 5.3 shows which Warsaw basis Wilson coefficients affect each set of observables, where the "4-fermion" category includes low energy precision measurements as well as $e^+e^- \to \bar{q}q$ off the Z pole.

5.4.2 Fit methodology

The SMEFT corrections to all the observables are linear in the dimension 6 Wilson coefficients (under our flavour and CP assumptions and working to $O(\Lambda^{-2})$), meaning that predictions for the observables can be written as a matrix equation

$$\boldsymbol{\mu}(\boldsymbol{\theta}) = \boldsymbol{\mu}_{\rm SM} + \mathbf{H} \cdot \boldsymbol{\theta}, \tag{5.35}$$

where $\boldsymbol{\mu}$ is the vector of predictions, $\boldsymbol{\mu}_{\rm SM}$ represents the SM predictions, $\boldsymbol{\theta}$ is a vector of SMEFT Wilson coefficients, and $\mathbf{H}$ is a matrix of functions that parameterise the SMEFT

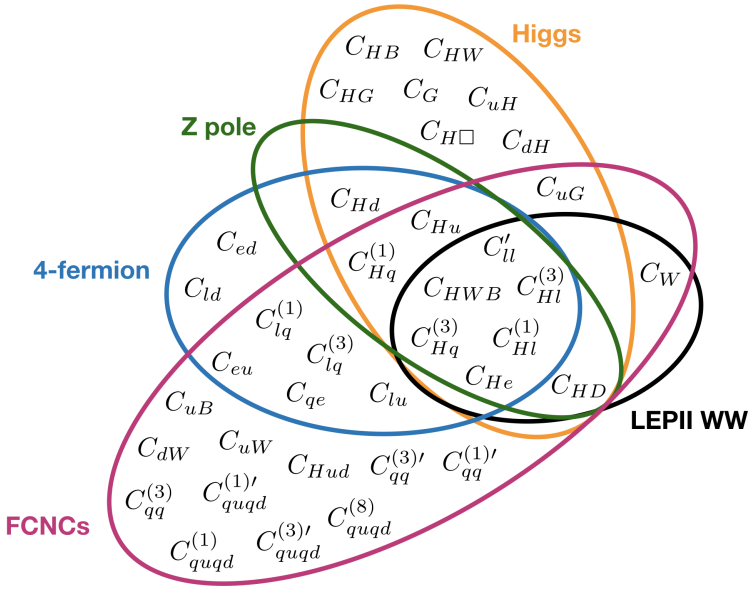

Figure 5.3: Diagram to show which Warsaw basis Wilson coefficients affect each of the types of observables included in the fit

corrections. The measured central values of the observables can be represented by a vector $\mathbf{y}$, with a covariance matrix $\mathbf{V}$. Then the χ^2 function is

$$\chi^2(\boldsymbol{\theta}) = (\mathbf{y} - \boldsymbol{\mu}(\boldsymbol{\theta}))^T \mathbf{V}^{-1} (\mathbf{y} - \boldsymbol{\mu}(\boldsymbol{\theta})) . \tag{5.36}$$

The least-squares estimators $\hat{\boldsymbol{\theta}}$ for the Wilson coefficients are found by minimising χ^2:

$$\hat{\boldsymbol{\theta}} = \left(\mathbf{H}^T \mathbf{V}^{-1} \mathbf{H}\right)^{-1} \mathbf{H}^T \mathbf{V}^{-1} \mathbf{y}. \tag{5.37}$$

The covariance matrix $\mathbf{U}$ for the least squares estimators is given by the inverse of the Fisher matrix $\mathbf{F}$, defined as

$$\mathbf{F} = \mathbf{H}^T \mathbf{V}^{-1} \mathbf{H} = \mathbf{U}^{-1}. \tag{5.38}$$

When the covariance matrix is diagonalised, its entries are the variances σ_i^2 of its eigenvectors, which are a set of linearly independent directions in Wilson coefficient space. The eigenvalues of the Fisher matrix are therefore $1/\sigma_i^2$. It is importance to note that if an eigenvector direction is unconstrained by the data, its corresponding Fisher matrix eigenvalue will be zero.

5.4.3 Flavour in the electroweak hyperplane

If we (artificially, but for purposes of illustration) restrict attention to the set of ten Wilson coefficients that enter the Z-pole observables (the green ellipse in Fig. 5.3),

$$\{C_{HWB}, C_{HD}, C_{Hl}^{(1)}, C_{Hl}^{(3)}, C_{Hq}^{(1)}, C_{Hq}^{(3)}, C_{Hu}, C_{Hd}, C_{He}, C'_{ll}\}, \tag{5.39}$$

then it is well-known that fitting only to Z-pole observables leaves two flat directions. We define these as

$$k_1 = 0.369\bigg(\frac{1}{3}C_{Hd} - 2C_{HD} + C_{He} + \frac{1}{2}C_{Hl}^{(1)} - \frac{1}{6}C_{Hq}^{(1)} - \frac{2}{3}C_{Hu} - 5.12(C_{Hq}^{(3)} + C_{Hl}^{(3)}) + 3.62C_{HWB}\bigg), \tag{5.40}$$

$$k_2 = -0.118\bigg(\frac{1}{3}C_{Hd} - 2C_{HD} + C_{He} + \frac{1}{2}C_{Hl}^{(1)} - \frac{1}{6}C_{Hq}^{(1)} - \frac{2}{3}C_{Hu} + 0.77(C_{Hq}^{(3)} + C_{Hl}^{(3)}) + 0.56C_{HWB}\bigg). \tag{5.41}$$

These are linear combinations of the flat directions given in Ref. [65]. This reference also provides an explanation of why these occur, in terms of a reparameterization invariance of $2 \to 2$ fermion scattering processes in the SMEFT, which we explain in the following.

5.4.4 Reparameterization Invariance

Consider the simple Lagrangian of a $\bar{\psi}\psi \to V \to \bar{\psi}\psi$

$$\mathcal{L}_{V\psi_i} = \frac{1}{2}m_V^2 V^\mu V_\mu - \frac{1}{4}V^{\mu\nu}V_{\mu\nu} - g\bar{\psi}\gamma^\mu\phi_j V_\mu - g\kappa\bar{\psi}_k\gamma^\mu\psi_l V_\mu + ... \tag{5.42}$$

From Sec 3, we know that we can always transform the boson kinetic term from canonical to a non-canonical form. Such field redefinition does not have any physical effect due to the LSZ formula. However, this particular shift can be cancelled by a shift in the coupling. This fact is used to take the kinetic term to the canonical form when we add the SMEFT corrections, $g_b \to g_b'(1-\epsilon)$ and $V_b \to V_b'(1+\epsilon)$. with $\epsilon \sim \bar{v}_T^2/\Lambda^2$ such that $g_b V_b \to g_b' V_b'$ is invariant for $V_b = \{G, B, W\}$.

This freedom defines an unobservable redundancy in the subset $\bar{\psi}\psi \to V \to \bar{\psi}\psi$, which are parametrized by the equivalence class of V and g where $(V, g) \leftrightarrow (V'(1+\epsilon), g'(1-\epsilon))$. The reparametrization invariance can be implemented via Equations of Motion, where operators identities can be obtained. These relations can then be projected in the process of interest $S_R : \bar{\psi}\psi \to \bar{\psi}\psi$, represented by $\langle ... \rangle_{S_R}$, in which we obtain

$$\langle y_h g_1^2 Q_{HB}\rangle_{S_R} = \langle \sum_{\psi_k} y_k g_1^2 \bar{\psi}_k\gamma_\beta\psi_k (H^\dagger i\overleftrightarrow{D} H) + \frac{g_1^2}{2}(Q_{H\Box} + 4Q_{HD}) - \frac{1}{2}g_1 g_2 Q_{HWB}\rangle_{S_R} \tag{5.43}$$

$$\langle g_2^2 Q_{HW}\rangle_{S_R} = \langle g_2^2(\bar{q}\tau^I\gamma_\beta q + \bar{l}\tau^I\gamma_\beta l)(H^\dagger \overleftrightarrow{D}^I_\beta H) + 2g_2^2 Q_{H\Box} - 2g_1 g_2 y_h Q_{HWB}\rangle_{S_R} \tag{5.44}$$

Due to a small Yukawa coupling the effect of $Q_{H\Box}$ can be ignored and we have for the four-point scattering

$$\langle y_h g_1^2 Q_{HB}\rangle_{S_R} \to \frac{g_1^2\bar{v}_T^2}{4\Lambda^2} B^{\mu\nu}B_{\mu\nu}, \quad \langle g_2^2 Q_{HW}\rangle_{S_R} \to \frac{g_2^2\bar{v}_T^2}{2\Lambda^2} W_I^{\mu\nu}W^I_{\mu\nu} \tag{5.45}$$

The reparametrization invariance tell us that, in scattering processes $S_R : \bar{\psi}\psi \to \bar{\psi}\psi$, we cannot access the Wilson coefficients C_{HB}, C_{HW} and nor the two linear combinations

$$g_1^2 w_B = g_1^2\frac{\bar{v}_T^2}{\Lambda^2}\left(-\frac{1}{3}C_{Hd} - C_{He} - \frac{1}{2}C_{Hl}^{(1)} + \frac{1}{6}C_{Hq}^{(1)} + \frac{2}{3}C_{Hu} + 2C_{HD} - \frac{1}{2t_{\hat{\theta}}}C_{HWB}\right) \tag{5.46}$$

$$g_2^2 w_W = g_2^2\frac{\bar{v}_T^2}{2\Lambda^2}\left(C_{Hq}^{(3)} + C_{Hl}^{(3)} - t_{\hat{\theta}}C_{HWB}\right) \tag{5.47}$$

Then, the unconstrained flat directions found by LEP I data $k_{1,2}$ can be projected in the space of unobservable direction from reparametrization invariance,

$$k_1 = -w_B - 2.59 w_W \qquad k_2 = -w_B + 4.31 w_W. \tag{5.48}$$

The way to close these flat directions is to obtain competitive constrains from orthogonal directions, which are provided by other observables. In [20], the LEP II WW production was used to break the reparametrization invariance in $2 \to 2$ fermion scattering. In Figure 5.4 we show, within the plane of the Wilson coefficients of these two flat directions. The LEP II WW is shown in orange. Another option is to use LHC Higgs measurements (shown in blue), which also provide observables able to close these directions. However, our goal here is to show the power of flavour constrains compared to other sectors, we show that, under our assumptions, it is competitive with existing constraints within this highly flavourless plane. In all cases the Z-pole data are also included in the fit.

We need to make further comments in Figure 5.4. The axes correspond to the k_1 and k_2 directions, which have been normalised to unit vectors in Wilson coefficient space. We define the norm $|k|$ of an operator direction by assuming an arbitrary Euclidean metric δ_{ij} in the Warsaw basis; if we write $k = \boldsymbol{c}\cdot\boldsymbol{\theta}$, where as before $\boldsymbol{\theta}$ is the vector of Warsaw basis Wilson coefficients, then $|k|^2 \equiv \delta_{ij}\, c_i c_j$. All of the ellipses in Figure 5.4 are obtained by taking only this set of 10 Wilson coefficients (5.39) to be non-zero, and profiling over the 8 linearly independent directions (which are already well constrained by the Z-pole data).

It is clear that there is an apparent tension on the central value of the flavour ellipsis. This tension is due to the recent measurements of $b \to s\mu\mu$ processes, which show a pattern of deviations from SM predictions, particularly among angular observables in $B \to K^*\mu\mu$ decays [181] and measurements of exclusive branching ratios [182, 183]. These processes provide some of the strongest constraints among the flavour data used, and drive the green ellipse away from the origin. These anomalous results can be explained either by

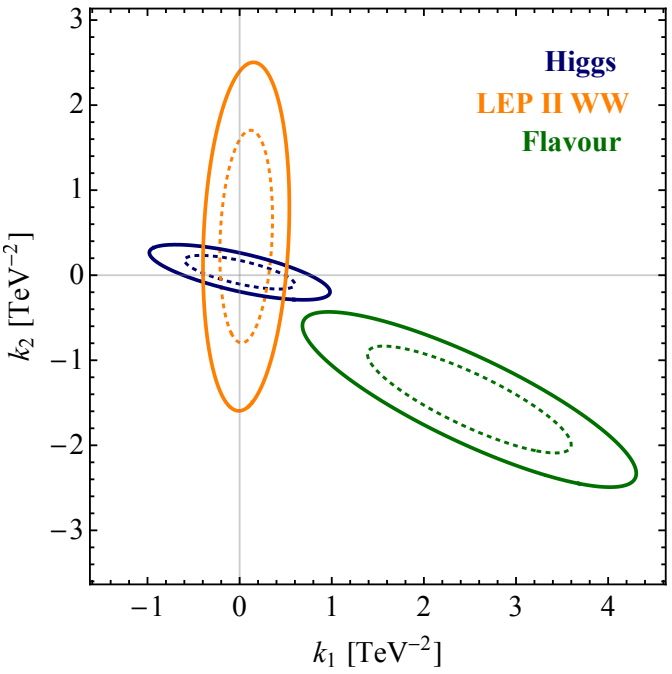

Figure 5.4: Flavour (green), Higgs (blue) and LEP II WW (orange) constraints on the plane of the Z-pole flat directions, under the assumptions explained in the text. The dotted lines are 1σ contours, the solid lines are 2σ contours. The axes correspond to the coefficients of the two independent linear combinations of Wilson coefficients that remain unconstrained by the Z-pole data.

lepton flavour universal new physics, or by lepton non-universal new physics which affects muons more strongly than electrons (see e.g. [184–189] for recent fits to WET coefficients). If the new physics explanation is lepton non-universal, it could simultaneously produce effects in ratios of decays involving muons to those involving electrons (R_K and R_{K^*}), recent measurements of which also deviate from the SM expectation [190, 191] (but have no impact on our lepton flavour universal fit). For this reason most recent models invoked to explain the anomalies are lepton flavour non-universal.

Whether these anomalies will persist in new data remains to be seen, but even if they are confirmed as signs of new physics, it does not imply that there is really a tension between electroweak, Higgs and flavour data. This is because we are only studying a subset of operators in this plot, when in reality many other operators could provide the explanation for the anomalies, which would in turn shift the favoured central value within the plane of Figure 5.4. Therefore under a less restrictive BSM situation, in which more operator coefficients were non-zero, it's likely that this discrepancy would be accounted for by an operator not among these ten (and which is less constrained by EW and Higgs data).

So while this limited fit gives an indication of the power of current flavour measurements when compared like-for-like with Higgs and LEP II WW measurements, it is clear that a more global picture is needed for a more realistic interpretation of the constraints, and this is the subject of the following subsections. We note, however, that our flavour symmetry assumption does not allow for lepton non-universality, and so if the $R_K^{(*)}$ anomalies were confirmed with more data, it would be a sure sign that this flavour symmetry is not

respected by BSM physics. Other flavour symmetries within the SMEFT which can induce lepton flavour non-universality have been explored in the literature, in the context of BSM explanations for the anomalies, see e.g. Refs. [192–195].

5.4.5 Eigensystem of the global fit

The observables we include in the fit, within our MFV flavour assumption, depend on a total of 37 Wilson coefficients in the Warsaw basis:

$$\begin{aligned}&\{C_{H\Box}, C_{HWB}, C_{HD}, C_{HW}, C_{HB}, C_{HG}, C_W, C_G, C_{Hl}^{(1)}, C_{Hl}^{(3)}, C_{Hq}^{(1)}, C_{Hq}^{(3)}, C_{Hu}, C_{Hd}, C_{He},\\ &C_{Hud}, C_{uH}, C_{dH}, C_{uW}, C_{dW}, C_{uB}, C_{uG}, C'_{ll}, C_{lq}^{(3)}, C_{lq}^{(1)}, C_{qe}, C_{lu}, C_{ld}, C_{eu}, C_{ed},\\ &C_{qq}^{(1)\prime}, C_{qq}^{(3)}, C_{qq}^{(3)\prime}, C_{quqd}^{(1)}, C_{quqd}^{(8)}, C_{quqd}^{(1)\prime}, C_{quqd}^{(8)\prime}\}. \end{aligned} \tag{5.49}$$

Including all observables above, we have 7 flat directions (corresponding to the null space of the Fisher matrix):

$$\begin{aligned}&(f_1,\, f_2,\, f_3,\, f_4,\, f_5, f_6,\, f_7)^T = \\ &\qquad \mathbb{A}\,(C_{qq}^{(1)\prime} + C_{qq}^{(3)\prime},\, C_{quqd}^{(1)},\, C_{quqd}^{(1)\prime},\, C_{quqd}^{(8)},\, C_{quqd}^{(8)\prime},\, C_{dW},\, C_G,\, C_{Hud},\, C_{uG},\, C_{uH})^T\end{aligned}$$

where the matrix $\mathbb{A}$ is given by

$$\mathbb{A} = \begin{pmatrix} -0.68 & 0.14 & 0.09 & 0.20 & 0.06 & -0.05 & 0.01 & -0.01 & 0.00 & -0.01 \\ -0.02 & 0.27 & 0.66 & -0.52 & -0.46 & -0.04 & 0.03 & -0.02 & 0.01 & -0.02 \\ -0.05 & 0.06 & -0.52 & 0.11 & -0.82 & 0.09 & 0.12 & 0.03 & 0.04 & -0.11 \\ 0.18 & 0.30 & 0.39 & 0.80 & -0.16 & -0.15 & -0.03 & 0.03 & -0.01 & 0.03 \\ 0.03 & 0.00 & 0.07 & 0.03 & 0.15 & -0.03 & 0.69 & -0.00 & 0.21 & -0.67 \\ 0.01 & -0.01 & -0.02 & 0.03 & -0.03 & -0.05 & 0.00 & -1.00 & 0.00 & 0.00 \\ -0.06 & -0.90 & 0.33 & 0.16 & -0.24 & 0.04 & 0.01 & 0.01 & 0.00 & -0.01 \end{pmatrix} \tag{5.50}$$

If the flavour observables are excluded from the fit, there are 12 flat directions — the flavour data adds 5 new constraints.

The set of simultaneous constraints that can be extracted from the fit can be illustrated by the eigenvalues of the Fisher matrix, $1/\sigma_i^2$, defined in Section 5.4.2. The values of σ_i can be taken as bounds on the coefficients C_i of the respective eigenvector directions, or equivalently $\sigma_i^{-1/2}$ provides a lower bound on the scale of suppression of the eigenvector operator ($1/\sqrt{|C_i|} > \sigma_i^{-1/2}$), remembering that the C_i's have dimension TeV^{-2}. In this way, the effect of adding flavour data to the fit is demonstrated in Figure 5.5. The addition of flavour data changes the eigenvector directions, and therefore not all the eigenvalues can be directly compared. With this in mind, we have plotted the eigenvalues of the full fit in size order, pairing each with the eigenvalue of the fit without flavour whose

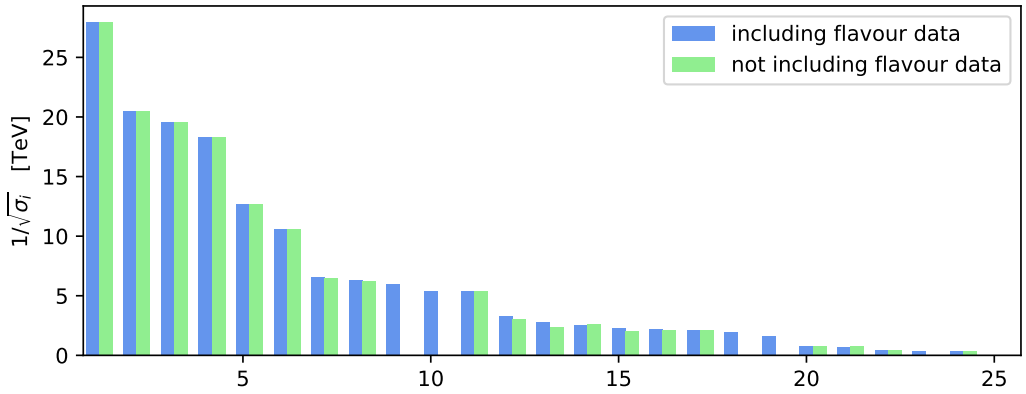

Figure 5.5: Comparison of the eigenvalues of the Fisher matrix, for the fit including the flavour data (blue), and the fit excluding flavour data (green). We have not plotted eigenvalues for which the fit including flavour data gives $1/\sqrt{\sigma_i} < 250$ GeV.

corresponding eigenvector ($\boldsymbol{e}^{\not F}$) has the largest overlap with the relevant eigenvector of the full fit ($\boldsymbol{e}^F$), where this overlap is defined as

$$\frac{\delta_{ij}\, e_i^{\not F} e_j^F}{|\boldsymbol{e}^{\not F}||\boldsymbol{e}^F|}. \tag{5.51}$$

For the well-constrained eigenvectors (towards the left of the plot), the overlap is close to 1. The five otherwise flat directions which are closed by flavour data can be seen in the plot as blue bars without an accompanying green bar. In particular, two directions which are unconstrained without flavour data are now rather well constrained ($1/\sqrt{|c|} > 5$ TeV). These directions are dependent on nearly all the Wilson coefficients in the fit, but can be written approximately as

$$\begin{aligned} C_1 \approx{}& 0.44\left(C_{qq}^{(1)\prime} - C_{qq}^{(3)\prime}\right) + 0.41 C_{He} + 0.32 C_{Hl}^{(1)} + 0.31 C_{dW} + 0.23 C_{HWB} + 0.22 C_{qq}^{(3)} \\ &+ 0.21 C_{Hq}^{(3)} + 0.14 C_{ll}' + 0.10 C_{Hl}^{(3)} - 0.10 C_{lq}^{(1)} + 0.10 C_{HB} + \cdots, \\ C_2 \approx{}& 0.76 C_{dW} - 0.33\left(C_{qq}^{(1)\prime} - C_{qq}^{(3)\prime}\right) + 0.29 C_{uB} - 0.22 C_{uW} - 0.17 C_{qq}^{(3)} \\ &+ 0.10 C_{quqd}^{(1)\prime} + \cdots, \end{aligned} \tag{5.52}$$

where we have dropped all terms with numerical coefficient less than 0.1, just to give an idea of their main dependence.

Some or all of the remaining flat directions can probably be closed by Tevatron and LHC top observables. The study and interpretation of top data in the language of effective

field theory is a very active field at the moment, see e.g. [196–198] for recent work in this area. Furthermore, fruitful results have been found by using flavour and top data in combination to constrain some top-containing operators (see e.g. [199–205]). However, to our knowledge a study of top observables within a global fit based on an exact or approximate $U(3)^5$ flavour symmetry has not been done, and is beyond the scope of our work.

5.4.6 Full flavour symmetry

We can imagine a situation in which the NP is completely flavour symmetric, and the symmetry breaking associated with the Yukawas can only enter through loops involving W bosons. In other words, the dimension 6 Lagrangian at the scale Λ only includes operators which are $U(3)^5$ singlets (without spurionic Yukawa insertions). In this case, the observables we include in the fit now depend on 26 Wilson coefficients in the Warsaw basis:

$$\{C_{H\Box}, C_{HWB}, C_{HD}, C_{HW}, C_{HB}, C_{HG}, C_W, C_G, C_{Hl}^{(1)}, C_{Hl}^{(3)}, C_{Hq}^{(1)}, C_{Hq}^{(3)}, C_{Hu}, C_{Hd}, C_{He},$$
$$C'_{ll}, C_{lq}^{(3)}, C_{lq}^{(1)}, C_{qe}, C_{lu}, C_{ld}, C_{eu}, C_{ed}, C_{qq}^{(1)\prime}, C_{qq}^{(3)}, C_{qq}^{(3)\prime}\}. \tag{5.53}$$

Including all observables, we now have only one flat direction in the fit:

$$\frac{1}{\sqrt{2}}\left(C_{qq}^{(1)\prime} + C_{qq}^{(3)\prime}\right), \tag{5.54}$$

whereas if the flavour observables are excluded, there are 3 flat directions, all within the $C_{qq}^{(1)\prime}$-$C_{qq}^{(3)\prime}$-$C_{qq}^{(3)}$ hyperplane. The reason for this remaining flat direction is clear by inspection of the matching calculations; the coefficients $C_{qq}^{(1)\prime}$ and $C_{qq}^{(3)\prime}$ always appear in the linear combination $(C_{qq}^{(1)\prime} - C_{qq}^{(3)\prime})$.

The set of simultaneous constraints that can be extracted from the fit can again be illustrated by the eigenvalues of the Fisher matrix. The effect of adding flavour data is demonstrated in Figure 5.6. It can be seen that one direction which is unconstrained without flavour data is now rather well constrained ($1/\sqrt{|C|} > 5$ TeV). This direction is[27]

$$\begin{aligned} C = &-0.56\,(C_{qq}^{(1)\prime} - C_{qq}^{(3)\prime}) - 0.28\,C_{qq}^{(3)} + 0.11\,C_{lq}^{(1)} - 0.09\,C_{lq}^{(3)} - 0.03\,C_{ed} + 0.01\,C_{eu} \\ &- 0.02\,C_{lu} - 0.11\,C_{qe} + 0.03\,C_{ld} - 0.07\,C_{Hu} - 0.03\,C_{Hd} + 0.02\,C_{Hq}^{(1)} - 0.14\,C_{Hq}^{(3)} - 0.32\,C_{He} \\ &- 0.27\,C_{Hl}^{(1)} - 0.02\,C_{Hl}^{(3)} - 0.08\,C'_{ll} - 0.10\,C_{HD} - 0.05\,C_{HW} - 0.20\,C_{HWB} \\ &- 0.09\,C_{HB} + 0.01\,C_W - 0.01\,C_{H\Box}. \end{aligned} \tag{5.55}$$

[27] The other strictly flat direction which is closed by the flavour data is represented by the eigenvalue at position 17 in the plot, whereas the eigenvalue at position 16 is not exactly zero for the fit without flavour data, but much too small to be visible.

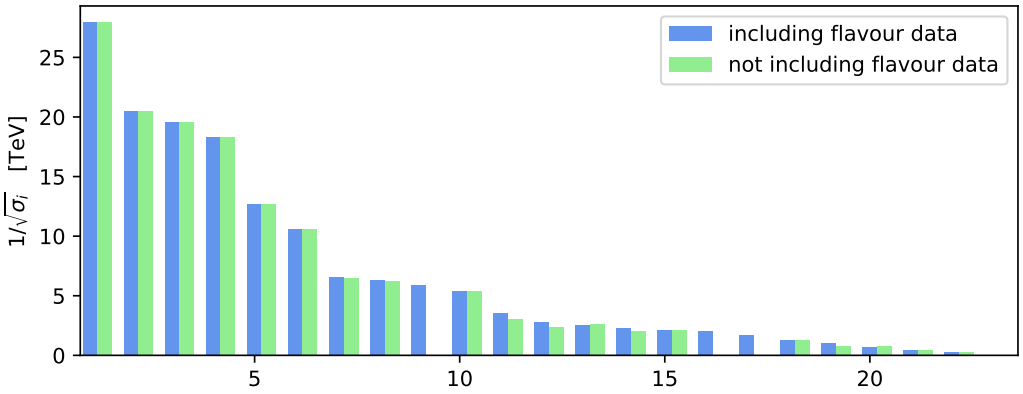

Figure 5.6: Comparison of the eigenvalues of the Fisher matrix assuming full $U(3)^5$ flavour symmetry, for the fit including the flavour data (blue), and the fit excluding flavour data (green). We have not plotted eigenvalues for which the fit including flavour data gives $1/\sqrt{\sigma_i} < 250$ GeV.

5.5 Summary

We have studied the impact of the flavour data in global fits of the leading order MFV SMEFT. We focus in particular to the down-type FCNC currents since they provide the strongest constrains. After performing one-loop matching we can see that flavour measurements not only constrains flavour-changing operators but also bosonic flavourless operators and flavour-conserving ones. An illustrative fit on the LEP I flat directions, which is due to reparametrization invariance, were used to show that flavour measurements have a competitive impact on closing the flat directions as the Higgs and LEP II WW data.

The most symmetric form of the SMEFT is obtained assuming $U(3)^5$, and any other breaking of this flavour assuming would lead to enhanced effects in flavour. Therefore, our findings may be taken as conservative bounds from flavour on generic new physics. However, the specific Wilson coefficient combinations that can be constrained by flavour data clearly depend rather strongly, both in their number and direction, on the flavour assumptions imposed at the scale Λ. Hence the results of our analysis cannot directly be extrapolated to other flavour scenarios which may be of interest, however in cases where the flavour assumption we make a few comments here.

If a flavour assumption forbids tree level FCNCs (this is true, for example, of an unbroken $U(2)^5$ flavour symmetry among the first two generations of fermions), then the matching calculations at m_W will not change considerably. The only change will be that extra terms that are independent of the top mass may now appear in the matching re-

sults involving operators that contain quarks, because GIM cancellations which occur in the MFV case will no longer happen. In the context of a global fit, the lifting of the $U(3)^5$ symmetry will have the effect of somewhat disconnecting the spheres of influence of the different constraints, since the flavour and Higgs observables depend strongly on top-containing operators, while the electroweak and 4-fermion observables are largely insensitive to the top.

If instead the theory at Λ contains both flavour violating and flavour conserving operators, then things become more complicated, not least because of the proliferation of Wilson coefficients. A likelihood for general flavour structures, including Higgs and electroweak observables, was recently calculated in Ref. [206]. Processes involving FCNCs will now depend on both flavour-violating operators at tree level and flavour-conserving operators at loop level. The CKM must also be consistently parametrised, as discussed in Ref. [139]. Understanding the messages that we can learn from studying this general case will clearly be an important goal over the next few years.

6 Modern Methods for Scattering Amplitudes

Modern methods are a collection of tools and efficient formalism to perform high-multiplicity and high-loop calculations for scattering amplitudes. There are three main ingredients for these calculations: spinor-helicity variables, recursion relations and generalized unitarity. The first one is the variables used in the calculations. Feynman diagrams use polarization vectors, Dirac spinors and momenta vectors. New modern methods use spinor-variables as building blocks. The second ingredient accounts for the construction of higher-point amplitudes, which is done recursively from on-shell lower-points. Finally, generalized unitarity makes use of the amplitude's analytical structure to construct loop amplitudes from tree-level ones. The idea of re-using amplitudes to increase the multiplicity and number of loops makes these methods efficient. In this thesis we are interested in the tree-level amplitudes with effective field theories, therefore we are not going to discuss generalized unitarity [207].

More than making the calculation efficient, these methods provide a deep understanding of hidden structures of gauge and gravity amplitudes. Among its successes, we can point out new soft theorems, double copy relations, colour-kinematics duality, Black Hole binary dynamics, momentum twistors, amplitudehedron, and many others (See [10, 208–212] for reviews).

One of the interesting directions is the construction of theories bypassing Lagrangians. Pure Yang-Mills is characterized by its only coupling constant $g_{\rm YM}$, and higher order amplitudes (in multiplicity and loops) can be computed from the three-point vertex, which already contains all the information of the theory. Moving to effective theories, where higher-dimensional operators with arbitrary coefficients are added, more information is required to construct the amplitude. One way to define some effective theories is to make use of the of the soft behaviour of these amplitudes. This point of view shed new light on how to define a theory [209].

However, most of the progress has been made in massless theories since masses add more complications. Pioneering works on trying to extend the formalism to massive amplitudes used many different approaches, for instance: [213–220], where the momenta are decomposed into a particular direction, [221] where the massive little-group is used to constrain the three-points amplitudes, and [222] using six-dimensional spinors assigning the last two components of the momenta to represent the masses. However, a simple formalism for massive particles that makes expressions compact was still missing. Recently, a new covariant formalism was presented by Arkani-Huang-Huang [8], where the spinors were constructed based on the little group of a massive particle, SU(2). Three-point amplitudes for all spins and masses were obtained, allowing one to perform higher point calculations. Among several applications, these modern methods were already applied to the Standard Model [223, 224], black hole binary calculations [225], Soft Theorems [226], etc. The natural question that follows is how to apply them for Effective Theories.

Naturally, the progress in on-shell effective theories was made for massless theories. In [227], the authors obtained recursion relations for EFTs making use of their soft behaviour. Modifications of soft theorems due to effective operators were also obtained, appearing at sub-leading order to Yang-Mills and sub-sub leading order to Gravity [228, 229]. In the context of SMEFT, the explanation of null entries of the anomalous matrices were easily obtained using on-shell methods [9] and, recently, the extension of these zeros for higher loops were discovered, leading to more non renormalization theorems [76].

A very natural direction is the use of the massive spinor-helicity formalism for effective theories. The third work presented in this thesis is the construction of SMEFT in the broken phase, where particles are massive. In this project, we construct the three-point amplitudes for SMEFT and use them to build higher point ones. Another application of the massive formalism for on-shell amplitudes, which will not be discussed here, is the classical gravitational potential calculation from massive spinors. In particular, we point out the construction of a heavy-particle spinor formalism developed by the author and collaborators [5].

In the following section we discuss the basis to construct the angle and square brackets from the particles' little group. These are the building blocks for the three-point amplitudes for massless and massive theories. We use them to recursively build higher points amplitudes at Section 6.4 and end the section with a discussion of on-shell effective theories. These ingredients will be all the machinery for the next section, where we introduce 'The Rise of SMEFT On-shell Amplitudes'.

6.1 Little Group

What is a particle? According to Wigner [230], a particle is a fundamental representation of the Poincaré Group in the Hilbert space. In the Lie algebra of the Poincaré Group, there is only one set of operators that commutes $[P^\mu, P^\nu] = 0$. Since we need to represent the one-particle state in the Hilbert space, it is natural to use these operators P^μ. Therefore, we can construct a basis of eigenvectors such that $P^\mu|\psi(p,\sigma)\rangle = p^\mu|\psi(p,\sigma)\rangle$, where σ represent the possible degeneracies of this eigenspace.

The realisation of the Poincaré transformation in the Hilbert space can be decomposed as a product of the Lorentz transformation Λ and a translation labelled by a, i.e. $\mathrm{U}(\Lambda, a) = \mathrm{U}(\Lambda, 0)\mathrm{U}(\mathbb{1}, \Lambda^{-1}a)$. Furthermore, any Lorentz transformation can be written as products of parity and time-reversal $\mathcal{P}, \mathcal{T}, \mathcal{PT}$ with transformation from the subgroup $\mathrm{SO}(1,3)$, which is the proper-orthocronus subgroup[28]. Transformations in this subgroup preserve the norm of the vector $p^\mu p_\mu = m^2$ and the sign of the zeroth-component. Therefore, the task to represent the Poincaré Group is reduced to represent the Lorentz group with p^2 and p^0 fixed, i.e. with the following transformation $W(\Lambda, p)k = k$.

[28]Proper indicates that $\det\Lambda = +1$ and orthocronus refers to $\Lambda^0_0 \geq 1$. With parity and time-reversal transformations one can obtain the whole homogeneous Lorentz group.

The set of all transformations that keep the momentum k invariant is called the *little group* (LG) and depends on the particle's mass. We refer to Weinberg's book [11] for the task of finding each type little group, where here we just state that for a massless little group is SO(2) and for a massive particle is SO(3). Therefore, the one-particle state transforms as

$$\mathrm{U}(\Lambda)|p,\sigma\rangle = D_{\sigma\sigma'}(W(\Lambda,p;k))|\Lambda p,\sigma'\rangle \tag{6.1}$$

where $D_{\sigma\sigma'}$ is the little group realisation and it is summed over the index σ'. Given the transformation of the one-particle states, we can obtain the transformation of the S-matrix, or the scattering amplitude, which is the object of central interest.

A scattering amplitude of n particles can be labelled by (p_i,σ_i) for $i=1,..,n$. The S-matrix element transforms under Poincaré transformation according with each one-particle state separately

$$A^{\Lambda}(p_i,\sigma_i) = \prod_i D_{\sigma_i\sigma_i'}(W)A((\Lambda p)_i,\sigma_i'). \tag{6.2}$$

where we stripped out the delta of momentum conservation $\delta^D(p^\mu_{i_1}+...p^\mu_{i_n})$.

The usual procedure in QFT is to formulate the action of the theory, derive the Feynman rules and then calculate the matrix elements, making sure that the final answer is gauge invariant. To do so, we start with off-shell fields in the Lagrangian that give external state wave functions which are Dirac spinors, $u(p,\sigma), v(p,\sigma)$, for fermions, and the polarization vectors $\epsilon^\mu(p)$ for external gauge bosons. Both of these wave-functions are four-element spinors and vectors which have to satisfy $p_\mu\epsilon^\mu_\sigma = 0$ to preserve gauge invariance. However, these constraints only appear because we are working with off-shell quantities, the fields. Moreover, the wave-functions do not transform correctly under Lorentz transformations. Consider a massless photon transforming under the Little Group [8]

$$(\Lambda p) = p \qquad \rightarrow \qquad (\Lambda\epsilon_\pm)^\mu = e^{\pm i\phi}\epsilon^\mu_\pm + \alpha(\Lambda,p)p^\mu. \tag{6.3}$$

Thus, the equivalence class $\{\epsilon^\mu_\pm|\epsilon^\mu_\pm+\alpha p^\mu\}$ is the object invariant under Lorentz transformations and one has to fix the gauge to froce $\epsilon^\mu_\pm$ to transform correctly under the little group. Polarization tensors and momentum vectors are very useful in Feynman diagrams computation, but it seems more natural to start with variables that from the beginning transform correctly under the little group those are called *spinor-helicity variables*.

6.2 Massless Spinor-Helicity Formalism

One of the reason behind the spinor-helicity formalism's [231–233] success is the ability to represent polarization vectors and momenta using the same spinor building blocks. We start constructing these blocks by noticing that we can generalize the universal covering

group $\mathrm{SL}(2,\mathbb{C})$ of the little group $\mathrm{SO}(1,3)$. In simple words, it maps a four vector to a 2 x 2 matrix:

$$p_{\alpha\dot{\beta}} = p_\mu \sigma^\mu_{\alpha\dot{\beta}} \qquad \text{and} \qquad p^{\dot{\alpha}\beta} = p^\mu \bar{\sigma}_\mu^{\dot{\alpha}\beta} \tag{6.4}$$

where the sigma matrices are given by $\sigma^\mu = (1, \vec{\sigma})$ and $\bar{\sigma}^\mu = (1, -\vec{\sigma})$. Here, we are going to use the following conventions for the Pauli matrices: $\sigma^0 = \left(\begin{smallmatrix} 1 & 0 \\ 0 & 1 \end{smallmatrix}\right), \sigma^1 = \left(\begin{smallmatrix} 0 & 1 \\ 1 & 0 \end{smallmatrix}\right), \sigma^2 = \left(\begin{smallmatrix} 0 & -i \\ i & 0 \end{smallmatrix}\right)$ and $\sigma^3 = \left(\begin{smallmatrix} 1 & 0 \\ 0 & -1 \end{smallmatrix}\right)$. With these conventions the momentum represented as a 2x2 matrix is given by:

$$\det(p_{\alpha\dot{\beta}}) = \det \begin{pmatrix} p_0 + p_3 & p_1 - ip_2 \\ p_1 + ip_2 & p_0 - p_3 \end{pmatrix} = p^2 = m^2 \tag{6.5}$$

Generally, the momentum matrix determinant is non-vanishing, meaning that the rank of the matrix is two.

6.2.1 Massless spinors

In the massless case the determinant is zero, $\det(p_{\alpha\dot{\beta}}) = 0$, meaning it is a matrix of rank 1. Thus, this matrix can be decomposed as a tensor product of two Weyl spinors, which we represent in the bracket notation as

$$p_{\alpha\dot{\beta}} = \lambda_{p\alpha}\tilde{\lambda}_{p\dot{\beta}} \equiv |p\rangle_\alpha [p|_{\dot{\beta}} \qquad \text{and} \qquad p^{\dot{\alpha}\beta} = \tilde{\lambda}_p^{\dot{\alpha}} \lambda_p^\beta \equiv |p]^{\dot{\alpha}} \langle p|^\beta \tag{6.6}$$

For real momenta, $p_{\alpha\dot{\beta}}$ is a hermitian matrix and therefore both variables are connected through $\tilde{\lambda}_{p\alpha} = (\lambda_{p\alpha})^*$. However, we are going to work with complex momenta where these variables are independent. The power of complex momenta will come through in the recursion relations. One of the advantages of working with these variables is the way that they transform under Lorentz transformations. Let $S \in \mathrm{SL}(2,\mathbb{C})$, which transforms the Weyl spinors, up to a U(1) rotation [223]

$$\lambda_{p\alpha} \to S_\alpha^\beta \lambda_{p\beta} = e^{i\phi/2}\lambda_{Lp\alpha} \qquad \text{and} \qquad \tilde{\lambda}_{p\dot{\alpha}} \to \tilde{\lambda}_{p\dot{\beta}} (S^\dagger)_{\dot{\alpha}}^{\dot{\beta}} = e^{-i\phi/2}\tilde{\lambda}_{Lp\dot{\alpha}} \tag{6.7}$$

and, as expected, leaving the momentum invariant under this transformation. The spinors were given with 'downstairs' indices, to raise the index one has to use the epsilon matrices $\epsilon^{\alpha\beta} = \left(\begin{smallmatrix} 0 & 1 \\ -1 & 0 \end{smallmatrix}\right)$ and $\epsilon_{\alpha\beta} = \left(\begin{smallmatrix} 0 & -1 \\ 1 & 0 \end{smallmatrix}\right)$. These matrices also contract the spinors to construct our basic building blocks

$$\langle pq\rangle \equiv \lambda_p^\alpha \lambda_{q\alpha} = \lambda_p^\alpha \epsilon_{\alpha\beta} \lambda_q^\beta \qquad [pq] \equiv \tilde{\lambda}_{p\dot{\alpha}} \tilde{\lambda}_q^{\dot{\alpha}} = \tilde{\lambda}_{p\dot{\alpha}} \epsilon^{\dot{\alpha}\dot{\beta}} \tilde{\lambda}_{q\dot{\beta}} \qquad \langle pq\rangle [qp] = \langle p|q|p] = 2p \cdot q \tag{6.8}$$

These angular and squared variables can represent the momentum and the Weyl spinors, which are components the Dirac spinors in the massless limit, which obey the massless

Dirac equation $\not{p}\, u_\pm(p) = 0$. Therefore,

$$u_+ = \begin{pmatrix} 0 \\ |p]^{\dot{\alpha}} \end{pmatrix} \qquad \text{and} \qquad u_- = \begin{pmatrix} |p\rangle_\alpha \\ 0 \end{pmatrix}. \tag{6.9}$$

But the spinors really come in handy for polarization vectors and its gauge invariance. These gauge bosons polarization vectors are constructed with an auxiliary reference vector

$$\epsilon^\mu_{p+} = \frac{1}{\sqrt{2}} \frac{\langle q|\sigma^\mu|p]}{\langle qp\rangle} \qquad \text{and} \qquad \epsilon^\mu_{p-} = -\frac{1}{\sqrt{2}} \frac{[q|\bar{\sigma}^\mu|p\rangle}{[qp]} \tag{6.10}$$

where q cannot be proportional to p. Seems that any amplitude constructed with these polarization vectors will depend on q. But this is not true, a choice of q is as choosing a gauge and the final answer will not depend on it. The goal in the calculation is to choose q as early as possible to get rid of several terms.

6.2.2 Massless three-point amplitudes

We know how the building blocks transform under LG and we know how the amplitude transforms. We are then equipped with the tools to completely determine the three-points massless amplitude $A(1^{h_1}, 2^{h_2}, 3^{h_3})$, where the particles are labelled by the numbers 1,2 and 3, and h_i represents the helicities. First, we impose momentum conservation [209],[29]

$$p_1 + p_2 + p_3 = 0 \qquad \Rightarrow \qquad \begin{aligned} (p_1+p_2)^2 &= \langle 12\rangle[21] = p_3^2 = 0 \\ (p_2+p_3)^2 &= \langle 23\rangle[32] = p_1^2 = 0 \\ (p_3+p_1)^2 &= \langle 31\rangle[13] = p_2^2 = 0 \end{aligned} \tag{6.11}$$

In the first line, if we choose the angular brackets $\langle 12\rangle$ to be zero, then the square bracket $[21] \neq 0$. Using momentum conservation $\langle 32\rangle[21] = -\langle 31\rangle[11] + \langle 33\rangle[31] = 0$, where we see that $\langle 32\rangle$ is also zero. Doing the same steps for all cases, we arrive at two options: either $\langle 12\rangle = \langle 23\rangle = \langle 31\rangle = 0$ or $[12] = [23] = [31] = 0$. The first solution is called anti-holomorphic, where all angle brackets vanish and the second is the holomorphic solution, with the square brackets vanishing. This means that the three-point massless amplitudes can only be written either with λ or with $\tilde{\lambda}$ but never with both. Taking the holomorphic type, we can write the three-point amplitude as

$$A(1^{h_1}, 2^{h_2}, 3^{h_3}) = \langle 12\rangle^{n_3} \langle 23\rangle^{n_1} \langle 31\rangle^{n_2} \tag{6.12}$$

and we just need to fix the exponents n_i. A n-point amplitude transforms accordingly to Eq. 6.2, which has $D_{\sigma\sigma'} = e^{i\phi}\delta_{\sigma\sigma'}$ for each massless particle. Since we are working with complex momenta $\tilde{\lambda} \neq (\lambda)^*$ and phase can be a complex number t, therefore

$$\lambda_i \to t_i \lambda_t \qquad \tilde{\lambda}_i \to t_i^{-1}\tilde{\lambda}_i \qquad A_n(1^{h_1}...n^{h_n}) \to \prod_i t_i^{-2h_i} A_n(1^{h_1}...n^{h_n}) \tag{6.13}$$

[29] Where our convention is all momenta outgoing.

where $t = e^{+i\phi/2}$ for real momenta. The LG scaling completely fixes the exponents n_i, such that $-2h_1 = n_2 + n_3$ and similarly for the others. Solving for the exponents we have

$$n_1 = h_1 - h_2 - h_3 \qquad n_2 = h_2 - h_3 - h_1 \qquad n_3 = h_3 - h_1 - h_2 \tag{6.14}$$

If we would have chosen the non-holomorphic amplitude $[12]^{\bar{n}_3}[23]^{\bar{n}_1}[31]^{\bar{n}_2}$, we would have arrived at $\bar{n}_i = -n_i$. The last ingredient to completely fix the amplitude is locality which implies that the amplitude has non-negative mass dimension [30]. Since each bracket has mass dimension one, the amplitude scales as $\sum_i n_i = -\sum_i \bar{n}_i = -\sum_i h_i = -h \geq 0$. Finally, we arrive at the general formula for the three-particle massless amplitude in four dimensions

$$A(1^{h_1}, 2^{h_2}, 3^{h_3}) = \begin{cases} \langle 12\rangle^{n_3}\langle 23\rangle^{n_1}\langle 31\rangle^{n_2}, & h < 0 \\ [12]^{\bar{n}_3}\ [23]^{\bar{n}_1}\ [31]^{\bar{n}_2}, & h > 0 \end{cases} \tag{6.15}$$

where $n_1 = -\bar{n}_1 = h_1 - h_2 - h_3$. Besides the exceptional case of three-scalars particles, where the amplitude is just a constant, the $h = 0$ is particular because it fails to construct local amplitudes at higher point, so it has to be zero at three-points [234]. It is incredible that just momentum conservation, LG scaling and locality completely fix the behaviour of a three point amplitude. In the next section we are going to upgrade them to massive spinors and afterwards construct higher points.

6.3 Massive Spinor-Helicity Formalism

There are several generalizations of the spinor-helicity formalism for massive particles [213–222]. In this work, we are going to use the one by Arkani-Huang-Huang [8] due to its simplicity and covariant formulation. In the case of massive particles, $\mathrm{rk}(p_{\alpha\dot{\beta}}) = 2$, which can be written as two rank-1 matrices. These matrices are tensor products of two Weyl spinors, i.e. the massive momentum can be decomposed into two null momenta

$$p_{\alpha\dot{\beta}} = \lambda^I_{p\alpha}\tilde{\lambda}_{p\dot{\beta}I} = \lambda^1_{p\alpha}\tilde{\lambda}_{p\dot{\beta}1} + \lambda^2_{p\alpha}\tilde{\lambda}_{p\dot{\beta}2} \tag{6.16}$$

and we can use the ϵ_{IJ} to lower or raise the index. With this decomposition, the on-shell condition becomes

$$\det(p_{\alpha\dot{\beta}}) = p^2 = m^2 \quad \Rightarrow \quad \det(\lambda^I_{p\alpha}) \cdot \det(\tilde{\lambda}^I_{p\dot{\alpha}}) = \mathfrak{M} \cdot \tilde{\mathfrak{M}} = m^2 \tag{6.17}$$

[30] In the Lagrangian, negative mass dimensions would require inverse powers of derivatives. For instance, the amplitude $A(1^-, 2^-, 3^+) = \frac{\langle 12\rangle^3}{\langle 23\rangle\langle 31\rangle}$ has the same little-group scaling as the amplitude $A(1^-, 2^-, 3^+) = \frac{[23][31]}{[12]^3}$. However, the kinetic term of the forms is positive, corresponding to the known term in the Lagrangian $\mathrm{Tr}F^2$. The latter has negative mass dimension for the kinetic term and correspond to $AA\frac{\partial}{\Box}A$, which is a non-local term

The natural choice for the determinant of each spinor is a democratic choice $\mathfrak{M} = \tilde{\mathfrak{M}} = m$. and the massive spinors transform under the massive LG as

$$\lambda^I_\alpha \to W^I_J \, \lambda^J_\alpha \qquad\qquad \tilde{\lambda}_{\dot{\beta}I} \to (W^{-1})^J_I \, \tilde{\lambda}_{\dot{\beta}J} \tag{6.18}$$

keeping the momenta invariant. As in the massless case, the amplitude will have a certain transformation under the LG of all particles and we are going to bootstrap, for three-points, which spinors structure should be included. In this language, the Dirac spinors become

$$u^{AI} = \begin{pmatrix} \lambda^I_\alpha \\ \tilde{\lambda}^{\dot{\alpha}I} \end{pmatrix} \qquad \bar{u}^I_A = \begin{pmatrix} -\lambda^{\alpha I} \\ \tilde{\lambda}^I_{\dot{\alpha}} \end{pmatrix} \qquad v^{AI} = \begin{pmatrix} -\lambda^I_\alpha \\ \tilde{\lambda}^{\dot{\alpha}I} \end{pmatrix} \qquad \bar{v}^I_A = \begin{pmatrix} \lambda^{\alpha I} \\ \tilde{\lambda}^I_{\dot{\alpha}} \end{pmatrix} \tag{6.19}$$

And as in the massless case, we want to introduce the bracket notation, which in this case will have the SU(2) index. An explicit representation of these variables is [223]

$$\lambda^I_{p\alpha} = \sqrt{E+P} \begin{pmatrix} -e^{-i\phi} \sin\frac{\theta}{2} \\ \cos\frac{\theta}{2} \end{pmatrix}_\alpha \otimes \begin{pmatrix} 0 \\ 1 \end{pmatrix}^I + \frac{m}{\sqrt{E+P}} \begin{pmatrix} \cos\frac{\theta}{2} \\ e^{i\phi} \sin\frac{\theta}{2} \end{pmatrix}_\alpha \otimes \begin{pmatrix} 1 \\ 0 \end{pmatrix}^I \tag{6.20}$$

$$\tilde{\lambda}^I_{p\alpha} = \sqrt{E+P} \begin{pmatrix} \cos\frac{\theta}{2} \\ e^{i\phi} \sin\frac{\theta}{2} \end{pmatrix}^{\dot{\alpha}} \otimes \begin{pmatrix} 1 \\ 0 \end{pmatrix}^I + \frac{m}{\sqrt{E+P}} \begin{pmatrix} -e^{-i\phi} \sin\frac{\theta}{2} \\ \cos\frac{\theta}{2} \end{pmatrix}^{\dot{\alpha}} \otimes \begin{pmatrix} 0 \\ 1 \end{pmatrix}^I \tag{6.21}$$

$$\tag{6.22}$$

which makes clear how to take the high energy limit ($m \to 0$), where one should recover the massless spinors

$$\lambda^I_{p\alpha} \to \lambda_{p\alpha} \zeta^I_-, \qquad \tilde{\lambda}^{\dot{\alpha}I}_p \to \tilde{\lambda}^{\dot{\alpha}}_p \zeta^I_+ \tag{6.23}$$

with $\zeta^I_- \equiv (0,1)$ and $\zeta^I_+ \equiv (1,0)$.

6.3.1 Massive Three-point Amplitudes

We then come to the task of defining all the possible 3-point massive amplitudes. These amplitudes will be labelled by the SU(2) little group indices. The main idea here is to factor out all the massive spinors such that the remaining amplitude contains only $\mathrm{SL}(2,\mathbb{C})$ indices. For example, take a three-point amplitude with massless particles and one spin-s massive, the amplitude will be a symmetrick rank $2s$ tensor in $\{I_1, ..., I_{2s}\}$, i.e. $A_3(1^{h_1}, 2^{h_2}, \mathbf{3}^{I_1,...,I_{2s}})$ [8]. This amplitude will have the massless LG h_1, h_2 and we strip out all the massive spinors λ or $\tilde{\lambda}$ from the third leg

$$\mathcal{A}_3(1^{h_1}, 2^{h_2}, \mathbf{3}^{I_1,...,I_{2s}}) = \boldsymbol{\lambda}^{I_1}_{\alpha_1} ... \boldsymbol{\lambda}^{I_{2s}}_{\alpha_{2s}} \, A_3^{h_1,h_2,\{\alpha_1,...,\alpha_{2S}\}} \tag{6.24}$$

$$\mathcal{A}_3(1^{h_1}, 2^{h_2}, \mathbf{3}^{I_1,...,I_{2s}}) = \tilde{\boldsymbol{\lambda}}^{I_1}_{\dot{\alpha}_1} ... \tilde{\boldsymbol{\lambda}}^{I_{2S}}_{\dot{\alpha}_{2s}} \, \tilde{A}_3^{h_1,h_2,\{\dot{\alpha}_1,...,\dot{\alpha}_{2s}\}} \tag{6.25}$$

where $I_a = 1, 2$ with $a = 1 \cdots 2s$ are $SU(2)$ indices. For more massive legs, we strip out for each massive leg. The amplitude without these spinor is called stripped amplitude and is a tensor in $\mathrm{SL}(2,\mathbb{C})$, and our task is to find the most general form of it. It is important to notice that we have removed the little group of the massive particle and we need to respect the massless little group. We also have shown two types of amplitude that resembles the holomorphic and anti-holomorphic options of the massless case. However, we will see that both representations are equivalent, since the kinematics do not force us to pick one of them.

To fully determine the amplitude, we need to look for two linear independent 2-component spinors (v_α, u_α) that span this $\mathrm{SL}(2,\mathbb{C})$ space.

- **Two-massless + One-massive**
  In this case, is natural to take the two massless spinors $(v_\alpha, u_\alpha) = (\lambda_{1\alpha}, \lambda_{2\alpha})$ and together with the square brackets, we can fix the *massless little group*

$$A_3^{h_1,h_2\{\alpha_1,\ldots,\alpha_{2s}\}} \propto (\lambda_1^{n_1}\lambda_2^{n_2})^{\{\alpha_1,..,\alpha_{2s}\}}[12]^{n_{12}}. \tag{6.26}$$

  where s is the spin of the massive particle. The helicities (h_1, h_2) completely fix the $2s$-polynomial in λ_1, λ_2. First, the polynomial has $2s$ indices, which constrains $n_1 + n_2 = 2s$. Secondly, the LG of 1 and 2 set $h_i = n_i + n_{12}$, for $i = 1, 2$. These conditions fix the n_i to be $n_1 = s + h_2 - h_1$, $n_2 = s + h_1 - h_2$ and $n_{12} = s + h_1 + h_2$. We thus obtain

$$A_3^{h_1,h_2\{\alpha_1,\ldots,\alpha_{2s}\}} = g\,(\lambda_1^{s+h_2-h_1}\lambda_2^{s+h_1-h_2})^{\{\alpha_1,..,\alpha_{2s}\}}[12]^{s+h_1+h_2}, \tag{6.27}$$

  and dimensional analysis gives $[g] = 1-(3s+h_1+h_2)$. A non-trivial constraint on the amplitude comes from the fact that the expression above only exist if $|h_2 - h_1| \leq s$. A similar analysis can be done to $\tilde{A}_3$, using $(v_\alpha, u_\alpha) = (\tilde{\lambda}_{1\alpha}, \tilde{\lambda}_{2\alpha})$

$$\tilde{A}_3^{h_1,h_2\{\alpha_1,\ldots,\alpha_{2s}\}} = g\,(\tilde{\lambda}_1^{s+h_2-h_1}\tilde{\lambda}_2^{s+h_1-h_2})^{\{\alpha_1,..,\alpha_{2s}\}}\langle 12\rangle^{s+h_1+h_2} \tag{6.28}$$

- **One massless + Two massive particles**
  An amplitude with two massive particles with spin s_1, s_2 and mass m_1, m_2 coupled to one massless particle with helicity h_3 can be decomposed as

$$\mathcal{A}_3(\mathbf{1}^{I_1\cdots I_{2s_1}}\,\mathbf{2}^{J_1\cdots J_{2s_2}}\,3^{h_3}) = \boldsymbol{\chi}^{I_1}_{\alpha_1}\cdots\boldsymbol{\chi}^{I_{2s_1}}_{\alpha_{2s_1}}\,\boldsymbol{\psi}^{J_1}_{\beta_1}\cdots\boldsymbol{\psi}^{J_{2s_2}}_{\beta_{2s_1}}\,A_3^{\{\alpha_1\cdots\alpha_{2s_1}\}\{\beta_1\cdots\beta_{2s_2}\}}, \tag{6.29}$$

  where $\boldsymbol{\chi}$ and $\boldsymbol{\psi}$ are the massive spinors for particles $\mathbf{1}$ and $\mathbf{2}$, respectively. A similar decomposition can be also made in the anti-chiral basis, constructed with $\tilde{\boldsymbol{\chi}}$ and $\tilde{\boldsymbol{\psi}}$. In the case where $m_1 \neq m_2$, the spinors $u^\alpha \equiv \lambda_3^\alpha$ and $v_\alpha \equiv p_{\mathbf{1}\alpha\dot{\alpha}}\tilde{\lambda}_3^{\dot{\alpha}}/\sqrt{m_1\,m_2}$ span the entire $2D$ spinor space allowing the amplitude to be written as

$$A^{\{\alpha_1\cdots\alpha_{2s_1}\}\{\beta_1\cdots\beta_{2s_2}\}} = \sum_{i=1}^{C} g_i\left(u^{s_1+s_2+h_3}v^{s_1+s_2-h_3}\right)^{\{\alpha_1\cdots\alpha_{2s_1}\}\{\beta_1\cdots\beta_{2s_2}\}},$$

where $C = 2\min(s_1, s_2) + 1$ is the number of different partitions of the two groups of $SL(2, \mathbb{C})$ indices.

In the case where $m_1 = m_2$, we have a problem because the two vectors that span the space are collinear

$$v_\alpha u^\alpha \propto \langle 3|p_{\mathbf{1}}|3] = 2p_{\mathbf{1}} \cdot p_3 = p_{\mathbf{2}}^2 - p_{\mathbf{1}}^2 = m_1^2 - m_2^2 = 0 \tag{6.30}$$

To solve this, we need to define auxiliary objects,

$$x \equiv \frac{\langle \zeta | p_{\mathbf{1}} | 3]}{\langle 3\, \zeta \rangle}, \qquad x^{-1} \equiv \frac{\langle 3 | p_{\mathbf{1}} | \tilde{\zeta}]}{[\tilde{\zeta}\, 3]}, \tag{6.31}$$

where 3 is the label of the massless particle. The amplitude is then given by

$$A^{\{\alpha_1 \cdots \alpha_{2s_1}\}\{\beta_1 \cdots \beta_{2s_2}\}} = \sum_{i=|s_1 - s_2|}^{s_1+s_2} g_i \, (m\, x)^{h+i} \left(\lambda_3^{2i} \varepsilon^{s_1+s_2-i}\right)^{\{\alpha_1 \cdots \alpha_{2s_1}\}\{\beta_1 \cdots \beta_{2s_2}\}} . \tag{6.32}$$

where $[g_i] = 1 - (i + s_1 + s_2)$.

- **Three massive particles**
  In order to construct this amplitude, we have two tensor structures: The antisymmetric tensor $\epsilon_{\alpha\beta}$ and the symmetric tensor $\mathcal{O}_{\alpha\beta} = \epsilon^{\dot{\alpha}\dot{\beta}}(p_{1\alpha\alpha} p_{2\beta\dot{\beta}} + p_{1\beta\dot{\alpha}} p_{2\alpha\dot{\beta}})$, which leads to the following three-point stripped amplitude

$$A_{\{\alpha_1 \cdots \alpha_{2s_1}\},\{\beta_1 \cdots \beta_{2s_2}\},\{\gamma_1 \cdots \gamma_{2s_3}\}} = \sum_{i=0}^{1} g_{\sigma_i} \left(\mathcal{O}^{s_1+s_2+s_3-i} \epsilon^i\right)_{\{\alpha_1 \cdots \alpha_{2s_1}\},\{\beta_1 \cdots \beta_{2s_2}\},\{\gamma_1 \cdots \gamma_{2s_3}\}} \tag{6.33}$$

  However, we noticed that is easier to just write down all possible terms consistent with the little group. Many structures cancel since $\langle \boldsymbol{i}\, \boldsymbol{i} \rangle = [\boldsymbol{i}\, \boldsymbol{i}] = 0$ after the symmetrization of the $SU(2)$ indices. Also, structures with a momentum insertion can be rewritten in terms of a contraction of angle and square brackets with the use of Schouten identities.

Given all the three-point amplitudes, how can we construct higher point amplitudes? For massless amplitudes, the success comes from the famous recursion relations where one takes advantage of the simple analytical structure at the tree-level to deform the amplitude and construct higher-points. We are going to see this method in detail in the next section. For massive amplitudes, a method introduced as 'gluing' uses correct factorization to just put amplitudes together and obtain four points. We are also going to compare these two methods in the following chapters.

6.4 Recursion Relations

At three-points, locality was the ingredient to fix the non-negative mass dimension of the amplitude. In order to go to higher-point amplitudes, we are going to make more use of locality. Imagine the situation that one could tune the external kinematics such that an intermediate particle goes on-shell. In this particular point, the tree-level amplitudes have a pole, exhibiting a singularity. The consequence of the intermediate particle going on-shell is that it travels a macroscopic distance. Moreover, the four-point amplitude factorizes into a product of lower-point sub-amplitudes, which corresponds to two processes occurring at two different points [209]. For example, imagine that we put the external data such that the s-channel is on-shell, as consequence, we will have:

$$\lim_{s\to 0} sA_4 = A_3^L A_3^R \tag{6.34}$$

where left (L) and right (R) label the sub-amplitudes. From this, we can see that locality allows us to relate lower-point amplitudes to higher-points, as a recursion relation. However, we need a general method to probe the analytical structure of this amplitude. This is achieved by shifting the external momenta and using the Cauchy theorem.

The on-shell recursion relations are a method to relate the amplitude at these singular values (poles) to the amplitude for general kinematics. In the following, we give the recipe for recursion relations which have three main ingredients: *(i)* momentum shift, *(ii)* Cauchy theorem and *(iii)* boundary terms. Consider an n-point amplitude A_n with momenta $p_i, i = 1 \cdots n$. We start shifting the external momenta by q_i

$$p_i \to p_i(z) = p_i + zq_i \tag{6.35}$$

where $z \in \mathbb{C}$ is a complex variable that the amplitude will depend on $A \to A(z)$, where the original amplitude is recovered when $z = 0$. These momentum shifts have to preserve momentum conservation and on-shellness

$$\text{mom. conserv.} \qquad \sum_i p_i(z) = 0 \quad \to \quad \sum_i q_i = 0 \tag{6.36}$$

$$\text{on-shellness} \qquad p_i(z)^2 = 0 \quad \to \quad q_i^2 = p_i \cdot q_i = 0 \tag{6.37}$$

Furthermore, we consider that $q_i \cdot q_j = 0$, which will simplify the calculations. Consider a non-trivial subset I of momenta $P_I = \sum_{i\in I} p_i$, then the shifted momenta will be linear in z:

$$P_I(z) = \sum_{i\in I} p_i(z) = P_I + zQ_I, \quad \text{where} \quad Q_I = \sum_{i\in I} q_i \tag{6.38}$$

Generally, the subset of momenta is off-shell $P_I^2 \neq 0$ and the shifted momenta is on-shell for the following value of $z = z_I$

$$0 = P_I^2(z) = P_I^2 + 2z_I P_I \cdot Q_I \quad \to \quad z_I = \frac{-P_I^2}{2P_I \cdot Q_I} \tag{6.39}$$

where the q_i can be chosen such that $q_i \cdot q_j = 0 \to Q_I^2 = 0$. Then, whenever $z = z_I$ the shifted amplitude has a singularity, which can be studied looking into the analytical structure of the function $A(z)/z$ in the complex plane. Choosing a contour that only captures the pole at the origin, we have

$$\oint_{\mathcal{C}_0} dz \, \frac{A(z)}{z} = 2\pi i \, A(z=0) \tag{6.40}$$

However, if we deform this contour to surround all the other poles, $\mathcal{C}_0 \to \mathcal{C}$, we will have

$$A(z=0) = \frac{1}{2\pi i} \oint_{\mathcal{C}_0} dz \, \frac{A(z)}{z} = \frac{1}{2\pi i} \oint_{\mathcal{C}} dz \, \frac{A(z)}{z} = -\sum_I \text{Res}_{z=z_I} \frac{A(z)}{z} + B_\infty \tag{6.41}$$

where B_∞ is the residue at infinity and the minus sign comes from the opposite direction in the Cauchy theorem. We know what happens when the amplitude is evaluated at its pole: the propagator $P_I(z)^2$ goes on-shell and in this factorization limit, the amplitude becomes a product of two sub-amplitudes

$$\lim_{z \to z_I} P_I^2(z) A(z) = A_L(z_I) A_R(z_I) \tag{6.42}$$

and the residue at this pole is [209]

$$\text{Res}_{z=z_I} \left[\frac{A(z)}{z} \right] = \frac{1}{z_I} \left(\frac{dP_I^2(z_I)}{dz_I} \right)^{-1} \lim_{z \to z_I} P_I^2(z) A(z) = -A_L(z_I) \frac{1}{P_I^2} A_R(z_I) \tag{6.43}$$

which allows us to construct the whole amplitude up to the boundary term

$$A(z=0) = \sum_I A_L(z_I) \frac{1}{P_I^2} A_R(z_I) + B_\infty \tag{6.44}$$

This equation is one of the pillars for the success of the modern methods for scattering amplitudes. However, we still have this elephant in the room that we cannot ignore, B_∞. Let's give some examples of a specific type of recursion relations, called BCFW, where only two legs are shifted and address the problems of B_∞.

6.4.1 BCFW

The Britto-Cachazo-Feng-Witten recursion relation [235, 236] is a special case where only two lines are shifted. In this case, the two momenta are shifted by $q_1 = -q_2 = q$. For example, let's evaluate the four-point colour-ordered[31] amplitude in pure Yang-Mills

[31] This means that one strips out all the colour factors and the amplitude only contains its kinematic information. The decomposition that makes use of the minimal amount of colour-factors was found in [237] and its called the DDM decomposition. Since we will be interested mainly in broken electroweak amplitudes, we do not discuss in detail the colour-decomposition.

$A(1^-, 2^-, 3^+, 4^+)$. We can implement this shift on the square spinors for 1 and angle spinors for 2, which is called the $[1, 2\rangle$-shift, and the reason for shifting this way is to cancel boundary term.

$$|\hat{1}] = |1] + z|2], \qquad |\hat{2}] = |2], \qquad |\hat{1}\rangle = |1\rangle, \qquad |\hat{2}\rangle = |2\rangle - z|1\rangle, \tag{6.45}$$

where we denoted the shifted variables by a hat, and no other spinor is shifted. Since the amplitude is colour-ordered, we only have one pole:

$$0 = \hat{P}_{23}^2 = \langle\hat{2}3\rangle[3\hat{2}] = (\langle 23\rangle - z\langle 13\rangle)\,[32] \qquad \Rightarrow \qquad z_{23} = \frac{\langle 23\rangle}{\langle 13\rangle} \tag{6.46}$$

Using the recursion formula, we obtain

$$\begin{aligned} A(1^-, 2^-, 3^+, 4^+) &= \sum_{h_I=\pm} A(\hat{1}^-, \hat{P}_I^{h_I}, 4^+)\,\frac{1}{P_I^2}\,A(-\hat{P}_I^{-h_I}, \hat{2}^-, 3^+) \\ &= A(\hat{1}^-, \hat{P}_I^-, 4^+)\,\frac{1}{P_I^2}\,A(-\hat{P}_I^+, \hat{2}^-, 3^+) \\ &= \frac{\langle 1\hat{P}\rangle^3}{\langle\hat{P}4\rangle\langle 41\rangle}\frac{1}{\langle 23\rangle[32]}\frac{[3\hat{P}]^3}{[\hat{P}2][23]} = -\frac{\langle 12\rangle^3[23]^3}{\langle 43\rangle[32]\langle 41\rangle\langle 23\rangle[32]^2} \end{aligned} \tag{6.47}$$

where the three-point amplitudes come from Eq. 6.15. In the first line we used the fact that $\langle\hat{2}3\rangle = 0$ to see that the term in the sum with $h_I = +$ vanish since it generates the $A(-\hat{P}_I^-, \hat{2}^-, 3^+)$, which contains $\langle\hat{2}3\rangle$. In the last step, we have used $\hat{P}_I = \hat{2} + 3$ in the numerator and denominator. Simplifying everything we arrive at the Parke-Taylor formula [238]

$$A(1^-, 2^-, 3^+, 4^+) = \frac{\langle 12\rangle^4}{\langle 12\rangle\langle 23\rangle\langle 34\rangle\langle 41\rangle} \tag{6.48}$$

This process can then be done iteratively to higher points and general expressions for the maximally helicity violating amplitudes MHV, where a n-point amplitude has 2 negative and $n-2$ positive helicity gluons, and anti-MHV amplitudes $\overline{\text{MHV}}$, where there the helicities and flipped, can be obtained. The boundary term, which we chose to ignore at first, was proven to have the behaviour z^{-1} at large-z for the following shifts $[-,-\rangle, [-,+\rangle, [+,+\rangle$ but z^1 for $[+,-\rangle$ [239, 240] and that is why we have chosen the $[1, 2\rangle$-shift. Therefore, the former shifts are said to be good-shifts whereas the latter is a bad-shift. The general structure of MHV and $\overline{\text{MHV}}$ Parke-Taylor amplitudes with only particles i, j as different helicities

$$A(1, ..., i^-, j^-, ..., n) = \frac{\langle ij\rangle^4}{\langle 12\rangle\langle 23\rangle ...\langle n1\rangle} \qquad A(1, ..., i^+, j^+, ..., n) = \frac{[ij]^4}{[12][23]...[n1]} \tag{6.49}$$

For massive particles, the recursion relations will depend on whether the shifted legs are massless or massive or one of each [241]. Again, one would have to solve the conditions of the shifted vector for the two line shift

$$q \cdot p_i = q \cdot p_j = q^2 = 0 \tag{6.50}$$

The first two conditions tell us that q lies in the plane orthogonal to the plane spanned by p_i, p_j, and the last one means that q lies in the intersection of this orthogonal plane with lightcone. In the case where the two particles are massless, we already know the solution from BCFW. In the case where we have particle i massless and particle j massive, the two solutions to these conditions are

$$q^{\alpha\dot{\beta}} = \lambda_i^{\alpha}(\lambda_i p_j)^{\dot{\beta}} \qquad \text{or} \qquad q'^{\alpha\dot{\beta}} = (p_j\tilde{\lambda}_i)^{\alpha}\tilde{\lambda}_i^{\dot{\beta}} \tag{6.51}$$

For the both massive cases, the expression is not simple, since p_i and p_j are not rank-1 matrices. In Section 7, we are going to use the massless and the mixed amplitudes derived here and apply it to the bosonic sector of the Standard Model Effective Theory. These amplitudes contain effective operators, which often include derivative couplings that worsen the large-z limit and problems with the boundary terms appear. Further studies on constructibility for massive recursion relations were done in [242].

6.5 On-shell effective theories

The massless amplitudes of Eq. 6.15 already contain a contribution from EFTs. If we set the three-amplitude to be all-plus or all-minus in pure YM, we obtain the following

$$A(1^-, 2^-, 3^-) = \frac{c}{\Lambda^2}\langle 12\rangle\langle 23\rangle\langle 31\rangle \qquad A(1^+, 2^+, 3^+) = \frac{\tilde{c}}{\Lambda^2}[12][23][31] \tag{6.52}$$

where the Λ^2 comes from dimensional analysis. Each bracket has mass dimension one, while the cross-section has dimension (length)^2 and then an n-point amplitude has mass dimension $4-n$ in $d=4$. These two amplitudes are generated by the dimension-six F^3 operator, which can be expanded in its holomorphic and the antiholomorphic parts.

In all, our task is to go further and construct higher point amplitudes, where the question of constructibility plays a major role. A vanishing B_∞ allows one to have a finite number of input seed amplitudes and from that, construct higher-points. However, we should expect that for an effective theory, where more derivative couplings enter, this fails.

The answer to the constructibility will be dictated by the symmetry in the theory. For instance, perturbative gravity tree-level amplitudes come from the Einstein-Hilbert Lagrangian expanded around the flat space

$$\mathcal{L}_{\text{EH}} = \frac{1}{2\kappa^2}\int d^4x\sqrt{-g}R \qquad\qquad g_{\mu\nu} = \eta_{\mu\nu} + \kappa h_{\mu\nu} \tag{6.53}$$

where the graviton is represented by the tensor field $h_{\mu\nu}$, which gives vertices at all orders. This seems to be a disaster; each order in multiplicity has a new vertex with more derivatives that could spoil the boundary term. However, gravity is completely constructible and well-behaved at tree-level. The only information we need to provide as seed is the three-point amplitude. This is all due to the diffeomorphism invariance that connects all the terms. Somehow, this information could be expected, since we only have the parameter κ in the Lagrangian as we only have g_{YM} in Yang-Mills.

Another example where the symmetry connects different multiplicity vertices is the non-linear sigma model (NLSM):

$$\mathcal{L}_{\text{NLSM}} = \frac{f^2}{4}\langle \partial_\mu U \partial^\mu U^{-1} \rangle, \qquad U = \exp\left(\sqrt{2}\frac{i}{f}\phi\right). \tag{6.54}$$

The difference for this model is that besides using the information of the poles of the amplitudes, we have to explore its zeros. For instance, taking the soft limit of the n-point NLSM amplitude,

$$A_n \sim p^\sigma, \qquad \text{for} \qquad p \to 0 \tag{6.55}$$

where σ is the soft degree and must be an integer. For the NLSM this quantity is one and using it to modify the Recursion Relations allows one to reconstruct any amplitude with only the 4-point as an input seed. We say that the NLSM is 6-point constructible.

However, how about other theories? With more parameters and different fields? A way to understand them is to study the structure in the IR and the UV behaviour of the theory. These two informations guide one on the constructibility of effective theories. A bad UV behaviour of an EFT can be circumvented by a soft general behaviour, i.e. a soft theorem.

For the Standard Model in the symmetric phase, particles are massless and the constructibility and recursion relations can be obtained. Whenever the Higgs bosons breaks the symmetry, particles acquire mass and a massive spinor helicity formalism has to be used. Moreover, as explored in Sec. 3, there are a lot of reasons to extend the SM. The SMEFT in its broken phase with on-shell methods, *i.e* using massive spinor helicity formalism and recursion relations, will be explored in the next chapter.

7 Effective Field Theories and Scattering Amplitudes

This section is based on the paper ***"The Rise of SMEFT On-shell Amplitudes"****.*

7.1 Introduction

The spinor helicity formalism has been an efficient tool to calculate scattering amplitudes with an enormous development over the past decades, especially for the case of massless particles, e.g. [243]. The application to massive particles is less explored, although processes involving massive quarks were calculated in [213–220] and massive gauge bosons in [239,244,245]. Recently, a convenient way to describe massive amplitudes, which makes the (massive) little group covariant, was presented in Ref. [8]. This formalism can be applied to supersymmetric theories [246,247], to the Standard Model (SM) [223,224] and to study amplitudes with higher spin particles [248–250]. A natural question that follows is: what can we learn in the context of Effective Field Theories (EFTs) using the formalism of massive on-shell amplitudes?

One way to study the effects of beyond SM (BSM) physics is to write all the possible (independent) higher dimensional operators assuming the SM symmetries. In particular, the *SM Effective Field Theory* (SMEFT) is built on the assumption of a linearly realized electroweak symmetry (for a recent review, see [20]).[32] Note that the operators may be related by field redefinitions and finding a basis is, in general, not a trivial task. The so-called Warsaw Basis, for example, was obtained using the equations of motion to remove the maximum number of covariant derivatives [59].[33] In addition, the calculation of observables with the inclusion of higher dimensional operators may involve the computation of diagrams with a large number of external particles and derivatives.

Thus it seems compelling to ask if it is possible to formulate the EFTs without dealing with Lagrangians and equations of motion, and use the spinor language to describe the physics only in terms of on-shell quantities instead. Indeed, this has been already explored, for instance, to calculate QCD amplitudes with the operators G^3 and hG^2 [115,252], to study helicity selection rules [112] and the anomalous matrix [9] in the SMEFT (with massless particles), and also for more general EFTs [227,239,253–255].

On the other hand, there are several obstacles to extend these results for the SMEFT at low energies, as many of them apply only to massless particles and theories with non-trivial soft limits. Besides, the recursion relations do not always work for EFTs, as contact interactions, which are non-factorizable, are needed as an extra input. There are

[32] If the electroweak symmetry is non-linearly realized we have the so-called *Higgs Effective Field Theory* (HEFT). We are not exploring this case here, although it is an interesting problem to understand how the difference between SMEFT and HEFT emerges in the on-shell construction.

[33] A general approach involving Hilbert series can be used to find the set of independent operators, see [52,53]. Moreover, a new approach on the construction of a operator basis using the Poincaré symmetry of spacetime was presented in [251].

a few ways to overcome this problem for certain classes of theories [227, 239, 255, 256] and recently, a new strategy was presented in [257] to construct amplitudes with higher dimensional operators for an EFT that consists of the SM plus a massive scalar that couples to gluons. This points in the direction of constructing generic EFTs without Lagrangians, fully in the on-shell language.

In this paper, we want to explore the formulation of the massive on-shell SMEFT focusing on the electroweak sector without fermions ($N_f = 0$). In the broken phase, we can use that the massive 3-point on-shell amplitudes and non-factorizable 4-point amplitudes are related by the Higgs vev to define the (electroweak) SMEFT deformations at dimension six level. The eleven dimension six operators can be described in terms of the hhh, $h\gamma\gamma$, $h\gamma Z$, $hW\bar{W}$, $hZ\bar{Z}$, $W\bar{W}Z$ and $W\bar{W}\gamma$ massive on-shell amplitudes. Independent structures can only appear from dimension eight operators or in a framework where the electroweak symmetry is non-linearly realized. Notice that this is only true because we are not considering the limit of massless particles, in which case, the purely bosonic operators of the Warsaw basis should be defined including explicitly the 4-point contact interactions [258].

Finally, the main goal is to find a fully on-shell description for the SMEFT in the lines of the bootstrap program, i.e. computing the S-matrix bypassing the usual quantum field theory machinery, and this work is a first step towards this direction. Although we are relying on Feynman rules to obtain the coefficients of on-shell amplitudes, the kinematic part is totally fixed by Lorentz symmetry and unitarity.[34] In addition, we explore the calculation of SM and SMEFT scattering amplitudes with massive particles. For the SM, we calculate the massive amplitude $WW\gamma\gamma$ with the Britto–Cachazo–Feng–Witten (BCFW) recursion relation [235,236] and we discuss how to obtain the $WWhh$ demanding correct factorization and unitarity in the high energy limit (HE). For the SMEFT, the recursion relations are challenging and we discuss some possible strategies to overcome the problems.

The paper is organized as follows: in Section 7.2 we discuss how to describe higher dimensional operators with the amplitude language, starting from the massless and moving to the massive case. In Section 7.3, we discuss our strategy to do the map of the dimension six operators in the Warsaw basis to the on-shell language which requires defining an appropriate input scheme. Next, in Section 7.4, we write the 3-point massive amplitudes and then define the *on-shell basis*. We then move to the discussion about scattering amplitudes using the on-shell basis in Section 7.5.

[34] Recently, Ref. [259] presented a bottom-up construction of the electroweak amplitudes, in which the $SU(2)_L \times U(1)_Y$ symmetry arises imposing perturbative unitarity in tree-level amplitudes. Although their construction applies for a theory with general non-renormalizable interactions, it was showed that it is possible to map the Warsaw basis and our results were recovered.

7.2 EFTs with amplitudes

The massless three point amplitudes are completely fixed by the $U(1)$ Little Group (LG), locality and by the special 3-point kinematics [260]. This means that there are two non-trivial solutions for the on-shell 3-point amplitudes if we allow the 4-momenta to be complex: the holomorphic (H) with all $[i\,j]=0$ and the anti-holomorphic (AH) with all $\langle i\,j\rangle=0$. Hence, the general formula for the 3-point massless amplitudes is given by

$$\mathcal{M}_3(1^{h_1}2^{h_2}3^{h_3}) = g\begin{cases}\langle 12\rangle^{-h_1-h_2+h_3}\langle 23\rangle^{h_1-h_2-h_3}\langle 31\rangle^{-h_1+h_2-h_3}\,, & h<0\ \ (\mathrm{H}),\\ [12]^{h_1+h_2-h_3}\ [23]^{-h_1+h_2+h_3}\,[31]^{h_1-h_2+h_3}\,, & h>0\ \ (\mathrm{AH}),\end{cases} \tag{7.1}$$

where $h\equiv\sum_i h_i$.[35] We can then see that there is a relation between the mass dimension of the coupling g and the allowed vertices. More precisely, a n-point amplitude has mass dimension $[\mathcal{M}_n]=4-n$, so using Eq. (7.1) we get that:

$$|h| = 1-[g]\,. \tag{7.2}$$

In order to connect this formula with terms in the Lagrangian, it is useful to define the complex field strength as [262]: [36]

$$X^{\pm}_{\mu\nu} = \frac{1}{2}(X_{\mu\nu}\mp i\tilde{X}_{\mu\nu})\,,\quad \tilde{X}^{\pm}_{\mu\nu} = \pm iX^{\pm}_{\mu\nu}\,, \tag{7.3}$$

with $\tilde{X}_{\mu\nu}=\epsilon_{\mu\nu\alpha\beta}X^{\alpha\beta}/2$. The holomorphic operators are constructed with X^+ fields and anti-holomorphic ones with X^-. For example, the $\mathcal{O}_X=X^3$ and $\mathcal{O}_{\tilde{X}}=\tilde{X}^3$ operators can be written as $\mathcal{O}^{\pm}_X\equiv(\mathcal{O}_X\mp i\mathcal{O}_{\tilde{X}})/2$, such that

$$\mathcal{L}\supset c_X\mathcal{O}_X + c_{\tilde{X}}\mathcal{O}_{\tilde{X}} = c^+_X\mathcal{O}^+_X + c^-_X\mathcal{O}^-_X\,, \tag{7.4}$$

where we define the H and AH complex Wilson coefficients as $c^{\pm}_X=c_X\pm ic_{\tilde{X}}$. We can then easily make the connection with Eq. (7.2). For a coupling with mass dimension $[g]=-2$, the only possible vertices have total helicity ±3, which are generated by the H/AH operators $X^{3,\pm}$. For $[g]=-1$, the possible 3-point amplitudes corresponds to the dimension five operators $(X^{\pm})^2\phi$, $\psi^2\phi$ and $\bar{\psi}^2\phi$, where ψ and $\bar{\psi}$ are Weyl spinors.

Moving to higher point amplitudes, we cannot use the 3-point special kinematics as in this case $s_{ij}=(p_i+p_j)^2$ is non-zero. However, we can still extract some information

[35] In the case of $h=0$, besides the trivial case where all helicities are zero (ϕ^3-theory), it is possible to prove that both cases reduces to a constant of mass dimension one, which vanish for all theories with coupling $[g]\leq 0$. Moreover, these theories fails to fullfill four-points consistency conditions [261].

[36] In terms of spinor indices the gauge field strength is $F_{\mu\nu}\sigma^{\mu}_{\alpha\dot{\alpha}}\sigma^{\nu}_{\beta\dot{\beta}}\equiv F_{\alpha\beta}\bar{\epsilon}_{\dot{\alpha}\dot{\beta}}+\bar{F}_{\dot{\alpha}\dot{\beta}}\epsilon_{\alpha\beta}$, where $F_{\alpha\beta}$, where $F_{\alpha\beta}$ ($\bar{F}_{\dot{\alpha}\dot{\beta}}$) corresponding to helicity $+1(-1)$. For a review on spinors, see [263].

using the LG scaling and dimensional analysis. In general, a n-point tree-level massless amplitude can be written as a sum of angles and square brackets with a common denominator [239]:

$$\mathcal{M}_n(1^{h_1}\cdots n^{h_n}) \sim g\,\frac{\sum\langle\cdots\rangle^{n_a}[\cdots]^{n_h}}{\sum\langle\cdots\rangle^{d_a}[\cdots]^{d_h}}\,, \tag{7.5}$$

which means that the numerator and denominator are a sum of Lorentz invariant objects. The difference of H/AH contraction is $\Delta_i \equiv n_i - d_i$, then dimensional analysis and LG gives

$$\Delta_a + \Delta_h + [g] = 4 - n\,, \quad \Delta_a - \Delta_h = -h\,. \tag{7.6}$$

For $n > 3$, all non-factorizable terms are polynomials in the spinor products. For example, in the case of a $n = 4$ with $[g] = -2$, Eq. (7.6) is simply $n_a + n_h = 2$, as a non-zero d_i would introduce a pole. For bosonic operators, the only possibility is then $\mathcal{M}_4 \sim \{\langle\cdots\rangle^2, [\cdots]^2, \langle\cdots\rangle[\cdots]\}$. This can be done systematically in order to construct a amplitude basis for higher dimensional operators without make use of a Lagrangian [258].

However, this simplicity holds just up to dimension six operators as beyond it is challenging to identify the independent terms, as there are terms with more derivatives contributing to the same helicity amplitude. Although arduous to do analytically, Ref. [253] suggests an numerical approach to identify the redundant terms, which can be useful, for instance, to find a dimension eight basis for the SMEFT. Another strategy is to explore the spacetime symmetries as in [251].

We are going to pursue a possibility less explored so far, that is to study higher dimensional operators with massive amplitudes. We are then able to study the broken phase of SMEFT amplitudes and define a dimension six basis only using 3-point amplitudes.

For 3-point massive amplitudes, the associated massive LG is the $SO(3) \simeq SU(2)/\mathbb{Z}_2$. The massive momenta can be represented by 4 spinors collected into two vectors $\boldsymbol{\chi}^I$ and $\widetilde{\boldsymbol{\chi}}^I$, with $I = 1, 2$ for the $SU(2)$ indices and greek letters for the Lorentz indices:

$$p_{\alpha\dot\beta} = \boldsymbol{\chi}^I_\alpha \widetilde{\boldsymbol{\chi}}_{\dot\beta,I} \;\text{ with }\; \mathbf{p}^2 = \det\boldsymbol{\chi}\det\widetilde{\boldsymbol{\chi}} = m^2\,, \tag{7.7}$$

where $\det\boldsymbol{\chi} = \frac{1}{2}\boldsymbol{\chi}^I\boldsymbol{\chi}_I$ and $\det\widetilde{\boldsymbol{\chi}} = \frac{1}{2}\widetilde{\boldsymbol{\chi}}^I\widetilde{\boldsymbol{\chi}}_I$. The conventions used here are shown in Sec. 6 and the massive particles quantities are represented with the **bold** notation, introduced in [8]. Moreover, we are going to omit the $SU(2)$ indices for the massive particles and use the short-hand notation as e.g. $[\mathbf{i}\,j]^2 \equiv \frac{1}{2}\left([\mathbf{i}^{I_1}\,j][\mathbf{i}^{I_2}\,j] + [\mathbf{i}^{I_2}\,j][\mathbf{i}^{I_1}\,j]\right)$. In the rest of the paper, we consider the symmetrization of the $SU(2)$ indices always implicit.

The massive complex momenta respecting the on-shell condition should have $8 - 2 = 6$ real degrees of freedom (d.o.f). Since we introduced 4 two-component spinors, i.e. 16 real d.o.f, where 2 of them are fixed by Eq. (7.7), the remaining 8 d.o.f corresponds to the $GL(2)$ redundancy $\boldsymbol{\chi}^J \to S^J_K\boldsymbol{\chi}_K$ and $\widetilde{\boldsymbol{\chi}}_J \to (S^{-1})^K_J\widetilde{\boldsymbol{\chi}}_K$, where $S \in GL(2)$. Whenever

the 4-momenta is real, the $GL(2)$ reduces to $SU(2) \otimes U(1)$, where the $SU(2)$ part act as rotations on the index J and the $U(1)$ is just a rephasing, as it commutes with the LG. A possible choice used to fix this transformation is given by $\det \boldsymbol{\chi} = \det \widetilde{\boldsymbol{\chi}} = m$ [8].[37]

The n-point amplitudes can then be written as Eq. (7.5), with the difference that now there is also the $SU(2)$ LG to be satisfied. In particular, the 3-point amplitudes can mix H and AH Lorentz invariants, as $(p_i + p_j)^2$ is non-zero:[38]

$$\mathcal{M}_3 \sim \sum_G g_i \langle \cdots \rangle^{N_a} [\cdots]^{N_h} , \tag{7.8}$$

where G is the set of all possible irreducible contractions of the massive/massless spinor variables. (Note that in the massless case $N_a = 0$ *or* $N_h = 0$ due to the special kinematics.) The size of G is set by the number of the massive external legs and their spinors, we show all possibly cases on the Sec. 2 (where we follow closely Ref. [8] but a different approach to build massive 3-point amplitudes can also be found in [221]). Note that dimensional analysis give $N_a + N_h = 1 - [g_i]$, similarly to the massless case. The difference is that g_i can have powers of masses, so $[g_i] = -2$ does not correspond necessarily to a dimension six operator.

For a theory with spontaneous symmetry breaking, in the broken phase, we choose to write g_i using powers of v and $m_{W,Z}$ times a dimensionless function, as showed in Table 7.1. As we are going to show in the next section, with these pre-factors, the dimensionless function depend only on the Wilson coefficients c_i, the Weinberg angle θ and the Higgs quartic coupling λ_h. We can see that for $[g_i] = \pm 1$ the natural dimensional parameter is the Higgs vev v, as the Higgs mechanism shows itself as a IR unification of the UV amplitudes [8]. Therefore, massless amplitudes apparently unrelated in the UV can be unified into different components of massive amplitudes in the IR. The only case in which no mass or vev should appear is the $[g_i] = -2$ term that corresponds exactly to the $(X^{\pm})^3$ operator, as it is the only possible dimension six operator for a massless 3-point amplitude. For the SM couplings, the HE limit of the amplitudes determines the power of masses (see also [224]). On the other hand, it is unclear how to 'bootstrap' the dimensionless functions. For some theories the soft limit of higher point amplitudes can encode information about the symmetries [255], but it is uncertain how this approach should be applied for the SMEFT. In the next sections, we are going to obtain these functions comparing with the SMEFT Feynman rules.

[37] Since its an arbitrary phase, it is possible to choose to transform, for instance, just the spinor with index $I = 2$ as in Ref. [221]. Requiring that the amplitude is invariant under the rephasing may lead to additional constraints on the massive amplitudes.

[38] There is a subtley in the case of two particles with same mass, as there is a term in the denominator to fix the LG of the massless particle (for further details, see Sec. 6).

Coupling dim.	$[g_i]=1$	$[g_i]=-1$	$[g_i]=-2$
Marginal	$v\,\mathcal{G}_{hhh}$	$\frac{1}{v}\,\mathcal{G}_{h\bar{V}V}$	$\frac{1}{v\,m_W}\,\mathcal{G}_{W\bar{W}\gamma}$, $\frac{1}{v\,m_W}\,\mathcal{G}_{W\bar{W}Z}$, $\frac{1}{v\,m_Z}\,\mathcal{G}_{W\bar{W}Z}$
Dim-6	$\frac{v^3}{\Lambda^2}\,\mathcal{C}_{hhh}$	$\frac{v}{\Lambda^2}\,\mathcal{C}_{hV_iV_j}$	$\frac{v}{\Lambda^2\,m_W}\,\mathcal{C}_{W\bar{W}V}$, $\frac{1}{\Lambda^2}\,\mathcal{C}'_{W\bar{W}V}$

Table 7.1: The mass dimension of g_i is fixed by the spin/helicities of the 3-point amplitude and we choose to write it as powers of v, $m_{W,Z}$ and Λ times a dimensionless functions (we use $\mathcal{G}_i$ for SM and $\mathcal{C}_i$ for dimension six structures). In order to do the map to the $N_f = 0$ SMEFT we need to write the following 3-point amplitudes: hhh, $h\gamma\gamma$, $h\gamma Z$, $hW\bar{W}$, $hZ\bar{Z}$, $W\bar{W}Z$ and $W\bar{W}\gamma$. The kinematic part is fixed by the massless/massive LG. The symmetries and UV properties of the theory are encoded in the dimensionless functions.

7.3 The Lagrangian side: Feynman rules and input parameters

In order to draw the map between the dimension six SMEFT and on-shell amplitudes, we are going to use the Warsaw basis, which is convenient as the number of derivatives are reduced to a minimum in trade for operators with more fields. One advantage is that there are no bivalent operators which makes the on-shell description more convenient (see also [9, 112]). The SMEFT Lagrangian is given by

$$\mathcal{L}_{\text{SMEFT}} = \mathcal{L}_{\text{SM}} + \sum_i \frac{c_i}{\Lambda^2}\mathcal{O}_i\,, \tag{7.9}$$

where Λ is the EFT expansion parameter (from now on we ignore Λ^{-4} effects), and the Wilson coefficient c_i and the dimension six operators $\mathcal{O}_i$ can be written in the H and AH form using Eq. (7.3) (see Table 7.2). We are considering the operators without fermions and gluons such that the space of higher dimensional operators is 11-dimensional. For the SMEFT Feynman rules we are following the conventions and results of Ref. [264].

Before writing the on-shell amplitudes, one important comment is in order. The SM has five free parameters which are g_L, g_Y, g_s, λ_h and v, i.e, three gauge couplings, the Higgs quartic coupling and the Higgs vev. A common choice to extract the values of SM electroweak parameters g_L, g_Y and v is through the measured experimental observables $\{m_Z, \alpha(0), G_F\}$. These observables will receive contributions from diagrams involving dimension six operators that are usually parametrized as $\bar{g}_L, \bar{g}_Y, \bar{\lambda}_h, \bar{v}$ where $\bar{x} \equiv \hat{x} + \delta x$ and we are considering just tree-level corrections of order $\mathcal{O}(\Lambda^{-2})$ in the δx parameters. To get the bar parameters we have to choose the measurements used to fix the Lagrangian parameters.

From the point of view of the on-shell amplitudes formalism, particle masses constitute natural input, as they label representations of the Poincaré group and do not receive any

Bosonic operators			
$\mathcal{O}_W^{\pm}$	$\epsilon^{ijk} W^{i,\pm}_{\mu\nu} W^{j,\pm}_{\nu\rho} W^{k,\pm}_{\rho\mu}$	$\mathcal{O}_H$	$(H^\dagger H)^3$
$\mathcal{O}_{HB}^{\pm}$	$H^\dagger H B^{\pm}_{\mu\nu} B^{\pm}_{\mu\nu}$	$\mathcal{O}_{H\Box}$	$(H^\dagger H)\Box(H^\dagger H)$
$\mathcal{O}_{HW}^{\pm}$	$H^\dagger H W^{\pm}_{\mu\nu} W^{\pm}_{\mu\nu}$	$\mathcal{O}_{HD}$	$\lvert H^\dagger D_\mu H\rvert^2$
$\mathcal{O}_{HWB}^{\pm}$	$H^\dagger \sigma^i H W^{i,\pm}_{\mu\nu} B^{\pm}_{\mu\nu}$		

Table 7.2: Bosonic operators in the Warsaw basis. We define the holomorphic and anti-holomorphic operators/Wilson coefficients as $\mathcal{O}_X^{\pm} \equiv (\mathcal{O}_X \mp i\mathcal{O}_{\tilde{X}})/2$ and $c_X^{\pm} = c_X \pm i\tilde{c}_X$. Note that the operators on the right side do not have defined holomorphic structure.

corrections. Since we need to fix four parameters (considering that g_s is fixed via the SM-like triple gluon self-coupling) and there are only three masses available, we are going to leave the fourth choice unspecified, which means that the formulas will depend explicitly on δv. Thus, we can define the *on-shell input scheme* as $\{\hat{m}_W, \hat{m}_Z, \hat{m}_h\}$, which follows the SM relations with the hat parameters:

$$\hat{m}_W = \frac{\bar{g}_L\,\bar{v}}{2}\,, \qquad \hat{m}_Z = \frac{\sqrt{\bar{g}_L^2 + \bar{g}_Y^2}\,\bar{v}}{2}\,, \qquad \hat{m}_h = \bar{\lambda}_h\,\bar{v}^2\,. \tag{7.10}$$

Solving these equations we obtain

$$\begin{aligned} \frac{\delta g_Y}{\hat{g}_Y} &= -\frac{\delta v}{\hat{v}} - \frac{\hat{v}^2}{\Lambda^2}\left(c_{HD}\,\frac{(\hat{g}_L^2 + \hat{g}_Y^2)}{4\,\hat{g}_Y^2} + c_{HWB}\,\frac{\hat{g}_L}{\hat{g}_Y}\right), \\ \frac{\delta\lambda_h}{\hat{\lambda}_h} &= -\frac{2\,\delta v}{\hat{v}} + \frac{\hat{v}^2}{\Lambda^2}\left(\frac{3\,c_H}{\hat{\lambda}_h} - 2\,c_{H\Box} + \frac{c_{HD}}{2}\right), \quad \frac{\delta g_L}{\hat{g}_L} = -\frac{\delta v}{\hat{v}}\,. \end{aligned} \tag{7.11}$$

One may choose a pseudo-observable for the fourth parameter as the electromagnetic SM-like coupling between the photon and a W pair. Then δv can be obtained using the fact that $\hat{e} \equiv \hat{g}_L\,\hat{g}_Y/\sqrt{\hat{g}_L^2 + \hat{g}_Y^2}$ and δg_L, δg_Y of Eq. (7.11), which leads to

$$\delta\tilde{v} \equiv \frac{\delta v \Lambda^2}{v^3} = -\frac{\hat{g}_L^2}{\hat{g}_Y^2}\left(c_{HWB}\,\frac{\hat{g}_L\hat{g}_Y}{\hat{g}_L^2 + \hat{g}_Y^2} + \frac{c_{HD}}{4}\right). \tag{7.12}$$

For now on, we are going to leave $\delta\tilde{v}$ unspecified. The Weinberg angle can then be defined as $c_{\hat{\theta}} \equiv \hat{m}_W/\hat{m}_Z$, which at $\mathcal{O}(\Lambda^{-2})$ gives $c_{\bar{\theta}} \equiv c_{\hat{\theta}} + \delta c_\theta$ where,[39]

$$\delta c_\theta \equiv \frac{\hat{g}_Y}{(\hat{g}_L^2 + \hat{g}_Y^2)^{3/2}}\,(\hat{g}_Y \delta g_L - \hat{g}_L \delta g_Y)\,. \tag{7.13}$$

[39] One should be careful with this definition as there are extra pieces in the rotation of gauge fields to the mass basis, however, in [264], this is already taken into account in the Feynman rules, and the Weinberg angle can be consistently defined in this way.

Notice that $\delta g_Y, \delta\lambda_h$ and δg_L are relevant only in the deviation of SM amplitudes, since whenever a dimension six Wilson coefficient multiplies them, the term is order Λ^{-4}. In the following, we drop the hat as it corresponds to the observable quantities.

7.4 The on-shell side: SMEFT 3-point amplitudes

We are going to write the massive 3-point amplitudes for hhh, $h\gamma\gamma$, $h\gamma Z$, $hW\bar{W}$, $hZ\bar{Z}$, $W\bar{W}Z$ and $W\bar{W}\gamma$. Comparing with the Feynman rules allows us to draw a 1-to-1 map from on-shell amplitude coefficients and the SM/Warsaw basis parameters.

7.4.1 Massive 3-point amplitudes

In the case of Higgs self-interactions, there are no little group indices, hence the most generic on-shell 3-point amplitude is just a constant as we can always trade momentum contractions with masses. The SM and dimension six contributions can be parametrized as

$$\mathcal{M}(\mathbf{1}_h\mathbf{2}_h\mathbf{3}_h) = v\,\mathcal{G}_{hhh} + \frac{v^3}{\Lambda^2}\,\mathcal{C}_{hhh}\,. \tag{7.14}$$

Moving to one massive with spin s and two massless particles with helicities h_2 and h_3, there is a non-trivial constraint on the amplitude given by $|h_3 - h_2| \leq s$, which is another way to see the Landau-Yang Theorem [8, 221]. Then, in the case of the coupling of the Higgs with two photons, the only possibility is to have the photons with the same helicity:

$$\mathcal{M}(\mathbf{1}_h 2_\gamma^+ 3_\gamma^+) = \frac{v}{\Lambda^2}\,\mathcal{C}^+_{h\gamma\gamma}\,[23]^2, \tag{7.15}$$

where the amplitude with photons of helicity -1 can be obtain just applying a parity transformation, which is equivalent to replacing $[2\,3] \leftrightarrow \langle 2\,3\rangle$ and $\mathcal{C}^+_{h\gamma\gamma} \leftrightarrow \mathcal{C}^-_{h\gamma\gamma}$.

In the case of two massive (with different masses) and one massless particle, the only constraint on the amplitude is $|h_3| \leq s_1 + s_2$. Then, we can write the amplitude with the Higgs, the Z boson and the photon as

$$\mathcal{M}(\mathbf{1}_h \mathbf{2}_Z^{J_{1,2}} 3_\gamma^+) = \frac{v}{\Lambda^2}\,\mathcal{C}^+_{hZ\gamma}[\mathbf{2}3]^2\,, \tag{7.16}$$

and similarly to the Eq. (7.15), the amplitude with the photon with helicity -1 can be obtained by parity.

For the amplitudes with three massive particles the number of terms can be reduced noticing that many structures are zero after the symmetrization of the $SU(2)$ indices.[40]

[40] This is a manifestation of the Ward identity for massive vectors, since $\epsilon_{\mathbf{3}}^{K_1K_2}\cdot p_{\mathbf{3}} \sim \langle \boldsymbol{\chi}_3|p_{\mathbf{3}}|\widetilde{\boldsymbol{\chi}}_3]^{K_1K_2} = -m_3\langle \mathbf{33}\rangle^{K_1K_2} = -m_3\,\varepsilon^{K_1K_3} \to 0$, where the last step is due the symmetrization of the antisymmetric tensor $\varepsilon^{K_1K_2}$. For massless particles, the Ward identity comes from the fact the brackets with the same particle vanish, i.e $\langle 33\rangle \to 0$.

The structures with a momentum insertion can be rewritten in terms of contractions of angle and square brackets with the use of Schouten identities (see Appendix I). Then, for $V = W, Z$ we have

$$\mathcal{M}(\mathbf{1}_h\mathbf{2}_V^{I_{1,2}}\mathbf{3}_{\bar{V}}^{J_{1,2}}) = \left(\frac{1}{v}\,\mathcal{G}_{hV\bar{V}} + \frac{v}{\Lambda^2}\,\mathcal{C}_{hV\bar{V}}\right)\langle\mathbf{23}\rangle[\mathbf{23}] + \frac{v}{\Lambda^2}\,\mathcal{C}^-_{hV\bar{V}}\langle\mathbf{23}\rangle^2 + \frac{v}{\Lambda^2}\,\mathcal{C}^+_{hV\bar{V}}[\mathbf{23}]^2\,, \tag{7.17}$$

and the triple gauge coupling $W\bar{W}Z$ can be written as:

$$\begin{aligned}\mathcal{M}(\mathbf{1}_W^{I_{1,2}}\mathbf{2}_{\bar{W}}^{J_{1,2}}\mathbf{3}_Z^{K_{1,2}}) = {}& F_1\Big(\langle\mathbf{12}\rangle[\mathbf{23}][\mathbf{31}] + [\mathbf{12}]\langle\mathbf{23}\rangle\langle\mathbf{31}\rangle\Big)\\ &+ F_2\Big(\langle\mathbf{31}\rangle[\mathbf{12}][\mathbf{23}] + [\mathbf{31}]\langle\mathbf{12}\rangle\langle\mathbf{23}\rangle\Big)\\ &+ F_3\Big(\langle\mathbf{23}\rangle[\mathbf{31}][\mathbf{12}] + [\mathbf{23}]\langle\mathbf{31}\rangle\langle\mathbf{12}\rangle\Big)\\ &+ \frac{v}{m_W\Lambda^2}\Big(\mathcal{C}^+_{W\bar{W}Z}\,\langle\mathbf{12}\rangle[\mathbf{23}][\mathbf{31}] + \mathcal{C}^-_{W\bar{W}Z}\,[\mathbf{12}]\langle\mathbf{23}\rangle\langle\mathbf{31}\rangle\Big)\\ &+ \frac{1}{\Lambda^2}\Big(\mathcal{C}'^+_{W\bar{W}Z}[\mathbf{12}][\mathbf{23}][\mathbf{31}] + \mathcal{C}'^-_{W\bar{W}Z}\langle\mathbf{12}\rangle\langle\mathbf{23}\rangle\langle\mathbf{31}\rangle\Big)\,,\end{aligned} \tag{7.18}$$

where,

$$F_1 = F_2 = \frac{1}{v\,m_Z}\mathcal{G}_{W\bar{W}Z} + \frac{v}{m_Z\Lambda^2}\mathcal{C}_{W\bar{W}Z}\,, \quad F_3 = \frac{1}{v\,m_W}\mathcal{G}_{W\bar{W}Z} + \frac{v}{m_W\Lambda^2}\mathcal{C}_{W\bar{W}Z}\,. \tag{7.19}$$

Since all invariants can be written as masses, e.g. $2p_{\mathbf{1}}\cdot p_{\mathbf{2}} = m_3^2 - m_1^2 - m_2^2$, the coefficients of the amplitudes can differ for each term. The form above is particularly convenient to compare with the Feynman rules. Alternatively, one may start with a momentum insertion as $\mathcal{M} \supset (\langle\mathbf{12}\rangle[\mathbf{12}]\,\langle\mathbf{3}|p_{\mathbf{1}}|\mathbf{3}] + \text{cyclic})$ and use the equations of motion and Schouten identities to write as Eq. (7.18). Moving to the amplitude of $W\bar{W}\gamma$, we have one massless and two massive particles with same mass and, consequently, only one spinor to construct the amplitude. Following [8], we can define an auxiliary object x and x^{-1}:[41]

$$x \equiv \frac{\langle\zeta|p_2|3]}{\langle\zeta 3\rangle} \quad \text{and} \quad x^{-1} \equiv \frac{\langle 3|p_2|\zeta]}{[\zeta 3]} \tag{7.20}$$

where ζ is an arbitrary spinor, 2 is a massive leg and 3 is the massless one. They transform as $x \to t_3^{-2}\,x$ and $x^{-1} \to t_3^2\,x^{-1}$ under the little group of the massless particle and relate to the momenta/polarization vector as:

$$x = \sqrt{2}p_1^\mu\epsilon_\mu^+(p_3) \quad \text{and} \quad x^{-1} = \sqrt{2}p_1^\mu\epsilon_\mu^-(p_3)\,. \tag{7.21}$$

[41]Note that our definition is slightly different from [8] since we do not have a mass in the denominator. This is useful to write the amplitude for $W\bar{W}\gamma$ and $W\bar{W}Z$ in a similar form.

Then, the amplitude can be organized with powers of x. This parametrization makes manifest the HE of the interactions, i.e. the minimal coupling appears as the first term in the expansion and it is the one with best UV behaviour (this has interesting applications in the context of black hole physics, see [248]). We can also use the relations

$$\langle \mathbf{21}\rangle = [\mathbf{21}] + \frac{[\mathbf{23}][\mathbf{31}]}{x} \quad \text{and} \quad \langle \mathbf{23}\rangle\langle \mathbf{31}\rangle = -[\mathbf{23}][\mathbf{31}]\,\frac{m_W^2}{x^2}\,, \tag{7.22}$$

to write the amplitude in a similar form as the $W\bar{W}Z$:

$$\begin{aligned}\mathcal{M}(\mathbf{1}_W^{I_{1,2}}\mathbf{2}_{\bar{W}}^{J_{1,2}}3_\gamma^-) = &\left(\frac{1}{v\,m_W}\mathcal{G}_{W\bar{W}\gamma} + \frac{v}{m_W\Lambda^2}\mathcal{C}_{W\bar{W}\gamma}\right)x^{-1}[\mathbf{12}]^2 \\ &+ \frac{v\,\mathcal{C}^-_{W\bar{W}\gamma}}{m_W\Lambda^2}\,[\mathbf{12}]\langle \mathbf{23}\rangle\langle \mathbf{31}\rangle \;+ \frac{\mathcal{C}'^-_{W\bar{W}\gamma}}{\Lambda^2}\langle \mathbf{12}\rangle\langle \mathbf{23}\rangle\langle \mathbf{31}\rangle\,.\end{aligned} \tag{7.23}$$

It is worth mentioning that the high energy limit of the amplitudes with massive gauge bosons are consistent with the Goldstone boson equivalence theorem. As we showed explicitly in Appendix H, the amplitudes with a longitudinal mode have the same structure as the amplitude in which the longitudinal mode is replaced by a scalar. Having the form of all 3-point amplitudes with gauge bosons allows us to map to the Feynman rules and obtain the dimensionless functions. We use the convention that $\mathcal{G}_i$ and $\mathcal{C}_i$ correspond to the SM-like structures and $\mathcal{G}_i^\pm$ correspond only to dimension six operators through H or AH combinations of operators showed in Table 7.2. The explicit form of all functions are showed in Tables 7.3 and 7.4.

$\mathcal{G}_i$	$\mathcal{G}_{hhh}$	$\mathcal{G}_{hV\bar{V}}$	$\mathcal{G}_{W\bar{W}Z}$	$\mathcal{G}_{W\bar{W}\gamma}$
SM	$-3\lambda_h$	-2	$2\sqrt{2}\,c_\theta$	$-2\sqrt{2}\,s_\theta$

Table 7.3: Map between the dimensionless $\mathcal{G}_i$ functions and the Standard Model parameters.

7.4.2 Defining an on-shell basis

In addition to the SM couplings, there are 11 parameters in the purely bosonic electroweak sector of SMEFT as can be seen in Table 7.2. However, the map from 3-point massive on-shell amplitudes to the Feynman rules has 21 dimensionless functions $\mathcal{C}_i, \mathcal{C}_i^\pm$ (see Table 7.4). This is because the gauge symmetries relate several amplitudes and, in order to define an *on-shell basis*, we need to reduce the 21 functions to a 11-dimensional space. There are many equivalent choices but a convenient set that we are going to use to define the *on-shell basis* is given by:

$$\mathcal{C}_{hhh},\ \mathcal{C}_{hZZ},\ \mathcal{C}_{hW\bar{W}},\ \mathcal{C}^\pm_{h\gamma\gamma},\ \mathcal{C}'^\pm_{W\bar{W}\gamma},\ \mathcal{C}^\pm_{W\bar{W}\gamma},\ \mathcal{C}^\pm_{hW\bar{W}}\,. \tag{7.24}$$

$\mathcal{C}_i$	Warsaw Basis
$\mathcal{C}_{hhh}$	$3\lambda_h\delta\tilde{v} + 6c_H - 9\lambda_h c_{H\Box} + 9/4\lambda_h c_{HD}$
$\mathcal{C}_{W\bar{W}Z}$	$-4\sqrt{2}\,c_\theta\left[c_{HD}/4 + c_{HWB}\,s_\theta c_\theta - \delta\tilde{v}\right]$
$\mathcal{C}_{W\bar{W}\gamma}$	$-\sqrt{2}\,c_\theta/t_\theta\left[c_{HD}/4 + c_{HWB}s_\theta c_\theta + \delta\tilde{v}\right]$
$\mathcal{C}_{hZZ}$	$-2\left[c_{H\Box} + c_{HD}/4 - \delta\tilde{v}\right]$
$\mathcal{C}_{hW\bar{W}}$	$-2\left[c_{H\Box} - c_{HD}/4 - \delta\tilde{v}\right]$
$\mathcal{C}^{\pm}_{h\gamma\gamma}$	$-2\left[s_\theta^2\,c^{\pm}_{HW} - s_\theta\,c_\theta\,c^{\pm}_{HWB} + c_\theta^2\,c^{\pm}_{HB}\right]$
$\mathcal{C}^{\pm}_{hZ\gamma}$	$-\left[(s_\theta^2 - c_\theta^2)\,c^{\pm}_{HWB} + 2s_\theta\,c_\theta\,(c^{\pm}_{HW} - c^{\pm}_{HB})\right]$
$\mathcal{C}^{\pm}_{hZZ}$	$-2\left[c_\theta^2\,c^{\pm}_{HW} + s_\theta^2\,c^{\pm}_{HB} + c_\theta\,s_\theta\,c^{\pm}_{HWB}\right]$
$\mathcal{C}^{\pm}_{hW\bar{W}}$	$-2\,c^{\pm}_{HW}$
$\mathcal{C}^{\pm}_{W\bar{W}Z}$	$c^{\pm}_{HWB}\sqrt{2}\,s_\theta$
$\mathcal{C}^{\pm}_{W\bar{W}\gamma}$	$c^{\pm}_{HWB}\,\sqrt{2}\,c_\theta$
$\mathcal{C}'^{\pm}_{W\bar{W}Z}$	$c^{\pm}_{W}\,3\sqrt{2}\,c_\theta$
$\mathcal{C}'^{\pm}_{W\bar{W}\gamma}$	$c^{\pm}_{W}\,3\sqrt{2}\,s_\theta$

Table 7.4: Map between the dimensionless functions $\mathcal{C}_i, \mathcal{C}_i^{\pm}$ and the dimension six SMEFT in the Warsaw basis, where we define $\delta\tilde{v} \equiv \Lambda^2\,\delta v/v^3$ (see also Eq.(7.12)).

The remaining 10 coefficients $(\mathcal{C}^{\pm}_{hZZ}, \mathcal{C}^{\pm}_{hZ\gamma}, \mathcal{C}^{\pm}_{W\bar{W}Z}, \mathcal{C}'^{\pm}_{W\bar{W}Z}, \mathcal{C}_{W\bar{W}Z}, \mathcal{C}_{W\bar{W}\gamma})$ can be related to the ones of the basis through the following relations:

$$\begin{aligned} c_\theta^2\,\mathcal{C}^{\pm}_{hZZ} &= -\sqrt{2}\,s_\theta\,\mathcal{C}^{\pm}_{W\bar{W}\gamma} + s_\theta^2\,\mathcal{C}^{\pm}_{h\gamma\gamma} + (c_\theta^2 - s_\theta^2)\,\mathcal{C}^{\pm}_{h\bar{W}W}\,, \\ c_\theta\,\mathcal{C}^{\pm}_{W\bar{W}Z} - s_\theta\,\mathcal{C}^{\pm}_{W\bar{W}\gamma} &= 0\,, \qquad s_\theta\,\mathcal{C}'^{\pm}_{W\bar{W}Z} - c_\theta\,\mathcal{C}'^{\pm}_{W\bar{W}\gamma} = 0\,, \\ 2\,c_\theta s_\theta\,\mathcal{C}^{\pm}_{hZ\gamma} &= \mathcal{C}^{\pm}_{h\bar{W}W} - c_\theta^2\,\mathcal{C}^{\pm}_{hZZ} - s_\theta^2\,\mathcal{C}^{\pm}_{h\gamma\gamma}\,, \end{aligned} \tag{7.25}$$

and we are still left with two SM-like structures $\mathcal{C}_{W\bar{W}Z}$ and $\mathcal{C}_{W\bar{W}\gamma}$. One linear combination is given by

$$\mathcal{C}_{W\bar{W}Z} + 4\,t_\theta\,\mathcal{C}_{W\bar{W}\gamma} = \left(\mathcal{C}_{hZZ} - \mathcal{C}_{hW\bar{W}}\right) 2\sqrt{2}\,c_\theta - 4\,s_\theta\,c_\theta\,\left(\mathcal{C}^{+}_{W\bar{W}\gamma} + \mathcal{C}^{-}_{W\bar{W}\gamma}\right)\,, \tag{7.26}$$

and another one is determined once δv is fixed. We can also write the Wilson coefficients c_i of the Warsaw basis in terms of the on-shell basis parameters:

$$
\begin{aligned}
c_W^{\pm} &= \frac{\mathcal{C}'^{\pm}_{W\bar{W}\gamma}}{3\sqrt{2}\,c_\theta}\,, \qquad c_{HW}^{\pm} = -\frac{\mathcal{C}^{\pm}_{hW\bar{W}}}{2}\,, \qquad c_{HWB}^{\pm} = \frac{\mathcal{C}^{\pm}_{W\bar{W}\gamma}}{\sqrt{2}\,c_\theta}, \\
c_{HB}^{\pm} &= -\frac{1}{2\,c_\theta^2}\left(\mathcal{C}^{\pm}_{h\gamma\gamma} - s_\theta^2\,\mathcal{C}^{\pm}_{hW\bar{W}} - \sqrt{2}\,s_\theta\,\mathcal{C}^{\pm}_{W\bar{W}\gamma}\right)\,, \qquad c_H = \frac{\mathcal{C}_{hhh}}{6} - \frac{3\lambda_h \mathcal{C}_{hW\bar{W}}}{4} + \lambda_h\,\delta\tilde{v}, \\
c_{H\Box} &= -\frac{1}{4}\left(\mathcal{C}_{hW\bar{W}} + \mathcal{C}_{hZZ}\right) + \delta\tilde{v}\,, \qquad c_{HD} = \left(\mathcal{C}_{hW\bar{W}} - \mathcal{C}_{hZZ}\right).
\end{aligned}
\tag{7.27}
$$

7.5 What about $2 \to 2$ scattering amplitudes?

The advantage of recursion relations is well-known in several cases and an important tool for LHC calculations (for a review, see [243, 265]). In particular, the BCFW recursion relations can be used to calculate massless [235,236] and massive amplitudes [217,241,266] at tree and loop level. On the other hand, for a general EFT the recursion relations can fail, as normally the amplitudes are not fixed just by factorization.[42] Once the information about independent interactions is supplied, the amplitude can be built recursively for a minimum number of external legs. Then, a good large-z behaviour can be obtained with the all-line shift [239] or with soft-shifts (for theories with massless particles and non-trivial soft degree) [227, 255].

Another way to calculate amplitudes requiring consistent factorization was presented in [8] (see also [248]). This means that for a set of 3-point amplitudes and particle spectrum, one may look for a function that factorizes correctly in each channel, noticing that the residue in one channel can manifest as a pole in another channel. Requiring that the amplitude factorize in all physical channels and that there are no other poles allows to iteratively build the correct amplitude up to polynomial terms (i.e. without poles).

In order to study massive amplitude with higher dimensional operators we are going to use the BCFW and/or the requirement of consistent factorization channels to build the factorizable part of the amplitude. For the SM, the coefficient of the contact interactions are going to be obtained demanding that the full amplitude asymptotes to a constant in the HE. For EFTs, the full amplitude in general grows with some energy power in the HE limit and we should look for different strategies to fix the coefficient of non-factorizable terms. However, since we are adding the information about the electroweak symmetry breaking explicitly, i.e. relying on the Feynman rules structure and doing a map to the on-shell amplitudes, the contact interactions are related to the 3-point amplitude once $\delta\tilde{v}$ is fixed. Generically, one may use of the following steps to build massive amplitudes:

[42] One could think that the obstacle for applying recursion relations to EFTs is the energy growth of the amplitudes. However, as discussed in [227], a bad high energy behaviour is not an obstacle to the BCFW, as many gravity amplitudes can be calculated correctly in this way. Indeed, in Ref. [240], it is shown that the BCFW works for any amplitude in two-derivatives gauge and (super)gravity theories.

1. Build the $\mathcal{M}_4$ amplitude using recursion relations (e.g. BCFW);

2. Check if the result factorizes correctly in all physical channels. If this is not the case, it means that the recursion relations failed, in the sense that there is a non-zero boundary term;

3. The boundary term can be calculated requiring consistent factorization (see also [267]);

4. Once the factorizable part is calculated, write all possible polynomials terms (without poles) consistent with the LG;

5. Compute the HE limit to obtain information about the coefficient of the non-factorizable terms.

Indeed, steps 1-3 can be replaced by simply starting with an ansatz (gluing lower point amplitudes) and building a function that factorizes correctly, as presented in [8]. We are going to show a few cases where this algorithm is useful and give the correct result.

7.5.1 $W\bar{W}\gamma\gamma$

Let us start with the SM amplitude $\mathcal{M}^{\rm SM}(\mathbf{1}_W\mathbf{2}_{\bar{W}}3^-_\gamma 4^+_\gamma)$. In this case, the easier choice is to shift the massless legs to the complex plane such that

$$|\hat{4}\rangle = |4\rangle + z|3\rangle, \qquad |\hat{3}] = |3] - z|4] \tag{7.28}$$

while $|\hat{4}] = |4]$ and $|\hat{3}\rangle = |3\rangle$. With the $[3^-, 4^+\rangle$-shift, there are two factorization channels that corresponds to

$$\begin{aligned}
\hat{p}^2_{\boldsymbol{q}} = (p_{\mathbf{1}} + \hat{p}_3(z_t))^2 = m_W^2 \Rightarrow z_t = \frac{2p_{\mathbf{1}}p_3}{\langle 3|p_{\mathbf{1}}|4]}\,, \\
\hat{p}^2_{\boldsymbol{q}} = (p_{\mathbf{1}} + \hat{p}_4(z_u))^2 = m_W^2 \Rightarrow z_u = -\frac{2p_{\mathbf{1}}p_4}{\langle 3|p_{\mathbf{1}}|4]}\,.
\end{aligned} \tag{7.29}$$

The amplitude can then be represented by

$$\begin{aligned}
\mathcal{M}(\mathbf{1}_W\mathbf{2}_{\bar{W}}3^-_\gamma 4^+_\gamma) &= \hat{\mathcal{M}}(\mathbf{1}_W 3^-_\gamma \boldsymbol{q}_{\bar{W}})\frac{1}{t-m_W^2}\hat{\mathcal{M}}(-\boldsymbol{q}_W\mathbf{2}_{\bar{W}}4^+_\gamma) \\
&\quad + \hat{\mathcal{M}}(\mathbf{2}_W 3^-_\gamma \boldsymbol{q}_{\bar{W}})\frac{1}{u-m_W^2}\hat{\mathcal{M}}(-\boldsymbol{q}_W\mathbf{1}_{\bar{W}}4^+_\gamma) \\
&= \hat{\mathcal{M}}_t + \hat{\mathcal{M}}_u\,,
\end{aligned} \tag{7.30}$$

where the $\hat{\mathcal{M}}$ indicate the 3-point amplitudes with the shifted legs of Eq. (7.28) corresponding to the t and u-channel. We can write the t-channel contribution explicitly as

$$\hat{\mathcal{M}}_t = \left(\frac{\mathcal{G}_{W\bar{W}\gamma}}{v\, m_W}\frac{\langle\hat{3}|p_{\mathbf{1}}|\xi_3]}{[\zeta_3\,\hat{3}]}[\mathbf{1}\hat{\boldsymbol{q}}]^2\right)\frac{1}{t-m_W^2}\left(\frac{\mathcal{G}_{W\bar{W}\gamma}}{v\, m_W}\frac{\langle\zeta_4|p_{\mathbf{2}}|\hat{4}]}{\langle\hat{4}\,\zeta_4\rangle}\langle\mathbf{2}\,\hat{\boldsymbol{q}}\rangle^2\right). \tag{7.31}$$

We can choose $\zeta_3 = 4$ and $\zeta_4 = 3$, then the z part is proportional to $\langle 3\,3\rangle = 0$ and $[4\,4] = 0$ which simplifies the calculation. It is also useful to use momentum conservation to write $\langle 3|p_{\mathbf{1}}|4] = -\langle 3|p_{\mathbf{2}}|4]$ and

$$\langle\mathbf{2}|p_{\boldsymbol{q}}|\mathbf{1}] = \frac{m_W^2}{\langle 3|p_{\mathbf{2}}|4]}\Big(\langle 3\,\mathbf{1}\rangle[4\,\mathbf{2}] + \langle 3\,\mathbf{2}\rangle[4\,\mathbf{1}]\Big). \tag{7.32}$$

The calculation for the $\hat{\mathcal{M}}_u$ is analogous as we can replace $3 \leftrightarrow 4$. We can then sum both contributions to obtain

$$\mathcal{M}(\mathbf{1}_W\mathbf{2}_{\bar{W}}3_\gamma^-4_\gamma^+) = -\frac{(\mathcal{G}_{W\bar{W}\gamma}\, m_W/v)^2}{(t-m_W^2)(u-m_W^2)}\Big(\langle 3\,\mathbf{1}\rangle[4\,\mathbf{2}] + \langle 3\,\mathbf{2}\rangle[4\,\mathbf{1}]\Big)^2, \tag{7.33}$$

The square indicates the contraction with the same term with different $SU(2)$ indices and the symmetrization is implicit. Using the map of Table 7.3, we get that $(\mathcal{G}_{W\bar{W}\gamma}\, m_W/v)^2 = 2e^2$. We can see that naively the amplitude goes as z^{-2}, which justifies us finding the correct result with the chosen shift. However, we should not make use of the final result to prove the large-z behaviour. A more detailed analysis for massive BCFW based on Feynman diagrams (in the case of gluons and massive quarks) can be seen in [217, 241] and it would be interesting to find a generalization for any shift on the lines of [256].

The good large-z behaviour and the absence of boundary terms can also be seen noticing that an independent contact interaction would have the form

$$\frac{\mathcal{G}_{W\bar{W}\gamma\gamma}}{v^4}\Big(\langle 3\,\mathbf{1}\rangle[4\,\mathbf{2}] + \langle 3\,\mathbf{2}\rangle[4\,\mathbf{1}]\Big)^2, \tag{7.34}$$

which blows up in the HE, so indeed $\mathcal{G}_{W\bar{W}\gamma\gamma} = 0$. This is the most generic structure consistent with the LG (at leading order in $1/v$) as any other term with a momentum insertion can be reduced to this one using Schouten identities.

For the amplitude where the photons have same helicities we can try a different shift where one of the legs is massive. The $[4^+, \mathbf{1}\rangle$- shift is given by

$$|\hat{\mathbf{1}}^I\rangle = |\mathbf{1}^I\rangle - z\langle 4\,\mathbf{1}^I\rangle|4\rangle, \qquad |\hat{4}] = |4] + z\langle 4\,\mathbf{1}^K\rangle|\mathbf{1}_K]. \tag{7.35}$$

Since it is clear how the $SU(2)$ indices should be contracted, we will omit the indices in the following. For this shift, the only factorization channel corresponds to $\hat{p}_{\boldsymbol{q}}^2 = (p_{\mathbf{1}} + \hat{p}_3(z_t))^2 =$

m_W^2. (The u-channel diagram would have both shifted legs in the same sub-amplitude so it vanishes and there is no s-channel as it is not allowed a vertex with photons of the opposite helicities). Solving the condition above for z_t, we get

$$z_t = \frac{t - m_W^2}{\langle 3\,4\rangle\langle 4|p_{\mathbf{1}}|3]} = \frac{\langle 3|p_{\mathbf{1}}|3]}{\langle 3\,4\rangle\langle 4|p_{\mathbf{1}}|3]}\,. \tag{7.36}$$

Then, the amplitude is given by

$$\begin{aligned}\mathcal{M}(\mathbf{1}_W\mathbf{2}_{\bar{W}}3_\gamma^-4_\gamma^-) &= \hat{\mathcal{M}}(\mathbf{1}_W 3_\gamma^- \boldsymbol{q}_{\bar{W}})\frac{1}{t-m_W^2}\hat{\mathcal{M}}(-\boldsymbol{q}_W\mathbf{2}_{\bar{W}}4_\gamma^-)\\ &= \left(\frac{\mathcal{G}_{W\bar{W}\gamma}}{v\,m_W}\frac{\langle 3|\hat{p}_{\mathbf{1}}|\zeta_3]}{[\zeta_3\,3]}[\mathbf{1}\hat{\boldsymbol{q}}]^2\right)\frac{1}{t-m_W^2}\left(\frac{\mathcal{G}_{W\bar{W}\gamma}}{v\,m_W}\frac{\langle 4|p_{\mathbf{2}}|\zeta_4]}{[\zeta_4\,\hat{4}]}[\mathbf{2}\hat{\boldsymbol{q}}]^2\right)\end{aligned} \tag{7.37}$$

It is convenient to choose $\zeta_3 = 4$ and $\zeta_4 = 3$. We can also use that

$$\langle 3|\hat{p}_{\mathbf{1}}|4] = \langle 3|p_{\mathbf{1}}|4] - z_t\langle 3\,4\rangle\langle 4|p_{\mathbf{1}}|4] = \frac{m_W^2 s}{\langle 4|p_{\mathbf{1}}|3]}, \tag{7.38}$$

where $\langle 3\,4\rangle[\hat{4}\,3] = m_W^2 - u$ and $\langle 3\,4\rangle[3\,4] = s$. This leads to

$$\mathcal{M}(\mathbf{1}_W\mathbf{2}_{\bar{W}}3_\gamma^-4_\gamma^-) = \frac{(\mathcal{G}_{W\bar{W}\gamma}\,m_W/v)^2}{(t-m_W^2)(u-m_W^2)}[\mathbf{1}\,\mathbf{2}]^2\langle 3\,4\rangle^2\,, \tag{7.39}$$

which agrees with the Feynman rules calculation. Naively, we can see that with the one massless/one massive shift the amplitude scales as z^{-2}. On the other hand, a shift on both massless legs would go as z^0, which explains our choice. In this case, an independent contact interaction is also forbidden due to the HE constraint. The next step is to calculate the amplitude with one insertion of a dimension six operator $\mathcal{M}^{\rm BSM}(\mathbf{1}_W\mathbf{2}_{\bar{W}}3_\gamma^-4_\gamma^+)$. The SM-like part gives the same result as Eq. (7.33), with the appropriate couplings. For the non-minimal coupling in the vertex $\hat{\mathcal{M}}(-\mathbf{q}_W\mathbf{2}_{\bar{W}}4_\gamma^-)$, we can use the $[3^-,4^+\rangle$-shift of Eq. (7.28). One of the 3-point amplitudes corresponds to the non-minimal coupling of Eq. (7.23) and we obtain:

$$\begin{aligned}\hat{\mathcal{M}}_t^{\rm BSM,-} &= \left(\frac{1}{v\,m_W}\mathcal{G}_{W\bar{W}\gamma} + \frac{v}{m_W\Lambda^2}\mathcal{C}_{W\bar{W}\gamma}\right)\frac{m_W^2}{s\,(t-m_W^2)}\times \\ &\times\left\{\frac{v\,\mathcal{C}^-_{W\bar{W}\gamma}}{\Lambda^2}\Big(\langle 3\,\mathbf{1}\rangle[4\,\mathbf{2}] + \langle 3\,\mathbf{2}\rangle[4\,\mathbf{1}]\Big)\langle 3\,\mathbf{1}\rangle\langle 3\,\mathbf{2}\rangle[4\,3] + \frac{\mathcal{C}'^-_{W\bar{W}\gamma}}{\Lambda^2}\frac{\langle\mathbf{1}\,\mathbf{2}\rangle[4\,3]}{m_W}\langle 3\,\mathbf{1}\rangle\langle 3\,\mathbf{2}\rangle\langle 3|p_{\mathbf{2}}|4]\right\}\,.\end{aligned} \tag{7.40}$$

Then, $\hat{\mathcal{M}}_t^{\rm BSM,+}$ can be obtained by parity and the u-channel using crossing symmetry. Summing the t and u contributions and keeping just $\mathcal{O}(\Lambda^{-2})$ terms leads to

$$\begin{aligned}\mathcal{M}^{\rm BSM,-}(\mathbf{1}_W\mathbf{2}_{\bar{W}}3_\gamma^-4_\gamma^+) &= \left(\frac{\mathcal{G}_{W\bar{W}\gamma}}{\Lambda^2}\right)\frac{1}{(t-m_W^2)\,(u-m_W^2)}\times \\ &\times\Big\{\mathcal{C}^-_{W\bar{W}\gamma}m_W\Big(\langle 3\,\mathbf{1}\rangle[4\,\mathbf{2}] + \langle 3\,\mathbf{2}\rangle[4\,\mathbf{1}]\Big)\langle 3\,\mathbf{1}\rangle\langle 3\,\mathbf{2}\rangle[4\,3] + \mathcal{C}'^-_{W\bar{W}\gamma}\langle\mathbf{1}\,\mathbf{2}\rangle\langle 3\,\mathbf{1}\rangle\langle 3\,\mathbf{2}\rangle\langle 3|p_{\mathbf{2}}|4][4\,3]\Big\}\,,\end{aligned} \tag{7.41}$$

which factorizes correctly in all channels. For the non-minimal coupling in the vertex $\hat{\mathcal{M}}(\mathbf{1}_W 3^-_\gamma \boldsymbol{q}_{\bar{W}})$ we obtain the same result with $\langle ... \rangle \leftrightarrow [...]$ and $3 \leftrightarrow 4$. Before discussing the non-factorizable contributions, let us analyse the HE of Eq. (7.41). Naively, we can just 'unbold' the amplitude and by the LG we can see that the term $\mathcal{C}^-_{W\bar{W}\gamma}$ contributes to amplitudes with longitudinal W's, and $\mathcal{C}'^-_{W\bar{W}\gamma}$ contributes at leading order to an amplitude with two transverse W's with the same polarization, which has the same structure as the gluon scattering with a G^3 insertion [115]. Notice that the factorizable terms of the amplitude can also be obtained without BCFW, and just starting with an ansatz and requiring consistent factorization [248]. However, both methods fail to get the polynomial terms correctly. Since the term of Eq. (7.34) is forbidden, the next candidate for contact interaction is

$$\frac{\mathcal{C}^-_{W\bar{W}\gamma\gamma}}{v^2\,\Lambda^2}\Big(\langle 3\,\mathbf{1}\rangle[4\,\mathbf{2}] + \langle 3\,\mathbf{2}\rangle[4\,\mathbf{1}]\Big)^2 . \tag{7.42}$$

In this case, we know that the coefficient $\mathcal{C}^-_{W\bar{W}\gamma\gamma}$ is related to the 3-point vertex, as the information about the gauge symmetries of the theory are already in the map of Table 7.4. Then, we can do the matching to the Feynman calculation, which means impose that the 4-point contact interaction is proportional to the 3-point amplitude if one leg corresponds to the Higgs vev, i.e. $\mathcal{C}_{hh\gamma\gamma} \equiv (2/\bar{v})\,\mathcal{C}_{h\gamma\gamma}$. Now, as discussed in Sec. 7.4, the Goldstone boson equivalence theorem can be seen in the HE of the massive amplitudes. This implies that the contact interactions $\mathcal{C}_{hh\gamma\gamma}$ and $\mathcal{C}^-_{W\bar{W}\gamma\gamma}$ have the same form. We leave the exploration of a bottom-up approach to obtain the non-factorizable interactions for a future work.

7.5.2 $W\bar{W}hh$

In the case of $\mathcal{M}(\mathbf{1}_W \mathbf{2}_{\bar{W}} \mathbf{3}_h \mathbf{4}_h)$, one may expect a bad large-z behaviour doing a BCFW shift due to the pure scalar amplitude with longitudinal W's and the Higgs. However, we may reconstruct the SM amplitude from the residues at the poles and requiring a well-behaved UV. The full amplitude can be written as

$$\mathcal{M}(\mathbf{1}_W \mathbf{2}_{\bar{W}} \mathbf{3}_h \mathbf{4}_h) = \frac{R_t}{t - m_W^2} + \frac{R_u}{u - m_W^2} + \frac{R_s}{s - m_h^2} + \mathcal{G}_{W\bar{W}hh}\langle \mathbf{12}\rangle[\mathbf{12}]\,, \tag{7.43}$$

where the form of the non-factorizable contribution is fixed by the $SU(2)$ LG[43] and we will discuss how to obtain $\mathcal{G}_{W\bar{W}hh}$ in the following. First, we can easily calculate the

[43]The structures $\langle \mathbf{12}\rangle^2$ and $[\mathbf{12}]^2$ are also consistent with the LG, but are not linearly independent as can be written in terms of $\langle \mathbf{12}\rangle[\mathbf{12}]$ using that $2p_1 \cdot p_2 = s - 2m_h^2$.

residues by just 'gluing' the corresponding 3-point amplitudes:

$$R_t = \mathcal{M}(\mathbf{1}_W \boldsymbol{q}_{\bar{W}} \mathbf{3}_h)\mathcal{M}(-\boldsymbol{q}_W \mathbf{2}_{\bar{W}} \mathbf{4}_h)|_{t\to m_W^2} = \frac{(\mathcal{G}_{W\bar{W}h})^2}{v^2}\Big(\langle \mathbf{1}\boldsymbol{q}\rangle[\mathbf{1}\boldsymbol{q}]\Big)\Big(\langle \boldsymbol{q}\mathbf{2}\rangle[\boldsymbol{q}\mathbf{2}]\Big)\,,$$
$$R_s = \mathcal{M}(\mathbf{1}_W \mathbf{2}_{\bar{W}} \boldsymbol{q}_h)\mathcal{M}(-\boldsymbol{q}_h \mathbf{3}_h \mathbf{4}_h)|_{s\to m_W^2} = (\mathcal{G}_{W\bar{W}h})(\mathcal{G}_{hhh})\Big(\langle \mathbf{12}\rangle[\mathbf{12}]\Big)\,, \tag{7.44}$$

where $\boldsymbol{q}$ is the momentum in the corresponding factorization channel. The residue in the u-channel can then be obtained as $R_u = R_t\,(\mathbf{3} \leftrightarrow \mathbf{4})$. Notice that we have to sum over the $SU(2)$ indices of the internal particle such that

$$\begin{aligned}\Big(\langle \mathbf{1}\boldsymbol{q}\rangle[\mathbf{1}\boldsymbol{q}]\Big)\Big(\langle \boldsymbol{q}\mathbf{2}\rangle[\boldsymbol{q}\mathbf{2}]\Big) &= \Big(\langle \mathbf{1}^{J_1}\boldsymbol{q}^{J}\rangle[\mathbf{1}^{K_1}\boldsymbol{q}^{K}] + \langle \mathbf{1}^{J_1}\boldsymbol{q}^{K}\rangle[\mathbf{1}^{K_1}\boldsymbol{q}^{J}]\Big)\Big(\langle \boldsymbol{q}_J\mathbf{2}^{J_2}\rangle[\boldsymbol{q}_K\mathbf{2}^{K_2}]\Big)\\ &= -m_1^2\,\langle \mathbf{1}^{J_1}\mathbf{2}^{J_2}\rangle[\mathbf{1}^{J_1}\mathbf{2}^{J_2}] + \langle \mathbf{1}^{J_1}|\,p_{\boldsymbol{q}}\,|\mathbf{2}^{K_2}][\mathbf{2}^{J_2}|\,p_{\boldsymbol{q}}\,|\mathbf{1}^{K_1}]\,,\end{aligned} \tag{7.45}$$

where $p_{\boldsymbol{q}} = p_{\mathbf{1}} + p_{\mathbf{3}}$ for the t-channel. Summing all the residues, we can use $\mathcal{G}_i$ from Table 7.3 and write Eq. (7.43) as

$$\begin{aligned}\mathcal{M}(\mathbf{1}_W\mathbf{2}_{\bar{W}}\mathbf{3}_h\mathbf{4}_h) =& \frac{(\mathcal{G}_{W\bar{W}h})^2}{v^2}\left[\frac{\langle \mathbf{1}|p_{\mathbf{3}}|\mathbf{1}][\mathbf{2}|p_{\mathbf{4}}|\mathbf{2}]}{t-m_W^2} + \frac{\langle \mathbf{1}|p_{\mathbf{4}}|\mathbf{1}][\mathbf{2}|p_{\mathbf{3}}|\mathbf{2}]}{u-m_W^2}\right] \\ &\left[-\frac{(\mathcal{G}_{W\bar{W}h})^2 m_W^2(2m_h^2-s)}{v^2(t-m_W^2)(u-m_W^2)} - \frac{(\mathcal{G}_{W\bar{W}h})(\mathcal{G}_{hhh})}{(s-m_h^2)} + \mathcal{G}_{W\bar{W}hh}\right]\langle \mathbf{12}\rangle[\mathbf{12}]\,.\end{aligned} \tag{7.46}$$

For the longitudinally polarized W's, in the HE limit we have that $\mathcal{M}_{\rm HE} \to (\mathcal{G}_{W\bar{W}h})^2 s/(2v^2) + \mathcal{G}_{W\bar{W}hh}s$ and demanding that the amplitude asymptotes to a constant in the UV, we have

$$\mathcal{G}_{W\bar{W}hh} = -\frac{1}{2}\frac{(\mathcal{G}_{W\bar{W}h})^2}{v^2} = -\frac{2}{v^2}\,, \tag{7.47}$$

which reproduces the Feynman rules calculation. This should not be a surprise, since the 3- and 4-point contact interactions are connected by a gauge symmetry in the Lagrangian language, which means that the higher point contact interactions of this type are fixed by the coefficient of the 3-point amplitude.

Moving to the SMEFT amplitude, the SM-like part gives the same result as Eq. (7.46) with the replacement $\mathcal{G}_{W\bar{W}h} \to \mathcal{C}_{W\bar{W}h}$ and one of $\mathcal{G}_{W\bar{W}hh} \to \mathcal{C}_{W\bar{W}hh}$. However, we cannot use the same argument as before to obtain the new coefficient of the 4-point contact interaction $\mathcal{C}_{W\bar{W}hh}$, since for the SMEFT the amplitude actually grows with s/v^2. In this case, we can proceed similarly to the $WW\gamma\gamma$ amplitude and use the relation $\mathcal{C}_{W\bar{W}hh} \equiv (2/\bar{v})\,\mathcal{C}_{W\bar{W}h}$.

This channel can be particularly interesting to study the origin of the electroweak symmetry breaking. For example, one may explore the difference between SMEFT and HEFT, where the symmetry is linearly and non-linearly realized, respectively [268–270].

7.6 Summary

In this paper, we started the exploration of the massive SMEFT in terms of on-shell amplitudes using the formulation of massive spinors of [8]. Although the kinematic structure is fixed by Lorentz invariance, LG and Bose symmetry, it is not clear how the information about the UV symmetries and the relation between amplitudes should appear in the on-shell language.

As a first step, we draw a map between the parameters of the SMEFT Lagrangian and the coefficients of the on-shell amplitudes using the Feynman rules derived in [264]. We also discussed how the BCFW recursion relation can be applied for the massive SM $WW\gamma\gamma$ scattering. Similar calculations could also be done for other SM processes as e.g. $WWh\gamma$ or with a Z boson instead. It also should be worthwhile to develop a more systematic way to analyse the large-z behaviour and in addition, study general recursion relations. For instance, a lot of progress was made using the soft and collinear limits in the massless and/or supersymmetric cases and one may ask if a similar approach can be useful also in the massive case, especially for the SMEFT.

Another question is how the difference between a linear and a non-linear realization of the electroweak symmetry arises in this language. In other words, it would be interesting to see how HEFT and SMEFT are described at the on-shell level and if this can shed some light on the description of the spontaneous symmetry breaking. Moreover, we are just working at tree-level, but there are several avenues to pursue loop calculation also with massive particles. We hope that this may be an initial step towards a deeper understanding of the intersection of on-shell amplitudes and SMEFT.

8 Final Conclusions

Much experimental evidence point towards the SM being an effective description of Nature. Moreover, theoretical inconsistencies with the Higgs boson reinforce the need for an extension of the current model and a more fundamental description of this boson. Many models were constructed trying to solve the theoretical problems and predict the experimental signals. However, the series of LHC null results shifts the interests towards a model-independent description of new physics with the least amount of UV assumptions possible. HEFT provides the effective description with the least number of assumptions, however it comes with too many parameters. Aiming for a simpler effective description, SMEFT is a good compromise.

Assuming $\mathrm{SU(2)_L}\otimes\ \mathrm{U(1)_Y}$, the SM is enlarged with higher-dimensional operators. The most relevant set of operators for LHC are the dimension-six, which contains several classes categorized accordingly to their field content. Various operators are connected through integration-by-parts and equations of motion, thus finding a minimal set of operators, i.e. a basis, is an essential task. The Warsaw basis is constructed aiming to remove higher derivatives operators and is the basis used in this thesis. Different sectors of the SMEFT contribute to different processes. Looking for observables sensitive to few operators lead to distinct clear signals at the LHC. In the first work of this thesis [1] we analyse the diboson production at the LHC, which probes the nature of the triple-gauge boson sector. In the second result [3], we have shown how the flavour sector can impact the operators in SMEFT. Last but not least, in the third result [2] we built the SMEFT amplitudes via on-shell methods. This new approach shed light on various aspects of SMEFT which can be obscure using Feynman diagrams.

In the SMEFT framework, the proliferation of dimension-six coefficients can lead to complex phenomenological analysis, where many parameters contribute. Thus, finding observables sensitive to a minimal amount of higher dimension operators is essential. The first work of this thesis provides an analysis where only one operator $\mathcal{O}_W$ comes in hand. In the study of diboson production at the LHC, we were able to set a bound on this particular operator. The production is given by the four-point amplitude $\bar{\psi}\psi \to VV$, which does not have an interference between the standard model and the SMEFT amplitudes. Therefore, this effect cannot be seen in the cross-section. However, when the bosons decay, which is the real final state, an interference resurrection emerges. The signal of this interference make itself clear in the azimuthal angles of the final state. We made use of jet substructure techniques to reconstruct and analyse the hadronic and semileptonic final state of the boson decay. The latter had competitive bounds with the purely leptonic final states, while the former is polluted by the four jet background. This analysis provides a valuable cross-check to the fully-leptonic case and developments on the jet substructure techniques can refine the analysis and improve the background rejection.

A very important effect in EFTs is the running of the Wilson coefficients. Starting

with a theory at a high scale Λ and then running down to the electroweak scale can mix into different operators. At LHC, Higgs, Top and electroweak physics normally occurs at their respective scale where bounds are set. However, we know that very strong bounds comes from flavour physics which is given at low-energy scale. Running a theory from Λ down to the flavour physics low-energy scale is a multi-step process. It involves running to electroweak, matching to the WET theory and running again to low-energy. The result is a Wilson coefficient at flavour scale as a linear combination of the SMEFT Wilson coefficients at Λ. Performing a one-loop matching relates coefficients which are naively unrelated, as electroweak operators at low energy, and can provide new bounds. In the second paper of this thesis, we continued with one-loop matching between SMEFT and WET done at [71], and analysed the impact of the flavour observables compared to the other scales observables. We saw that even starting with the most flavourless scenario, these measurements can provide competitive bounds to the electroweak observables.

In the second part of this thesis, we discussed modern methods for scattering amplitudes. This is a rapidly growing field and has enormous applications, from higher loop order QCD calculations to black hole binary dynamics. Using spinor-helicity variables, recursion relations and generalized unitarity, one can build an n-point amplitude very effectively and discover hidden symmetries. The main obstruction to the recursive construction is the boundary term B_∞. This term is avoided in YM and GR by choosing a good shift in the momenta that makes it vanish. For EFTs, the boundary term also sets an obstruction to the recursion relations, and one has to rely on the soft behaviour of the amplitude to circumvent it. The story is simple for massless amplitude but is becomes harder when masses are included. In this case, the definition of good/bad shift becomes harder since the massive particles contains both polarizations. With the addition of EFT operators, more complications come to the recursive construction of the amplitudes and this is what we explore in the last paper.

In the last paper presented in this thesis we studied the three-point SMEFT amplitudes in the massive on-shell formalism. An incredible simplification and compact form of this amplitude is obtained and compared with Feynman rules. This is due to the massive spinor-helicity formalism that has simple transformations under the little group. We also explore four-point amplitudes, where the recursion relations for BCFW works for limited cases. Another explored technique to obtain these amplitudes was consistent factorization, where we also made use of perturbative unitarity to obtain contact terms of the amplitude. This study was the first step in obtaining the SMEFT 3-point massive amplitudes and exploring four-points. Many developments and avenues can be explored after it and an on-shell development of the SMEFT is crucial for the LHC precision calculations and to discover new hidden structures in those amplitudes.

We motivated the study of SMEFT arguing in favour of the independence for any model. However, the search for a new physics model that explains the experimental evidences and predicts new particles is the major goal. In the lack of this model, possible LHC

signals that appears in the effective theory will guide any model building. For instance, many models can be matched to SMEFT and existing bounds on the Wilson Coefficients give information on the parameters and scales of the given model. Therefore, is essential to have consistent bounds on all of the SMEFT coefficients. To do so, global analysis are indispensable, since they give the allowed values of the coefficients and, consequently, to the new physics models parameters. As we shown in the first part, providing all the data possible to complete global analysis is essential to understand the nature of physics beyond the SM.

In conclusion, the study of EFT has a clear motivation in the current times. The use of SMEFT for it is the best available tool to identify and parametrize the new physics effects that might come. Finding observables sensitive to the minimal set of Wilson coefficients is an important task to pursue. Moreover, connecting different set of data tell us more about how the UV theory should behave. And lastly, calculation via Lagrangians can be a bottleneck for the 'EFT precision era' of LHC. Therefore, sharpening the tools for these computations is essential. The use of modern methods has proven many times its effectiveness of precision calculation and ability to find hidden structures in the amplitudes.

Appendices

This section contains the appendices of the papers [1–3].

A Two-to-four partonic cross section calculations

The SM diboson production matrix elements at leading order in the squared center of mass energy s are given by (for $u\bar{u} \to W^+W^-$, other cases are similar) [271]

$$\mathcal{M}^{\rm SM}(-+ \to 00) = \frac{3g_L^2 + g_Y^2}{12}\sin\theta + \mathcal{O}(m_W^2/s), \quad \mathcal{M}^{\rm SM}(+- \to 00) = -\frac{g_Y^2}{3}\sin\theta + \mathcal{O}(m_W^2/s),$$
$$\mathcal{M}^{\rm SM}(-+ \to \pm\mp) = -\frac{\mp 1 + \cos\theta}{1+\cos\theta}\frac{g_L^2}{2}\sin\theta, \qquad \mathcal{M}^{\rm SM}(+- \to \pm\mp) = 0,$$

for the BSM, and for the single-insertion of the effective coupling $\delta\lambda_Z$:

$$\mathcal{M}^{\rm BSM}(-+ \to \pm 0) = \frac{\sqrt{s}}{M_W}\frac{g_L}{12\sqrt{2}}(\pm 1 - \cos\theta)3\delta\lambda_Z, \quad \mathcal{M}^{\rm BSM}(-+ \to \pm\pm) = \frac{s}{M_W^2}\frac{g_L^2}{4}\sin\theta\delta\lambda_Z.$$

The vector boson decay amplitudes for helicity λ can be decomposed as:

$$\mathcal{A}^\lambda = (g_\psi\sqrt{2s}/s_w)e^{\lambda\phi_{ij}}d_\lambda(\theta_{ij}) \tag{A.1}$$

where $d_\lambda(\theta_{ij})$ are the Wigner functions $d_\pm(\theta_{ij}) = (1 \mp \cos\theta_{ij})/2$ and $d_0(\theta_{ij}) = (\sin\theta_{ij})/\sqrt{2}$.

λ	$\mathcal{A}_\lambda/(g_\psi\sqrt{2s}/s_w)$
0	$-\sqrt{2}\sin\theta_{ij}$
+	$(1-\cos\theta_{ij})e^{i\phi_{ij}}$
−	$(1+\cos\theta_{ij})e^{-i\phi_{ij}}$

With the above constituents, we can define the total partonic spin-averaged two-to-four cross section

$$\sigma(s) = \int \frac{\sum|\mathcal{M}|^2}{8s}\frac{ds_{12}ds_{34}}{(2\pi)^2}\left[\frac{1}{8\pi}\frac{d\cos\theta_{12}}{2}\frac{d\phi_{12}}{2\pi}\right]\left[\frac{1}{8\pi}\frac{d\cos\theta_{34}}{2}\frac{d\phi_{34}}{2\pi}\right]\left[\frac{\beta}{8\pi}\frac{d\cos\theta}{2}\frac{d\phi}{2\pi}\right], \tag{A.2}$$

with

$$\sum|\mathcal{M}|^2 = |D_W(s_{12})D_W(s_{34})|^2\sum_{\lambda_{12}\lambda'_{12}}\sum_{\lambda_{34}\lambda'_{34}}\left(\mathcal{A}^{\lambda_{12}}\mathcal{A}^{\lambda_{34}}\right)\left(\mathcal{A}^{\lambda'_{12}}\mathcal{A}^{\lambda'_{34}}\right)^* \tag{A.3}$$
$$\sum_{\lambda_+\lambda_-}\left(\mathcal{M}_{q\bar{q}\to WW}^{\lambda_+\lambda_-,\lambda_{12}\lambda_{34}}\right)\left(\mathcal{M}_{q\bar{q}\to WW}^{\lambda_+\lambda_-,\lambda'_{12}\lambda'_{34}}\right)^*,$$

where $D_W(s)$ is the W boson propagator stripped of Lorentz structure, $\lambda_\pm$ are initial state quark polarizations, and $\lambda^{(\prime)}_{12,34}$ are the polarizations of the intermediate, decaying W bosons. Crucially, because these particles are internal to the process, the summation over their helicities takes place independently in the amplitude and its complex conjugate.

A.1 Single-insertion interference

The total BSM amplitude including decays is

$$\mathcal{M}^{\rm BSM}(-+\to\pm\pm)\sim\left(-\frac{\delta\lambda_Z s}{m_W^2}\right)\left(\frac{g_L^2}{2}\sin\theta\right)(1\mp\cos\theta_{12})(1\mp\cos\theta_{34})e^{\pm i(\phi_{12}-\phi_{34})}, \quad \text{(A.4)}$$

and the interference with the SM amplitude can be written as

$$\sum|\mathcal{M}|^2\sim\sum_{\lambda_{12}\lambda_{34}}2{\rm Re}\left[\mathcal{M}^{\rm SM}_{-+,\lambda_{12}\lambda_{34}}(\mathcal{M}^{\rm BSM}_{-+,--})^*+\mathcal{M}^{\rm SM}_{-+,\lambda_{12}\lambda_{34}}(\mathcal{M}^{\rm BSM}_{-+,++})^*\mathcal{M}\right]. \quad \text{(A.5)}$$

In the equation above, two BSM three SM helicities configuration contribute for the sum. The azimuthal behaviour of SM and BSM can be seen in table below, where $\Delta\phi=\phi_{12}-\phi_{34}$.

$(\lambda'_{12}\lambda'_{34})$	$(\lambda_{12}\lambda_{34})$	polar	azimuthal
$(++)$	(00)	$(1-\cos\theta_{12})(1-\cos\theta_{34})(2\sin\theta_{12}\sin\theta_{34})$	$2\cos\Delta\phi$
	$(+-)$	$(1-\cos\theta_{12})^2\sin^2\theta_{34}$	$2\cos 2\phi_{34}$
	$(-+)$	$(1-\cos\theta_{34})^2\sin^2\theta_{12}$	$2\cos 2\phi_{12}$
$(--)$	(00)	$(1+\cos\theta_{12})(1+\cos\theta_{34})(2\sin\theta_{12}\sin\theta_{34})$	$2\cos\Delta\phi$
	$(+-)$	$(1+\cos\theta_{34})^2\sin^2\theta_{12}$	$2\cos 2\phi_{34}$
	$(-+)$	$(1+\cos\theta_{12})^2\sin^2\theta_{34}$	$2\cos 2\phi_{12}$

One should notice here that the coefficient of $\cos 2\phi_{12}(2\phi_{34})$ goes to zero whenever $\theta_{34}(\theta_{12})\to 0,\pi$ and vice versa. This means that the interference vanishes again whenever $\theta_{(12),(34)}\to 0,\pi$, i.e. in the limit where decay products of either W boson are either collinear or anti-collinear with the W momentum. This is intuitive to understand as arising from the fact that in this limit the decay angle, which determines whether the interference is constructive or destructive in the normal case, cannot be defined leading to an effectively-longitudinal polar angle distribution of the vector boson decay products, even though it is the result of interference of two distinct transverse polarizations.

Integrated over the polar angles of W pair production and W boson decays, the interference term becomes:

$$\frac{d\sigma_{\rm int}(s)}{d\phi_{12}d\phi_{34}}\sim\left(-\frac{\delta\lambda_Z s}{m_W^2}\right)\left\{[g_L^2(3g_L^3+g_Y^2)\frac{\pi}{2}]\cos\Delta\phi+g_L^4(\cos 2\phi_{12}+\cos 2\phi_{34})\right\} \quad \text{(A.6)}$$

where the first term vanish after the proper foldings.

A.2 SM self-interference

In the purely SM case, the squared amplitude is given by

$$\begin{aligned}\sum|\mathcal{M}|^2 &= \sum_{\lambda_{12}\lambda'_{12}}\sum_{\lambda_{34}\lambda'_{34}}\sum_{\lambda_+\lambda_-}\mathcal{M}^{\mathrm{SM}}_{\lambda_+\lambda_-,\lambda_{12}\lambda_{34}}(\mathcal{M}^{\mathrm{SM}}_{\lambda_+\lambda_-,\lambda_{12}\lambda_{34}})^* \\ &= \sum_{\lambda_{12}\lambda'_{12}}\sum_{\lambda_{34}\lambda'_{34}}\mathcal{M}^{\mathrm{SM}}_{+-,\lambda_{12}\lambda_{34}}(\mathcal{M}^{\mathrm{SM}}_{+-,\lambda_{12}\lambda_{34}})^* + \mathcal{M}^{\mathrm{SM}}_{-+,\lambda_{12}\lambda_{34}}(\mathcal{M}^{\mathrm{SM}}_{-+,\lambda_{12}\lambda_{34}})^*\end{aligned} \tag{A.7}$$

The first term, coupling to right-handed fermions, produces only longitudinal gauge bosons at leading order. Thus, it has no azimuthal dependence, as there is no non-trivial combination of helicities to interfere. The helicity interference structure of the second term is:

$(\lambda'_{12}\lambda'_{34})$	$(\lambda_{12}\lambda_{34})$	polar	azimuthal
(00)	(00)	$4(\sin\theta_{12})^2(\sin\theta_{34})^2$	1
	(+−)	$2(\sin\theta_{12})(\sin\theta_{34})(1-\cos\theta_{12})(1-\cos\theta_{34})$	$e^{-i\Delta\phi}$
	(−+)	$2(\sin\theta_{12})(\sin\theta_{34})(1+\cos\theta_{12})(1+\cos\theta_{34})$	$e^{+i\Delta\phi}$
(+−)	(00)	$2(\sin\theta_{12})(\sin\theta_{34})(1-\cos\theta_{12})(1-\cos\theta_{34})$	$e^{+i\Delta\phi}$
	(+−)	$(1-\cos\theta_{12})^2(1+\cos\theta_{34})^2$	1
	(−+)	$(1-\cos\theta_{12}^2)(1-\cos^2\theta_{34})$	$e^{+2i\Delta\phi}$
(−+)	(00)	$2(\sin\theta_{12})(\sin\theta_{34})(1+\cos\theta_{12})(1+\cos\theta_{34})$	$e^{-i\Delta\phi}$
	(+−)	$(1-\cos\theta_{12}^2)(1-\cos^2\theta_{34})$	$e^{-2i\Delta\phi}$
	(−+)	$(1+\cos\theta_{12})^2(1-\cos\theta_{34})^2$	1

Note that in this case there are combinations of helicities which allow for nonvanishing forward decay amplitudes, in contrast to the interference case. This means that there is a higher probability of a W boson decaying into something which appears to be a simple QCD jet, yielding different tagging efficiencies for SM diboson pair production as compared to single-insertion of $\delta\lambda_Z$ diboson production. This is again due to the SM amplitude having a large contribution from straightforward transverse polarizations, something forbidden by the non-interference effects for the single-insertion SMEFT case.

Summing and integrating over the polar decay angles θ_{12} and θ_{34},

$$\begin{aligned}\sum|\mathcal{M}|^2 \sim \frac{64}{9}&\left[\left(\frac{g_Y^2\sin\theta}{3}\right)^2+\left(\frac{3g_L^2+g_Y^2}{12}\sin\theta\right)^2\right]+\frac{\pi^2}{2}\left[\left(\frac{1-\cos\theta}{1+\cos\theta}\frac{g_L^2}{2}\sin\theta\right)^2+\left(\frac{g_L^2}{2}\sin\theta\right)^2\right] \\ &+\frac{512}{9}\left(\frac{1-\cos\theta}{1+\cos\theta}\frac{g_L^2}{2}\sin\theta\right)\left(\frac{g_L^2}{2}\sin\theta\right)\cos 2\phi_{12}\cos 2\phi_{34}.\end{aligned}$$

Naïvely, one expects a divergence whenever $\cos\theta = -1$ which corresponds to the coulomb pole for t-channel quark exchange, but integrating over the detector acceptance $|\eta| \leq 4.9$

regulates this divergence. The constant term dominates over the term with nontrivial azimuthal structure. Therefore, for practical terms one can consider the SM self-interference to be effectively independent of azimuthal decay angles.

A.3 EFT self-interference

Finally, for the $\delta\lambda_Z^2$ cross section, we have

$$\begin{aligned}\sum|\mathcal{M}|^2 &= \sum_{\lambda_{12}\lambda'_{12}}\sum_{\lambda_{34}\lambda'_{34}}\sum_{\lambda_+\lambda_-}\mathcal{M}^{\mathrm{BSM}}_{\lambda_+\lambda_-,\lambda_{12}\lambda_{34}}(\mathcal{M}^{\mathrm{BSM}}_{\lambda_+\lambda_-,\lambda_{12}\lambda_{34}})^* \\ &= \left(\frac{s}{m_W^2}\frac{g_L^2}{4}\sin\theta\delta\lambda_Z\right)^2\sum_{\lambda_{12}\lambda'_{12}}\sum_{\lambda_{34}\lambda'_{34}}\mathcal{M}_{\lambda_{12}}\mathcal{M}_{\lambda_{34}}(\mathcal{M}_{\lambda'_{12}}\mathcal{M}_{\lambda'_{34}})^*\end{aligned} \tag{A.8}$$

The structure of the individual terms of this sum with respect to decay angles is:

$(\lambda'_{12}\lambda'_{34})$	$(\lambda_{12}\lambda_{34})$	polar	azimuthal
$(++)$	$(++)$	$(1-\cos\theta_{12})^2(1-\cos\theta_{34})^2$	no
	$(--)$	$\sin^2\theta_{12}\sin^2\theta_{34}$	$e^{2i\Delta\phi}$
$(--)$	$(++)$	$\sin^2\theta_{12}\sin^2\theta_{34}$	$e^{-2i\Delta\phi}$
	$(--)$	$(1+\cos\theta_{12})^2(1+\cos\theta_{34})^2$	no

Note again that there exist here terms which allow for forward W decays. Integrating over polar decay angles leads to

$$\sum|\mathcal{M}^{\mathrm{BSM}}|^2 \sim \left(\frac{s}{m_W^2}g_L^2\delta\lambda_Z\right)^2\left(\frac{32}{27}\right)(1+4\cos 2\phi_{12}\cos 2\phi_{34}) \tag{A.9}$$

We can see that it is composed of the same azimuthal structures as the pure SM case, but with differing weights between the constant and ϕ_{ij}-dependent terms.

B Effects of additional operators

Considering the effects of the other contributions to triple gauge boson couplings $\delta g_{1,Z}$, $\delta\kappa_Z$ and $\delta\kappa_\gamma$, we have the following LO amplitudes:

$$\begin{aligned}\mathcal{M}^{\mathrm{BSM}}(-+\to 00) &= \frac{\sqrt{s}}{m_W}\frac{g_L}{12}\sin\theta[-3\delta\kappa_Z - 4s_W^2(\delta\kappa_\gamma-\delta\kappa_Z)] \\ \mathcal{M}^{\mathrm{BSM}}(+-\to 00) &= \mathcal{M}\frac{s}{m_W^2}\frac{g_L^2}{4}\sin\theta[2s_W^2(\delta\kappa_\gamma-\delta\kappa_Z)],\end{aligned} \tag{B.1}$$

where we have replaced $\delta\kappa_\gamma$ using the relation $\delta\kappa_Z = \delta g_{1,Z} - s_W^2\delta\kappa_\gamma$, which holds for our chosen SMEFT input scheme. Interfering with the SM amplitudes with $\lambda_{12}, \lambda_{34} = \pm\mp$ will give terms as $\cos(\phi_{12} + \phi_{34})$ which cancel after the two foldings. One should notice that also exist the possibility of these operators generating the same transverse amplitudes as the SM: $(\lambda_{12}, \lambda_{34} = \pm\mp)$, however this comes at $\mathcal{O}(s^0)$ and no energy growth relative to the SM cross section is expected. The terms $\lambda_{12}, \lambda_{34} = 00$ are of course independent of the azimuthal decay angles. The total squared amplitude integrated over polar decay angles is

$$\sum |\mathcal{M}|^2 \sim \left(\frac{s}{m_W^2} g_L^2 \sin\theta\right)^2 \left(\frac{512}{324}\right) \left[-\delta g_{1,Z}\left(\frac{9g_L^2 + g_Y^2}{3}\right) + \delta\kappa_Z\left((4s_W + 1)\frac{3g_L^2 + g_Y^2}{12} - 2g_L^2 c_W^2\right)\right]. \tag{B.2}$$

An additional potential source of azimuthal behaviour that could fake this signal is singly-resonant diagrams involving a four-fermion operator. The azimuthal behaviour of the non-resonant fermion pair in this case would not be dictated by the helicity of an on-shell vector boson, and as such is more challenging to calculate analytically. We have numerically explored these processes and found no operator which contributes to the asymmetries studied here.

C Signal and Background Events Tables

In this Appendix we present some illustrative numbers for (N_A, N_B), as defined in Section 4.3, as a function of the Wilson coefficients for linear and quadratic in Table C.1. Moreover, we present the same numbers for various backgrounds in Table C.2. All the numbers are for an integrated Luminosity of 300 $[\text{fb}]^{-1}$.

	Hadronic	Semileptonic
linear	(2.22, -1.95) $10^3 \times \delta\lambda_Z$	(1.28, -1.28) $10^3 \times \delta\lambda_Z$
quadratic	(3.45,3.53) $10^6 \times (\delta\lambda_Z)^2$	(0.68,0.67) $10^6 \times (\delta\lambda_Z)^2$

Table C.1: The number of events $(N_A\,, N_B)$ for linear and quadratic of the cross-section. One could easily obtain the same numbers for different Wilson Coefficient values just rescaling the showed numbers with the aid of Eq. 3.49 in Section 3.6. The numbers of N_B for the linear part can be negative since the interference cross-section has oppostive sign in these two regions. Note that the numbers of events from the quadratic contributions are equal up to statistical errors in Monte Carlo samples, justifying our claim that theoretical errrors have reduced impact on this asymmetry observable.

Hadronic			Semileptonic		
SM	jets	$t\bar{t}$	SM	Z+jets	$t\bar{t}$
(2.95,2.97) 10^3	(4.60,4.49) 10^4	(4.28,4.32) 10^5	(1.26,1.26) 10^3	(2.88,2.88) 10^3	(0.46,0.46) 10^3

Table C.2: Number of events for some of the hadronic and semileptonic backgrounds $(N_A\,, N_B)$, after histogram normalisations and cuts.As expected, both regions A and B have equal numbers of events (within statistical errors of our Monte Carlo sampling) and the same sign, making their expected contribution to the defined asymmetry vanish.

D General MFV expansions of SMEFT operator coefficients

The coefficients of operators with quark flavour indices can be written in the MFV framework as expansions in terms of the spurionic Yukawas. We classify the different forms of the expansions in terms of the charges of the operators under the quark flavour symmetry $U(3)_q \times U(3)_u \times U(3)_d$. All operators of the Warsaw basis containing quarks are classified in this way, in Tab. D.1. The schematic MFV expansions of the Wilson coefficients of each of these classes of operators are given in Tab. D.2.

$U(3)_q$	$U(3)_u$	$U(3)_d$	Operators
$\bar{3}\otimes 3$	1	1	$Q^{(1)}_{Hq}$, $Q^{(3)}_{Hq}$, Q_{qe}, $Q^{(1)}_{lq}$, $Q^{(3)}_{lq}$
1	$\bar{3}\otimes 3$	1	Q_{Hu}, Q_{lu}
1	1	$\bar{3}\otimes 3$	Q_{Hd}, Q_{ld}
$\bar{3}\otimes 3$	$\bar{3}\otimes 3$	1	$Q^{(1)}_{qu}$, $Q^{(8)}_{qu}$
$\bar{3}\otimes 3$	1	$\bar{3}\otimes 3$	$Q^{(1)}_{ud}$, $Q^{(8)}_{ud}$
$\bar{3}\otimes 3$	3	3	$Q^{(1)}_{quqd}$, $Q^{(8)}_{quqd}$
$\bar{3}\otimes 3\otimes\bar{3}\otimes 3$	1	1	$Q^{(1)}_{qq}$, $Q^{(3)}_{qq}$
1	$\bar{3}\otimes 3\otimes\bar{3}\otimes 3$	1	Q_{uu}
1	1	$\bar{3}\otimes 3\otimes\bar{3}\otimes 3$	Q_{dd}
$\bar{3}$	3	1	Q_{uB}, Q_{uW}, Q_{uG}, Q_{uH}, $Q^{(1)}_{lequ}$, $Q^{(3)}_{lequ}$
$\bar{3}$	1	3	Q_{dB}, Q_{dW}, Q_{dG}, Q_{dH}, $Q^{\dagger}_{ledq}$
1	$\bar{3}$	3	Q_{Hud}

Table D.1: Classification of quark-containing operators in terms of their charges under the $U(3)_q \times U(3)_u \times U(3)_d$ flavour symmetry

Charges under $U(3)_q \times U(3)_u \times U(3)_d$	Example operator	Operator coefficient in the MFV expansion
$(\bar{3} \otimes 3, 1, 1)$	$(H^\dagger i \overleftrightarrow{D}_\mu H)(\bar{q}_p \gamma^\mu q_r)$	$C^{(0)}\delta_{pr} + C_1^{(2)}[Y_u Y_u^\dagger]_{pr} + C_2^{(2)}[Y_d Y_d^\dagger]_{pr} + \dots$
$(1, \bar{3} \otimes 3, 1)$	$(H^\dagger i \overleftrightarrow{D}_\mu H)(\bar{u}_p \gamma^\mu u_r)$	$C^{(0)}\delta_{pr} + C^{(2)}[Y_u^\dagger Y_u]_{pr} + \dots$
$(1, 1, \bar{3} \otimes 3)$	$(H^\dagger i \overleftrightarrow{D}_\mu H)(\bar{d}_p \gamma^\mu d_r)$	$C^{(0)}\delta_{pr} + C^{(2)}[Y_d^\dagger Y_d]_{pr} + \dots$
$(\bar{3} \otimes 3, \bar{3} \otimes 3, 1)$	$(\bar{q}_p \gamma^\mu q_r)(\bar{u}_s \gamma^\mu u_t)$	$C^{(0)}\delta_{pr}\delta_{st} + C_1^{(2)}\delta_{pr}[Y_u^\dagger Y_u]_{st}$ $+C_2^{(2)}\delta_{st}[Y_u Y_u^\dagger]_{pr} + C_3^{(2)}\delta_{st}[Y_d Y_d^\dagger]_{pr} + \dots$
$(\bar{3} \otimes 3, 1, \bar{3} \otimes 3)$	$(\bar{q}_p \gamma^\mu q_r)(\bar{d}_s \gamma^\mu d_t)$	$C^{(0)}\delta_{pr}\delta_{st} + C_1^{(2)}\delta_{pr}[Y_d^\dagger Y_d]_{st}$ $+C_2^{(2)}\delta_{st}[Y_u Y_u^\dagger]_{pr} + C_3^{(2)}\delta_{st}[Y_d Y_d^\dagger]_{pr} + \dots$
$(1, \bar{3} \otimes 3, \bar{3} \otimes 3)$	$(\bar{u}_p \gamma^\mu u_r)(\bar{d}_s \gamma^\mu d_t)$	$C^{(0)}\delta_{pr}\delta_{st} + C_1^{(2)}\delta_{st}[Y_u^\dagger Y_u]_{st} + C_2^{(2)}\delta_{pr}[Y_d^\dagger Y_d]_{st} + \dots$
$(\bar{3} \otimes 3 \otimes \bar{3} \otimes 3, 1, 1)$	$(\bar{q}_p \gamma_\mu q_r)(\bar{q}_s \gamma^\mu q_t)$	$C_1^{(0)}\delta_{pr}\delta_{st} + C_2^{(0)}\delta_{pt}\delta_{sr} + C_1^{(2)}\delta_{pr}[Y_u Y_u^\dagger]_{st} + C_2^{(2)}\delta_{st}[Y_u Y_u^\dagger]_{pr}$ $+C_3^{(2)}\delta_{pt}[Y_u Y_u^\dagger]_{sr} + C_4^{(2)}\delta_{sr}[Y_u Y_u^\dagger]_{pt} + C_5^{(2)}\delta_{pr}[Y_d Y_d^\dagger]_{st}$ $+C_6^{(2)}\delta_{st}[Y_d Y_d^\dagger]_{pr} + C_7^{(2)}\delta_{pt}[Y_d Y_d^\dagger]_{sr} + C_8^{(2)}\delta_{sr}[Y_d Y_d^\dagger]_{pt} + \dots$
$(1, \bar{3} \otimes 3 \otimes \bar{3} \otimes 3, 1)$	$(\bar{u}_p \gamma_\mu u_r)(\bar{u}_s \gamma^\mu u_t)$	$C_1^{(0)}\delta_{pr}\delta_{st} + C_2^{(0)}\delta_{pt}\delta_{sr} + C_1^{(2)}\delta_{pr}[Y_u^\dagger Y_u]_{st} + C_2^{(2)}\delta_{st}[Y_u^\dagger Y_u]_{pr} + \dots$
$(1, 1, \bar{3} \otimes 3 \otimes \bar{3} \otimes 3)$	$(\bar{d}_p \gamma_\mu d_r)(\bar{d}_s \gamma^\mu d_t)$	$C_1^{(0)}\delta_{pr}\delta_{st} + C_2^{(0)}\delta_{pt}\delta_{sr} + C_1^{(2)}\delta_{pr}[Y_d^\dagger Y_d]_{st} + C_2^{(2)}\delta_{st}[Y_d^\dagger Y_d]_{pr} + \dots$
$(\bar{3}, 3, 1)$	$(\bar{q}_p \sigma^{\mu\nu} u_r)\widetilde{H}\, B_{\mu\nu}$	$C^{(1)}[Y_u]_{pr} + \dots$
$(\bar{3}, 1, 3)$	$(\bar{q}_p \sigma^{\mu\nu} d_r)\widetilde{H}\, B_{\mu\nu}$	$C^{(1)}[Y_d]_{pr} + \dots$
$(1, \bar{3}, 3)$	$i(\widetilde{H}^\dagger D_\mu H)(\bar{u}_p \gamma^\mu d_r)$	$C^{(2)}[Y_u^\dagger Y_d]_{pr} + \dots$

Table D.2: The MFV expansion of the Wilson coefficients of operators containing quarks. The $C_i^{(n)}$ coefficients represent scalar (i.e. without quark flavour indices) Wilson coefficients, with n the number of Yukawa matrices they multiply. Ellipses represent terms of third order or higher in the Yukawas.

E Yukawa-suppressed Operator Matching

Here we calculate the effects of each Yukawa-suppressed operator which contributes to $d_i \to d_j\gamma$, $d_i \to d_j l^+ l^-$ or down-type meson mixing, as identified in Table 5.3. Some of the Feynman diagrams for these calculations are shown in Figures F.1, F.2, F.3, and F.4. The results of these calculations are the SMEFT contributions to the Wilson coefficients of the effective Hamiltonians defined in Section 5.3.1, at the scale m_W. Since many of these contributions are quark flavour universal, if the quark flavour indices are not made explicit, $C_\alpha \equiv C_\alpha^{bs} = C_\alpha^{bd} = C_\alpha^{sd}$ is meant. In addition to individually-identified references below, these results have also been checked against [138].

E.1 Q_{Hud}

This operator matches to $C_7^{bd_j}$ through diagrams in Figure F.1, as well as to $C_8^{bd_j}$ through diagrams similar to the second and sixth diagram in Figure F.1 (with the photon replaced

by a gluon):

$$C_7^{bd_j} = v^2 y_t^2 C_{Hud} \left(\frac{-5x_t^2 + 31x_t - 20}{24(x_t-1)^2} + \frac{x_t(2-3x_t)}{4(x_t-1)^3} \log x_t \right) \tag{E.1}$$

$$C_8^{bd_j} = v^2 y_t^2 C_{Hud} \left(-\frac{x_t^2 + x_t + 4}{8(x_t-1)^2} + \frac{3x_t}{4(x_t-1)^3} \log x_t \right) \tag{E.2}$$

which is in agreement with Ref. [272].

E.2 Q_{uW}

This operator matches to $C_{1,\text{mix}}$ via box diagrams involving W bosons, as well as to $C_{7,8,9,10}$ through the diagrams shown in Figure F.2 and similar:

$$C_{1,\text{mix}} = \frac{m_t}{m_W} \sqrt{2} v^2 y_t \, C_{uW} \, \frac{9x_t}{4} \left(\frac{x_t+1}{(x_t-1)^2} - \frac{2x_t}{(x_t-1)^3} \log x_t \right), \tag{E.3}$$

$$\begin{aligned} C_7 = \frac{m_t}{m_W} \sqrt{2} v^2 y_t \, C_{uW} \Bigg(& \frac{1}{4} \log \frac{m_W}{\mu} + \frac{11 - 69x_t + 97x_t^2 - 15x_t^3}{48(x_t-1)^3} \\ & + \frac{-8 + 32x_t - 27x_t^2 - 12x_t^3 + 3x_t^4}{24(x_t-1)^4} \log x_t \Bigg), \end{aligned} \tag{E.4}$$

$$C_8 = \frac{m_t}{m_W} \sqrt{2} v^2 y_t \, C_{uW} \left(\frac{1 - 9x_t + 2x_t^2}{4(x_t-1)^3} + \frac{-1 + 4x_t}{2(x_t-1)^4} \log x_t \right), \tag{E.5}$$

$$C_9 = \frac{m_t}{m_W} \sqrt{2} v^2 y_t \, C_{uW} \left(\frac{1 - 4\sin^2\theta}{\sin^2\theta} Y_{uW}(x_t) + X_{uW}(x_t) \right), \tag{E.6}$$

$$C_{10} = -\frac{m_t}{m_W} \sqrt{2} v^2 y_t \, C_{uW} \frac{Y_{uW}(x_t)}{\sin^2\theta} \tag{E.7}$$

where

$$Y_{uW}(x_t) = \frac{3x_t}{4(x_t-1)} - \frac{3x_t}{4(x_t-1)^2} \log x_t \tag{E.8}$$

$$X_{uW}(x_t) = \frac{-50 + 133x_t - 80x_t^2 + 9x_t^3}{36(x_t-1)^3} + \frac{2 - x_t - 9x_t^2 + 6x_t^3}{6(x_t-1)^4} \log x_t \tag{E.9}$$

Our meson mixing result agrees with that of Ref. [273], while the other results are all in agreement with Ref. [272].

E.3 Q_{uB}

This operator matches to $C_{7,9}$ through the third and fourth diagrams in Figure F.2:

$$C_7 = -\frac{\cos\theta}{\sin\theta}\frac{m_t}{m_W}\sqrt{2}v^2 y_t\, C_{uB}\left(\frac{1}{4}\log\frac{m_W}{\mu} + \frac{3-2x_t+3x_t^2}{16(x_t-1)^2} - \frac{x_t^2(x_t-3)}{8(x_t-1)^3}\log x_t\right), \quad \text{(E.10)}$$

$$C_9 = \frac{\cos\theta}{\sin\theta}\frac{m_t}{m_W}\sqrt{2}v^2 y_t\, C_{uB}\left(\frac{x_t^2+3x_t-2}{4(x_t-1)^2} - \frac{3x_t-2}{2(x_t-1)^3}\log x_t\right), \quad \text{(E.11)}$$

in agreement with Ref. [272].

E.4 Q_{uG}

$$C_8 = -\frac{m_t}{m_W}\sqrt{2}v^2 y_t\, C_{uG}\left(\frac{1}{4}\log\frac{m_W}{\mu} + \frac{3-2x_t+3x_t^2}{16(x_t-1)^2} - \frac{x_t^2(x_t-3)}{8(x_t-1)^3}\log x_t\right) \quad \text{(E.12)}$$

This is in agreement with Ref. [272].

E.5 Q_{dW}

This operator matches to C_7, through the diagrams in Figure F.3, as well as to C_8 through a diagram similar to the second one of Figure F.3 (with the photon replaced by a gluon):

$$C_7 = \frac{m_t}{m_W}\sqrt{2}v^2 y_t\, C_{dW}\left(-\log\frac{m_W}{\mu} + \frac{6x_t^3-31x_t^2+19x_t}{12(x_t-1)^2} + \frac{-3x_t^4+16x_t^3-12x_t^2+2x_t}{6(x_t-1)^3}\log x_t\right) \quad \text{(E.13)}$$

$$C_8 = \frac{m_t}{m_W}\sqrt{2}v^2 y_t\, C_{dW}\left(\frac{5+x_t}{4(x_t-1)^2} + \frac{2x_t^2-6x_t+1}{2(x_t-1)^3}\log x_t\right) \quad \text{(E.14)}$$

which all agrees with Ref. [205].

E.6 $Q^{(1,8)}_{quqd}$

These operators produce effects in C_7 and C_8 through the diagram in Figure F.4 (and similar with the photon replaced by a gluon):

$$C_7 = -\frac{1}{3}m_t^2\log\frac{m_t^2}{\mu^2}\left(C^{(1)}_{quqd} + \frac{5}{3}C^{(1)\prime}_{quqd} + \frac{4}{3}C^{(8)}_{quqd} + \frac{4}{9}C^{(8)\prime}_{quqd}\right), \quad \text{(E.15)}$$

$$C_8 = -\frac{1}{2}m_t^2\log\frac{m_t^2}{\mu^2}\left(C^{(1)}_{quqd} + \frac{1}{6}C^{(1)\prime}_{quqd} - \frac{1}{6}C^{(8)}_{quqd} + \frac{17}{18}C^{(8)\prime}_{quqd}\right), \quad \text{(E.16)}$$

in agreement with Ref. [272] (taking into account our different flavour assumptions).

F Matching to neutrino-containing operators

Here we present the matching of all operators to the coefficients $C_L^{d_i d_j}$ of the effective Hamiltonian in Eqn. 5.5. Since all contributions are quark flavour universal, we define $C_L \equiv C_L^{bs} = C_L^{bd} = C_L^{sd}$. We do not show the Feynman diagrams, but they are always simply related to diagrams which match to the C_{10} operator (by exchanging charged leptons for neutrinos and vice versa), so can be inferred from diagrams in Ref. [71] and in Figure F.2.

We provide results for both the $\{m_W, m_Z, G_F\}$ and $\{\alpha_{em}, m_Z, G_F\}$ input parameter schemes. The full result for either input scheme is the sum of an input scheme independent piece, $C_L^{S.I.}$, and an input scheme dependent piece. For a fuller explanation of the different schemes, please see Ref. [71] Section 3 (and references therein). The input scheme independent piece is

$$\begin{aligned} C_L^{S.I.} &= v^2 \left(-C_{Hl}^{(1)} - C_{Hq}^{(1)} + C_{Hu} - C_{lq}^{(1)} + C_{lu} - \frac{1}{2} C_{HD} \right) I(x_t) + v^2 C_{lq}^{(3)} I^{lq}(x_t) \\ &+ v^2 C_{Hl}^{(3)} I_{\nu,S.I.}^{Hl3}(x_t) - v^2 C_{Hq}^{(3)} I_\nu^{Hq3}(x_t) - \sqrt{2} y_t \frac{m_t}{m_W} v^2 C_{uW} I_\nu^{uW} \\ &+ v^2 C_{qq}^{(3)} I_\nu^{qq}(x_t) + v^2 \left(C_{qq}^{(3)\prime} - C_{qq}^{(1)\prime} \right) I_\nu^{qq\prime}(x_t), \end{aligned} \tag{F.1}$$

where

$$I(x_t) = \frac{x_t}{16} \left[-\log \frac{m_W^2}{\mu^2} + \frac{x_t - 7}{2(1-x_t)} - \frac{x_t^2 - 2x_t + 4}{(1-x_t)^2} \log x_t \right], \tag{F.2}$$

$$I^{lq}(x_t) = \frac{x_t}{16} \left[-\log \frac{m_W^2}{\mu^2} + \frac{1 - 7x_t}{2(1-x_t)} - \frac{x_t^2 - 2x_t + 4}{(1-x_t)^2} \log x_t \right], \tag{F.3}$$

$$I_{\nu,S.I.}^{Hl3}(x_t) = \frac{x_t}{16} \left[\log \frac{m_W^2}{\mu^2} + \frac{7x_t + 23}{2(1-x_t)} + \frac{x_t^2 - 14x_t + 28}{(1-x_t)^2} \log x_t \right] \tag{F.4}$$

$$I_\nu^{Hq3}(x_t) = \frac{x_t}{16} \left[7 \log \frac{m_W^2}{\mu^2} + \frac{x_t - 31}{2(1-x_t)} + \frac{7x_t^2 - 2x_t - 20}{(1-x_t)^2} \log x_t \right], \tag{F.5}$$

$$I_\nu^{uW}(x_t) = \frac{3}{4} \left[\frac{2 - 3x_t + x_t^2}{(1-x_t)^2} + \frac{x_t}{(1-x_t)^2} \log x_t \right], \tag{F.6}$$

$$I_\nu^{qq}(x_t) = \frac{x_t}{2} \left[1 + \log \frac{m_t^2}{\mu^2} \right], \tag{F.7}$$

$$I_\nu^{qq\prime}(x_t) = -\frac{N_c}{4} x_t \log \frac{m_t^2}{\mu^2}. \tag{F.8}$$

The above must be added to an input scheme dependent piece. This piece in the

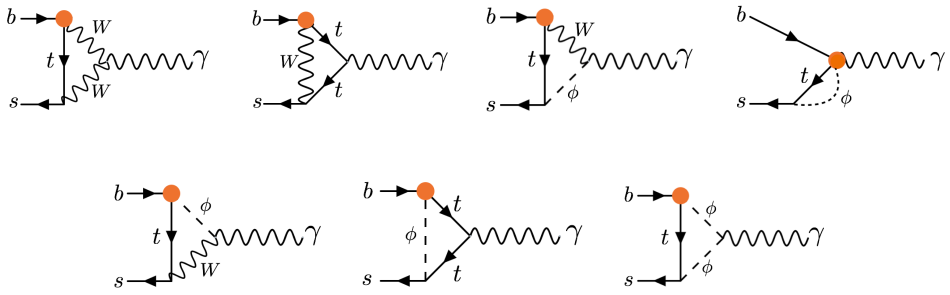

Figure F.1: Diagrams generating contributions to $b \to s\gamma$ from the Q_{Hud} operator

$\{\alpha_{em}, m_Z, G_F\}$ scheme is:

$$C_L^{\{\alpha_{em},m_Z,G_F\}} = v^2\left(C_{Hl}^{(3)} - \frac{1}{2}C'_{ll}\right)\left[\frac{x_t(x_t^2+x_t-5)}{2(1-x_t)^2} - \frac{3x_t(x_t^2-3x_t+4)}{(1-x_t)^3}\log x_t\right] - v^2\frac{g_2^2}{(g_1^2-g_2^2)}\left(\frac{1}{4}C_{HD} + \frac{g_1}{g_2}C_{HWB}\right)\left[\frac{3x_t}{2(x_t-1)^2} + \frac{3x_t^2(x_t-3)}{4(x_t-1)^3}\log x_t\right] \tag{F.9}$$

Instead the scheme dependent piece in the $\{m_W, m_Z, G_F\}$ scheme is:

$$C_L^{\{m_W,m_Z,G_F\}} = 4v^2\left(C_{Hl}^{(3)} - \frac{1}{2}C'_{ll}\right)\left(C_0(x_t) - 4B_0(x_t)\right), \tag{F.10}$$

where

$$B_0(x_t) = \frac{1}{4}\left[\frac{x_t}{1-x_t} + \frac{x_t}{(x_t-1)^2}\log x_t\right], \tag{F.11}$$

$$C_0(x_t) = \frac{x_t}{8}\left[\frac{x_t-6}{x_t-1} + \frac{3x_t+2}{(x_t-1)^2}\log x_t\right], \tag{F.12}$$

are the usual Inami Lim [18] functions.

G Numerical matching results

In this appendix we present the results of our matching calculations in numerical form, as tables of the $N_{\alpha k}^{(1,2)}$ coefficients of Eqn. (5.7). The index α labels the WET coefficients in the columns of the tables, while the index k labels the SMEFT coefficients in the rows. The coefficients $N_{\alpha k}^{(1)}$, which are independent of the choice of input scheme, are given in Table G.1, while the coefficients $N_{\alpha k}^{(2)}$ are given in Table G.2 for the $\{\alpha_{em}, m_Z, G_F\}$ input scheme, and in Table G.3 for the $\{m_W, m_Z, G_F\}$ input scheme.

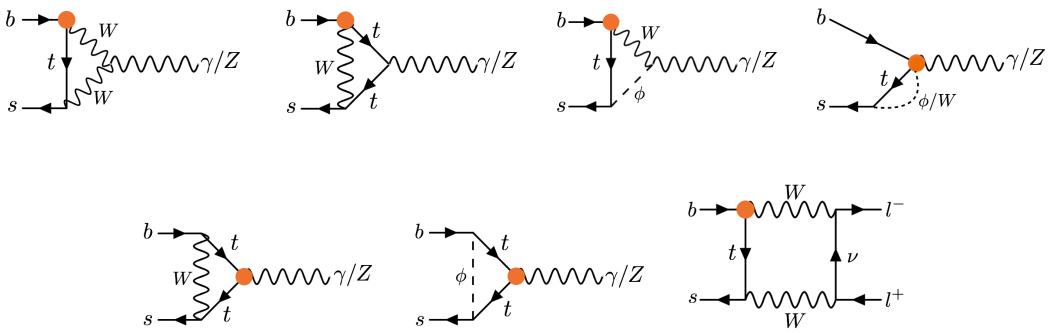

Figure F.2: Diagrams generating contributions to $b \to s l^+ l^-$ and/or $b \to s\gamma$ from the Q_{uW} and Q_{uB} (3rd and 4th diagrams only) operators. Diagrams in which the operator attaches to the b quark leg imply also the existence (and inclusion in our calculations) of similar diagrams with the operator attached to the s quark leg

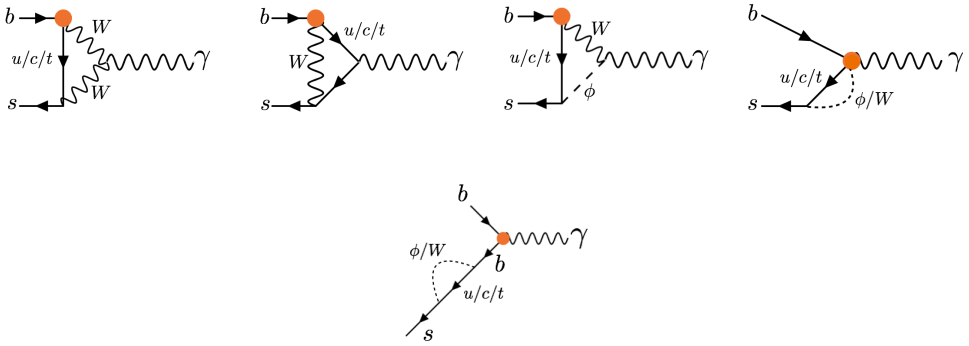

Figure F.3: Diagrams generating contributions to $b \to s\gamma$ from the Q_{dW} operator

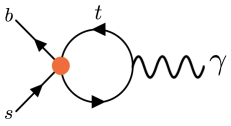

Figure F.4: Diagram generating contributions to $b \to s\gamma$ from the operators $Q^{(1)}_{quqd}$ and $Q^{(8)}_{quqd}$

$N^{(1)}_{\alpha k}$	C_7	C_8	C_9	C_{10}	C_L
C_W	-	-	-	-	-
C_{HD}	-	-	$-1.23\cdot10^{-2}$	$8.15\cdot10^{-2}$	$1.73\cdot10^{-2}$
C_{HWB}	-	-	-	-	-
C_{uG}	-	$-4.55\cdot10^{-2}$	-	-	-
C_{uW}	$4.58\cdot10^{-2}$	-	-	-	-
C_{uB}	$-8.76\cdot10^{-2}$	-	-	-	-
C_{dW}	-0.182^*	-	-	-	-
$C^{(1)}_{Hl}$	-	-	0.163	-0.163	$3.46\cdot10^{-2}$
$C^{(3)}_{Hl}$	-	-	-0.163	0.163	$3.46\cdot10^{-2}$
C_{He}	-	-	0.163	0.163	-
$C^{(1)}_{Hq}$	-	-	$2.47\cdot10^{-2}$	0.163	$3.46\cdot10^{-2}$
$C^{(3)}_{Hq}$	-	-	0.173	-1.14	-0.242
C_{Hu}	-	-	$-2.47\cdot10^{-2}$	-0.163	$-3.46\cdot10^{-2}$
C_{Hud}	-	-	-	-	-
C'_{ll}	-	-	-	-	-
$C^{(1)\prime}_{qq}$	-	-	-0.458	1.96	-0.415
$C^{(3)\prime}_{qq}$	-	-	0.458	-1.96	0.415
$C^{(3)}_{qq}$	-	-	0.305	1.30	-0.277
$C^{(1)}_{lq}$	-	-	0.163	-0.163	$3.46\cdot10^{-2}$
$C^{(3)}_{lq}$	-	-	0.163	0.163	$-3.46\cdot10^{-2}$
C_{lu}	-	-	-0.163	0.163	$-3.46\cdot10^{-2}$
C_{qe}	-	-	0.163	0.163	-
$C^{(1)}_{quqd}$	$-1.99\cdot10^{-2*}$	$-2.99\cdot10^{-2*}$	-	-	-
$C^{(8)}_{quqd}$	$-2.66\cdot10^{-2*}$	$4.98\cdot10^{-3*}$	-	-	-
$C^{(1)\prime}_{quqd}$	$-3.32\cdot10^{-2*}$	$-4.98\cdot10^{-3*}$	-	-	-
$C^{(8)\prime}_{quqd}$	$-8.86\cdot10^{-3*}$	$-2.82\cdot10^{-2*}$	-	-	-

Table G.1: Numerical values of the coefficients $N^{(1)}_{\alpha k}$ of the matching equation Eqn. (5.7). Note that the matching to $C_{1,\mathrm{mix}}$, C_1 and C_2 does not have any divergent diagrams so the corresponding $N^{(1)}_{\alpha k}$ coefficients are all zero (and are not listed here). All results are quark-flavour universal ($C_\alpha \equiv C^{bs}_\alpha = C^{bd}_\alpha = C^{sd}_\alpha$), *except* for results indicated by an asterisk (*), for which only $C^{bd_j}_\alpha$ is meant ($d_j = s, d$).

$N^{(2)}_{\alpha k}$	C_1	C_2	C_7	C_8	C_9	C_{10}	C_L	$C_{1,\mathrm{mix}}$
C_W	-	-	$-2.03\cdot10^{-2}$	-	$-6.12\cdot10^{-2}$	-	-	-
C_{HD}	-	-	$1.38\cdot10^{-2}$	-	0.400	$6.25\cdot10^{-2}$	$1.33\cdot10^{-2}$	-
C_{HWB}	-	-	$-2.05\cdot10^{-2}$	-	0.483	-	-	-
C_{uG}	-	-	-	$-2.56\cdot10^{-2}$	-	-	-	-
C_{uW}	-	-	$5.53\cdot10^{-3}$	$1.64\cdot10^{-2}$	0.152	-0.473	0.172	0.246
C_{uB}	-	-	$-4.94\cdot10^{-2}$	-	0.156	-	-	-
C_{dW}	-	-	$-8.10\cdot10^{-3*}$	$6.06\cdot10^{-2*}$	-	-	-	-
$C^{(1)}_{Hl}$	-	-	-	-	0.125	0.125	$2.65\cdot10^{-2}$	-
$C^{(3)}_{Hl}$	-	-	$3.52\cdot10^{-2}$	$1.17\cdot10^{-2}$	$-1.52\cdot10^{-2}$	0.710	-0.218	-1.22
C_{He}	-	-	-	-	0.125	0.125	-	-
$C^{(1)}_{Hq}$	-	-	-	-	$1.89\cdot10^{-2}$	0.125	$2.65\cdot10^{-2}$	-
$C^{(3)}_{Hq}$	-	-	$-2.35\cdot10^{-2}$	$-1.17\cdot10^{-2}$	0.449	-1.98	-0.305.	0.608
C_{Hu}	-	-	-	-	$-1.89\cdot10^{-2}$	-0.125	$-2.65\cdot10^{-2}$	-
C_{Hud}	-	-	$-2.34\cdot10^{-2*}$	$-1.04\cdot10^{-2*}$	-	-	-	-
C'_{ll}	-	-	$-1.76\cdot10^{-2}$	$-5.86\cdot10^{-3}$	0.475	-0.585	-0.191	0.608
$C^{(1)\prime}_{qq}$	$-6.06\cdot10^{-2}$	-	-	-	-0.347	1.48	0.315	-0.277
$C^{(3)\prime}_{qq}$	$6.06\cdot10^{-2}$	-	-	-	0.347	1.48	-0.315	0.277
$C^{(3)}_{qq}$	-	-0.121	-	-	-0.384	1.64	0.348	-0.554
$C^{(1)}_{lq}$	-	-	-	-	0.125	-0.125	$2.65\cdot10^{-2}$	-
$C^{(3)}_{lq}$	-	-	-	-	-0.201	-0.201	$4.26\cdot10^{-2}$	-
C_{lu}	-	-	-	-	-0.125	0.125	$-2.65\cdot10^{-2}$	-
C_{qe}	-	-	-	-	0.125	0.125	-	-
C_{eu}	-	-	-	-	-0.125	-0.125	-	-
$C^{(1)}_{quqd}$	-	-	$-1.51\cdot10^{-2*}$	$-2.27\cdot10^{-2*}$	-	-	-	-
$C^{(8)}_{quqd}$	-	-	$-2.02\cdot10^{-2*}$	$3.78\cdot10^{-3*}$	-	-	-	-
$C^{(1)\prime}_{quqd}$	-	-	$-2.52\cdot10^{-2*}$	$-3.78\cdot10^{-3*}$	-	-	-	-
$C^{(8)\prime}_{quqd}$	-	-	$-6.72\cdot10^{-3*}$	$-2.14\cdot10^{-2*}$	-	-	-	-

Table G.2: Numerical values of the coefficients $N^{(2)}_{\alpha k}$ of the matching equation Eqn. (5.7), in the $\{m_W, m_Z, G_F\}$ input scheme. All results are quark-flavour universal ($C_\alpha \equiv C^{bs}_\alpha = C^{bd}_\alpha = C^{sd}_\alpha$), *except* for results indicated by an asterisk (*), for which only $C^{bd_j}_\alpha$ is meant ($d_j = s, d$).

$N^{(2)}_{\alpha k}$	C_1	C_2	C_7	C_8	C_9	C_{10}	C_L	$C_{1,\mathrm{mix}}$
C_W	-	-	$-1.80\cdot10^{-2}$	-	$-5.43\cdot10^{-2}$	-	-	-
C_{HD}	-	-	$8.42\cdot10^{-3}$	$6.06\cdot10^{-3}$	-0.185	0.112	$4.45\cdot10^{-2}$	-
C_{HWB}	-	-	$-1.10\cdot10^{-2}$	$1.42\cdot10^{-2}$	-0.451	0.116	$7.31\cdot10^{-2}$	-
C_{uG}	-	-	-	$-2.56\cdot10^{-2}$	-	-	-	-
C_{uW}	-	-	$5.53\cdot10^{-3}$	$1.64\cdot10^{-2}$	$5.17\cdot10^{-2}$	-0.473	0.173	0.246
C_{uB}	-	-	$-4.94\cdot10^{-2}$	-	0.156	-	-	-
C_{dW}	-	-	$-8.10\cdot10^{-3*}$	$6.06\cdot10^{-2*}$	-	-	-	-
$C^{(1)}_{Hl}$	-	-	-	-	0.125	0.125	$2.65\cdot10^{-2}$	-
$C^{(3)}_{Hl}$	-	-	-0.179	$-4.24\cdot10^{-3}$	0.174	1.52	0.368	-1.22
C_{He}	-	-	-	-	0.125	0.125	-	-
$C^{(1)}_{Hq}$	-	-	-	-	$1.89\cdot10^{-2}$	0.125	$2.65\cdot10^{-2}$	-
$C^{(3)}_{Hq}$	-	-	$2.35\cdot10^{-2}$	$-1.17\cdot10^{-2}$	0.449	-1.98	-0.305	0.608
C_{Hu}	-	-	-	-	$-1.89\cdot10^{-2}$	-0.125	$-2.65\cdot10^{-2}$	-
C_{Hud}	-	-	$-2.34\cdot10^{-2*}$	$-1.04\cdot10^{-2*}$	-	-	-	-
C'_{ll}	-	-	$8.96\cdot10^{-2}$	$2.12\cdot10^{-3}$	0.381	-0.989	-0.266	0.608
$C^{(1)\prime}_{qq}$	$-6.06\cdot10^{-2}$	-	-	-	-0.347	1.48	0.315	-0.277
$C^{(3)\prime}_{qq}$	$-6.06\cdot10^{-2}$	-	-	-	0.347	-1.48	-0.315	0.277
$C^{(3)}_{qq}$	-	-0.121	-	-	-0.384	1.64	0.348	-0.554
$C^{(1)}_{lq}$	-	-	-	-	0.125	-0.125	$2.65\cdot10^{-2}$	-
$C^{(3)}_{lq}$	-	-	-	-	-0.201	-0.201	$4.26\cdot10^{-2}$	-
C_{lu}	-	-	-	-	-0.125	0.125	$-2.65\cdot10^{-2}$	-
C_{qe}	-	-	-	-	0.125	0.125	-	-
C_{eu}	-	-	-	-	-0.125	-0.125	-	-
$C^{(1)}_{quqd}$	-	-	$-1.51\cdot10^{-2*}$	$-2.27\cdot10^{-2*}$	-	-	-	-
$C^{(8)}_{quqd}$	-	-	$-2.02\cdot10^{-2*}$	$3.78\cdot10^{-3*}$	-	-	-	-
$C^{(1)\prime}_{quqd}$	-	-	$-2.52\cdot10^{-2*}$	$-3.78\cdot10^{-3*}$	-	-	-	-
$C^{(8)\prime}_{quqd}$	-	-	$-6.72\cdot10^{-3*}$	$-2.14\cdot10^{-2*}$	-	-	-	-

Table G.3: Numerical values of the coefficients $N^{(2)}_{\alpha k}$ of the matching equation Eqn. (5.7), in the $\{\alpha_{em}, m_Z, G_F\}$ input scheme. All results are quark-flavour universal ($C_\alpha \equiv C^{bs}_\alpha = C^{bd}_\alpha = C^{sd}_\alpha$), *except* for results indicated by an asterisk (*), for which only $C^{bd_j}_\alpha$ is meant ($d_j = s, d$).

H High energy limit of SMEFT Amplitudes

For $\mathbf{p}^\mu = (E, Ps_\theta c_\phi, Ps_\theta s_\phi, Pc_\theta)$ we have $E^2 - P^2 = m^2$ and the explicit solution for the spinors is given by,

$$\boldsymbol{\chi}^I_\alpha = \begin{pmatrix} \sqrt{E-P}\, c & -\sqrt{E+P}\, s^* \\ \sqrt{E-P}\, s & \sqrt{E+P}\, c \end{pmatrix}, \qquad \tilde{\boldsymbol{\chi}}^J_{\dot\beta} = \begin{pmatrix} \sqrt{E-P}\, c & -\sqrt{E+P}\, s \\ \sqrt{E-P}\, s^* & \sqrt{E+P}\, c \end{pmatrix},$$

which can be written as

$$\begin{aligned} \boldsymbol{\chi}^I_\alpha &= \sqrt{E-P}\zeta^+_\alpha(\theta) \otimes \zeta^{-\,I} - \sqrt{E+P}\zeta^-_\alpha(\theta) \otimes \zeta^{+\,I}, \\ \tilde{\boldsymbol{\chi}}^J_{\dot\beta} &= \sqrt{E+P}\tilde{\zeta}^-_{\dot\beta}(\theta) \otimes \zeta^{+\,J} + \sqrt{E-P}\tilde{\zeta}^+_{\dot\beta}(\theta) \otimes \zeta^{-\,J}, \end{aligned} \tag{H.1}$$

making clear that the two indices belong to two different spaces. The high energy limit can be obtain taking $m/E \ll 1$, leading to the following

$$\sqrt{E+P} \approx \sqrt{2E}\left(\frac{m}{2E}\right) \qquad \sqrt{E-P} \approx \sqrt{2E}\left(1 - \frac{m^2}{8E^2}\right). \tag{H.2}$$

It is useful to define

$$\begin{aligned} \lambda &= \sqrt{E+P}\,\zeta^-(\theta), \quad \tilde\lambda = \sqrt{E+P}\,\tilde\zeta^+(\theta), \\ \eta &= \sqrt{E-P}\,\zeta^+(\theta), \quad \tilde\eta = \sqrt{E-P}\,\tilde\zeta^-(\theta), \end{aligned} \tag{H.3}$$

from which follows immediately that η and $\tilde\eta$ are suppressed by a mass term while λ and $\tilde\lambda$ are the massless spinors. With these, we can write the massive spinors as:

$$\boldsymbol{\chi}^J_\alpha = -\lambda_\alpha \zeta^J_+ + \eta_\alpha \zeta^J_-, \qquad \tilde{\boldsymbol{\chi}}^J_{\dot\beta} = \tilde\lambda_{\dot\beta}\zeta^J_- + \tilde\eta_{\dot\beta}\tilde\zeta^J_+ \,. \tag{H.4}$$

where, $\langle\lambda\eta\rangle = -[\tilde\lambda\tilde\eta] = m$, leading to the following assignments

$$\boldsymbol{\chi}^1_\alpha = \eta_\alpha, \quad \boldsymbol{\chi}^2_\alpha = \lambda_\alpha, \quad \tilde{\boldsymbol{\chi}}^1_{\dot\beta} = \tilde\lambda_{\dot\beta}, \quad \text{and} \quad \tilde{\boldsymbol{\chi}}^2_{\dot\beta} = -\tilde\eta_{\dot\beta} \tag{H.5}$$

With those, we have the $\langle \mathbf{2}^I \mathbf{3}^J \rangle$ and $[\mathbf{2}^I \mathbf{3}^J]$ as

$$\begin{aligned} &\langle \mathbf{2}^1\mathbf{3}^1\rangle = \langle \eta_2 \eta_3\rangle, \quad \langle \mathbf{2}^1\mathbf{3}^2\rangle = \langle \eta_2 3\rangle, \quad \langle \mathbf{2}^2\mathbf{3}^1\rangle = \langle 2\eta_3\rangle, \quad \langle \mathbf{2}^2\mathbf{3}^2\rangle = \langle 23\rangle, \\ &[\mathbf{2}^1\mathbf{3}^1] = [23], \quad [\mathbf{2}^1\mathbf{3}^2] = -[2\eta_3], \quad [\mathbf{2}^2\mathbf{3}^1] = -[\eta_2 3], \quad [\mathbf{2}^2\mathbf{3}^2] = [\eta_2\eta_3], \end{aligned} \tag{H.6}$$

which enable us to write the massive spinors in the HE limit as

$$\boldsymbol{\chi}^I_\alpha \approx \sqrt{2E}\begin{pmatrix} \frac{m}{2E}\, c & \left(-1 + \frac{m^2}{8E^2}\right) s^* \\ \frac{m}{2E}\, s & \left(1 - \frac{m^2}{8E^2}\right) c \end{pmatrix}, \qquad \tilde{\boldsymbol{\chi}}^J_{\dot\beta} = \sqrt{2E}\begin{pmatrix} \frac{m}{2E}\, c & \left(-1 + \frac{m^2}{8E^2}\right) s \\ \frac{m}{2E}\, s^* & \left(1 - \frac{m^2}{8E^2}\right) c \end{pmatrix}.$$

Writing the Lorentz invariants as matrices in the $SU(2)$ Little-Group space, at order $\mathcal{O}(m^2)$ we have that:

$$\langle\mathbf{12}\rangle^{\rm IJ} \approx \begin{pmatrix} \left(1-\frac{m_1^2}{8E_1^2}-\frac{m_2^2}{8E_2^2}\right)\langle 12\rangle & -\frac{m_2}{\sqrt{2E_2}}\langle 1\eta_2\rangle \\ -\frac{m_1}{\sqrt{2E_1}}\langle \eta_1 2\rangle & \frac{m_1 m_2}{4E_1E_2}[12] \end{pmatrix}, \qquad [\mathbf{12}]^{\rm IJ} \approx \begin{pmatrix} \frac{m_1 m_2}{4E_1E_2}\langle 12\rangle & -\frac{m_1}{\sqrt{2E_1}}[\eta_1 2] \\ -\frac{m_2}{\sqrt{2E_2}}[1\eta_2] & \left(1-\frac{m_1^2}{8E_1^2}-\frac{m_2^2}{8E_2^2}\right)[12] \end{pmatrix}.$$

For the $W\bar{W}\gamma$ case is important to recall the HE limits of the x and x^{-1} factors, which are given by

$$x = \frac{\langle\zeta|p_2|3]}{\langle\zeta 3\rangle} \to \frac{[13][23]}{[12]}, \quad x^{-1} = \frac{\langle 3|p_2|\zeta]}{[\zeta 3]} \to -\frac{\langle 13\rangle\langle 23\rangle}{\langle 12\rangle}. \tag{H.7}$$

Once we have the HE limit of the building blocks, it is straightforward to obtain the HE for the massive 3-point amplitudes of Sec. 7.4. As an example, we show in Tables H.1 and H.2 the HE of the amplitude $\mathcal{M}(\mathbf{1}_h\mathbf{2}_V^{I_{1,2}}\mathbf{3}_V^{I_{1,2}})$ and $\mathcal{M}(\mathbf{1}_W\mathbf{2}_{\bar{W}}3_\gamma^-)$ at leading order in the (m/E) expansion.

$\mathcal{M}(\mathbf{1}_h\mathbf{2}_V\mathbf{3}_V)$	$\langle\mathbf{23}\rangle[\mathbf{23}]$	$\langle\mathbf{23}\rangle^2$	$[\mathbf{23}]^2$
$(1_h,2_V^+,3_V^+)$	-	-	$[23]^2$
$(1_h,2_V^-,3_V^-)$	-	$\langle 23\rangle^2$	-
$(1_h,2_V^+,3_V^-)$	$-[21]^2[31]^{-2}$	$[21]^2[31]^{-2}$	$[21]^2[31]^{-2}$
$(1_h,2_V^-,3_V^+)$	$-[31]^2[21]^{-2}$	$[31]^2[21]^{-2}$	$[31]^2[21]^{-2}$
$(1_h,2_V^+,3_V^0)$	$[12][23][31]^{-1}$	-	$[12][23][31]^{-1}$
$(1_h,2_V^-,3_V^0)$	$\langle 12\rangle\langle 23\rangle\langle 31\rangle^{-1}$	$\langle 12\rangle\langle 23\rangle\langle 31\rangle^{-1}$	-
$(1_h,2_V^0,3_V^+)$	$[23][31][12]^{-1}$	-	$[23][31][12]^{-1}$
$(1_h,2_V^0,3_V^-)$	$\langle 23\rangle\langle 31\rangle\langle 12\rangle^{-1}$	$\langle 23\rangle\langle 31\rangle\langle 12\rangle^{-1}$	-
$(1_h,2_V^0,3_V^0)$	-	-	-

Table H.1: High-Energy limit of the three independent structures of the $\mathcal{M}(\mathbf{1}_h\mathbf{2}_V\mathbf{3}_V)$ amplitude. Entries denoted by '-' appears only at order $\mathcal{O}(m^3/E^3)$. The SMEFT coefficients were omitted for convenience, see Eq. (7.17) for the full massive amplitude.

I Useful identities

In the following we are going to list useful identities for the manipulation of the massive amplitudes. For σ_μ and $\bar{\sigma}_\mu$ we can write that

$$\sigma^\mu_{\alpha\dot{\alpha}} = \epsilon_{\alpha\beta}\epsilon_{\dot{\alpha}\dot{\beta}}\bar{\sigma}_\mu^{\beta\dot{\beta}}, \qquad \bar{\sigma}_\mu^{\alpha\dot{\alpha}} = \epsilon^{\alpha\beta}\epsilon^{\dot{\alpha}\dot{\beta}}\sigma^\mu_{\beta\dot{\beta}}. \tag{I.1}$$

$\mathcal{M}(\mathbf{1}_W\mathbf{2}_{\bar{W}}3^-_\gamma)$	$x^{-1}[\mathbf{12}]^2$	$[\mathbf{12}]\langle\mathbf{23}\rangle\langle\mathbf{31}\rangle$	$\langle\mathbf{12}\rangle\langle\mathbf{23}\rangle\langle\mathbf{31}\rangle$
$(1^+_W,2^+_{\bar{W}},3^-_\gamma)$	$\frac{[21]^3}{[31][32]}$	$\frac{[21]^3}{[31][32]}$	-
$(1^-_W,2^-_{\bar{W}},3^-_\gamma)$	-	-	$\langle12\rangle\langle23\rangle\langle31\rangle$
$(1^+_W,2^-_{\bar{W}},3^-_\gamma)$	$-\frac{\langle23\rangle^3}{\langle12\rangle\langle13\rangle}$	$-\frac{\langle23\rangle^3}{\langle12\rangle\langle13\rangle}$	-
$(1^-_W,2^+_{\bar{W}},3^-_\gamma)$	$-\frac{\langle13\rangle^3}{\langle12\rangle\langle23\rangle}$	$-\frac{\langle23\rangle^3}{\langle12\rangle\langle13\rangle}$	-
$(1^+_W,2^0_{\bar{W}},3^-_\gamma)$	-	-	-
$(1^-_W,2^0_{\bar{W}},3^-_\gamma)$	-	-	-
$(1^0_W,2^0_{\bar{W}},3^-_\gamma)$	$\frac{\langle13\rangle\langle23\rangle}{\langle12\rangle}$	-	-

Table H.2: High-Energy limit of the three independent structures of the $\mathcal{M}(\mathbf{1}_W\mathbf{2}_{\bar{W}}3^-_\gamma)$ amplitude. Entries denoted by '-' appears only at order $\mathcal{O}(m^3/E^3)$. The SMEFT coefficients were omitted for convenience, see Eq. (7.23) for the full massive amplitude.

Therefore, the Fierz identities for σ matrices can be written as

$$
\begin{aligned}
&[\sigma^\mu]_{\alpha\dot\alpha}[\sigma^\nu]_{\alpha\dot\alpha} = 2\epsilon_{\alpha\beta}\epsilon_{\dot\alpha\dot\beta}\,,\\
&[\sigma^\mu]_{\alpha\dot\alpha}[\sigma^\nu]_{\alpha\dot\alpha} = \frac{1}{2}([\sigma^\mu]_{\alpha\dot\beta}[\sigma^\nu]_{\beta\dot\alpha} + [\sigma^\nu]_{\alpha\dot\beta}[\sigma^\mu]_{\beta\dot\alpha}2\eta^{\mu\nu}\epsilon_{\alpha\beta}\epsilon_{\dot\alpha\dot\beta} + i\epsilon^{\mu\nu\rho\sigma}[\sigma^\rho]_{\alpha\dot\beta}[\sigma^\sigma]_{\beta\dot\alpha})\,.
\end{aligned}
$$

With these identities, one can write the Fierz identities for the spinors (omitting the $SU(2)$ indices):

$$
\begin{aligned}
\langle\mathbf{1}|\sigma_\mu|\mathbf{2}]\,\langle\mathbf{3}|\sigma^\mu|\mathbf{4}] &= -2\langle\mathbf{13}\rangle[\mathbf{24}]\,,\\
\langle\mathbf{1}|q\sigma|\mathbf{2}]\,\langle\mathbf{3}|q\sigma|\mathbf{4}] &= \langle\mathbf{1}|q\sigma|\mathbf{4}]\,\langle\mathbf{3}|q\sigma|\mathbf{2}] + q^2\langle\mathbf{13}\rangle[\mathbf{24}]\,,\\
\langle\mathbf{1}|\sigma^\mu|\mathbf{2}]\,\langle\mathbf{3}|\sigma^\nu|\mathbf{4}] &= \frac{1}{2}\Big\{\langle\mathbf{1}|\sigma^\mu|\mathbf{4}]\,\langle\mathbf{3}|\sigma^\nu|\mathbf{2}] + \langle\mathbf{1}|\sigma^\nu|\mathbf{4}]\,\langle\mathbf{3}|\sigma^\mu|\mathbf{2}]\\
&\qquad + 2\eta^{\mu\nu}\langle\mathbf{13}\rangle[\mathbf{24}] + i\epsilon^{\mu\nu\rho\sigma}\,\langle\mathbf{1}|\sigma^\rho|\mathbf{4}]\,\langle\mathbf{3}|\sigma^\sigma|\mathbf{2}]\Big\}\,.
\end{aligned}
$$

The Schouten identity is given by

$$
\langle\mathbf{12}\rangle\langle\mathbf{34}\rangle - \langle\mathbf{13}\rangle\langle\mathbf{24}\rangle + \langle\mathbf{14}\rangle\langle\mathbf{23}\rangle = 0\,, \tag{I.2}
$$

and similarly for the square brackets. We can also write this directly in terms of polarization vector contractions:

$$
\langle\mathbf{1}|\sigma^\mu|\mathbf{2}]\,\langle\mathbf{2}|\sigma^\nu|\mathbf{1}] = (m_1m_2)\{\epsilon_1^\mu\epsilon_2^\nu + \epsilon_1^\mu\epsilon_2^\nu + \eta^{\mu\nu}(\epsilon_1\cdot\epsilon_2) + i\epsilon^{\mu\nu\rho\sigma}\epsilon_{1\rho}\epsilon_{2\sigma}\}\,, \tag{I.3}
$$

and, for three massive vectors, we can write

$$
\begin{aligned}
(\epsilon_i \cdot \epsilon_j)(\epsilon_k \cdot p) &= -\left(\frac{\langle \mathbf{ij}\rangle [\mathbf{ij}]\, \langle \mathbf{k}|p|\mathbf{k}]}{\sqrt{2} m_i m_j m_k}\right), \\
(\epsilon_k \cdot p)(\epsilon_i \cdot p_j)(\epsilon_j \cdot p_i) &= -\frac{\langle \mathbf{k}|p|\mathbf{k}]}{2\sqrt{2} m_k}\left(\langle \mathbf{ij}\rangle \langle \mathbf{ij}\rangle + [\mathbf{ij}][\mathbf{ij}] - \frac{M_k \langle \mathbf{ij}\rangle [\mathbf{ij}]}{m_i m_j m_k}\right), \\
i(\epsilon_k \cdot p)\varepsilon^{\mu\nu\rho\sigma} p_j^\mu p_i^\nu \epsilon_j^\sigma \epsilon_i^\rho &= -\frac{\langle \mathbf{k}|p|\mathbf{k}]}{2\sqrt{2} m_k}\Big(\langle \mathbf{ij}\rangle \langle \mathbf{ij}\rangle - [\mathbf{ij}][\mathbf{ij}]\Big),
\end{aligned}
\tag{I.4}
$$

where $M_k = m_k^2 - m_i^2 - m_j^2$.

J Warsaw Basis

$1: X^3$		$2: H^6$		$3: H^4D^2$		$5: \psi^2H^3 + \text{h.c.}$	
Q_G	$f^{ABC}G_\mu^{A\nu}G_\nu^{B\rho}G_\rho^{C\mu}$	Q_H	$(H^\dagger H)^3$	$Q_{H\Box}$	$(H^\dagger H)\Box(H^\dagger H)$	Q_{eH}	$(H^\dagger H)(\bar{l}_p e_r H)$
$Q_{\widetilde{G}}$	$f^{ABC}\widetilde{G}_\mu^{A\nu}G_\nu^{B\rho}G_\rho^{C\mu}$			Q_{HD}	$\left(H^\dagger D_\mu H\right)^*\left(H^\dagger D_\mu H\right)$	Q_{uH}	$(H^\dagger H)(\bar{q}_p u_r \widetilde{H})$
Q_W	$\epsilon^{IJK}W_\mu^{I\nu}W_\nu^{J\rho}W_\rho^{K\mu}$					Q_{dH}	$(H^\dagger H)(\bar{q}_p d_r H)$
$Q_{\widetilde{W}}$	$\epsilon^{IJK}\widetilde{W}_\mu^{I\nu}W_\nu^{J\rho}W_\rho^{K\mu}$						

$4: X^2H^2$		$6: \psi^2XH + \text{h.c.}$		$7: \psi^2H^2D$	
Q_{HG}	$H^\dagger H\, G_{\mu\nu}^A G^{A\mu\nu}$	Q_{eW}	$(\bar{l}_p\sigma^{\mu\nu}e_r)\tau^I H W_{\mu\nu}^I$	$Q_{Hl}^{(1)}$	$(H^\dagger i\overleftrightarrow{D}_\mu H)(\bar{l}_p\gamma^\mu l_r)$
$Q_{H\widetilde{G}}$	$H^\dagger H\, \widetilde{G}_{\mu\nu}^A G^{A\mu\nu}$	Q_{eB}	$(\bar{l}_p\sigma^{\mu\nu}e_r)H B_{\mu\nu}$	$Q_{Hl}^{(3)}$	$(H^\dagger i\overleftrightarrow{D}_\mu^I H)(\bar{l}_p\tau^I\gamma^\mu l_r)$
Q_{HW}	$H^\dagger H\, W_{\mu\nu}^I W^{I\mu\nu}$	Q_{uG}	$(\bar{q}_p\sigma^{\mu\nu}T^A u_r)\widetilde{H}\, G_{\mu\nu}^A$	Q_{He}	$(H^\dagger i\overleftrightarrow{D}_\mu H)(\bar{e}_p\gamma^\mu e_r)$
$Q_{H\widetilde{W}}$	$H^\dagger H\, \widetilde{W}_{\mu\nu}^I W^{I\mu\nu}$	Q_{uW}	$(\bar{q}_p\sigma^{\mu\nu}u_r)\tau^I\widetilde{H}\, W_{\mu\nu}^I$	$Q_{Hq}^{(1)}$	$(H^\dagger i\overleftrightarrow{D}_\mu H)(\bar{q}_p\gamma^\mu q_r)$
Q_{HB}	$H^\dagger H\, B_{\mu\nu}B^{\mu\nu}$	Q_{uB}	$(\bar{q}_p\sigma^{\mu\nu}u_r)\widetilde{H}\, B_{\mu\nu}$	$Q_{Hq}^{(3)}$	$(H^\dagger i\overleftrightarrow{D}_\mu^I H)(\bar{q}_p\tau^I\gamma^\mu q_r)$
$Q_{H\widetilde{B}}$	$H^\dagger H\, \widetilde{B}_{\mu\nu}B^{\mu\nu}$	Q_{dG}	$(\bar{q}_p\sigma^{\mu\nu}T^A d_r)H\, G_{\mu\nu}^A$	Q_{Hu}	$(H^\dagger i\overleftrightarrow{D}_\mu H)(\bar{u}_p\gamma^\mu u_r)$
Q_{HWB}	$H^\dagger\tau^I H\, W_{\mu\nu}^I B^{\mu\nu}$	Q_{dW}	$(\bar{q}_p\sigma^{\mu\nu}d_r)\tau^I H\, W_{\mu\nu}^I$	Q_{Hd}	$(H^\dagger i\overleftrightarrow{D}_\mu H)(\bar{d}_p\gamma^\mu d_r)$
$Q_{H\widetilde{W}B}$	$H^\dagger\tau^I H\, \widetilde{W}_{\mu\nu}^I B^{\mu\nu}$	Q_{dB}	$(\bar{q}_p\sigma^{\mu\nu}d_r)H\, B_{\mu\nu}$	Q_{Hud} + h.c.	$i(\widetilde{H}^\dagger D_\mu H)(\bar{u}_p\gamma^\mu d_r)$

$8: (\bar{L}L)(\bar{L}L)$		$8: (\bar{R}R)(\bar{R}R)$		$8: (\bar{L}L)(\bar{R}R)$	
$Q_{\ell\ell}$	$(\bar{l}_p\gamma_\mu l_r)(\bar{l}_s\gamma^\mu l_t)$	Q_{ee}	$(\bar{e}_p\gamma_\mu e_r)(\bar{e}_s\gamma^\mu e_t)$	Q_{le}	$(\bar{l}_p\gamma_\mu l_r)(\bar{e}_s\gamma^\mu e_t)$
$Q_{qq}^{(1)}$	$(\bar{q}_p\gamma_\mu q_r)(\bar{q}_s\gamma^\mu q_t)$	Q_{uu}	$(\bar{u}_p\gamma_\mu u_r)(\bar{u}_s\gamma^\mu u_t)$	Q_{lu}	$(\bar{l}_p\gamma_\mu l_r)(\bar{u}_s\gamma^\mu u_t)$
$Q_{qq}^{(3)}$	$(\bar{q}_p\gamma_\mu\tau^I q_r)(\bar{q}_s\gamma^\mu\tau^I q_t)$	Q_{dd}	$(\bar{d}_p\gamma_\mu d_r)(\bar{d}_s\gamma^\mu d_t)$	Q_{ld}	$(\bar{l}_p\gamma_\mu l_r)(\bar{d}_s\gamma^\mu d_t)$
$Q_{\ell q}^{(1)}$	$(\bar{l}_p\gamma_\mu l_r)(\bar{q}_s\gamma^\mu q_t)$	Q_{eu}	$(\bar{e}_p\gamma_\mu e_r)(\bar{u}_s\gamma^\mu u_t)$	Q_{qe}	$(\bar{q}_p\gamma_\mu q_r)(\bar{e}_s\gamma^\mu e_t)$
$Q_{\ell q}^{(3)}$	$(\bar{l}_p\gamma_\mu\tau^I l_r)(\bar{q}_s\gamma^\mu\tau^I q_t)$	Q_{ed}	$(\bar{e}_p\gamma_\mu e_r)(\bar{d}_s\gamma^\mu d_t)$	$Q_{qu}^{(1)}$	$(\bar{q}_p\gamma_\mu q_r)(\bar{u}_s\gamma^\mu u_t)$
		$Q_{ud}^{(1)}$	$(\bar{u}_p\gamma_\mu u_r)(\bar{d}_s\gamma^\mu d_t)$	$Q_{qu}^{(8)}$	$(\bar{q}_p\gamma_\mu T^A q_r)(\bar{u}_s\gamma^\mu T^A u_t)$
		$Q_{ud}^{(8)}$	$(\bar{u}_p\gamma_\mu T^A u_r)(\bar{d}_s\gamma^\mu T^A d_t)$	$Q_{qd}^{(1)}$	$(\bar{q}_p\gamma_\mu q_r)(\bar{d}_s\gamma^\mu d_t)$
				$Q_{qd}^{(8)}$	$(\bar{q}_p\gamma_\mu T^A q_r)(\bar{d}_s\gamma^\mu T^A d_t)$

$8: (\bar{L}R)(\bar{R}L) + \text{h.c.}$		$8: (\bar{L}R)(\bar{L}R) + \text{h.c.}$	
Q_{ledq}	$(\bar{l}_p^j e_r)(\bar{d}_s q_{tj})$	$Q_{quqd}^{(1)}$	$(\bar{q}_p^j u_r)\epsilon_{jk}(\bar{q}_s^k d_t)$
		$Q_{quqd}^{(8)}$	$(\bar{q}_p^j T^A u_r)\epsilon_{jk}(\bar{q}_s^k T^A d_t)$
		$Q_{lequ}^{(1)}$	$(\bar{l}_p^j e_r)\epsilon_{jk}(\bar{q}_s^k u_t)$
		$Q_{lequ}^{(3)}$	$(\bar{l}_p^j\sigma_{\mu\nu}e_r)\epsilon_{jk}(\bar{q}_s^k\sigma^{\mu\nu}u_t)$

Table J.1: The independent dimension-six operators built from Standard Model fields which conserve baryon number, as given in Ref. [59]. The flavour labels p, r, s, t on the Q operators are suppressed on the left hand side of the tables.

List of Figures

List of Tables

Acknowledgments

The Acknowledgements were omitted according to the University Regulations.

Bibliography

[1] Rafael Aoude and William Shepherd. Jet Substructure Measurements of Interference in Non-Interfering SMEFT Effects. *JHEP*, 08:009, 2019.

[2] Rafael Aoude and Camila S. Machado. The Rise of SMEFT On-shell Amplitudes. *JHEP*, 12:058, 2019.

[3] Rafael Aoude, Tobias Hurth, Sophie Renner, and William Shepherd. The impact of flavour data on global fits of the MFV SMEFT. 3 2020.

[4] Rafael Aoude and Andreas Helset. Soft Theorems and the KLT-Relation. *JHEP*, 04:044, 2020.

[5] Rafael Aoude, Kays Haddad, and Andreas Helset. On-shell heavy particle effective theories. *JHEP*, 05:051, 2020.

[6] Georges Aad et al. Observation of a new particle in the search for the Standard Model Higgs boson with the ATLAS detector at the LHC. *Phys. Lett.*, B716:1–29, 2012.

[7] Serguei Chatrchyan et al. Observation of a New Boson at a Mass of 125 GeV with the CMS Experiment at the LHC. *Phys. Lett. B*, 716:30–61, 2012.

[8] Nima Arkani-Hamed, Tzu-Chen Huang, and Yu-tin Huang. Scattering Amplitudes For All Masses and Spins. 2017.

[9] Clifford Cheung and Chia-Hsien Shen. Nonrenormalization Theorems without Supersymmetry. *Phys. Rev. Lett.*, 115(7):071601, 2015.

[10] Zvi Bern, Andres Luna, Radu Roiban, Chia-Hsien Shen, and Mao Zeng. Spinning Black Hole Binary Dynamics, Scattering Amplitudes and Effective Field Theory. 5 2020.

[11] Steven Weinberg. *The Quantum theory of fields. Vol. 1: Foundations.* Cambridge University Press, 2005.

[12] B.M. Gavela, E.E. Jenkins, A.V. Manohar, and L. Merlo. Analysis of General Power Counting Rules in Effective Field Theory. *Eur. Phys. J. C*, 76(9):485, 2016.

[13] A. V. Manohar. Effective field theories. *Lect. Notes Phys.*, 479:311–362, 1997.

[14] Steven Weinberg. Phenomenological Lagrangians. *Physica A*, 96(1-2):327–340, 1979.

[15] Gino Isidori. Quantum Field Theory III Lectures.

[16] Gino Isidori. Flavor physics and CP violation. In *2012 European School of High-Energy Physics*, pages 69–105, 2014.

[17] S. L. Glashow, J. Iliopoulos, and L. Maiani. Weak interactions with lepton-hadron symmetry. *Phys. Rev. D*, 2:1285–1292, Oct 1970.

[18] T. Inami and C. S. Lim. Effects of Superheavy Quarks and Leptons in Low-Energy Weak Processes $K_L \to \mu\bar{\mu}$, $K^+ \to \pi^+\nu\bar{\nu}$ and $K^0 \leftrightarrow \bar{K}^0$. *Prog. Theor. Phys.*, 65:297, 1981. [Erratum: Prog. Theor. Phys.65,1772(1981)].

[19] Thomas Appelquist and J. Carazzone. Infrared singularities and massive fields. *Phys. Rev. D*, 11:2856–2861, May 1975.

[20] Ilaria Brivio and Michael Trott. The Standard Model as an Effective Field Theory. *Phys. Rept.*, 793:1–98, 2019.

[21] Matthew D. Schwartz. *Quantum Field Theory and the Standard Model*. Cambridge University Press, 3 2014.

[22] Aneesh V. Manohar. Introduction to Effective Field Theories. In *Les Houches summer school: EFT in Particle Physics and Cosmology Les Houches, Chamonix Valley, France, July 3-28, 2017*, 2018.

[23] S.L. Glashow. Partial Symmetries of Weak Interactions. *Nucl. Phys.*, 22:579–588, 1961.

[24] Steven Weinberg. A model of leptons. *Phys. Rev. Lett.*, 19:1264–1266, Nov 1967.

[25] Abdus Salam. Weak and Electromagnetic Interactions. *Conf. Proc. C*, 680519:367–377, 1968.

[26] G. 't Hooft. Symmetry breaking through bell-jackiw anomalies. *Phys. Rev. Lett.*, 37:8–11, Jul 1976.

[27] R. D. Peccei and Helen R. Quinn. Constraints imposed by CP conservation in the presence of pseudoparticles. *Phys. Rev. D*, 16:1791–1797, Sep 1977.

[28] Jr. Callan, Curtis G., R.F. Dashen, and David J. Gross. The Structure of the Gauge Theory Vacuum. *Phys. Lett. B*, 63:334–340, 1976.

[29] A.A. Belavin, A.M. Polyakov, A.S. Schwartz, and Yu.S. Tyupkin. Pseudoparticle solutions of the yang-mills equations. *Physics Letters B*, 59(1):85 – 87, 1975.

[30] Nicola Cabibbo. Unitary symmetry and leptonic decays. *Phys. Rev. Lett.*, 10:531–533, Jun 1963.

[31] Makoto Kobayashi and Toshihide Maskawa. CP-Violation in the Renormalizable Theory of Weak Interaction. *Progress of Theoretical Physics*, 49(2):652–657, 02 1973.

[32] Jason Aebischer, Jacky Kumar, Peter Stangl, and David M. Straub. A Global Likelihood for Precision Constraints and Flavour Anomalies. *Eur. Phys. J.*, C79(6):509, 2019.

[33] John N. Bahcall. Solar neutrinos. i. theoretical. *Phys. Rev. Lett.*, 12:300–302, Mar 1964.

[34] Raymond Davis. Solar neutrinos. ii. experimental. *Phys. Rev. Lett.*, 12:303–305, Mar 1964.

[35] Q. R. Ahmad, R. C. Allen, T. C. Andersen, J. D. Anglin, G. Bühler, J. C. Barton, E. W. Beier, M. Bercovitch, J. Bigu, S. Biller, and et al. Measurement of the rate of ve + d -¿ p +p+e- interactions produced by b8 solar neutrinos at the sudbury neutrino observatory. *Physical Review Letters*, 87(7), Jul 2001.

[36] Q. R. Ahmad, R. C. Allen, T. C. Andersen, J. D.Anglin, J. C. Barton, E. W. Beier, M. Bercovitch, J. Bigu, S. D. Biller, R. A. Black, and et al. Direct evidence for neutrino flavor transformation from neutral-current interactions in the sudbury neutrino observatory. *Physical Review Letters*, 89(1), Jun 2002.

[37] Y. Fukuda, T. Hayakawa, E. Ichihara, K. Inoue, K. Ishihara, H. Ishino, Y. Itow, T. Kajita, J. Kameda, S. Kasuga, and et al. Evidence for oscillation of atmospheric neutrinos. *Physical Review Letters*, 81(8):1562–1567, Aug 1998.

[38] F. Zwicky. Die Rotverschiebung von extragalaktischen Nebeln. *Helv. Phys. Acta*, 6:110–127, 1933.

[39] Vera C. Rubin and Jr. Ford, W. Kent. Rotation of the Andromeda Nebula from a Spectroscopic Survey of Emission Regions. 159:379, February 1970.

[40] P. A. R. Ade, N. Aghanim, M. Arnaud, M. Ashdown, J. Aumont, C. Baccigalupi, A. J. Banday, R. B. Barreiro, J. G. Bartlett, and et al. Planck2015 results. *Astronomy & Astrophysics*, 594:A13, Sep 2016.

[41] V. A. Kuzmin, V. A. Rubakov, and M. E. Shaposhnikov. On anomalous electroweak baryon-number non-conservation in the early universe. *Physics Letters B*, 155(1-2):36–42, May 1985.

[42] A.D. Sakharov. Violation of CP Invariance, C asymmetry, and baryon asymmetry of the universe. *Sov. Phys. Usp.*, 34(5):392–393, 1991.

[43] K. Abe et al. Constraint on the matter–antimatter symmetry-violating phase in neutrino oscillations. *Nature*, 580(7803):339–344, 2020.

[44] B. Pontecorvo. Inverse beta processes and nonconservation of lepton charge. *Sov. Phys. JETP*, 7:172–173, 1958.

[45] Ziro Maki, Masami Nakagawa, and Shoichi Sakata. Remarks on the Unified Model of Elementary Particles. *Progress of Theoretical Physics*, 28(5):870–880, 11 1962.

[46] Gerard 't Hooft. Naturalness, chiral symmetry, and spontaneous chiral symmetry breaking. *NATO Sci. Ser. B*, 59:135–157, 1980.

[47] F. Feruglio. The Chiral approach to the electroweak interactions. *Int. J. Mod. Phys. A*, 8:4937–4972, 1993.

[48] Benjamin Grinstein and Michael Trott. Higgs-higgs bound state due to new physics at a tev. *Phys. Rev. D*, 76:073002, Oct 2007.

[49] Andrew Kobach. Baryon Number, Lepton Number, and Operator Dimension in the Standard Model. *Phys. Lett.*, B758:455–457, 2016.

[50] Hao-Lin Li, Zhe Ren, Jing Shu, Ming-Lei Xiao, Jiang-Hao Yu, and Yu-Hui Zheng. Complete set of dimension-8 operators in the standard model effective field theory, 2020.

[51] Christopher W. Murphy. Dimension-8 Operators in the Standard Model Effective Field Theory. 4 2020.

[52] Brian Henning, Xiaochuan Lu, Tom Melia, and Hitoshi Murayama. Hilbert series and operator bases with derivatives in effective field theories. *Commun. Math. Phys.*, 347(2):363–388, 2016.

[53] Brian Henning, Xiaochuan Lu, Tom Melia, and Hitoshi Murayama. 2, 84, 30, 993, 560, 15456, 11962, 261485, ...: Higher dimension operators in the SM EFT. *JHEP*, 08:016, 2017. [Erratum: JHEP09,019(2019)].

[54] Brian Henning, Xiaochuan Lu, Tom Melia, and Hitoshi Murayama. Operator bases, S-matrices, and their partition functions. *JHEP*, 10:199, 2017.

[55] Maximilian Ruhdorfer, Javi Serra, and Andreas Weiler. Effective Field Theory of Gravity to All Orders. 8 2019.

[56] Grant N. Remmen and Nicholas L. Rodd. Consistency of the Standard Model Effective Field Theory. *JHEP*, 12:032, 2019.

[57] Grant N. Remmen and Nicholas L. Rodd. Flavor Constraints from Unitarity and Analyticity. 2020.

[58] W. Buchmuller and D. Wyler. Effective Lagrangian Analysis of New Interactions and Flavor Conservation. *Nucl. Phys. B*, 268:621–653, 1986.

[59] B. Grzadkowski, M. Iskrzynski, M. Misiak, and J. Rosiek. Dimension-Six Terms in the Standard Model Lagrangian. *JHEP*, 10:085, 2010.

[60] Howard Georgi. On-shell effective field theory. *Nucl. Phys.*, B361:339–350, 1991.

[61] H. David Politzer. Power Corrections at Short Distances. *Nucl. Phys.*, B172:349–382, 1980.

[62] Rodrigo Alonso, Elizabeth E. Jenkins, Aneesh V. Manohar, and Michael Trott. Renormalization Group Evolution of the Standard Model Dimension Six Operators III: Gauge Coupling Dependence and Phenomenology. *JHEP*, 04:159, 2014.

[63] Ilaria Brivio, Tyler Corbett, and Michael Trott. The Higgs width in the SMEFT. *JHEP*, 10:056, 2019.

[64] Andreas Helset, Adam Martin, and Michael Trott. The Geometric Standard Model Effective Field Theory. *JHEP*, 03:163, 2020.

[65] Ilaria Brivio and Michael Trott. Scheming in the SMEFT... and a reparameterization invariance! *JHEP*, 07:148, 2017. [Addendum: JHEP05,136(2018)].

[66] Rhorry Gauld, Benjamin D. Pecjak, and Darren J. Scott. One-loop corrections to $h \to b\bar{b}$ and $h \to \tau\bar{\tau}$ decays in the Standard Model Dimension-6 EFT: four-fermion operators and the large-m_t limit. *JHEP*, 05:080, 2016.

[67] Rhorry Gauld, Benjamin D. Pecjak, and Darren J. Scott. QCD radiative corrections for $h \to b\bar{b}$ in the Standard Model Dimension-6 EFT. *Phys. Rev.*, D94(7):074045, 2016.

[68] Laure Berthier, Mikkel Bjørn, and Michael Trott. Incorporating doubly resonant $W^{\pm}$ data in a global fit of SMEFT parameters to lift flat directions. *JHEP*, 09:157, 2016.

[69] K. Hagiwara, S. Ishihara, R. Szalapski, and D. Zeppenfeld. Low energy effects of new interactions in the electroweak boson sector. *Phys. Rev. D*, 48:2182–2203, Sep 1993.

[70] Gerhard Buchalla, Andrzej J. Buras, and Markus E. Lautenbacher. Weak decays beyond leading logarithms. *Rev. Mod. Phys.*, 68:1125–1144, 1996.

[71] Tobias Hurth, Sophie Renner, and William Shepherd. Matching for FCNC effects in the flavour-symmetric SMEFT. *JHEP*, 06:029, 2019.

[72] G. D'Ambrosio, G.F. Giudice, G. Isidori, and A. Strumia. Minimal flavor violation: An Effective field theory approach. *Nucl. Phys. B*, 645:155–187, 2002.

[73] Elizabeth E. Jenkins, Aneesh V. Manohar, and Michael Trott. Renormalization group evolution of the standard model dimension six operators. i: formalism and λ dependence. *Journal of High Energy Physics*, 2013(10), Oct 2013.

[74] Elizabeth E. Jenkins, Aneesh V. Manohar, and Michael Trott. Renormalization group evolution of the standard model dimension six operators ii: Yukawa dependence. *Journal of High Energy Physics*, 2014(1), Jan 2014.

[75] Rodrigo Alonso, Elizabeth E. Jenkins, Aneesh V. Manohar, and Michael Trott. Renormalization group evolution of the standard model dimension six operators iii: gauge coupling dependence and phenomenology. *Journal of High Energy Physics*, 2014(4), Apr 2014.

[76] Zvi Bern, Julio Parra-Martinez, and Eric Sawyer. Nonrenormalization and Operator Mixing via On-Shell Methods. *Phys. Rev. Lett.*, 124(5):051601, 2020.

[77] Serguei Chatrchyan et al. Observation of a new boson at a mass of 125 GeV with the CMS experiment at the LHC. *Phys. Lett.*, B716:30–61, 2012.

[78] Jorge de Blas, Otto Eberhardt, and Claudius Krause. Current and Future Constraints on Higgs Couplings in the Nonlinear Effective Theory. *JHEP*, 07:048, 2018.

[79] Kaoru Hagiwara, S. Ishihara, R. Szalapski, and D. Zeppenfeld. Low-energy effects of new interactions in the electroweak boson sector. *Phys. Rev.*, D48:2182–2203, 1993.

[80] C. Arzt, M. B. Einhorn, and J. Wudka. Patterns of deviation from the standard model. *Nucl. Phys.*, B433:41–66, 1995.

[81] G. J. Gounaris, J. Layssac, and F. M. Renard. Testing the Higgs boson gluonic couplings at CERN LHC. *Phys. Rev.*, D58:075006, 1998.

[82] Aneesh V. Manohar and Mark B. Wise. Modifications to the properties of the Higgs boson. *Phys. Lett.*, B636:107–113, 2006.

[83] Aneesh V. Manohar and Mark B. Wise. Flavor changing neutral currents, an extended scalar sector, and the Higgs production rate at the CERN LHC. *Phys. Rev.*, D74:035009, 2006.

[84] Vernon Barger, Tao Han, Paul Langacker, Bob McElrath, and Peter Zerwas. Effects of genuine dimension-six Higgs operators. *Phys. Rev.*, D67:115001, 2003.

[85] G. F. Giudice, C. Grojean, A. Pomarol, and R. Rattazzi. The Strongly-Interacting Light Higgs. *JHEP*, 06:045, 2007.

[86] Benjamin Grinstein and Michael Trott. A Higgs-Higgs bound state due to new physics at a TeV. *Phys. Rev.*, D76:073002, 2007.

[87] Laure Berthier and Michael Trott. Consistent constraints on the Standard Model Effective Field Theory. *JHEP*, 02:069, 2016.

[88] John Ellis, Veronica Sanz, and Tevong You. Complete Higgs Sector Constraints on Dimension-6 Operators. *JHEP*, 07:036, 2014.

[89] Christine Hartmann and Michael Trott. Higgs Decay to Two Photons at One Loop in the Standard Model Effective Field Theory. *Phys. Rev. Lett.*, 115(19):191801, 2015.

[90] Anja Butter, Oscar J. P. Eboli, J. Gonzalez-Fraile, M. C. Gonzalez-Garcia, Tilman Plehn, and Michael Rauch. The Gauge-Higgs Legacy of the LHC Run I. *JHEP*, 07:152, 2016.

[91] Anke Biekötter, Tyler Corbett, and Tilman Plehn. The Gauge-Higgs Legacy of the LHC Run II. 2018.

[92] Eduardo da Silva Almeida, Alexandre Alves, N. Rosa Agostinho, Oscar J.P. Éboli, and M.C. Gonzalez-Garcia. Electroweak Sector Under Scrutiny: A Combined Analysis of LHC and Electroweak Precision Data. *Phys. Rev. D*, 99(3):033001, 2019.

[93] Elizabeth E. Jenkins, Aneesh V. Manohar, and Michael Trott. Renormalization Group Evolution of the Standard Model Dimension Six Operators I: Formalism and lambda Dependence. *JHEP*, 10:087, 2013.

[94] Elizabeth E. Jenkins, Aneesh V. Manohar, and Michael Trott. Renormalization Group Evolution of the Standard Model Dimension Six Operators II: Yukawa Dependence. *JHEP*, 01:035, 2014.

[95] Christine Hartmann, William Shepherd, and Michael Trott. The Z decay width in the SMEFT: y_t and λ corrections at one loop. *JHEP*, 03:060, 2017.

[96] Christine Hartmann and Michael Trott. On one-loop corrections in the standard model effective field theory; the $\Gamma(h \to \gamma\,\gamma)$ case. *JHEP*, 07:151, 2015.

[97] S. Dawson and Pier Paolo Giardino. Higgs decays to ZZ and $Z\gamma$ in the standard model effective field theory: An NLO analysis. *Phys. Rev.*, D97(9):093003, 2018.

[98] Sally Dawson and Ahmed Ismail. Standard model EFT corrections to Z boson decays. *Phys. Rev.*, D98(9):093003, 2018.

[99] Cen Zhang and Fabio Maltoni. Top-quark decay into Higgs boson and a light quark at next-to-leading order in QCD. *Phys. Rev.*, D88:054005, 2013.

[100] Sally Dawson and Pier Paolo Giardino. Electroweak corrections to Higgs boson decays to $\gamma\gamma$ and W^+W^- in standard model EFT. *Phys. Rev.*, D98(9):095005, 2018.

[101] A. Dedes, M. Paraskevas, J. Rosiek, K. Suxho, and L. Trifyllis. The decay $h \to \gamma\gamma$ in the Standard-Model Effective Field Theory. *JHEP*, 08:103, 2018.

[102] Eleni Vryonidou and Cen Zhang. Dimension-six electroweak top-loop effects in Higgs production and decay. *JHEP*, 08:036, 2018.

[103] Fabio Maltoni, Eleni Vryonidou, and Cen Zhang. Higgs production in association with a top-antitop pair in the Standard Model Effective Field Theory at NLO in QCD. *JHEP*, 10:123, 2016.

[104] Cen Zhang. Single Top Production at Next-to-Leading Order in the Standard Model Effective Field Theory. *Phys. Rev. Lett.*, 116(16):162002, 2016.

[105] S. Dawson, P. P. Giardino, and A. Ismail. SMEFT and the Drell-Yan Process at High Energy. 2018.

[106] Julien Baglio, Sally Dawson, and Ian M. Lewis. An NLO QCD effective field theory analysis of W^+W^- production at the LHC including fermionic operators. *Phys. Rev.*, D96(7):073003, 2017.

[107] Julien Baglio, Sally Dawson, and Ian M. Lewis. NLO Effects in EFT Fits to W^+W^- Production at the LHC. 2018.

[108] Vardan Khachatryan et al. Search for quark contact interactions and extra spatial dimensions using dijet angular distributions in proton–proton collisions at $\sqrt{s} = 8$ TeV. *Phys. Lett.*, B746:79–99, 2015.

[109] Serguei Chatrchyan et al. Search for quark compositeness in dijet angular distributions from pp collisions at $\sqrt{s} = 7$ TeV. *JHEP*, 05:055, 2012.

[110] Stefan Alte, Matthias König, and William Shepherd. Consistent Searches for SMEFT Effects in Non-Resonant Dijet Events. *JHEP*, 01:094, 2018.

[111] Stefan Alte, Matthias König, and William Shepherd. Consistent Searches for SMEFT Effects in Non-Resonant Dilepton Events. 2018.

[112] Aleksandr Azatov, Roberto Contino, Camila S. Machado, and Francesco Riva. Helicity selection rules and noninterference for BSM amplitudes. *Phys. Rev.*, D95(6):065014, 2017.

[113] A. Azatov, J. Elias-Miro, Y. Reyimuaji, and E. Venturini. Novel measurements of anomalous triple gauge couplings for the LHC. *JHEP*, 10:027, 2017.

[114] Giuliano Panico, Francesco Riva, and Andrea Wulzer. Diboson Interference Resurrection. *Phys. Lett.*, B776:473–480, 2018.

[115] Lance J. Dixon and Yael Shadmi. Testing gluon selfinteractions in three jet events at hadron colliders. *Nucl. Phys.*, B423:3–32, 1994. [Erratum: Nucl. Phys. B452, 724 (1995)].

[116] A. Abdesselam et al. Boosted objects: A Probe of beyond the Standard Model physics. *Eur. Phys. J.*, C71:1661, 2011.

[117] A. Altheimer et al. Jet Substructure at the Tevatron and LHC: New results, new tools, new benchmarks. *J. Phys.*, G39:063001, 2012.

[118] A. Altheimer et al. Boosted objects and jet substructure at the LHC. Report of BOOST2012, held at IFIC Valencia, 23rd-27th of July 2012. *Eur. Phys. J.*, C74(3):2792, 2014.

[119] A. Azatov, D. Barducci, and E. Venturini. Precision diboson measurements at hadron colliders. 2019.

[120] E. Venturini. Talk at Planck 2018.

[121] Ben Gripaios and Dave Sutherland. Searches for CP-violating dimension-6 electroweak gauge boson operators. *Phys. Rev.*, D89(7):076004, 2014.

[122] Jonathan M. Butterworth, Adam R. Davison, Mathieu Rubin, and Gavin P. Salam. Jet substructure as a new Higgs search channel at the LHC. *Phys. Rev. Lett.*, 100:242001, 2008.

[123] J. M. Butterworth, B. E. Cox, and Jeffrey R. Forshaw. WW scattering at the CERN LHC. *Phys. Rev.*, D65:096014, 2002.

[124] David E. Kaplan, Keith Rehermann, Matthew D. Schwartz, and Brock Tweedie. Top Tagging: A Method for Identifying Boosted Hadronically Decaying Top Quarks. *Phys. Rev. Lett.*, 101:142001, 2008.

[125] Tilman Plehn, Gavin P. Salam, and Michael Spannowsky. Fat Jets for a Light Higgs. *Phys. Rev. Lett.*, 104:111801, 2010.

[126] Andrew J. Larkoski, Simone Marzani, Gregory Soyez, and Jesse Thaler. Soft Drop. *JHEP*, 05:146, 2014.

[127] Jesse Thaler and Ken Van Tilburg. Identifying Boosted Objects with N-subjettiness. *JHEP*, 03:015, 2011.

[128] Andrew J. Larkoski, Duff Neill, and Jesse Thaler. Jet Shapes with the Broadening Axis. *JHEP*, 04:017, 2014.

[129] Adam Alloul, Neil D. Christensen, Celine Degrande, Claude Duhr, and Benjamin Fuks. FeynRules 2.0 - A complete toolbox for tree-level phenomenology. *Comput. Phys. Commun.*, 185:2250–2300, 2014.

[130] J. Alwall, R. Frederix, S. Frixione, V. Hirschi, F. Maltoni, O. Mattelaer, H. S. Shao, T. Stelzer, P. Torrielli, and M. Zaro. The automated computation of tree-level and next-to-leading order differential cross sections, and their matching to parton shower simulations. *JHEP*, 07:079, 2014.

[131] Torbjorn Sjostrand, Stephen Mrenna, and Peter Z. Skands. PYTHIA 6.4 Physics and Manual. *JHEP*, 05:026, 2006.

[132] Matteo Cacciari, Gavin P. Salam, and Gregory Soyez. FastJet User Manual. *Eur. Phys. J.*, C72:1896, 2012.

[133] Matteo Cacciari and Gavin P. Salam. Dispelling the N^3 myth for the k_t jet-finder. *Phys. Lett.*, B641:57–61, 2006.

[134] Morad Aaboud et al. Search for diboson resonances with boson-tagged jets in pp collisions at $\sqrt{s} = 13$ TeV with the ATLAS detector. *Phys. Lett.*, B777:91–113, 2018.

[135] S. Schael et al. Electroweak Measurements in Electron-Positron Collisions at W-Boson-Pair Energies at LEP. *Phys. Rept.*, 532:119–244, 2013.

[136] Valentin Hirschi, Fabio Maltoni, Ioannis Tsinikos, and Eleni Vryonidou. Constraining anomalous gluon self-interactions at the LHC: a reappraisal. *JHEP*, 07:093, 2018.

[137] Luca Silvestrini and Mauro Valli. Model-independent Bounds on the Standard Model Effective Theory from Flavour Physics. *Phys. Lett.*, B799:135062, 2019.

[138] Wouter Dekens and Peter Stoffer. Low-energy effective field theory below the electroweak scale: matching at one loop. *JHEP*, 10:197, 2019.

[139] Sébastien Descotes-Genon, Adam Falkowski, Marco Fedele, Martín González-Alonso, and Javier Virto. The CKM parameters in the SMEFT. *JHEP*, 05:172, 2019.

[140] S. Aoki et al. FLAG Review 2019: Flavour Lattice Averaging Group (FLAG). *Eur. Phys. J.*, C80(2):113, 2020.

[141] Jason Aebischer, Jacky Kumar, and David M. Straub. Wilson: a Python package for the running and matching of Wilson coefficients above and below the electroweak scale. *Eur. Phys. J.*, C78(12):1026, 2018.

[142] Jason Aebischer, Matteo Fael, Christoph Greub, and Javier Virto. B physics Beyond the Standard Model at One Loop: Complete Renormalization Group Evolution below the Electroweak Scale. *JHEP*, 09:158, 2017.

[143] Elizabeth E. Jenkins, Aneesh V. Manohar, and Peter Stoffer. Low-Energy Effective Field Theory below the Electroweak Scale: Anomalous Dimensions. *JHEP*, 01:084, 2018.

[144] Luca Di Luzio, Matthew Kirk, Alexander Lenz, and Thomas Rauh. ΔM_s theory precision confronts flavour anomalies. 2019.

[145] Y. Amhis et al. Averages of b-hadron, c-hadron, and τ-lepton properties as of summer 2016. *Eur. Phys. J.*, C77(12):895, 2017.

[146] Sebastian Jäger, Matthew Kirk, Alexander Lenz, and Kirsten Leslie. Charming new physics in rare B-decays and mixing? *Phys. Rev.*, D97(1):015021, 2018.

[147] Martin Gorbahn and Ulrich Haisch. Effective Hamiltonian for non-leptonic $|\Delta F| = 1$ decays at NNLO in QCD. *Nucl. Phys.*, B713:291–332, 2005.

[148] Sebastian Jäger, Matthew Kirk, Alexander Lenz, and Kirsten Leslie. Charming New B-Physics. 2019.

[149] Marina Artuso, Guennadi Borissov, and Alexander Lenz. CP violation in the B_s^0 system. *Rev. Mod. Phys.*, 88(4):045002, 2016. [Addendum: Rev. Mod. Phys.91,no.4,049901(2019)].

[150] Andrzej J. Buras, Dario Buttazzo, and Robert Knegjens. $K \to \pi\nu\overline{\nu}$ and ϵ'/ϵ in simplified new physics models. *JHEP*, 11:166, 2015.

[151] Andrzej J. Buras, Dario Buttazzo, Jennifer Girrbach-Noe, and Robert Knegjens. $K^+ \to \pi^+\nu\overline{\nu}$ and $K_L \to \pi^0\nu\overline{\nu}$ in the Standard Model: status and perspectives. *JHEP*, 11:033, 2015.

[152] Giuseppe Ruggiero. New Results on $K^+ \to \pi^+\bar{\nu}\nu$ from the NA62 Experiment, Talk given at KAON 2019, Perugia Italy. In *Talk given at KAON 2019, Perugia Italy*, 2019.

[153] J. K. Ahn et al. Search for the $K_L \to \pi^0\nu\overline{\nu}$ and $K_L \to \pi^0 X^0$ decays at the J-PARC KOTO experiment. *Phys. Rev. Lett.*, 122(2):021802, 2019.

[154] Andrzej J. Buras, Jennifer Girrbach-Noe, Christoph Niehoff, and David M. Straub. $B \to K^{(*)}\nu\overline{\nu}$ decays in the Standard Model and beyond. *JHEP*, 02:184, 2015.

[155] J. P. Lees et al. Search for $B \to K^{(*)}\nu\overline{\nu}$ and invisible quarkonium decays. *Phys. Rev.*, D87(11):112005, 2013.

[156] O. Lutz et al. Search for $B \to h^{(*)}\nu\overline{\nu}$ with the full Belle $\Upsilon(4S)$ data sample. *Phys. Rev.*, D87(11):111103, 2013.

[157] Andreas Crivellin and Lorenzo Mercolli. $B- > X_d\gamma$ and constraints on new physics. *Phys. Rev.*, D84:114005, 2011.

[158] Tobias Huber, Tobias Hurth, Jack Jenkins, Enrico Lunghi, Qin Qin, and K. Keri Vos. Long distance effects in inclusive rare B decays and phenomenology of $\bar{B} \to X_d\ell^+\ell^-$. 2019. [JHEP10,228(2019)].

[159] David M. Straub. flavio: a Python package for flavour and precision phenomenology in the Standard Model and beyond. 2018.

[160] Wolfgang Altmannshofer, Christoph Niehoff, Peter Stangl, and David M. Straub. Status of the $B \to K^*\mu^+\mu^-$ anomaly after Moriond 2017. *Eur. Phys. J.*, C77(6):377, 2017.

[161] Ayan Paul and David M. Straub. Constraints on new physics from radiative B decays. 2016.

[162] S. Schael et al. Precision electroweak measurements on the Z resonance. *Phys. Rept.*, 427:257–454, 2006.

[163] P. Achard et al. Measurement of the cross section of W-boson pair production at LEP. *Phys. Lett.*, B600:22–40, 2004.

[164] G. Abbiendi et al. Measurement of the $e^+e^- \to W^+W^-$ cross section and W decay branching fractions at LEP. *Eur. Phys. J.*, C52:767–785, 2007.

[165] A. Heister et al. Measurement of W-pair production in e+ e- collisions at centre-of-mass energies from 183-GeV to 209-GeV. *Eur. Phys. J.*, C38:147–160, 2004.

[166] Georges Aad et al. Measurements of the Higgs boson production and decay rates and constraints on its couplings from a combined ATLAS and CMS analysis of the LHC pp collision data at $\sqrt{s} = 7$ and 8 TeV. *JHEP*, 08:045, 2016.

[167] John Ellis, Christopher W. Murphy, Verónica Sanz, and Tevong You. Updated Global SMEFT Fit to Higgs, Diboson and Electroweak Data. *JHEP*, 06:146, 2018.

[168] Albert M Sirunyan et al. Combined measurements of Higgs boson couplings in proton–proton collisions at $\sqrt{s} = 13\,\text{TeV}$. *Eur. Phys. J.*, C79(5):421, 2019.

[169] Georges Aad et al. Combined measurements of Higgs boson production and decay using up to 80 fb^{-1} of proton-proton collision data at $\sqrt{s} = 13$ TeV collected with the ATLAS experiment. 2019.

[170] Morad Aaboud et al. Measurement of the W^+W^- production cross section in pp collisions at a centre-of-mass energy of $\sqrt{s} = 13$ TeV with the ATLAS experiment. *Phys. Lett.*, B773:354–374, 2017.

[171] H. Sagawa, T. Tauchi, M. Tanabashi, and S Uehara. TRISTAN physics at high luminosities, in Proceedings, 3rd Workshop, Tsukuba Japan, November 16-18. 1994.

[172] A. B. Arbuzov, M. Awramik, M. Czakon, A. Freitas, M. W. Grunewald, Klaus Monig, S. Riemann, and T. Riemann. ZFITTER: A Semi-analytical program for fermion pair production in e+ e- annihilation, from version 6.21 to version 6.42. *Comput. Phys. Commun.*, 174:728–758, 2006.

[173] P. A. Vetter, D. M. Meekhof, P. K. Majumder, S. K. Lamoreaux, and E. N. Fortson. Precise test of electroweak theory from a new measurement of parity nonconservation in atomic thallium. *Phys. Rev. Lett.*, 74:2658–2661, 1995.

[174] C. S. Wood, S. C. Bennett, D. Cho, B. P. Masterson, J. L. Roberts, C. E. Tanner, and Carl E. Wieman. Measurement of parity nonconservation and an anapole moment in cesium. *Science*, 275:1759–1763, 1997.

[175] C. Y. Prescott et al. Further Measurements of Parity Nonconservation in Inelastic electron Scattering. *Phys. Lett.*, 84B:524–528, 1979.

[176] Adam Falkowski, Martín González-Alonso, and Kin Mimouni. Compilation of low-energy constraints on 4-fermion operators in the SMEFT. *JHEP*, 08:123, 2017.

[177] J. V. Allaby et al. A Precise Determination of the Electroweak Mixing Angle from Semileptonic Neutrino Scattering. *Z. Phys.*, C36:611, 1987.

[178] M. Tanabashi et al. Review of Particle Physics. *Phys. Rev. D*, 98(3):030001, 2018.

[179] E. J. Beise, M. L. Pitt, and D. T. Spayde. The SAMPLE experiment and weak nucleon structure. *Prog. Part. Nucl. Phys.*, 54:289–350, 2005.

[180] A. Argento et al. Electroweak Asymmetry in Deep Inelastic Muon - Nucleon Scattering. *Phys. Lett.*, 120B:245, 1983.

[181] Roel Aaij et al. Angular analysis of the $B^0 \to K^{*0}\mu^+\mu^-$ decay using 3 fb^{-1} of integrated luminosity. *JHEP*, 02:104, 2016.

[182] R. Aaij et al. Differential branching fractions and isospin asymmetries of $B \to K^{(*)}\mu^+\mu^-$ decays. *JHEP*, 06:133, 2014.

[183] Roel Aaij et al. Angular analysis and differential branching fraction of the decay $B_s^0 \to \phi\mu^+\mu^-$. *JHEP*, 09:179, 2015.

[184] A. Arbey, T. Hurth, F. Mahmoudi, D. Martínez Santos, and S. Neshatpour. Update on the b $\to$ s anomalies. *Phys. Rev.*, D100(1):015045, 2019.

[185] Marcel Algueró, Bernat Capdevila, Andreas Crivellin, Sébastien Descotes-Genon, Pere Masjuan, Joaquim Matias, and Javier Virto. Emerging patterns of New Physics with and without Lepton Flavour Universal contributions. *Eur. Phys. J.*, C79(8):714, 2019.

[186] Marco Ciuchini, António M. Coutinho, Marco Fedele, Enrico Franco, Ayan Paul, Luca Silvestrini, and Mauro Valli. New Physics in $b \to s\ell^+\ell^-$ confronts new data on Lepton Universality. *Eur. Phys. J.*, C79(8):719, 2019.

[187] Jason Aebischer, Wolfgang Altmannshofer, Diego Guadagnoli, Méril Reboud, Peter Stangl, and David M. Straub. B-decay discrepancies after Moriond 2019. 2019.

[188] Kamila Kowalska, Dinesh Kumar, and Enrico Maria Sessolo. Implications for new physics in $b \to s\mu\mu$ transitions after recent measurements by Belle and LHCb. *Eur. Phys. J.*, C79(10):840, 2019.

[189] Ashutosh Kumar Alok, Amol Dighe, Shireen Gangal, and Dinesh Kumar. Continuing search for new physics in $b \to s\mu\mu$ decays: two operators at a time. *JHEP*, 06:089, 2019.

[190] Roel Aaij et al. Search for lepton-universality violation in $B^+ \to K^+\ell^+\ell^-$ decays. *Phys. Rev. Lett.*, 122(19):191801, 2019.

[191] R. Aaij et al. Test of lepton universality with $B^0 \to K^{*0}\ell^+\ell^-$ decays. *JHEP*, 08:055, 2017.

[192] Dario Buttazzo, Admir Greljo, Gino Isidori, and David Marzocca. B-physics anomalies: a guide to combined explanations. *JHEP*, 11:044, 2017.

[193] Marzia Bordone, Gino Isidori, and Sokratis Trifinopoulos. Semileptonic B-physics anomalies: A general EFT analysis within $U(2)^n$ flavor symmetry. *Phys. Rev.*, D96(1):015038, 2017.

[194] Javier Fuentes-Martín, Gino Isidori, Julie Pagès, and Kei Yamamoto. With or without U(2)? Probing non-standard flavor and helicity structures in semileptonic B decays. *Phys. Lett.*, B800:135080, 2020.

[195] Marzia Bordone, Oscar Catà, and Thorsten Feldmann. Effective Theory Approach to New Physics with Flavour: General Framework and a Leptoquark Example. *JHEP*, 01:067, 2020.

[196] Ilaria Brivio, Sebastian Bruggisser, Fabio Maltoni, Rhea Moutafis, Tilman Plehn, Eleni Vryonidou, Susanne Westhoff, and C. Zhang. O new physics, where art thou? A global search in the top sector. 2019.

[197] Nathan P. Hartland, Fabio Maltoni, Emanuele R. Nocera, Juan Rojo, Emma Slade, Eleni Vryonidou, and Cen Zhang. A Monte Carlo global analysis of the Standard Model Effective Field Theory: the top quark sector. *JHEP*, 04:100, 2019.

[198] Marco Farina, Cristina Mondino, Duccio Pappadopulo, and Joshua T. Ruderman. New Physics from High Energy Tops. *JHEP*, 01:231, 2019.

[199] Stefan Bißmann, Johannes Erdmann, Cornelius Grunwald, Gudrun Hiller, and Kevin Kröninger. Constraining top-quark couplings combining top-quark and $\boldsymbol{B}$ decay observables. 2019.

[200] S. Alioli, V. Cirigliano, W. Dekens, J. de Vries, and E. Mereghetti. Right-handed charged currents in the era of the Large Hadron Collider. *JHEP*, 05:086, 2017.

[201] V. Cirigliano, W. Dekens, J. de Vries, and E. Mereghetti. Constraining the top-Higgs sector of the Standard Model Effective Field Theory. *Phys. Rev.*, D94(3):034031, 2016.

[202] V. Cirigliano, W. Dekens, J. de Vries, and E. Mereghetti. Is there room for CP violation in the top-Higgs sector? *Phys. Rev.*, D94(1):016002, 2016.

[203] Joachim Brod, Admir Greljo, Emmanuel Stamou, and Patipan Uttayarat. Probing anomalous $t\bar{t}Z$ interactions with rare meson decays. *JHEP*, 02:141, 2015.

[204] Jernej F. Kamenik, Michele Papucci, and Andreas Weiler. Constraining the dipole moments of the top quark. *Phys. Rev.*, D85:071501, 2012. [Erratum: Phys. Rev.D88,no.3,039903(2013)].

[205] Jure Drobnak, Svjetlana Fajfer, and Jernej F. Kamenik. Probing anomalous tWb interactions with rare B decays. *Nucl. Phys.*, B855:82–99, 2012.

[206] Adam Falkowski and David Straub. Flavourful SMEFT likelihood for Higgs and electroweak data. 2019.

[207] Zvi Bern and Yu-tin Huang. Basics of Generalized Unitarity. *J. Phys. A*, 44:454003, 2011.

[208] Andrew Hodges. Twistors and amplitudes. *Phil. Trans. Roy. Soc. Lond. A*, 373:20140248, 2015.

[209] Clifford Cheung. *TASI Lectures on Scattering Amplitudes*, pages 571–623. 2018.

[210] Lance J. Dixon. Calculating scattering amplitudes efficiently. In *Theoretical Advanced Study Institute in Elementary Particle Physics (TASI 95): QCD and Beyond*, pages 539–584, 1 1996.

[211] Lance J. Dixon. A Brief Introduction to Modern Amplitude Methods. In *Theoretical Advanced Study Institute in Elementary Particle Physics: Journeys Through the Precision Frontier: Amplitudes for Colliders*, pages 39–97, 2015.

[212] Zvi Bern, John Joseph Carrasco, Marco Chiodaroli, Henrik Johansson, and Radu Roiban. The Duality Between Color and Kinematics and its Applications. 9 2019.

[213] Stefan Dittmaier. Weyl-van der Waerden formalism for helicity amplitudes of massive particles. *Phys. Rev.*, D59:016007, 1998.

[214] Darren Forde and David A. Kosower. All-multiplicity amplitudes with massive scalars. *Phys. Rev.*, D73:065007, 2006.

[215] German Rodrigo. Multigluonic scattering amplitudes of heavy quarks. *JHEP*, 09:079, 2005.

[216] Christian Schwinn and Stefan Weinzierl. SUSY ward identities for multi-gluon helicity amplitudes with massive quarks. *JHEP*, 03:030, 2006.

[217] Christian Schwinn and Stefan Weinzierl. On-shell recursion relations for all Born QCD amplitudes. *JHEP*, 04:072, 2007.

[218] Anthony Hall. Massive Quark-Gluon Scattering Amplitudes at Tree Level. *Phys. Rev.*, D77:025011, 2008.

[219] Rutger H. Boels and Christian Schwinn. On-shell supersymmetry for massive multiplets. *Phys. Rev.*, D84:065006, 2011.

[220] Ruth Britto and Alexander Ochirov. On-shell recursion for massive fermion currents. *JHEP*, 01:002, 2013.

[221] Eduardo Conde and Andrea Marzolla. Lorentz Constraints on Massive Three-Point Amplitudes. *JHEP*, 09:041, 2016.

[222] Clifford Cheung and Donal O'Connell. Amplitudes and Spinor-Helicity in Six Dimensions. *JHEP*, 07:075, 2009.

[223] Alexander Ochirov. Helicity amplitudes for QCD with massive quarks. *JHEP*, 04:089, 2018.

[224] Neil Christensen and Bryan Field. The Constructive Standard Model: Part I. 2018.

[225] Zvi Bern, Clifford Cheung, Radu Roiban, Chia-Hsien Shen, Mikhail P. Solon, and Mao Zeng. Black Hole Binary Dynamics from the Double Copy and Effective Theory. *JHEP*, 10:206, 2019.

[226] Freddy Cachazo and Andrew Strominger. Evidence for a New Soft Graviton Theorem. 4 2014.

[227] Clifford Cheung, Karol Kampf, Jiri Novotny, Chia-Hsien Shen, and Jaroslav Trnka. On-Shell Recursion Relations for Effective Field Theories. *Phys. Rev. Lett.*, 116(4):041601, 2016.

[228] Henriette Elvang, Callum R. T. Jones, and Stephen G. Naculich. Soft Photon and Graviton Theorems in Effective Field Theory. *Phys. Rev. Lett.*, 118(23):231601, 2017.

[229] Massimo Bianchi, Song He, Yu-tin Huang, and Congkao Wen. More on Soft Theorems: Trees, Loops and Strings. *Phys. Rev. D*, 92(6):065022, 2015.

[230] Eugene P. Wigner. On Unitary Representations of the Inhomogeneous Lorentz Group. *Annals Math.*, 40:149–204, 1939.

[231] P. [De Causmaecker], R. Gastmans, W. Troost, and Tai Tsun Wu. Multiple bremsstrahlung in gauge theories at high energies (i). general formalism for quantum electrodynamics. *Nuclear Physics B*, 206(1):53 – 60, 1982.

[232] R. Kleiss and W.J. Stirling. Spinor techniques for calculating pp $\rightarrow$ w$\pm$/z0 + jets. *Nuclear Physics B*, 262(2):235 – 262, 1985.

[233] Zhan Xu, Da-Hua Zhang, and Lee Chang. Helicity amplitudes for multiple bremsstrahlung in massless non-abelian gauge theories. *Nuclear Physics B*, 291:392 – 428, 1987.

[234] David A. McGady and Laurentiu Rodina. Higher-spin massless s matrices in four dimensions. *Phys. Rev. D*, 90:084048, Oct 2014.

[235] Ruth Britto, Freddy Cachazo, Bo Feng, and Edward Witten. Direct proof of tree-level recursion relation in Yang-Mills theory. *Phys. Rev. Lett.*, 94:181602, 2005.

[236] Ruth Britto, Freddy Cachazo, and Bo Feng. New recursion relations for tree amplitudes of gluons. *Nucl. Phys. B*, 715:499–522, 2005.

[237] Vittorio Del Duca, Lance J. Dixon, and Fabio Maltoni. New color decompositions for gauge amplitudes at tree and loop level. *Nucl. Phys. B*, 571:51–70, 2000.

[238] Stephen J. Parke and T. R. Taylor. Amplitude for n-gluon scattering. *Phys. Rev. Lett.*, 56:2459–2460, Jun 1986.

[239] Timothy Cohen, Henriette Elvang, and Michael Kiermaier. On-shell constructibility of tree amplitudes in general field theories. *JHEP*, 04:053, 2011.

[240] Clifford Cheung. On-Shell Recursion Relations for Generic Theories. *JHEP*, 03:098, 2010.

[241] S.D. Badger, E.W.Nigel Glover, V.V. Khoze, and P. Svrcek. Recursion relations for gauge theory amplitudes with massive particles. *JHEP*, 07:025, 2005.

[242] Robert Franken and Christian Schwinn. On-shell constructibility of Born amplitudes in spontaneously broken gauge theories. *JHEP*, 02:073, 2020.

[243] Henriette Elvang and Yu-tin Huang. Scattering Amplitudes. 2013.

[244] Michael Kiermaier. The Coulomb-branch S-matrix from massless amplitudes. 2011.

[245] Nathaniel Craig, Henriette Elvang, Michael Kiermaier, and Tracy Slatyer. Massive amplitudes on the Coulomb branch of N=4 SYM. *JHEP*, 12:097, 2011.

[246] Aidan Herderschee, Seth Koren, and Timothy Trott. Massive On-Shell Supersymmetric Scattering Amplitudes. 2019.

[247] Aidan Herderschee, Seth Koren, and Timothy Trott. Constructing $\mathcal{N} = 4$ Coulomb Branch Superamplitudes. 2019.

[248] Ming-Zhi Chung, Yu-Tin Huang, Jung-Wook Kim, and Sangmin Lee. The simplest massive S-matrix: from minimal coupling to Black Holes. *JHEP*, 04:156, 2019.

[249] Alfredo Guevara, Alexander Ochirov, and Justin Vines. Scattering of Spinning Black Holes from Exponentiated Soft Factors. 2018.

[250] Nathan Moynihan and Jeff Murugan. Comments on scattering in massive gravity, vDVZ and BCFW. 2017.

[251] Brian Henning and Tom Melia. Constructing effective field theories via their harmonics. 2019.

[252] Lance J. Dixon, E. W. Nigel Glover, and Valentin V. Khoze. MHV rules for Higgs plus multi-gluon amplitudes. *JHEP*, 12:015, 2004.

[253] Clifford Cheung, Karol Kampf, Jiri Novotny, Chia-Hsien Shen, and Jaroslav Trnka. A Periodic Table of Effective Field Theories. *JHEP*, 02:020, 2017.

[254] Clifford Cheung, Karol Kampf, Jiri Novotny, Chia-Hsien Shen, Jaroslav Trnka, and Congkao Wen. Vector Effective Field Theories from Soft Limits. *Phys. Rev. Lett.*, 120(26):261602, 2018.

[255] Henriette Elvang, Marios Hadjiantonis, Callum R. T. Jones, and Shruti Paranjape. Soft Bootstrap and Supersymmetry. 2018.

[256] Clifford Cheung, Chia-Hsien Shen, and Jaroslav Trnka. Simple Recursion Relations for General Field Theories. *JHEP*, 06:118, 2015.

[257] Yael Shadmi and Yaniv Weiss. Effective Field Theory Amplitudes the On-Shell Way: Scalar and Vector Couplings to Gluons. 2018.

[258] Teng Ma, Jing Shu, and Ming-Lei Xiao. Standard Model Effective Field Theory from On-shell Amplitudes. 2019.

[259] Gauthier Durieux, Teppei Kitahara, Yael Shadmi, and Yaniv Weiss. The electroweak effective field theory from on-shell amplitudes. 2019.

[260] Freddy Cachazo, Peter Svrcek, and Edward Witten. MHV vertices and tree amplitudes in gauge theory. *JHEP*, 09:006, 2004.

[261] David A. McGady and Laurentiu Rodina. Higher-spin massless S-matrices in four-dimensions. *Phys. Rev.*, D90(8):084048, 2014.

[262] Rodrigo Alonso, Elizabeth E. Jenkins, and Aneesh V. Manohar. Holomorphy without Supersymmetry in the Standard Model Effective Field Theory. *Phys. Lett.*, B739:95–98, 2014.

[263] Herbi K. Dreiner, Howard E. Haber, and Stephen P. Martin. Two-component spinor techniques and Feynman rules for quantum field theory and supersymmetry. *Phys. Rept.*, 494:1–196, 2010.

[264] A. Dedes, W. Materkowska, M. Paraskevas, J. Rosiek, and K. Suxho. Feynman Rules for the Standard Model Effective Field Theory in R_ξ-gauges. *JHEP*, 06:143, 2017.

[265] Bo Feng and Mingxing Luo. An Introduction to On-shell Recursion Relations. *Front. Phys.(Beijing)*, 7:533–575, 2012.

[266] S. D. Badger, E. W. Nigel Glover, and Valentin V. Khoze. Recursion relations for gauge theory amplitudes with massive vector bosons and fermions. *JHEP*, 01:066, 2006.

[267] Kang Zhou and Chenkai Qiao. General tree-level amplitudes by factorization limits. *Eur. Phys. J.*, C75(4):163, 2015.

[268] Adam Falkowski and Riccardo Rattazzi. Which EFT. 2019.

[269] Spencer Chang and Markus A. Luty. The Higgs Trilinear Coupling and the Scale of New Physics. 2019.

[270] Rodrigo Alonso, Elizabeth E. Jenkins, and Aneesh V. Manohar. A Geometric Formulation of Higgs Effective Field Theory: Measuring the Curvature of Scalar Field Space. *Phys. Lett.*, B754:335–342, 2016.

[271] Adam Falkowski, Martin Gonzalez-Alonso, Admir Greljo, David Marzocca, and Minho Son. Anomalous Triple Gauge Couplings in the Effective Field Theory Approach at the LHC. *JHEP*, 02:115, 2017.

[272] Jason Aebischer, Andreas Crivellin, Matteo Fael, and Christoph Greub. Matching of gauge invariant dimension-six operators for $b \to s$ and $b \to c$ transitions. *JHEP*, 05:037, 2016.

[273] Jure Drobnak, Svjetlana Fajfer, and Jernej F. Kamenik. Interplay of $t \to bW$ Decay and B_q Meson Mixing in Minimal Flavor Violating Models. *Phys. Lett.*, B701:234–239, 2011.